Timing and Structural Control of Gold Mineralization,

Santa Gertrudis, Sonora, Mexico

by
John Jeffrey Geier

A Thesis Presented in Partial Fulfillment
of the Requirements for the Degree of
Master of Science

Approved April 2011 by the
Graduate Supervisory Committee:

Stephen J Reynolds, Chair
Donald Burt
Edmund Stump

ARIZONA STATE UNIVERSITY

May 2011

ABSTRACT

The Santa Gertrudis Mining District of Sonora, Mexico, located 80 km southeast of Nogales, contains more than a dozen purported Carlin-like, sedimentary-hosted, disseminated-gold deposits. Following discovery of the district by Phelps Dodge Corporation in 1985, a series of near-surface, mostly oxidized gold deposits were open-pit mined from the calcareous and clastic units of the Cretaceous Bisbee Group. Mining ceased in 2000, with 600,000 ounces of gold mined at an average grade of 2.13 g/t with an estimated 700,000 ounces remaining.

Gold occurs as finely disseminated, sub-micron coatings on sulfides, associated with argillization and silicification of calcareous, carbonaceous, and siliciclastic sedimentary rocks in structural settings. Gold occurs with elevated levels of As, Hg, Sb, Pb, and Zn. There are strong relationships among alteration, mineralization, and structural control. Downhole drill data within distal disseminated gold zones reveal a 5:1 ratio of Ag:Au and strong correlations of Au to Pb and Zn, a geochemistry that is unlike most of the deposits at Carlin, Nevada.

Despite 25 years of exploration and mining in the district, little is known about the timing and structural control of the mineralization. This study explores the timing and structural control of mineralization utilizing 1:2,000 field mapping, geochemical studies, radiometric dating, drilling, core logging, and structural analysis. Structural controls for mineralization include a 15-km-long northwest trend of gold and tracer elements in brittle-ductile structures and north- to northeast-trending, high-angle, brittle structures. The highest grades of mineralization occur in the intersections of northwest and north to northeast structures, yet economic gold grades do not strike or dip vertically or laterally along any structure for more than 300 m. North-to-northeast-trending structures seem to have acted as conduits for concentrating decalcification, silicification and mineralization in favorable stratigraphic units.

Timing of mineralization is constrained between the age of the hornfels and the age of the low-angle structures that decapitate the deposits. Although there are suggestions of multiple,

unrelated pulses of mineralization, most field evidence indicates that mineralization is related to a single pulse of moderately differentiated, Eocene intrusives that may be best described as Mo-Cu-Au skarn with structurally controlled distal disseminated As-Ag-Au.

TABLE OF CONTENTS

CHAPTER Page

LIST OF TABLES

Table Page

LIST OF FIGURES

Figure Page

Figure Page

Figure Page

Figure Page

I. INTRODUCTION

General Overview

The Santa Gertrudis Mining District, Sonora, Mexico is located 80 km southeast of Nogales, Sonora (Figure 1-1). The district is located within the Basin and Range physiographic province (Wendt, 1997) as a series of low rolling hills along the southern flank of the 2,450 m Sierra Azul (Figure 1-2). The climate is semi-arid, with a variety of cacti, catclaw, black oak and mesquite interspersed with grasses (Figure 1-3). During the study, the property consisted of 55 concessions totaling 62,494 hectares (Ristorcelli, 2009). Access to the district is via the two-lane Magdalena-Cucurpé Highway and then along 39 km of graded haul road. Cattle ranching and farming are the main land uses.

The district is underlain by gently dipping to upright or steeply overturned, Cretaceous Bisbee Group, expressed in the limbs of a southwest-verging, asymmetric, regional-scale fold. The contact between the Glance Conglomerate and the rest of the Bisbee Group is conformable; the upper contact of the Bisbee Group is not exposed in the district. Intrusives from oldest to youngest include chloritized diorite, two-mica granite, felsic dikes, lamproites, and andesites. Early Miocene ignimbrites are exposed on the southern and eastern edges of the district as distinct, fault-bounded tilt blocks. The ignimbrites unconformably overly a Late Eocene, two-mica granite with associated Cu-Mo-Au mineralization and greisen alteration.

The study includes three areas of primary interest within the district: Enedina, Mirador, and Toro-to-Gregorio. These areas were chosen due to their abundance of the typical styles of structural deformation, mineralization, and alteration. Two additional areas are mentioned throughout this study: the Main District and San Enrique (Figure 1-4).

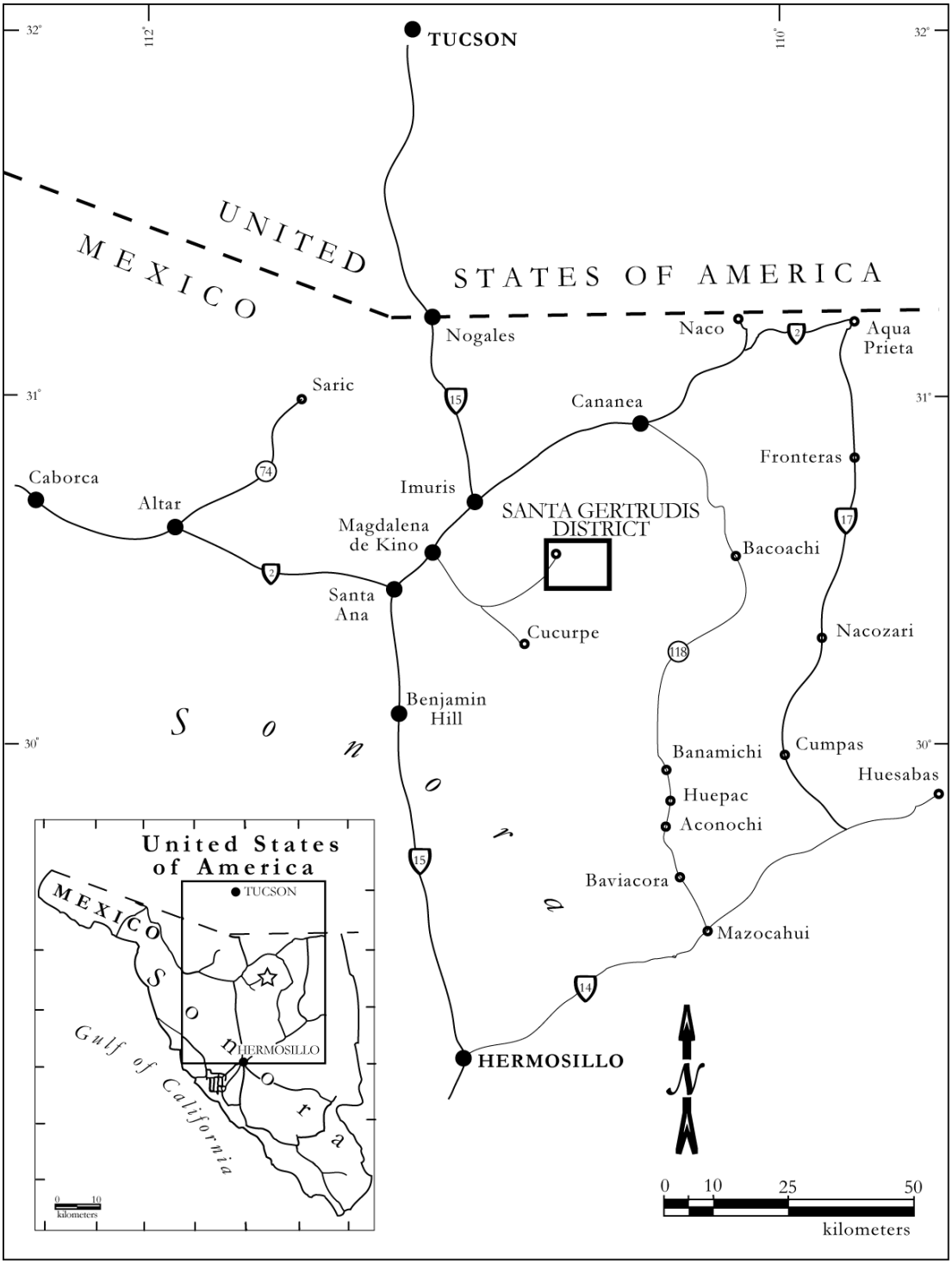

Figure 1-1 Map of the Santa Gertrudis Mining District and surrounding municipalities.

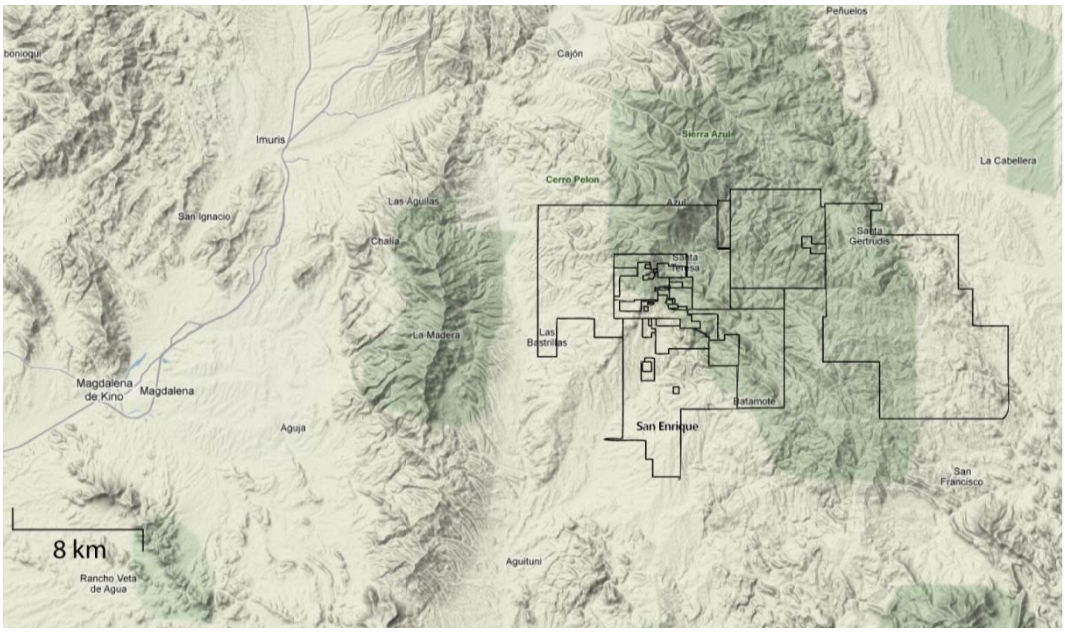

Figure 1-2 Physiography and claim boundaries for the Santa Gertrudis Mining District.

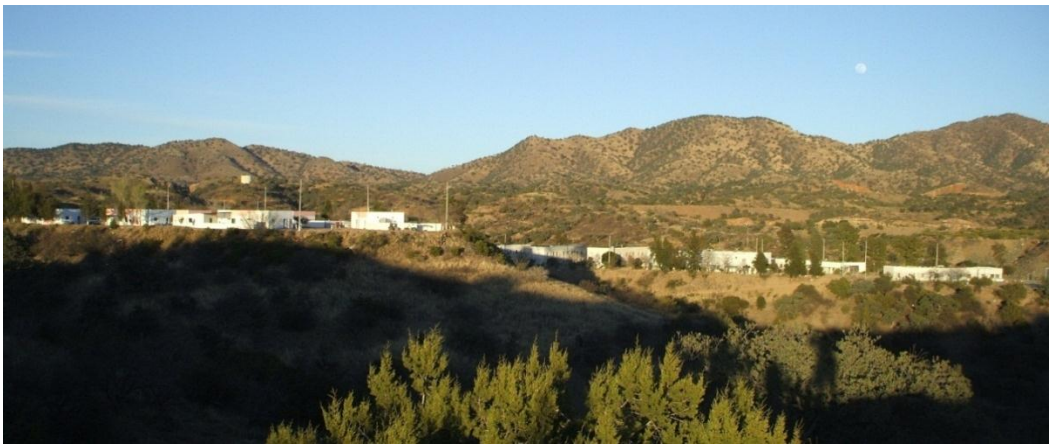

Figure 1-3 View looking northeast at the Santa Gertrudis mining camp and exploration offices. Background, higher hills are Glance Conglomerate.

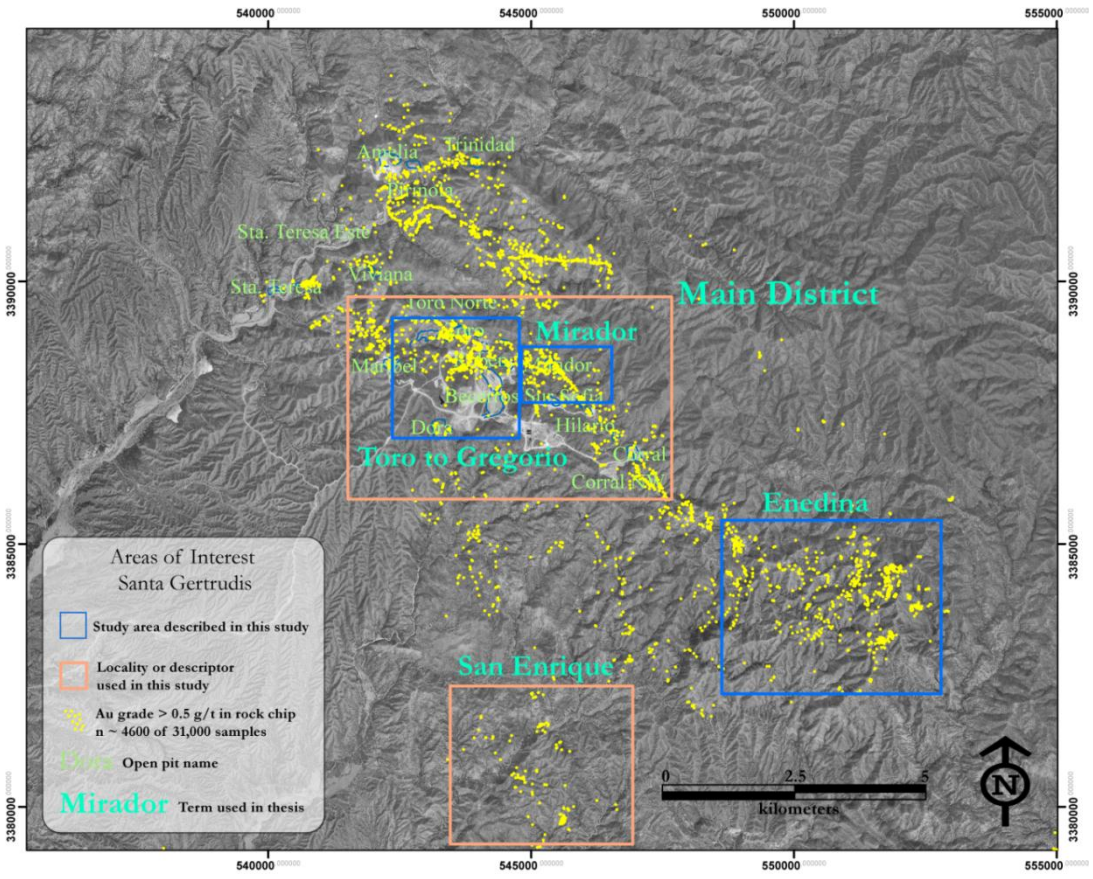

Figure 1-4 Localities identified in this thesis as study areas and commonly used geographic names plotted against rock-chip samples greater than 0.5 g/t Au.

The Main District lies in the center of the Santa Gertrudis mining district (Figure 1-4). Representing the bulk of the mining within the district, the Main District includes the following open-pits from northwest to southeast: Toro, Toro Norte, Katman, Manueles Sur, Dora, Maribel, Ruben, Camello, San Ignacio, Gregorio, Agua Blanca, Becerros Norte, Becerros Sur, Mirador, Sofia, Hilario, Corral Northwest, and Corral. The Main District covers 6.5 km^2 and contains 18 open mines, which produced approximately 450,000 ounces of gold. Upright, northwest-striking, and southwest-dipping Bisbee Group units abruptly roll over within the Main District to steep, northeast dips. The overturned stratigraphy defines a large, northwest-plunging, regional syncline referred to as the Gregorio syncline in this study (Figure 1-5).

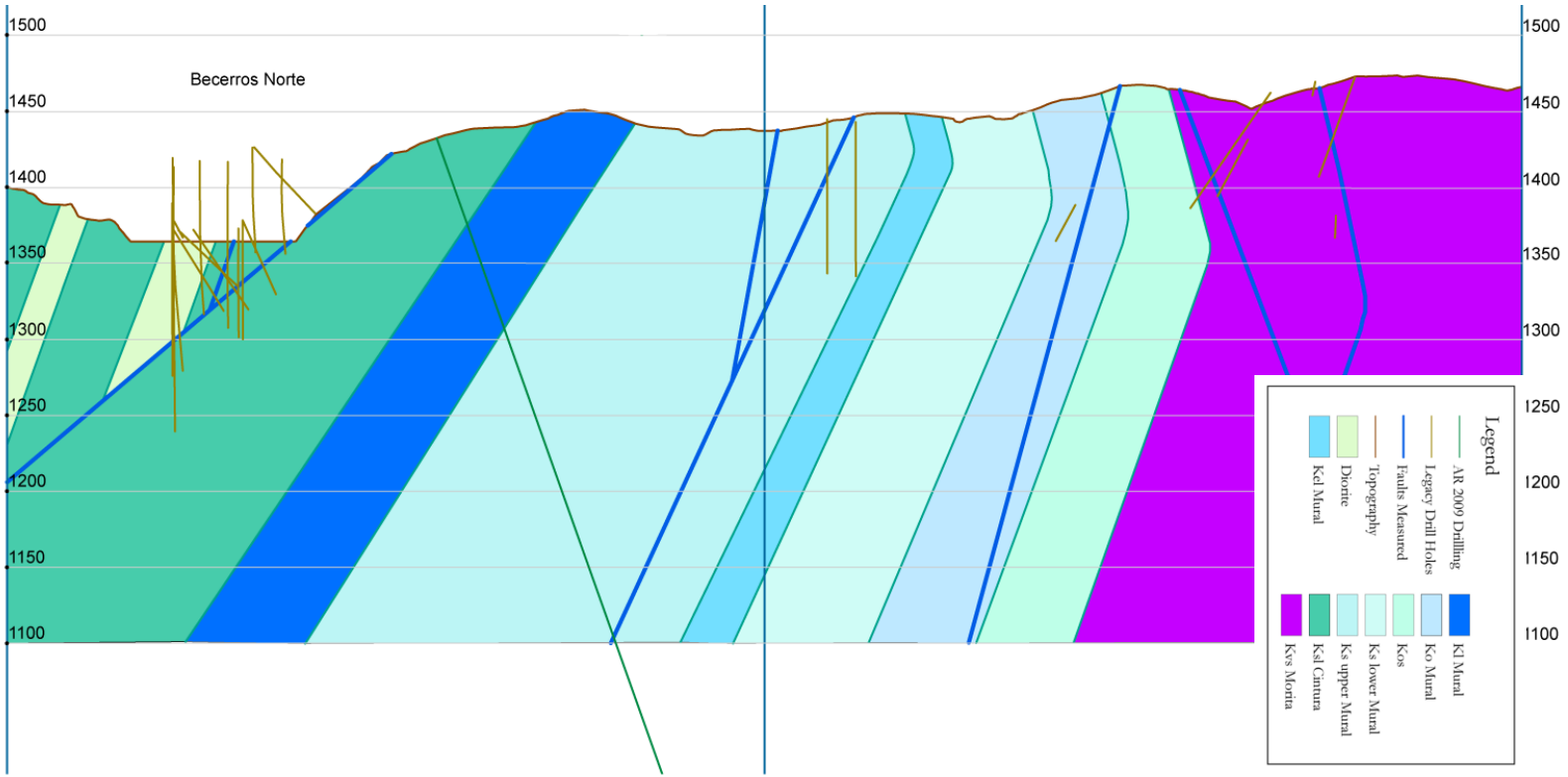

Figure 1-5 Cross section of Gregorio syncline and Becerros Norte Mine. Bisbee Group units abruptly roll over from southwest-dipping to northwest-dipping in the subsurface.

The Toro-to-Gregorio and Mirador study areas lie within the Main District. The Toro-to-Gregorio study area contains non-hornfels Bisbee Group units overturned in the Gregorio syncline and bedding-parallel shear zones hosting distal disseminated gold mineralization. The Mirador study area is east of the Toro-to-Gregorio study area and is characterized by metamorphism of the Bisbee Group to brown-biotite hornfels and minor andradite skarn. Post-hornfels faults in the Mirador study area separate the Toro-to-Gregorio study area from the Mirador study area.

The Enedina study area lies 8.5 km southeast of the Main District (Figure 1-4). Within the study area several prospects have been identified: La Gloria, Greta, Santiago, and Laura in the north; Tracy, Nadia, and Lupita to the south; and El Tigre, Enedina, and Lupita Sur further to the south. Enedina is characterized by increasing grades of hornfels and skarn in Bisbee Group units. The area with the highest grade of hornfels is called Enedina Hill and has been interpreted as the zone of highest metamorphism. The metamorphism may be related to a buried intrusive that lies deeper than 650 meters (Animas Resources, 2009). Hornfels extends for 2.5 km in diameter in a circular ring from Enedina Hill.

San Enrique, 8 km south of the Main District and 6 km southwest of Enedina Hill (Figure 1-4), is characterized by brown-biotite hornfels and skarn surrounding a 2 km, northeast-oriented, Eocene, two-mica granite. The granite intrudes the Bisbee Group and may be associated with the hornfels and skarn flanking the intrusive.

The Batamote graben, 1 km north of San Enrique, is a west-northwest-trending basin with northeast-dipping units bounded on the northeast by a southwest-dipping normal fault. The

basin has a basal trachyandesite overlain by an indurated conglomerate locally showing fanning dips.

Mineralization is best characterized as distal disseminated, sediment-hosted within the Main District and along the periphery of the hornfels zones. Minor decalcification and silicification, associated with minor stratiform replacement along structural pathways in calcareous rocks, acted as the primary hosts for ore grade. Gold and tracer elements are widely distributed throughout the district's sedimentary lithologies as distal disseminated haloes. Argillization, color leaching, and silicification are the primary alterations in the mineralized shear and fracture zones; oxidation of the primary sulfide hosts has overprinted the entire district with varying degrees of hematite, goethite, and jarosite.

Mineralization within the hornfels and skarn is disseminated, fault-controlled, and associated with quartz veins. Visible sphalerite, galena, and stibnite are present in the hornfels. Oxidation of primary mineralization is minor within the hornfels, and intensifies on the margins of the hornfels.

Previous Work

The geology and tectonic evolution of the region has been investigated by a number of workers on both sides of the U.S. – Mexico border. Detailed work, focused on gold exploration, has occurred in the area of Santa Gertrudis.

Previous investigators have documented that during the Late Jurassic, active marine basin formation was occurring due to rifting of the southern portion of the North American craton. This basin may have stretched from the Gulf of Mexico to southern California, with the seaway bearing different names according to its geographic position: Bisbee Basin, Sabinas

Basin, Chihuahua Trough, and McCoy Basin (Dickinson et al., 1989; Dickinson and Lawton, 2001). Within the district, sequences record volcanic and sedimentary environments from the Late Jurassic and Early Cretaceous to the mid-Cretaceous. Dumble (1900) was the first to describe the Bisbee Group units in Sonora, Mexico. Although he separated them into four separate units, he did not designate any formal names. Ransome (1904), working in southern Arizona, formally described and named the four units, designating them as separate formations, and giving the name Bisbee Group. He named the units, from bottom to top, the Glance Conglomerate, Morita Formation, Mural Limestone, and Cintura Formation. He measured the sequence to at least 1,580 m thick near Bisbee, AZ

More recent studies in northern Sonora include descriptions of Cretaceous rocks at Sierra de Santa Rosa (Hardy, 1973), Sierra La Gloria and Cerro Basura (Corona, 1979, 1980), Cerros Chino and Rayón in Caborca (Longoria and Pérez, 1979) and Sierra El Chanate (Jacques-Ayala, 1983). Gonzalez-Leon (1988) studied the fossils of the Cerro de Oro area and proposed that a new stratigraphic unit, the Cerro de Oro Formation (Barremian-Aptian), be added to the Bisbee Group. McKee and Anderson (1998) described the Jurassic and Cretaceous rocks south of Sierra Azul, north of Santa Gertrudis, and inferred they were equivalent to Bisbee Group rocks as described in southern Arizona and northern Sonora. Garcia y Barragán (2003) described the 2,000-m-thick La Palma Formation, a late Cretaceous sedimentary sequence of basal polymictic conglomerates overlain by a series of interbedded siltstones and sandstones that unconformably overlie the Bisbee Group. Gonzalez-Leon and Lucas (1995) studied the paleontology of the Cerro de Oro, Mural, and Morita formations. Jacques-Ayala (1995) described the Bisbee Group in the Caborca-Santa Ana area, and Monreal and Longoria (2000b) described the Lower Cretaceous stratigraphy of the Lampazos area in eastern Sonora.

Within the district, several academic studies have been conducted, including McKee's 1991 PhD dissertation on the Cretaceous stratigraphy and gravity mass sliding in the northwestern portion of the district. McKee and Anderson (1998) concluded that the Cretaceous Bisbee Group in the district had formed in the Sonora Basin, a small basin separated from the Bisbee Basin by a proposed Cananea Island. They continued McKee's 1991 notion of mass sliding of Bisbee Group stratigraphy into the basin. Bennett (1993) completed a M.S. thesis study of the district with the support of Minera Zapata, the Mexican subsidiary of Phelps Dodge. His study utilized field-based mapping and Landsat Thematic Mapper images with post-processing, along with lab-based studies to assemble an integrated GIS for gold exploration and target identification. He was also successful in obtaining K-Ar radiometric dates of the Las Panochas Granite (36.1 ± 0.9 Ma) and a biotite-rich diorite (26.1 ± 0.7 Ma). Garcia y Barragan (2008) completed a study of the Mesozoic conglomerates of Sonora, including the Early Cretaceous El Tuli Formation on the margins of the district. He succeeded in measuring two sections of the El Tuli Formation and one section of the Bisbee Group to the east of the Enedina study area.

According to Phelps Dodge reports (Rodriguez; Lopez, 1992), early in 1985, Walt Gauge of the Douglas smelter, in Douglas, Arizona, contacted Phelps Dodge exploration personnel to encourage a visit to a small mine making substantial shipments of gold-bearing silica flux to the smelter. Shipments over a period of several months yielded the following averages: 67.1% silica, 0.77 % arsenic, 0.35 ounces of gold per ton (l0.8 g Au/t), and silver less than one-half ounce per ton. Phelps Dodge representatives visited the area, collecting samples from the Amelia Mine in May 1985, as well as two small pits from which a local prospector was making

periodic shipments. These initial samples from the two pits confirmed the presence of gold in what will later become the Carmen and EI Toro deposits.

According to the Phelps Dodge 1992 report on the geology and history of the district:

> John Forrester (Phelps Dodge Corp.) visited the prospect with Herb Mendoza in May 1985 and recognized the potential for sediment-hosted gold mineralization similar to the gold deposits of Carlin, Nevada. The Agua Blanca claim was acquired by agreement on April 1, 1986 and by April 26, on the first hole, the Aqua Blanca deposit was discovered. Soon additional deposits were discovered: San Ignacio, Los Manueles, Rubin, Santa Teressa, Gregorio, Hilario and El Corral.
>
> The initial prospecting program incorporated geologic mapping as the primary guide to identifying the favorable zone of mineralization and alteration. Outcrop sampling was an integral part of this program. Soil and stream sampling were completed in the district as well. The principal exploration tool used to evaluate the gold deposits was core drilling. In 1988 and subsequent years, reverse circulation drilling has proven to be an economic and reliable sub-surface sampling technique. Rock sampling of the alteration zones exposed on the gently rolling hills often documented gold anomalies well above 1 ppm gold. Many of the deposits cropped out and drilling targets were easily defined by the wide zones of gold mineralization observed in shallow trenches. Stream silt sampling led to the discovery of Los Becerros in 1987.

Following the discovery of gold mineralization at Santa Gertrudis in 1985, Phelps Dodge Mining Company ("Phelps Dodge") began systematic exploration mapping and reconnaissance of the district to define deposits of recoverable gold. Phelps Dodge was the first major exploration company to recognize the potential of the Santa Teresa district. Using a Carlin-type (sedimentary-rock-hosted, disseminated-gold) model as a guide, Phelps Dodge completed soil and stream-sediment sampling, induced-polarization surveys, and reverse circulation and diamond drilling. An initial discovery was made in 1986; a feasibility study was completed in 1988, and mining commenced at the Santa Gertrudis district in 1991. The mining regulations at that time dictated that Phelps Dodge must secure a Mexican partner. In 1989, Grupo Ariztegui

became 51% owner of Minera Santa Gertrudis. Phelps Dodge, through a Mexican operating company, Sonoran Mining Company, agreed to be the operator of the mine. A decision to begin production was made in 1989, and construction started in May 1990. The first shipment of gold precipitate was made on June 10, 1991 from the 2,200-ton-per-day (tpd) heap leach facility. The initial capital investment was $22,000,000 to develop a mine based on reserves of 7,300,000 tons of 0.07 ounces of gold per ton.

Initially, production was 2000 tpd and was increased to 3000 tpd, in an open pit, heap-leach operation exploiting shallow oxide ore (Hamilton, 2003). Although much of this exploration work has been misplaced or lost, several studies and maps do remain on the property and were utilized by future concessionaires (Ristorcelli, 2009).

According to Strathcona Mineral Services Limited, 3,000,000 tons of ore were mined with an average grade of 2.0 g Au/t. From this 4300 kg of gold was recovered by heap leaching for a cumulative recovery of approximately 70% (Thalenhorst, 1994). This would have resulted in total recovered gold for Phelps Dodge at the Santa Gertrudis mine of approximately 138,000 ounces. Phelps Dodge was aware of the potential for deep Carlin-like deposits, but only drilled four holes deeper than 250 m to test for deep, unoxidized, down-dip potential and/or possible causative intrusives (G. McKelvey, pers. comm., 2009). Phelps Dodge developed the Santa Gertrudis district and produced gold from 1991 to 1994, then sold the property to Campbell Red Lake Resources Inc. ("Campbell") in 1994.

After purchasing the property through its Mexican subsidiary Oro de Sotula, S. A. de C. V., Campbell continued to mine shallow oxide ore in the Santa Gertrudis district at a rate of 3000 tpd from 1994 until late 1997 and then on a smaller scale from late 1999 until October 2000.

Hamilton (2003) stated, "The Santa Gertrudis mine-site has produced 332,000 ounces of gold since 1991." This would include production by Phelps Dodge and by Campbell (Ristorcelli, 2009; Table 1-1).

:os Sur	54,869	2.16	Cintura	9.71	37.9	2.10	Arg/ser/oxidation
ın	17,756	1.48	Cintura	3.14			Arg/ser/oxidation
el	24,406	2.19	Cintura	4.32			Arg/ser/oxidation
les Sur	11,027	2.69	Cintura	1.95			Arg/ser/oxidation
Blanca	43,038	2.12	upper Mural	7.62	11.7	1.82	Arg/ser/oxidation
	22,870	1.51	upper Mural	4.05			Arg/ser/oxidation
	77,039	2.35	middle Mural	13.64			Arg/ser/oxidation
	39,164	2.50	middle Mural	6.93			Arg/ser/oxidation
rio	11,794	1.45	middle Mural	2.09			Arg/ser/oxidation
or	10,202	1.43	middle Mural	1.81	1	8	Hornfels/ qtz vein

Table 1-1 Table of open-pit names, ore grade, host formation, percent of total production, percent sum by formation, and gold grade by formation

As reported by Hamilton (2003), Campbell carried out a systematic exploration program from 1994 through November 2000, spending a total of ~$13,000,000 while mining the Mirador, Dora, and Trinidad deposits. Much of the exploration and mining records from Campbell Resources have been preserved in paper and digital format including: 34,000 rock-chip samples, 98,620 m of reverse-circulation drilling in 1,017 holes, and 21,122 m of diamond drilling in 225 holes, geophysical surveys (induced-polarization, airborne magnetic, electromagnetic, radiometric geophysical surveys), detailed field mapping, whole-rock studies, monthly and yearly reports, and model analysis. According to Anderson and Hamilton (2000) "In the Santa Teresa district, between 1991 and 2000, in excess of 564,000 ounces were mined from 8.244 million tons of ore grading 2.13 g Au/t in twenty-two, sedimentary-rock-hosted, disseminated-gold deposits." Detailed structural studies were carried out by Scott Anderson, who generated monthly reports for the 2½ years that he spent mapping the district. He concluded that the Main District mineralization was most likely Tertiary in age, associated with the low-angle extensional structures and possibly related to the lamproite dikes ("lamprophyre" of Anderson; Phelps Dodge) and undifferentiated dikes discussed later in this study.

Campbell ceased operations at Santa Gertrudis in 2000 and through a series of transactions, the property was again divided, with the López-Limón concessions under the control of Sonora Copper LLC and the remainder of the property under the control of Sonora Gold Corporation. In 2005, Teck Cominco Ltd., operating as Minera Teck Cominco, S. A. DE C.V. in Mexico, optioned the San Enrique property, approximately 10 km south of the Main District of Santa Gertrudis. Although their focus was potential porphyry Cu-Mo associated with the Las Panochas Granite, they investigated distal gold deposits in San Enrique, mapped, and sampled the Enedina study area for gold and porphyry Cu-Mo potential. Their

contribution to this study includes eight diamond core drill-holes in the San Enrique area, numerous soil and rock-chip samples, and digital geologic maps at 1:2500 covering San Enrique northeast to the La Gloria prospect. Additionally, Teck Cominco commissioned six lines of large separation, time-domain IP survey on the San Enrique Project, totaling 23.9 line-km and testing three target areas. Teck Cominco also acquired a Re/Os date on molybdenite mineralization associated with the Las Panochas Granite. Reports by Moira Smith, Mario Canela Barboza, and Peter Lewis (Teck Cominco, 2006; 2007) summarize the results and conclusions drawn by Teck Cominco in San Enrique and Enedina. Teck Cominco optioned the property to Sonora Copper in 2007 after determining that the potential for porphyry Cu-Mo in San Enrique and Enedina areas was sub-economic.

In 2007, Animas Resources Ltd. (Animas) acquired the Sonora Copper and Sonora Gold properties and the majority of the legacy data remaining from the previous exploration and mining operations. The acquisitions amalgamated scattered prospects from Amelia in the northwest to La Gloria in the southeast, consolidating 750 km^2 of the Santa Teresa Mining District. Following the leasing and reconsolidation of the district by Animas in 2007, exploration focused on the further discovery of shallow, mineable targets, exploration of the potential for deeper extensions of shallow oxide gold, or the discovery of non-oxidized bonanzas. This exploration was accomplished through 2,700 rock-chip samples, whole-rock studies, 1:2,000 field mapping, and its digitization in G.I.S., induced-polarization studies, magnetic surveying and modeling, 13,000 m of diamond drilling, data compilation, and structural analysis.

Although much of the older data from Phelps Dodge and the smaller concessionaires has been lost, to date there have been over 36,000 rock-chip samples, over 100,000 grid-pattern

soil samples, more than 1300 diamond and reverse circulation drill-holes and multiple generations of detailed field maps over 700 km^2. Animas spent considerable effort compiling and digitizing the data, including scanning paper reports and applying optical character recognition (OCR) to the scans, georectifying legacy paper maps and field sheets for G.I.S. applications, and merging multiple data sets into a useful and searchable database. The database has proven a valuable resource in the current study and for exploration efforts.

Within the district, Phelps Dodge exploration geologists had separated out and given informal designations to distinct units within the Bisbee Group. The naming convention remained in use by the geologists of Campbell, Teck Cominco, and Animas Resources. These informal names help to designate calcareous and carbonaceous siltstones, mudstones, and sandstones from the massive limestones. Distinguishing these units was critical for exploration, structural analysis, mine planning, and ore processing. This study will utilize the district relevant, modified stratigraphy established in the mid-1980s by the Phelps Dodge geologists (Figure 2-2).

Focus of this study

Following the discovery of gold at Santa Gertrudis, multiple attempts were made to establish the source, timing, structural, and lithological controls of the mineralization. Utilizing soil and rock-chip sampling, a 15-km long, northwest trend of gold mineralization and tracer arsenic was discovered associated with the oxidation of iron sulfides. Mineralization is closely tied to northwest-trending, bedding-parallel, brittle-ductile structures that pinch-and-swell in much of the district, with the intersections of northwest-trending and north-to northeast-trending structures providing key sites for the economic concentration of gold. North-to northeast-trending structures post-date and offset the northwest-trending shear-zones, yet they are also

mineralized and have been reactivated post-mineralization. Lithological controls for mineralization were also recognized, with mineralization common by association with calcareous siltstones and sandstones of the Bisbee Group.

It was soon discovered that mineralization was not continuous beyond the intersections, in any orientation, or with depth. Down-dip extensions of favorable lithology and bedding-parallel structures bearing gold did not continue, nor did the trend and plunge of the intersections of the surficial, mineral-bearing structures. Deeper drill-holes, designed to test for unoxidized bonanzas or feeder structures, were generally unsuccessful in encountering significant mineralization. Despite decades of geologic manpower and multi-millions of dollars spent in the district, a complete understanding of the controls of emplacement and the timing of gold mineralization was still lacking.

This study focused on delineating the structural and/or lithological controls to the mineralization and assigning a relative age to the mineralization in the district. This has been accomplished by tying geochemical associations, alteration, metamorphism and mineralization styles to known, radiometric ages for mineralization and alteration at the San Enrique prospect.

Methodology

A brief summary of the methods will follow here, with an in-depth Methodology section presented in Appendix A. All of the study areas were mapped at 1:2,000 scale. The open pits in the Main District were mapped at 1:500 scale. Attention was placed on lithology, structural relationships to mineralization, and alteration styles. Geochemical sampling includes rock chips, soil samples, whole-rock analysis, and drill core data spanning the 35-year history of exploration and mining in the district. Most of the legacy and Animas data was digitized and

utilized in ESRI ArcGIS 9.3. Legacy and Animas geophysics, geochemistry, petrographic studies, and mapping assisted in designing several drill programs in 2008 and 2009, and in compiling this thesis.

II. GEOLOGY

Regional Geology

Santa Gertrudis lies within the Basin and Range physiographic province, wedged between the Tertiary Sierra Occidental to the east and the actively rifting Gulf of California to the west. The geologic history of the study area begins with the conversion from a passive to an active margin along the entire western coast of the North American continent during the mid-Mesozoic Era (Bilodeau, 1982, Dickinson, 1989). Marine basin formation via continental and backarc extensional rifting (Bilodeau, 1982; 1987) created a series of shallow, northwest-trending, fault-bounded grabens or half grabens. (Bilodeau, 1982; 1987). Dickinson and others (1986) proposed a transtensional model for the opening of the Bisbee Basin related to the Jurassic backarc rifting and opening of the Gulf of Mexico (Stern and Dickinson, 2010). Subsequent filling of the basin from locally derived terrestrial and marine sediments, through subsidence and transgression, deposited the Bisbee Group, with deeper marine sediments dominating to the southeast.

The Bisbee Group, exposed in mountain ranges in southeastern Arizona, northern Mexico, and southwestern New Mexico (Figure 2-1), was deposited at the northwestern extremity of the Chihuahua Trough, a northwest-trending, marine extension of the Gulf of Mexico depression (Dickinson et al., 1989). The type locality, in the Mule Mountains near Bisbee Arizona, contains strata recording the opening of the Bisbee Basin and the subsequent filling of the basin with nonmarine, marginal-marine, and marine limestone, followed by deposition of near-shore and terrestrial clastic deposits. The strata record the active rifting of the Late

Jurassic and several transgressive-regressive cycles of the Early Cretaceous. They have a maximum thickness of 3000 m (Bilodeau and Lindberg, 1983).

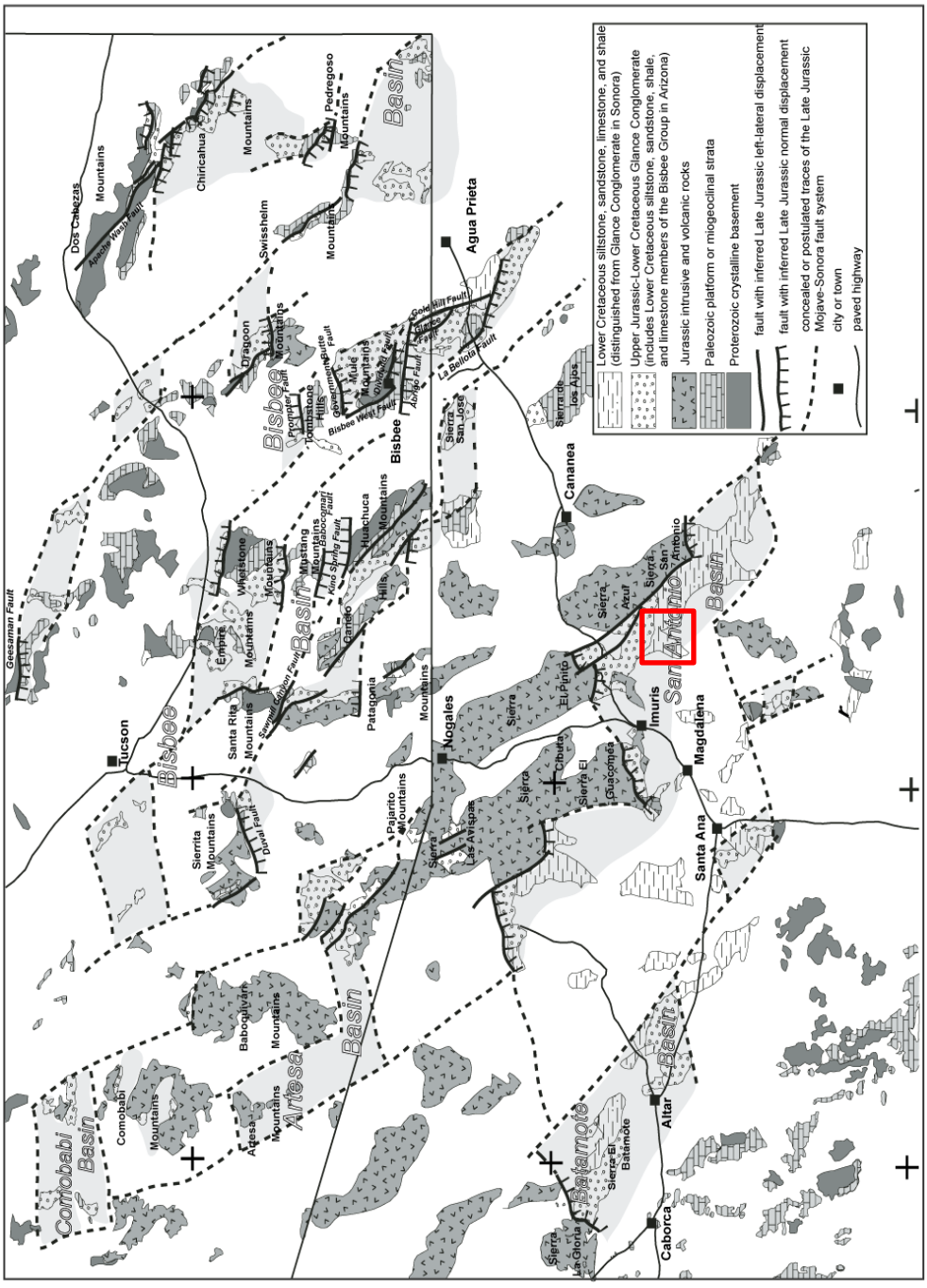

Figure 2-1 Regional map of southern Arizona and northern Sonora showing the relationship to the Jurassic and Cretaceous geology, Jurassic structures, localities and mountain ranges. Adapted from Anderson and Nourse, 2005 by (Richard et al., 2000) and geology of Sonora modified from Nourse (1995, 2001)

Glance Conglomerate, the basal unit of the Bisbee Group, marks the initiation of rifting and the onset of deposition of locally derived sediments in subaerial alluvial fans (Bilodeau, 1979). It was deposited on a highly variable and broken topography with strong local relief, in part generated by block faulting (Dickinson et al., 1989). Bilodeau (1979) recognized inverted clast stratigraphy in the Glance Conglomerate, with clasts of the basal Paleozoic sedimentary units and Precambrian basement in the upper portions of the Glance. Overlying the Glance Conglomerate, the gradational contact into the overlying Morita Formation represents a time-transgressive sequence (Dickinson et al., 1989) of fluvial and near-shore deposits as the basin continued to fill with more mature sediments. The first transgressions were recorded, during the deposition of the Morita Formation.

Overlying the Morita Formation is the Mural Limestone of mid-Cretaceous age. Nations (1989) states the Mural Limestone recorded the maximum marine transgression in late Aptian-Albian time. Black shale deposits in the central Chiricahua Mountains (Hayes, 1970), southern Whetstone Mountains (Tyrrell, 1957), and Patagonia Mountains are correlative to the Mural Limestone. They accumulated in the northwestern facies of southern Arizona, in areas of shallow, restricted water circulation, and lack the limestone units in the Bisbee Group type section and in sections south into Sonora. Local, coral-algal-rudist patch reefs of the upper Mural Limestone in southern Arizona and into Sonora developed on slightly submerged, residual paleostructural highs during the maximum transgression of the Bisbee Sea (Hayes, 1970; Bilodeau and Lindberg, 1983; Dickinson et al., 1989).

By the end of Albian time, the Bisbee Basin was invaded by an alluvial plain draining into the marine Chihuahua trough (Dickinson et al., 1989). Fan-delta deposits, topped by braided

fluvial systems of the Cintura Formation, outpaced subsidence, marking the end of marine transgression (Lindberg, 1987).

Initially, source material for the Bisbee Basin included locally derived sediment consisting primarily of clasts of Precambrian granite and schist, Paleozoic units, and Jurassic volcanic rocks. The sediment was deposited in irregular, fault-bounded basins. This is reflected in the inverted clast stratigraphy of the Glance Conglomerate, as progressively older units are exposed, weathered, eroded, and deposited into the actively faulting basins. The finer-grained, well-sorted, terrestrial sediment of the Morita Formation gradationally caps the Glance Conglomerate and marks the input of terrestrial and volcanic material into the basin, as well as the influence of marine deposition. Deposition of the Mural stratigraphy marks the presence of near-shore marine conditions with fluctuations in sea level marked by calcareous siltstones, carbonaceous mudstones, patch-reef and limestones. Finally, the Cintura Formation, a thick sequence of terrestrial sediments, marks the end of marine transgression. Dickinson et al. (1989) proposed that the terrestrial sediments deposited in the Bisbee Basin were derived from the Arizonan Mogollon Highlands to the north and east of Sonora.

The age of the Bisbee Group in southern Arizona and northern Mexico is constrained by paleontological studies of the Mural Limestone, including *Orbitolina texana* (Roemer, 1852). Pérez-Ramos (1986) described *Coalcomana ramose* near Santa Ana, and in the Cabullona Basin, and Warzeski (1987) observed calpionellids, caprinids, gastropods, echinoids, *Orbitolina,* milliolids, and diverse types of algae and corals.

Within the district, an unconformity exists between the uppermost Bisbee Group member, the Cintura Formation, and the overlying Late Cretaceous/Early Tertiary El Tuli Formation

(Barragán, 2003). Nowhere within the three study areas is the El Tuli Formation exposed. Legacy mapping from Phelps Dodge and Campbell as well as the current mapping completed by Animas, omits the El Tuli Formation, either lumping it with the Glance Conglomerate or mapping it as undifferentiated conglomerate. This is a reflection of the un-economic nature of the Glance/Tuli Formations, the similarity in clast size and type, the structural complexities of the district, and the similar deformations apparently experienced by both of the units. According to Barragán (2003), 76 Ma is a probable age for the upper sections of the El Tuli based on a rhyolitic tuff collected by Rodríquez-Castaneda (1994).

Active sedimentation ceased in the latest Cretaceous, contemporaneous with the initiation of the Laramide Orogeny along the western margin of the North American continent. Presumably, the northwest-trending basins bounded by high-angle normal faults were closed by the northeast-directed compression of the Laramide Orogeny, burying and ductilely deforming the sediments of the Bisbee Basin and the El Tuli Formation and possibly inverting the basin sediments. Hayes (1970) proposed that deformation, uplift, and erosion of the Bisbee Basin rocks might have begun as early as the mid-Late Cretaceous (Turonian). Dickinson et al. (1989) state that the Bisbee Group and overlying Cretaceous units were folded, faulted, uplifted, and exposed to erosion no later than the Eocene.

Throughout southern Arizona and northern Sonora, Laramide structures, including thrust faults, folds, and strike-slip faults are exposed cutting Mesozoic and older rocks. Vergence directions include top-to-the-northeast and top-to-the-southwest in northwest-striking thrust faults and fold hinges. Krantz (1989) states that in the western Huachuca Mountains, Arizona, and south into Sonora, folds have consistent overturning to the southwest and are disrupted by minor southwest-vergent reverse faults.

Evidence supporting Laramide deformation at Santa Gertrudis includes small, large, and regional-scale structures with consistent top-to-the-northeast orientation, followed by structures with top-to-the-southwest vergence. Multiple cleavages are present and pressure shadows are evident in diagenetic pyrite within the Bisbee Group. Asymmetric folds, along with structural thinning of less competent units and stretched pebble conglomerates in the Glance Conglomerate pre-date, and are preserved by a younger, metamorphosing event. Small-scale ductile deformation is evident in the drill core of all of the holes drilled by Animas.

Bracketing the end of Laramide Orogeny within the district is accomplished with relative and absolute timing relationships. The Las Panochas Granite, with a K-Ar date of 36 Ma (Bennett, 1993), lacks ductile shear fabrics. The lack of Laramide-style deformation may imply that deformation had ceased within the district by the mid-Eocene.

The earliest timing for extension in northern Mexico is evidenced by a moderate angular unconformity in 42 to 37 Ma Oligocene ignimbrites south of Chihuahua (Ferrari et al., 2007). Crustal extension commenced after the first pulse of ignimbrites during the Eocene, with rapid extension following rhyolitic volcanism at 30 Ma (Ferrari et al., 2007). Sweeping magmatism, from east to west, related to steepening of the subduction angle of the Farallon Plate in the Eocene provided the impetus to warm the upper crust as the relaxing of the compressive stress allowed the crust to collapse and extend.

Within the district, the Batamote trachyandesite, the basal unit of the Batamote half graben, has been assigned to the early Oligocene, with the overlying sandstones and conglomerates filling the basin assigned to the mid-to late-Oligocene Magdalena Formation. These units and the basin they fill may represent the first major extensional period at Santa Gertrudis.

According to Ferrari et al., (2007), normal faulting postdates the 28-27 Ma ignimbrites with extension extending from Durango to eastern Sonora, forming the basins that would host the Báucarit Formation and to the sites of formation of metamorphic core complexes. Metamorphic core complexes, which developed between 26 and 16 Ma in northern Sonora (Anderson and Silver, 1981; Nourse et al., 1994), are recognized in Magdalena (Nourse et al., 1994), Anóchi (Rodriquez-Castańeda, 1994), Puerto del Sol (Nourse et al., 1994) and Mazatán (Vega-Granillo and Calmus, 2003; Gans et al., 2003; Wong and Gans, 2003). Along with core complexes, extensional basins bounded by high-angle faults are common in central-eastern Sonora, with basal basaltic to andesitic lavas ranging in age from 27 to 20 Ma being capped with highly compacted sandstone and conglomerates of the Báucarit Formation (Ferrari et al., 2007). By the mid-Miocene, the Las Panochas granite had been exhumed and unconformably overlain by early Miocene Báucarit Formation and middle Miocene rhyolite tuffs. The final pulse of extension in Sonora occurred at the end of the middle Miocene between ca. 12 and 9 Ma (Ferrari, 2007; Gans et al., 2003) and is also recognized in Sinaloa (Henry and Aranda-Gómez, 2000) and Nayarit (Ferrari and Rosas-Elguera, 2000; Ferrari et al., 2002).

Differences between Basin and Range extension in the western United States and Mexico led to dramatically different outcomes. In the United States, extension occurred over a region 1000 km in width without rupturing the continental crust, whereas in Mexico extension became localized, leading to the rupture of the continental crust and the formation of the Gulf of California in the Pliocene (Ferrari, 2007).

The geologic history of Sonora has been dominated by the formation, variable-angle subduction and associated magmatism followed by the ultimate destruction of the active subduction margin along the western margin of the North American continent. Crustal

flexures led to the formation of marine basins, followed by the closure of the basins and ductile deformation of the sedimentary basin fill by the compressive forces of the Laramide Orogeny. Relaxation of the crust and partial melting (Huppert and Sparks, 1988) led to calc-alkaline peraluminous felsic intrusives, the ignimbrite flare-ups, and episodic extension accommodated by high-angle and low-angle structures from the Eocene until the end of the middle Miocene.

Rock Units

Within the study area (Figure 1-4) and the mining district, the local stratigraphy of the Bisbee Group has been subdivided into informal units to facilitate field mapping, ore-grade control, identification of favorable lithology, and identification of structural deformation of less competent units. This stratigraphy, initiated with the earliest exploration mapping by Phelps Dodge, has remained a time-tested and useful framework and will be used in this study (Figure 2-3).

Determining stratigraphic younging direction was important for drawing cross sections and predicting stratigraphy at depth for drill targeting. Tops were established using basic sedimentological up-indicators including crossbeds, graded beds, flame structures and other features (Figure 2-2).

Figure 2-2 Stratigraphic tops were determined using graded beds, crossbeds and other sedimentological indicators. Top is up in this photo. Graded beds and crossbeds in the Ksl. Tops were important for determining structural overturning present in the Animas 2009 deep drilling.

Some units are variable in thickness along strike. This is due to facies changes, structural and depositional lensing, and pinch-and-swell structures. Structural deformations include stacked, imbricated thrust sheets, bedding-parallel slip and attenuation, regional folding, low-angle extensional structures, strike-slip, and high-angle normal faulting. In each of the three study areas, mapping followed the individual beds for kilometers as they entered and exited the study zones. In addition to the study areas, 2½ years of mapping at the 1:2,000 scale was accomplished by the author, covering more than 100 km^2 within the district. In collaboration with Bryan MacFarlane and Miguel Angel Fernandez, we mapped the majority of the district and produced various maps at the 1:2,000 and 1:5,000 scales (Figure 2-4).

Abbreviations have been implemented to simplify the nomenclature of the local Bisbee Group stratigraphy: Jgc (Jurassic Glance Conglomerate), Kvs (Cretaceous Mortia Formation), Kos (oyster and sandstone), Ko (oyster-bearing massive limestone), Ks-lower (siltstone), Kel

(El Toro limestone), Ks-upper (siltstone), Kl (limestone), and Ksl (silty-limey) (Adapted from Phelps Dodge, 1986; modified from Bennett, 1993; Campbell, 1994). Abbreviations for the Tertiary intrusives and basin fill conglomerates have been modified from the Servicio Geológico Mexicano 1:50,000 "Carta Geológico-Minera, Santa Teresa" (2003). Tpg (Panochas granite), ToTr (Batamote andesite), Tmc (Magdalena Formation), Tbc (Báucarit Formation), Tmr (rhyolite), and the catch-all symbol is Qal (modern alluvium) are used to portray the Quaternary units (Figure 2-3).

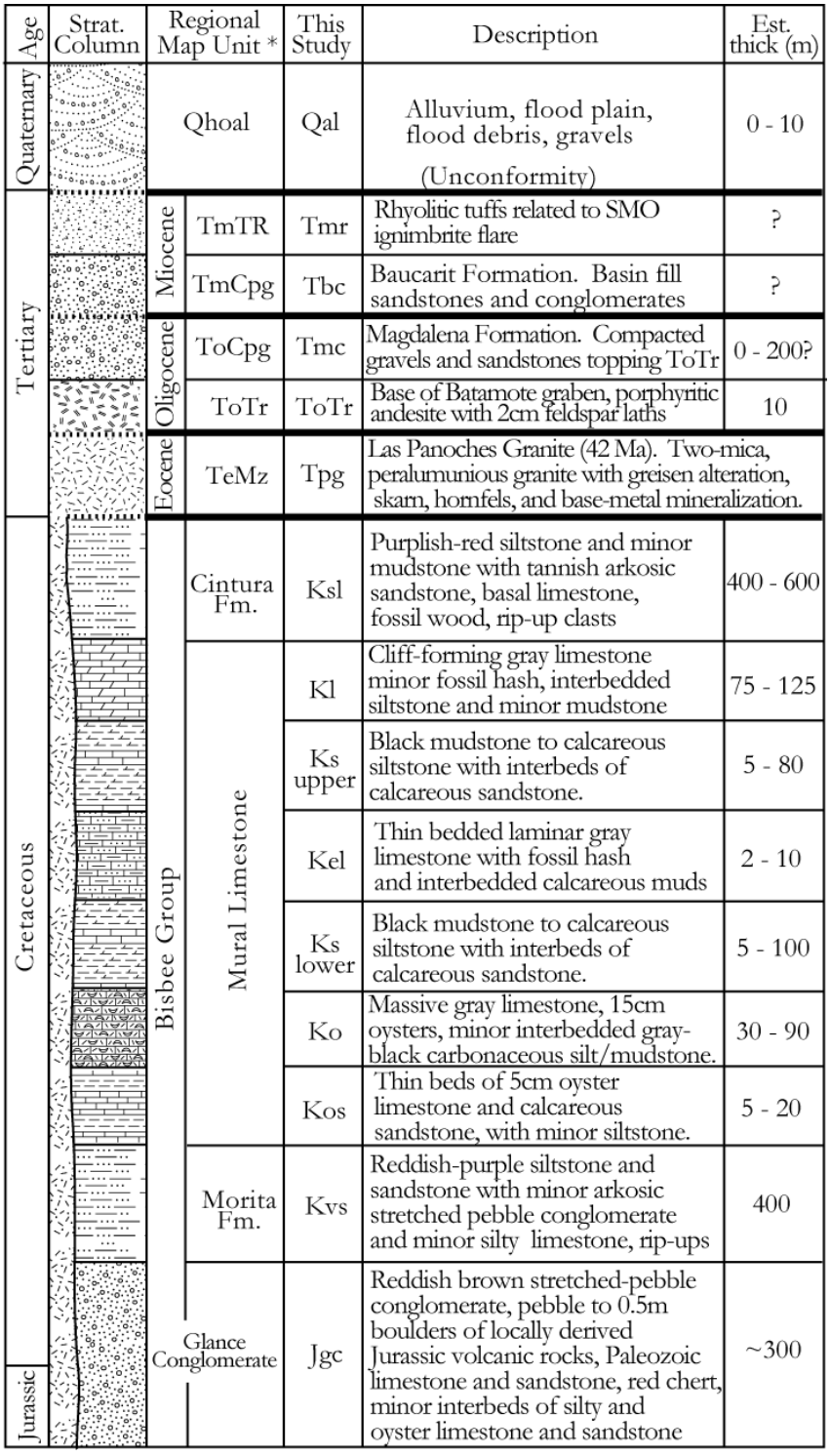

Figure 2-3 Generalized stratigraphic column of the district and study areas. Adapted from Phelps Dodge, Campbell, and Bennett (1993).

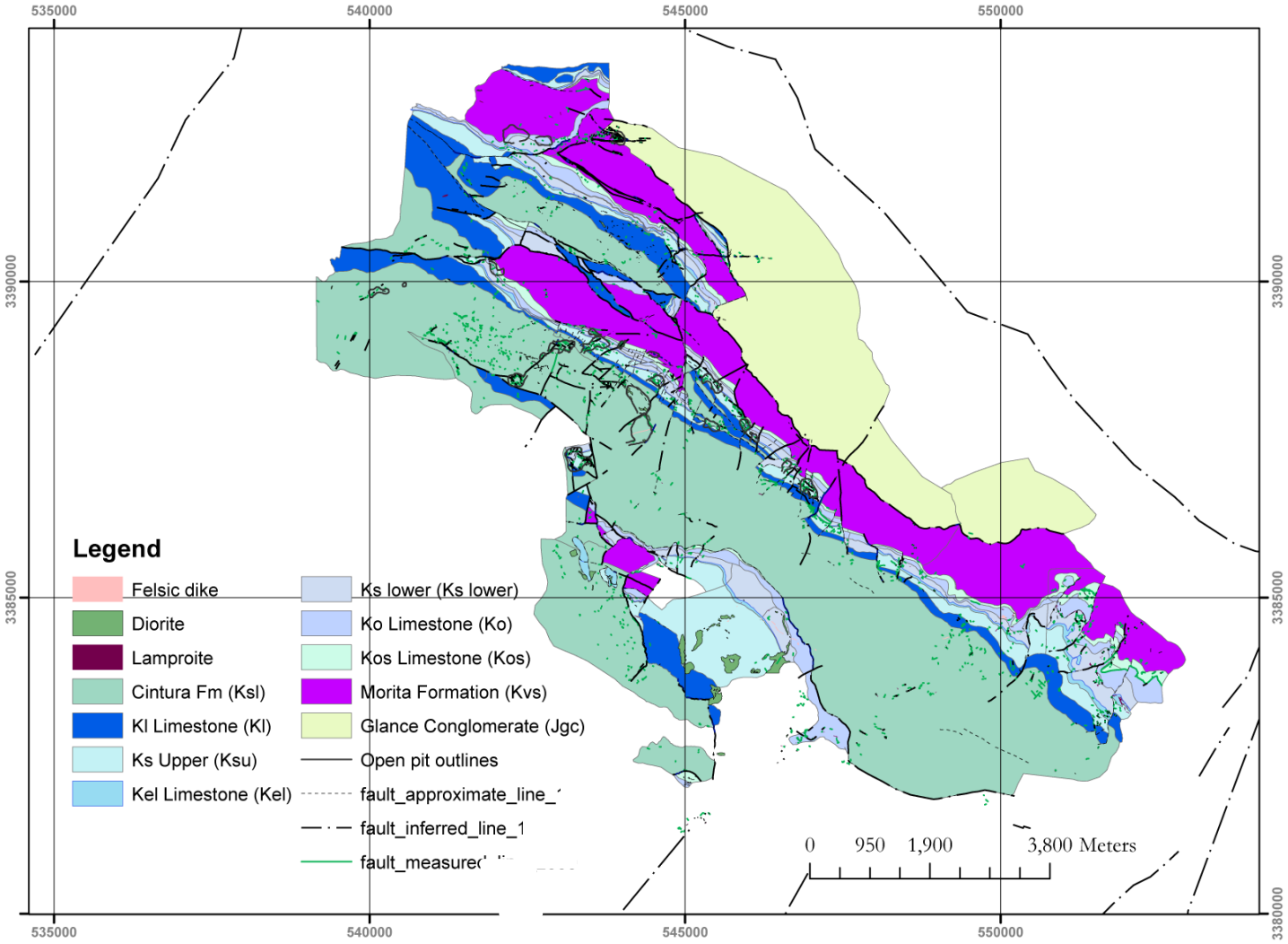

Figure 2-4 Animas Resources geology of the Santa Gertrudis district.

Jurassic - Cretaceous Glance Conglomerate

Within the district, the oldest unit appears to be the equivalent of the Late Jurassic to Early Cretaceous Glance Conglomerate (Jgc), the basal member of the Bisbee Group (Bilodeau, 1978; Dickinson et al., 1986; Bilodeau, 1987; Scott, 1987; Nourse, 1994). Nowhere within the district is the underlying contact between the Glance Conglomerate and older rocks exposed, but Jurassic volcanic rocks are reported north of the district.

In the Santa Gertrudis district, Jgc consists of more than 300 m of repeating, polymictic conglomerate beds, commonly showing normal grading from conglomerate into coarse-grained, arkosic sandstone with minor siltstone. Although no ages have been determined for the Glance Conglomerate in the district, it is in conformable gradational contact with the overlying Cretaceous Morita Formation, and so it is in part probably Early Cretaceous. In outcrop, the conglomerate is reddish-brown with dark green overtones related to chlorite-grade metamorphism. The conglomerate beds are predominately clast supported with a coarse sand matrix. Clasts within the conglomerate range from 2 mm to 1 m in diameter and include intrusive and extrusive volcanic rocks, quartzite, Paleozoic sedimentary rocks, and reddish chert. Interbedded sandstones generally match the arkosic nature and color of the conglomerate matrix. Siltstones tend to be less than 0.25 m thick and are thinly bedded.

Throughout southeastern Arizona, southwestern New Mexico, and northern Mexico, the Glance Conglomerate has tremendous variability in substrate, unit thickness, clast composition and size, sediment provenance, and even age (Bilodeau, 1979; Dickinson et al., 1986; Bilodeau, 1987). The conglomerate represents clastic sediments shed into the newly forming Bisbee Basin in proximal alluvial fan deposits, with varying paleotopography and sediment source reflected in the variability of the Glance Conglomerate throughout the region. Regional

thickness varies from 0 to 2000 m, mimicking the active fault-controlled topography during deposition (Fergusson, 1959; Schafroth, 1968; Dickinson et al., 1986).

Cretaceous Morita Formation

Within the district, the equivalent to the Morita Formation (Kvs) is 400 m thick, consisting of dark reddish purple siltstone and tannish sandstone with 0.5-to-3-m-thick pebble conglomerate beds, a basal sequence of mudstone and limestone, and upper limestone beds associated with the transition to the overlying oyster limestone (Kos). The base of the Morita Formation is in depositional contact with the underlying Glance Conglomerate, grading from matrix-supported pebble conglomerate to tannish-white coarse sandstone or fine sandstone, and then to 5 m of pale green siltstones, that mark the transition to lower energy depositional environments. Locally, black, carbonaceous mudstone and oyster-bearing, dark gray, silty limestones up to 10 m thick form lenses that are scattered within the Morita Formation. Early exploration workers separated this unit out of the Glance Conglomerate and Morita Formation, calling it the Cerro de Oro formation, but given the discontinuous, lens-like and thin nature of the limestones, they are, pending further work, best lumped into the basal Morita Formation. Animas Resources 2009 drilling in the northern portion of the district penetrated 40 m of carbonaceous shale and oyster-bearing limestone with gradational contacts out of and into the Morita Formation (Figure 2-5A; 2-5B; 2-5C). Further up section, the Morita Formation varies between non-calcareous, purplish siltstone to mudstone and tannish white sandstones, some with minor cross bedding. In some sections of the Morita Formation (Figure 2-6), rip-up clasts of the purple mudstone are evident in the lighter purple sandstones. Near the upper contact of the Kvs with the Kos and thin, discontinuous, fossiliferous limestone beds.

(Figure continued on next page)

Figure 2-5 6.50 m of core from ARES-001 showing lower gradational contact between interbedded, basal oyster-bearing limestones of the Morita Formation (Figure A and B) grading into greenish sandstones and pea-sized, pebble conglomerate (Figure C) of the Morita Formation. Calc-silicates between the limestone and sandstone (top of Figure C) are strong, brown-biotite hornfels. Core length is 2.4 m per box.

Figure 2-6 Purplish shale rip-up clasts in Morita Formation sandstones, south of Dora Mine.

The Morita Formation is interpreted to represent the transition from terrestrial-basin fill to inter-tidal and shallow-marine conditions (Schafroth, 1968; Dickinson et al., 1986), reflecting a rise in sea level relative to the region. The active tectonism that had created the Bisbee Basin had ceased prior to the deposition of the Morita Formation, as evident in the contrasts in sand grain-size and sorting compared to the Glance Conglomerate and in the size and abundance of the conglomerate clasts between the two formations (Jamison, 1987). The contact between the Morita Formation and the Glance Conglomerate within the district is consistent with observations made by Bilodeau (1987) and Vedder (1984) on the western flank of the Huachuca Mountains, Papago Springs, and Canelo Hills, all located in southern Arizona.

Cretaceous Kos

The Kos is a local designation given to a discontinuous, 0-to-5-m-thick sequence of alternating calcareous sandstone and 0.5-m-thick oyster limestone beds marking the transition

from the clastic Morita Formation to the overlying marine sequences of the Mural Limestone. In regional studies, the Kos sequence is often described and mapped with the Morita Formation or the overlying limestones of the Ko sequence, but within the district, its reaction to mineralizing fluids and the function of concentrating gold has earned it a separate, recognizable status. The limestones are whitish to cream colored and react to HCl vigorously, as do the sandstones. Within the limestone, molds of clam and oyster shells up to 3 cm in diameter are prevalent; body fossils are mostly missing. Sandy units are whitish to cream colored and, well sorted, with rounded, medium-grained sugary quartz grains and a calcite matrix. Thin, calcareous siltstone and mudstone beds intervene between sandstone and limestone. The sequence seems typical of near-shore marine conditions, with inter-tidal or terrestrial sands periodically washing over shallow reef environments.

Cretaceous Ko Limestone

Representing the basal unit of the Mural Limestone, the Ko Limestone is a thick, gray, massive limestone. The limestone is 15-to-90-meters thick and fossil-rich, limestone with individual beds greater than 3 m thick and interbedded carbonaceous, calcareous siltstone to organic-rich mudstone. It is distinguished from the Kos by the darker gray color, more massive beds, larger oyster fossils, and a general lack of sandstone. Oyster fossils contained within the Ko limestone are larger than 8 cm in diameter and can number more than 40 per cubic meter (Figure 2-7), representing a patch-reef facies. *Orbitolina texana,* 7 mm to 1 cm in diameter, are abundant as are *Nerinea*, an extinct genus of gastropod.

Figure 2-7 *Nerinea* and large oysters of the Ko limestone.

Patch-reef facies within the Ko are irregular bodies that can grade into calcareous, oyster-rich mudstone and siltstone, time-equivalents to the patch-reef facies. This occurs northwest of Corral Pit, west of Ruben Pit, and in the La Gloria/Greta prospects. This irregularity in the continuity of the bedding, along with other speculations has led others to the conclusion that the Ko stratigraphy has been involved in gravity-slide mechanics (McKee, 1991; McKee and Anderson, 1998). Although not a focus of this study, the slide block hypothesis was tested multiple times by field mapping and by Animas 2008 and 2009 drilling, and it is clear that gravity sliding does not play a role in altering the stratigraphy of the district. Time correlative, interfingering facies combined with post-Jurassic structural deformation can explain the complexities of the Ko in the district.

Depending on the facies of the Ko, there are interbedded, organic-rich, black to dark gray shales and siltstones, which when fresh, have an organic earthy odor with a hint of sulfur. Typically, these interbeds are thin within the massive limestone patch-reef facies, but thicken away from interpreted reef fronts. At the apron of the postulated reef front, within the mudstones, there can be fossil hash and oysters interspersed, which typically decrease in abundance with distance away from the patch-reef facies. This is best seen on a transect from La Gloria to Greta, then down to Ontario prospects. The shales and siltstones in the Ko are variably calcareous.

Within the district, the Ko reef facies seem typical of shallow marine, open basin, patch-reef limestones with debris fields stretching off into slightly deeper, but organic-rich, offshore muds. Deposition of the Ko coincides with the largest of the transgressions of the Bisbee Sea into the Bisbee Basin (Hayes, 1970; Monreal, 1989; Dickinson, 1989) and the oyster reefs would have lined the edge of the basin, sloping off into deeper marine facies.

Cretaceous Ks lower

Conformably grading out of the Ko, the Ks lower is a 5-to-100-m-thick sequence of black, calcareous and carbonaceous mudstones to siltstones, a 10-m thick sequence of coarse-grained, calcareous sandstones, and a capping tan to gray, calcareous siltstone. In outcrop, the light tan to dark gray units are easily eroded, forming subdued topography. Fossils are rare, but include petrified wood, ammonites, and pyritized, vertebrate ribs. The sequence has an average of 1% disseminated hematite after pyrite, with zones having greater concentrations.

Cretaceous Kel Limestone

Characterized as a thin-bedded, laminar limestone with minor fossil hash, the 2-to-10-m-thick Kel Limestone serves to separate the upper and lower Ks units. In outcrop, the limestone beds are beige to light gray in color and more resistant to erosion that the surrounding mudstones and siltstones (Figure 2-8). The unit was less prominent in the Animas 2008 and 2009 drill core since most of the surrounding rock is a similar dark gray color and equally as calcareous as the limestone. There do not appear to be any disconformities between the Ks units and the Kel Limestone, and thin, calcareous mudstones interbedded in the Kel are indistinguishable from similar mudstones above and below the Kel, so the contacts are most likely gradational.

Figure 2-8 Kel limestone striking northwest and dipping steeply to the northeast (right). Note the typical weathering, thickness and laminar nature of individual beds.

The Kel is useful as a surface maker bed within the stratigraphy of the district, with prominent, resistant weathering compared to the surrounding mud and siltstones of adjacent Ks units. The Kel represents a transition to slightly shallower marine conditions and the return of laminar-limestone deposition with pulses of calcareous muds temporarily covering the limestone.

Cretaceous Ks upper

Conformably grading from the Kel limestone, the 10-to-80-m-thick Ks upper consists of calcareous, carbonaceous mudstones, calcareous and non-calcareous siltstones, and minor sandstones (Figure 2-9). Light tan sandstone beds less than 2-m-thick are evident in the basal portions of the Ks upper. The majority of the Ks upper consists of dark gray, carbonaceous, fissile siltstones. Light tan siltstones with ripple marks are near the contact of the Ks upper with the Kl Limestone. The Ks upper is comparable to the Ks lower, with fewer sandy units.

Figure 2-9 Exposure of Ks upper in Gregorio Mine showing variable oxidation and deformation. The slivers of black, carbonaceous rock on the mid-wall are typical of unoxidized Ks. Nearly the entire unit has lost the original dark color contributed by organic carbon.

Cretaceous Kl Limestone

The Kl Limestone, the upper unit of the Mural Limestone, is 75-to-125-m-thick. It consists of interbedded, ledge-forming limestone and slope-forming clastic rocks. Limestone beds are finely bedded-to-massive and each approximately one-meter thick, and locally includes fossil hash. Typically, the limestone beds are lighter gray in color than the Ko and Kel Limestones and the upper limestone beds become dolomitic and beige in color. The siltstones are variably calcareous and typically light gray to tan. The Kl Limestone marks the last major marine transgression within the district and the region.

Cretaceous Cintura Formation (Ksl)

Within the district, the lowermost Ksl consists of greenish calcareous sandstones and interbedded, purplish siltstones with minor, massive limestones less than 0.5 m thick (Figure 2-10). The calcareous nature of the base of the Cintura Formation extends upward for less than 100 m, possibly marking the final expression of fan-delta, marine conditions and a return to fluvial, terrestrial deposition. Within the Cintura Formation, there are repeating sequences of fine to coarse sandstones and purplish siltstones to minor mudstones.

Figure 2-10 18 cm thick bed of massive limestone in lowermost Cintura Formation with apparent left-lateral separation of less than 20 cm.

Micritic, calcareous nodules, contained within the non-calcareous siltstones and mudstones, range in size from 1 mm to 10 cm in diameter (Figure 2-11). The nodules can contain solid calcareous cores or calcareous rims with hematite cores. Within the hornfels units surrounding Enedina and San Enrique, the Ksl nodules have been converted to quartz, magnetite, calcite, and rare base metals. The micritic nodules are useful for distinguishing the Cintura Formation from the Morita Formation.

Figure 2-11 Micrite nodules in Cintura Formation. Calcareous rind and pinkish white center with calcareous, hematite-clay infill, the surrounding purplish siltstone is non-calcareous.

The upper contact of the Cintura is not exposed within the district so; the true thickness of the formation is unknown. An angular unconformity exists between the Cintura Formation and the overlying Tertiary Magdalena Formation in the southern part of the district.

The Cretaceous Cintura Formation was first recognized throughout southern Arizona and northern Mexico by Ransome (1904) as repeating sequences of sandstones and purplish mudstones. Throughout the region, the unit has time-correlative sequences that represent the end of marine transgressions during the Aptian-Albian and a return to terrestrial, fluvial deposition. The Mojado Formation in the Big Hatchet and Animas Mountains (Hayes, 1970) in southwestern New Mexico, as well as the Schellenberger Canyon Formation in the Whetstone (Archibald, 1987) and Santa Rita Mountains (Hayes, 1970; Archibald, 1987; Inman, 1987) are likely correlative to the Cintura Formation (Inman, 1987). Lindberg (1987) describes the Cintura Formation as subaerial fan-delta deposits transitioning to braided fluvial systems that buried the older Bisbee Group rocks under hundreds of meters of fluvial deposits.

Tertiary Magdalena Formation

Unconformably overlying the Cretaceous Cintura Formation, the Tertiary Magdalena Formation is a well-indurated conglomerate consisting of locally derived, subangular to rounded clasts derived from the Bisbee Group, diorite, and granitic bodies. South and east of Dora, the Magdalena Formation is exposed, filling the Batamote half graben and capping an Oligocene andesite (S.G.M., 2003), referred to as the Batamote trachyandesite in this study. Fanning dips are observed within the conglomerate beds in the Batamote half graben. A younger Miocene ignimbrite sequence and the Báucarit Formation cap the Magdalena Formation south of the Main District.

Tertiary Báucarit Formation

The Miocene Báucarit Formation, unconformably capping the Magdalena Formation and overlain by the Miocene ignimbrite sequence, is composed of pebble-to-cobble sized felsic and intermediate volcanic rocks and sedimentary rocks with interbedded sandstones and clay horizons. The clasts are typically moderately rounded and moderately sorted, and the unit is poorly consolidated. The underlying Bisbee Group rocks and the younger intrusive rocks are the sources of the clasts in the Báucarit Formation conglomerate. The conglomerate is post-mineralization, containing clasts of hornfels and quartz fragments with oxidized sulfides.

Intrusives

Chloritized diorite

The oldest documented intrusive in the district is a medium-to coarse-grained diorite with a chloritized, dark green, subophitic texture defined by euhedral to subhedral plagioclase and pyroxene (Figure 2-12). The texture and composition of the diorite are rather homogeneous, but pyroxenite, gabbro, and granodiorite were locally present, along with screens of hornfels derived from Cintura Formation.

Figure 2-12 Disseminated and fracture chlorite in diorite, cut by late-stage calcite stained with hematite.

Hornfels is locally associated with the diorites, with pyroxene hornfels extending 1 to 5 m into the country rock. The best exposure of the diorite is along the southern wall of Becerros Norte, where diorite and associated hornfels are cut by a northwest-trending, mineralized shear zone (Figure 2-13).

Figure 2-13 Contact of diorite (upper right) with Cintura Formation, forming hornfels (middle of photo). The hornfels is less than 5 m thick, and is in fault contact with sheared, mineralized, non-hornfels Ksl (left side of photo).

Las Panochas Granite

The Las Panochas Granite is exposed south of the Main District, in the San Enrique area. The granite (Table 2-1) is a coarse-grained, peraluminous, two-mica, leucocratic granite consisting primarily of quartz, microcline, muscovite, and minor biotite, apatite, and garnet. The contact with country rocks is irregular, cuts the chloritized diorite and is intruded by numerous dikes. Diffuse, aplitic dikes are common in border areas, and are labeled as the Grasero Granite by Bennett (1993). The main stock is elongate in a NE-SW direction, with a 2 km-by-1-km aspect ratio. According to Smith (2006), the northeastern area of the stock grades

northeastward into coarse material consisting dominantly of coarse-grained quartz with minor K-feldspar, possibly representing a very late, pegmatitic, volatile-rich phase of the stock (Smith, 2006). This northeastern part of the stock is the site of historical drilling by Sonora Gold and Teck Cominco.

Greisen alteration cuts the granite and tens of meters of the associated hornfels and skarn on the margins of the granite. Greisen consists of quartz, books of muscovite, rare fluorine and reported topaz (Anderson, 1998) cutting the granite as veins. Bennett (1993) obtained a K-Ar age from muscovite in the greisen alteration of 36.1 ± 0.9 Ma. Elevated fluorine and tin were noted in Teck Cominco whole-rock geochemistry, presumably associated with the greisen event.

Roldán-Quintana (1991) reports the presence of two-mica, S-type granites in the Anochi-El Jaralito area of northern Sonora, west of Banamichi, with one K-Ar age of 35.96 ± 0.70 Ma. He notes the importance of these intrusives in Sonora due to their association to porphyry copper (Cu-Mo) and W and Fe skarn deposits. Major element geochemistry designates the granite as high-K calcalkaline (Peccerillo and Taylor, 1976), and the Rb/Sr ratio is relatively low at 3.1:1. Plots of major oxides of average granite (Blatt and Tracy, 2007), the Las Panochas granite, and a felsic dike phase of the Las Panochas granite are listed in Figure 2-14.

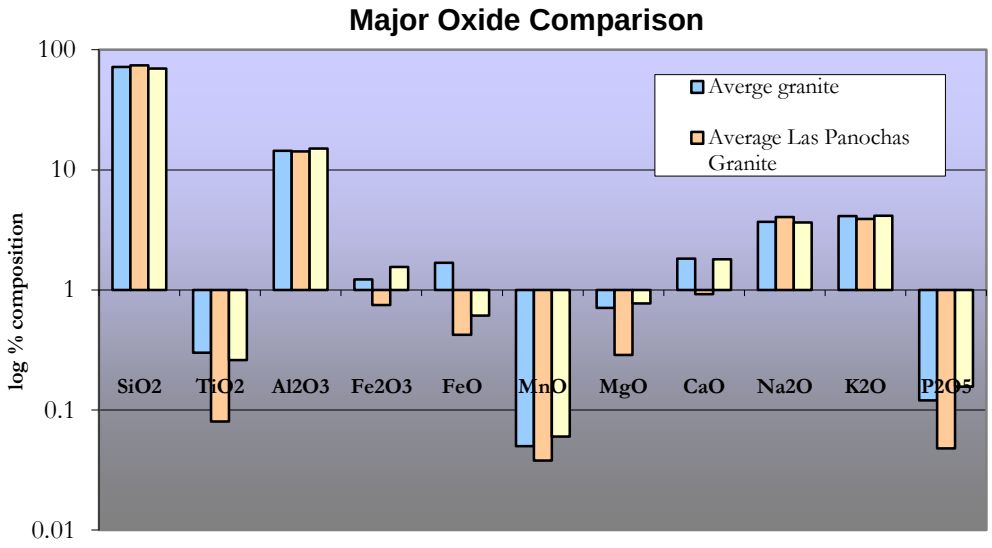

Figure 2-14 Whole-rock analysis of average granite, (n = 2485) (Blatt and Tracy, 2007), Las Panochas Granite (n = 5) and feldspar porphyry dike, (n = 3).

Table of comparative geochemistry of peraluminous granites of the SW U.S. and Sonora

Location	SiO_2 %	Al_2O_3 %	CaO %	Na_2O %	K_2O %
Sta. Catalina Mtns., AZ*	72.9	14.6	1.6	4.1	3.7
Whipple Mtns, CA*	71.8	15	2.2	4.1	3.4
Ruby Mtns, NV*	73.0	13.8	1.1	3.4	4.5
Rancho La Rosca, Sonora†	71.59	14.88	0.88	3.77	4.03
5 Km NW of El Torreón, Sonora†	73.54	13.91	1.21	3.96	3.57
Las Panochas, Santa Gertrudis, Sonora	74.04	14.27	0.64	3.64	4.38

Table 2-1 Comparative geochemistry of peraluminous granites of the southwestern U.S. and Sonora. Data from Reynolds and Keith (1982)* and Roldán-Quintana (1991)† and this study.

A Re-Os age of 42.3 ± 0.3 Ma obtained on molybdenite from a quartz vein in diamond drill-hole SE 15-05 places an absolute age on mineralization. The 6 million year difference between the Bennett's K-Ar age and Teck Cominco's Re-Os age may be explained by late-stage, Cu/Mo-bearing hydrothermal fluids resetting the muscovite K-Ar age or by a complex cooling history. Suzuki et al. (1996) state that in vein-type deposits there is a 3-12 Ma difference in the K-Ar versus the Re-Os ages, while Re-Os ages tend to agree with K-Ar ages of the host rocks in skarn, pegmatite, and greisen-type ore deposits.

Based on limited exploration and exposure of altered rock associated with the Las Panochas Granite, a tentative series of events would include formation of biotite hornfels, potassium feldspar and pyroxene hornfels, followed by skarn formation and propyllitic alteration, all cut by quartz-chalcopyrite-molybdenite-pyrite veins and limited distal disseminated mineralization, contemporaneous with late-stage greisen alteration.

Batamote trachyandesite

The Batamote trachyandesite unconformably overlies the hornfels and mineralized Bisbee Group rocks as the basal sequence of the Batamote half graben. Assigned (Toa) by S.G.M. (Servicio Geológico Mexicano, 2003), the Oligocene volcanic sequence has a dark brown aphanitic matrix and elongated laths of whitish plagioclase. The sequence dips moderately to the northeast. Presumably, the trachyandesite represents volcanic flows, erupted as part of the mid-Tertiary volcanic episode.

Lamproite dikes

Phlogopite-leucite-augite lamproite dikes and sills (Figure 2-46) are present throughout the district as 0.5-to-3-m-thick, continuous, sheet-like intrusives. Consisting of a grayish, aphanitic

matrix with euhedral books of phlogopite and whitish grains of leucite, the dikes are unaltered but exhibit strong grus weathering. Due to the presence of phlogopite, the dikes could be described as shoshonitic lamprophyre, variety kersantite Rock (1991), but are better classified as lamproite, variety fitzroyite due to: 1) the lower than average SiO_2 (~40 wt %) and Al_2O_3 (~12 wt %) (Figure 2-15), 2) the lack of plagioclase (Bergman, 1987), and 3) the presence of leucite (Mitchell and Bergman, 1991; Müller and Groves, 2000). The lamproites are ultrapotassic, with a K_2O/Na_2O ratio of 2.65, MgO > 3 wt % and K_2O > 3 wt % (Winter, 2001; Foley et al., 1987). Petrographic inspection of the lamproite dikes present in ARTG-002 at 303 m depth reveal phlogopite phenocrysts zoned with dark brown, Fe-rich rims and pale, Mg-rich cores (Figure 2-16) and the leucite phenocrysts.

Xenoliths of rounded granite, present in the lamproite dikes, could be related to the underlying Las Panochas-style intrusive or could reflect older Precambrian basement granite. Dr. Efrén Pérez Segura, Hermosillo, Mexico speculated that the xenoliths were Precambrian based on his experience and on petrographic inspection, and there is no recognizable alteration or mineralization present within the granitic xenoliths. The lamproite dikes cut the Las Panochas Granite and associated Cu-Mo bearing quartz veins.

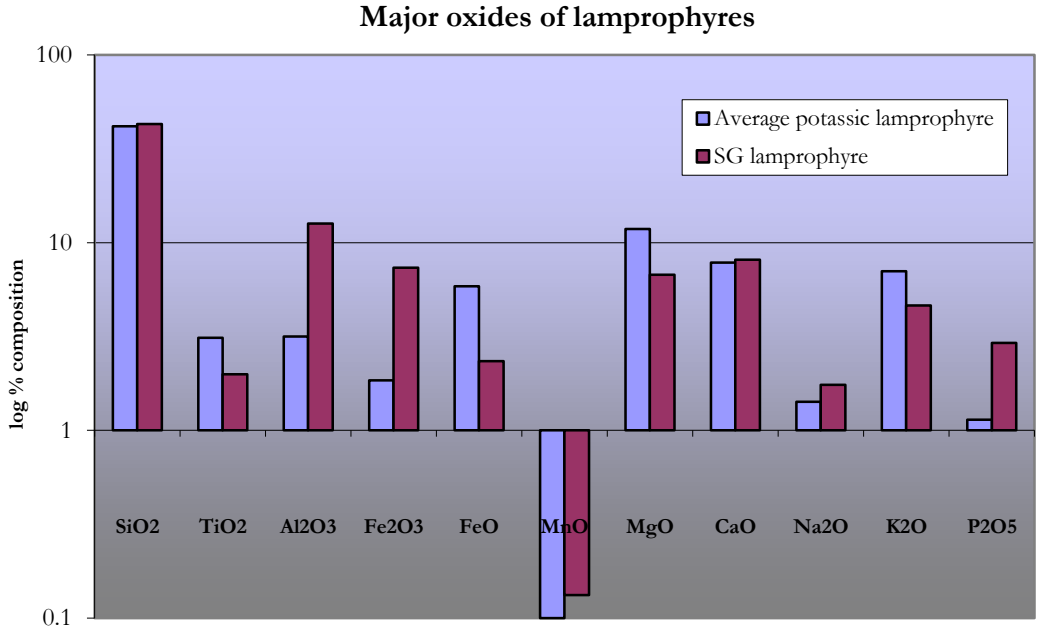

Figure 2-15 Comparative oxide geochemistry of average potassic lamprophyres (Scott, 1979) and lamproite, n = 5, observed at Santa Gertrudis. TiO_2, CaO, Na_2O and K_2O < 10%, typical of lamprophyres. Large excessive anomalies exist in Al_2O_3 and P_2O_5.

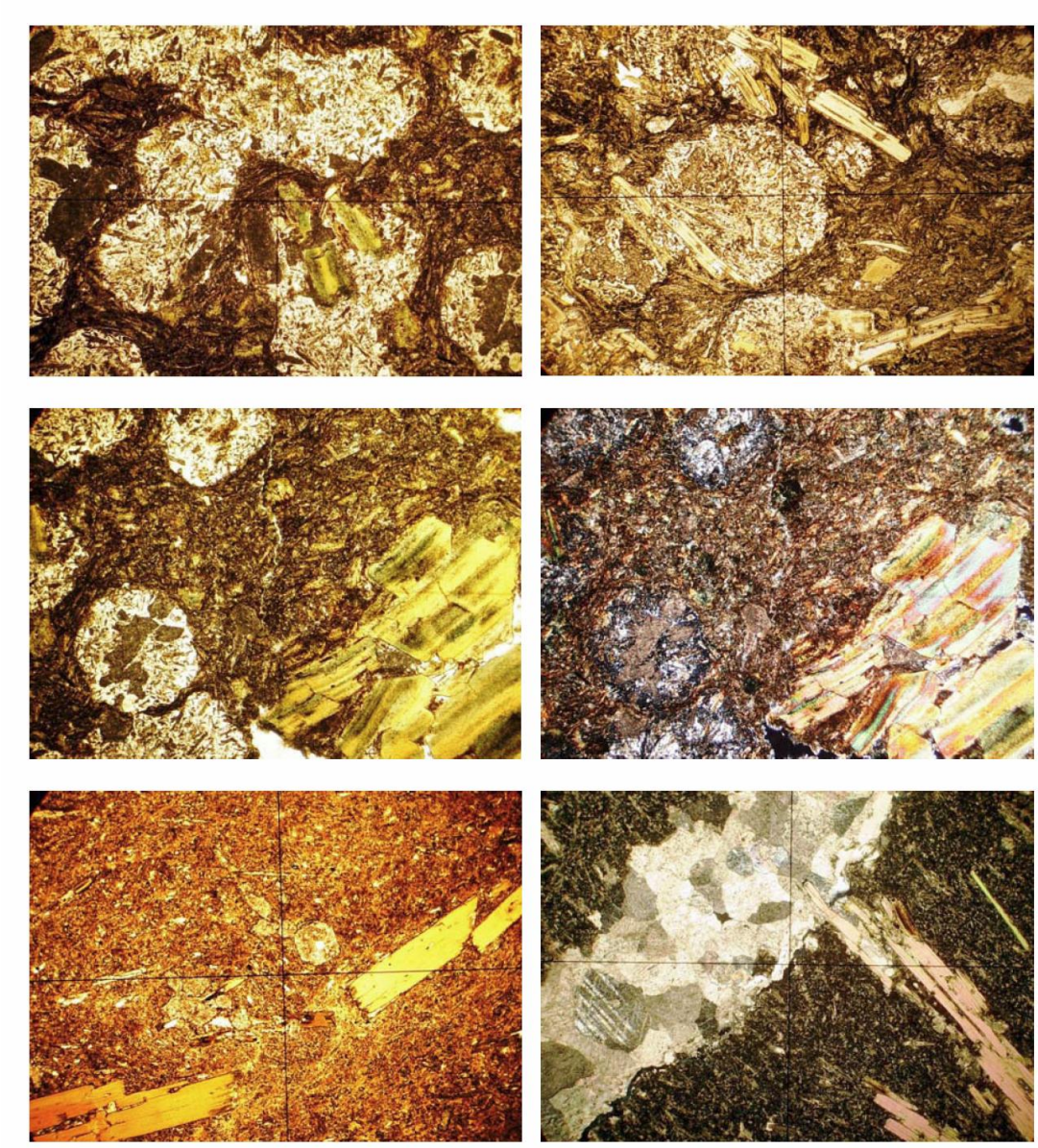

Figure 2-16 ARTG-002 303 m. Photomicrographs of phlogopite-leucite-augite lamproite. Top photos show white leucite phenocrysts with inclusions of biotite and augite. Middle row of photos highlight leucite phenocrysts with augite inclusions and brown biotite laths. (Left (PP) Plane-polar light; right (XP) Crossed Nichols). Bottom row of photos show chilled dike margin with biotite phenocrysts. Right photo (XP) shows late calcite vein cutting devitrified glass of the chilled margin with biotite phenocrysts. All photos are 5.7 mm wide. (Burnham Petrographics, 2009).

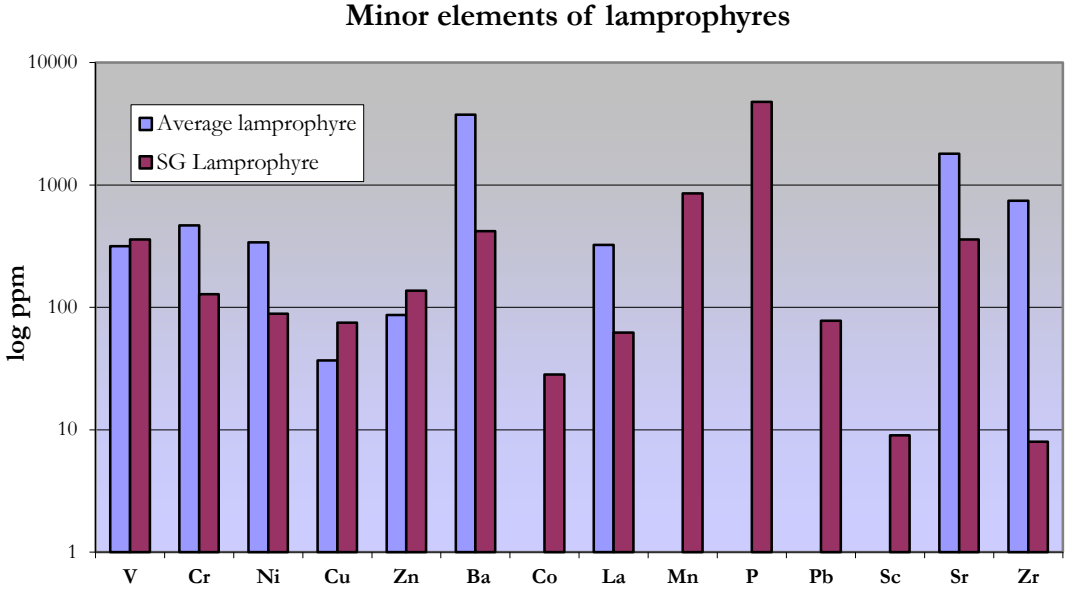

Figure 2-17 Comparative minor element geochemistry of average lamprophyres (Scott, 1979) and Santa Gertrudis lamproites (n = 5).

Undifferentiated, post-mineral dikes

Throughout the district there are numerous varieties of, post-mineral dikes and sills that vary in composition but are referred to as andesite dikes, diorite, or 'turkey track' andesite dikes. They intrude pre-existing shear-zones and structural weaknesses. Bennett acquired a K-Ar radiometric date from biotite on a dike he referred to as a biotite-rich diorite (26.1 ± 0.7 Ma) in the eastern part of the district. This age corresponds to the main pulse of mid-Tertiary magmatism (Nourse, 1994).

Whole-Rock Geochemistry

A plot of total alkali versus silica (Cox et. al., 1979) of all of the available legacy and Animas whole-rock data (n = 38) reveals three distinct chemistries (Figure 2-18). The felsic dikes and Las Panochas Granite plot in a tight cluster, possibly due to a temporal association. The

abundant aluminum and the sub-alkaline nature of the felsic intrusives hint at a sedimentary, crustal contribution, as is typical for S-type granites. The intrusive dikes and sills, identified as porphyritic trachyandesite and andesite plot in the hawaiite-basalt-picrite field. The lamproites are very peculiar and rare on a global scale and their unaltered leucite phenocryst and low silica content may imply a mantle source of partially depleted harzburgite, perhaps due to partial melting during collapse of an orogeny and decompression melting of the asthenosphere (Winter, 2000). At Santa Gertrudis, this could be consistent with the timing of mid-Tertiary crustal extension if the lamproites are indeed syntectonic with the observed low-angle structures.

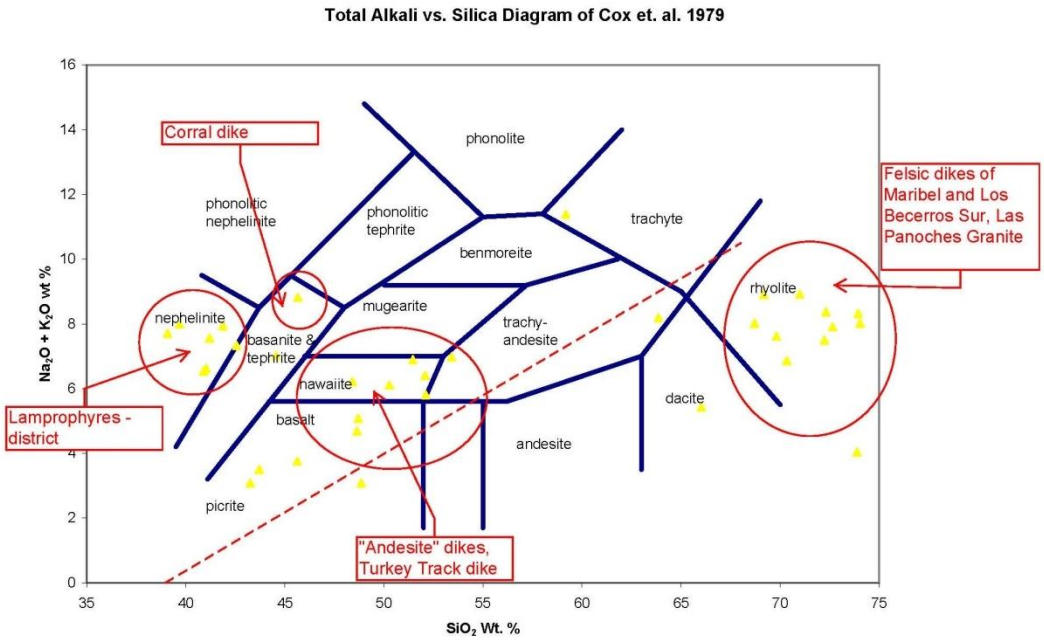

Figure 2-18 Whole-rock geochemistry of multiple igneous intrusive samples classified on total alkali vs. silica diagram from Cox et al., 1979.

Structural Geology

The structures present in the district record a complex history of deformation. The Bisbee Group rocks contain two phases of thrust faults, folds, and associated cleavages that are cut by younger low-angle and high-angle extensional structures. From oldest to youngest, the structures are: 1) bedding-parallel shear zones, 2) a southwest-dipping cleavage, 3) northeast-vergent thrusts and folds, 4) a northeast-dipping cleavage, 4) southwest-vergent thrusts and folds, 5) the southwest-vergent, stratigraphy-overturning Gregorio syncline and related folds, 6) northeast-trending brittle faults, 7) low-angle, southwest-dipping normal faults, and 8) high-angle normal faults.

Bedding-parallel structures

The oldest recognized structures in the district are zones of slip and cleavage that are parallel to subparallel to bedding in all of the units of the Bisbee Group. They include shear zones of intense cleavage development and bedding-parallel slip planes with cohesive breccia, non-cohesive gouge, and other evidence of shearing. The deformation is recognized throughout the district, and has a profound effect on unit thickness in certain locations (Figure 3-39). In outcrop, the structures produce a pinch-and-swell character and are generally discontinuous along strike. Rock type influences the style of these structures and the amount of deformation expressed on the stratigraphy. The Ks and Ksl units, along with interbedded shale and mudstone units in the other Bisbee Group rocks are more highly sheared and deformed (Figure 2-19; Figure 2-20), whereas the massive limestones and conglomerates are more intact. In limestones, these bedding-parallel structures are dominated by ductile features, such as sigmoid of features and S-C fabrics; they generally only affect the thinner bedded limestones of the Kl and Kel (Figure 2-21).

These bedding-parallel structures strike northwest, parallel to the host rocks. They dip gently to moderately to the southwest in the southwestern portion of the district, where the beds also dip to the southwest and are upright. They are more steeply dipping where the beds are steep in the Main District. They are also present in overturned beds (Figure 2-23), dipping northeast, paralleling the overturned beds.

Figure 2-19 Bedding-parallel shear-zones, upper right and along back wall, cutting otherwise weakly altered, purplish and greenish Ksl siltstone and sandstones. Katman Pit, Main District.

Shear fabrics, including S-C fabrics, and folds related to the shearing reveal a top-to-the-northeast transport direction. Shear fabrics, such as sigmoidal foliation and phacoids (Figure 2-22) along with rotated pyrite cubes with pressure shadows, are best revealed in the Ks mudstones. Thrust faulting, parallel to and at low angles to bedding, is most evident in the Ks interbedded siltstone and sandstone layers and within the limestone marker beds of the Kl and Kel limestones (Figure 2-23; Figure 2-24).

Figure 2-20 Bedding-parallel shear and subsequent leaching, mineralization, and oxidation in Cintura Formation greenish siltstones. Note healed, cohesive nature of shear-zones. Drill core from ARTG-006.

Figure 2-21 Bedding-parallel ductile shear-zones in the Kl in the Toro-Gregorio study area.

Figure 2-22 Ductile shear fabrics in carbonaceous Ks lower mudstones, Sargento prospect. Sigmoidal shapes and elongation show top-to-the-northeast shear (top-to-the-left in this view).

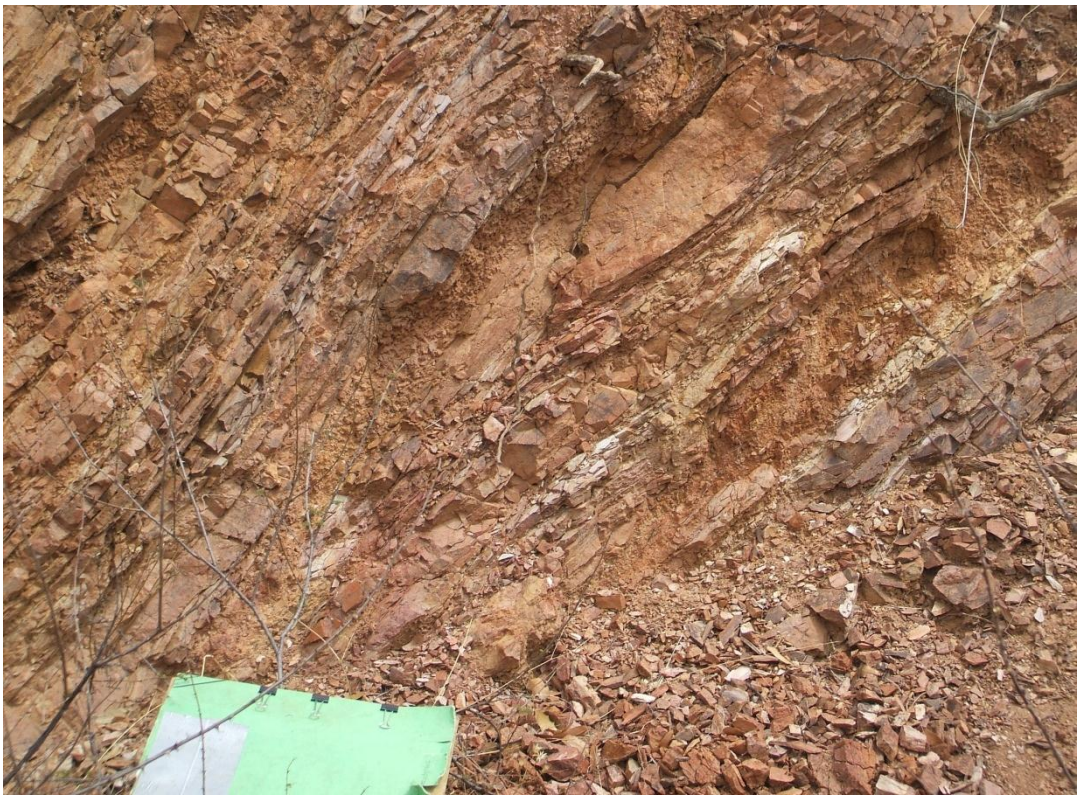

Figure 2-23 Sub-bedding-parallel thrusting within overturned Ks siltstones, looking southeast. Scale is 12 inches across.

This fabric is interpreted to be related to northeast directed shortening was accommodated, in part by thrusting, duplexing and thickening of the Bisbee Group with northwest-trending, brittle-ductile shear-zones that are parallel or subparallel to bedding. The anastomosing, lenticular, en-échelon zones of deformation with brittle patches of variably calcareous gouge to breccia would later act as important sites for mineralization (Figure 2-25).

Presumably, the repetition of stratigraphy throughout the district can, in part, be attributed to the initial, top-to-the-northeast thrusting. A transect from Mirador Pit to south of Aqua Blanca Pit reveals repeated and folded Kl stratigraphy separated by northwest-trending structures subparallel to bedding.

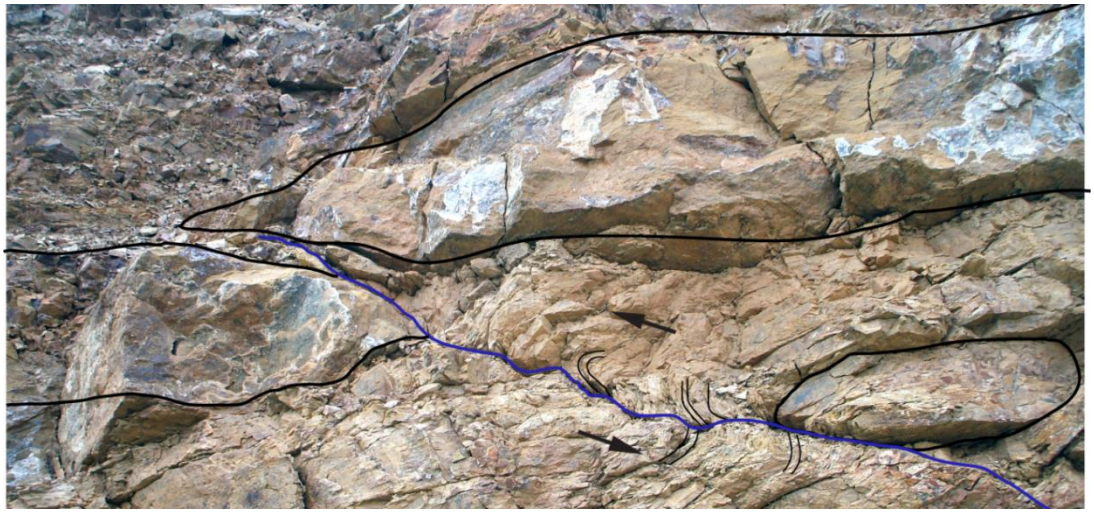

Figure 2-24 Photo and interpretation of a top-to-the-northeast thrust fault in Dora Pit, Main District showing offset of massive limestone bedding and drag folds along the structure in less competent siltstones. Massive limestone bed is approximately 30 cm thick. Looking south.

Figure 2-25 Bedding-parallel structure that hosted mineralization within Ruben Pit, looking southeast. The beds strike northwest, dip northeast and are overturned. Mineralization was sited at the intersection of the northwest-trending reddish oxide zones and a northeast structure, now the long axis of the pit (from left to right).

Cleavages

Cleavages are persistent throughout the district, with a great deal of variability to their degree of development and orientations. Cleavages are most notable in the siltstones and mudstones in the district, but are locally present in every rock type. There are two main cleavages, an older, more pervasive (S_1) and a younger, locally developed spaced cleavage (S_2). The oldest cleavage (S_1) (Figure 2-26) is a spaced to penetrative, well developed platy cleavage; it strikes and dips approximately sub-parallel to the bedding, varying from moderately southwest-dipping in the upright sections to vertical to moderately northeast-dipping in the overturned sections. This variation in the orientation of the S_1 cleavage, and its nearly parallel relationship to bedding, which is folded, indicates that the S_1 cleavage is folded. Restoring bedding to

horizontal would maintain the southwest dip to the cleavage. In Gregorio and elsewhere, quartz veins crosscut the S_1 cleavage (Figure 2-70; Figure 2-73).

The second cleavage (S_2) is a weakly developed, spaced cleavage striking 310 and dipping 60° NE (Figure 2-31). Typically the cleavage is most obvious in weaker lithologies and is roughly axial planar to the Gregorio syncline. Pencils due to cleavage intersections are present in the areas of the district that are most affected by the generation of the S_2 cleavage (Figure 2-27). Quartz veins crosscut the S_2 cleavage.

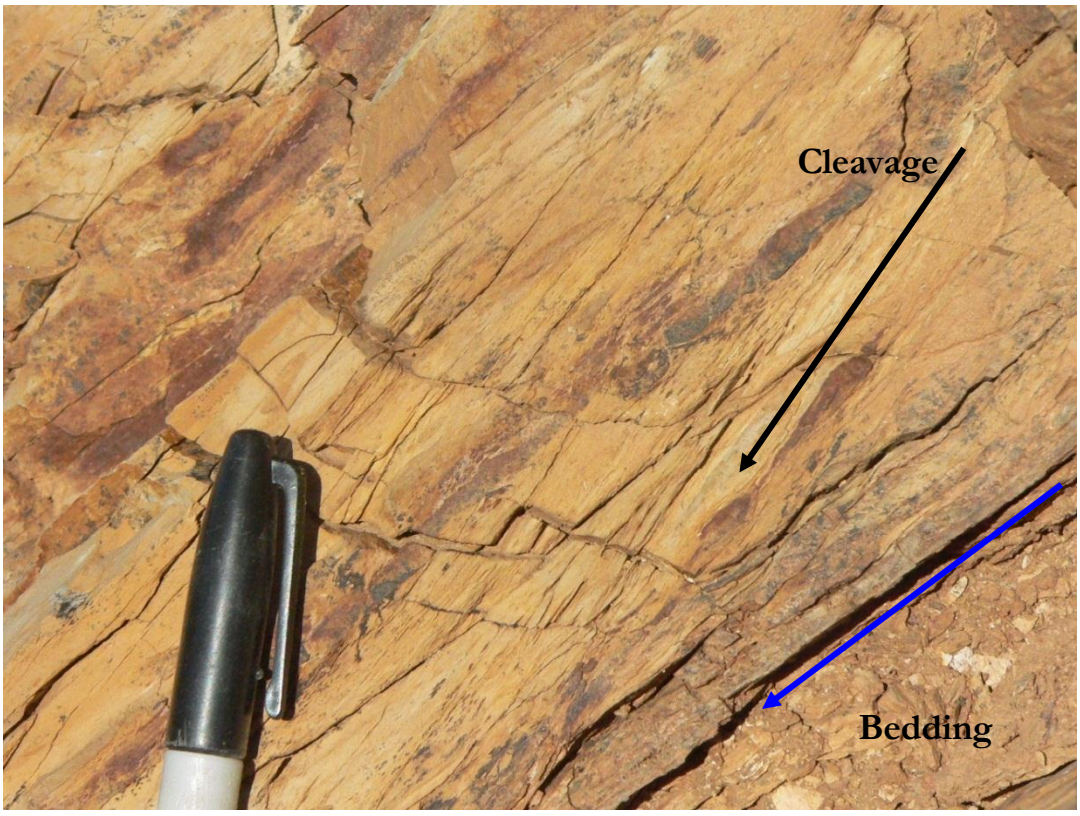

Figure 2-26 Photo of intersection of S_1 cleavage (black) and bedding (blue) at Gregorio Mine. Restoring bedding to horizontal would maintain the southwest dip to the cleavage. Arrows drawn in orientation of cleavage and bedding. Photo courtesy of S.J. Reynolds.

Figure 2-27 Strong, spaced cleavages at a low angle to bedding in the siltstones of the Cintura Formation south of Dora Mine. Penciling of the units is due to intersecting S_1 and S_2 cleavages.

Folds

The oldest folds (F_1) are small to medium-sized isoclinal to nearly isoclinal folds that are obvious throughout the district (Figure 2-29; 2-30). The folds are northwest-trending, northeast-verging, with axial surfaces parallel to S_1 cleavage, associated with bedding-parallel slip and northeast-directed shearing. Measurements of F_1 hinge-line orientations are variable, consistent with the variable orientations of the S_1 cleavages.

The next generation of folds (F_2a) are small to medium-sized folds that warp S_0 bedding and S_1 cleavage. The largest F_2a folds are tens of meters in amplitude. The folds are open to tight, asymmetric, with a top-to-the-southwest vergence in upright sections. The hinges of the folds

trend northwest or southeast and generally have gentle plunges. Axial surfaces dip northeast in upright sections, but are subhorizontal or dip southwest in overturned sections. A weak cleavage (S_2) is locally developed parallel to the axial surfaces of some F_2 folds, but many F_2 folds lack an associated cleavage, (Figure 2-28; Figure 2-31). This folding event may be the progenitor of the dramatic folds witnessed in Dora, Corral, and Corral NW Pits (Figure 2-29; Figure 2-30; Figure 2-31; Figure 2-42)

Figure 2-28 Asymmetric fold in Kl limestone. Note the strong, bedding-parallel, spaced cleavage, S_1, being folded and the lack of axial planar cleavage, S_2.

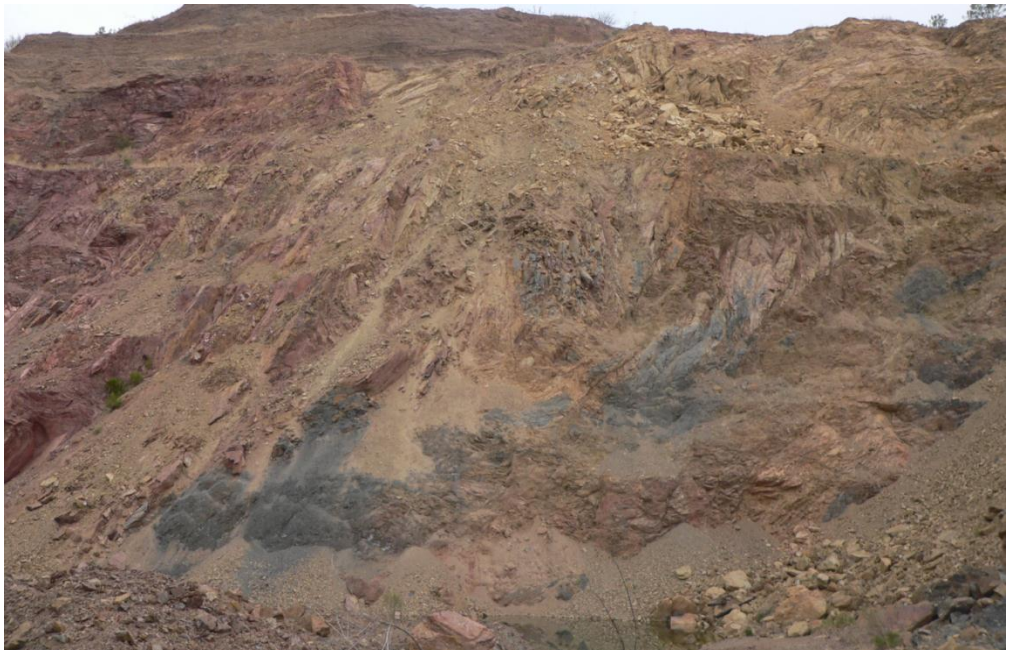

Figure 2-29 Photo of northwestern wall of Dora Pit with complex F_2 folding of S_1 cleavage and bedding S_0. Color variations reflect oxidation of Ks mudstones and siltstones.

Figure 2-30 Interpretation of F_2a (visible) and F_2b (regional limb) structures within the northwestern wall of Dora Pit. Illustrated folds are F_2a, but are overturned in the large-scale F_2b, Gregorio syncline.

Figure 2-31 Asymmetric folds in the Kl limestone, with an axial plane of 309 / 58° NE, and fold hinge 7°→131 trend and plunge. Note the strong axial planar parallel S_2 cleavage in the mudstones in upper left of photo. Brunton compass for scale.

The largest fold (F_2b) is a northwest-trending, southwest-facing fold that runs through the main part of the district. This fold, named the Gregorio syncline in this study, is an overturned syncline. Southwest-dipping beds, which dominate the district and form an upright limb, are in the southwestern part of the district. Northeast-dipping beds are in the northeastern part of the district representing the overturned limb. Vertical beds exposed between Gregorio and Ruben pits represent the exposed hinge of the fold. The axial surface dips gently to the northeast in most places. This fold is the major control of dips of bedding and S_1 cleavage in the district.

Within the Toro-to-Gregorio study area, 131 measurements of poles of bedding planes and bedding-parallel cleavage are plotted on an equal axis stereonet (Figure 2-32) and contours reveal a best fit girdle and beta axis of 7°→ 299, representing the fold axis of the syncline.

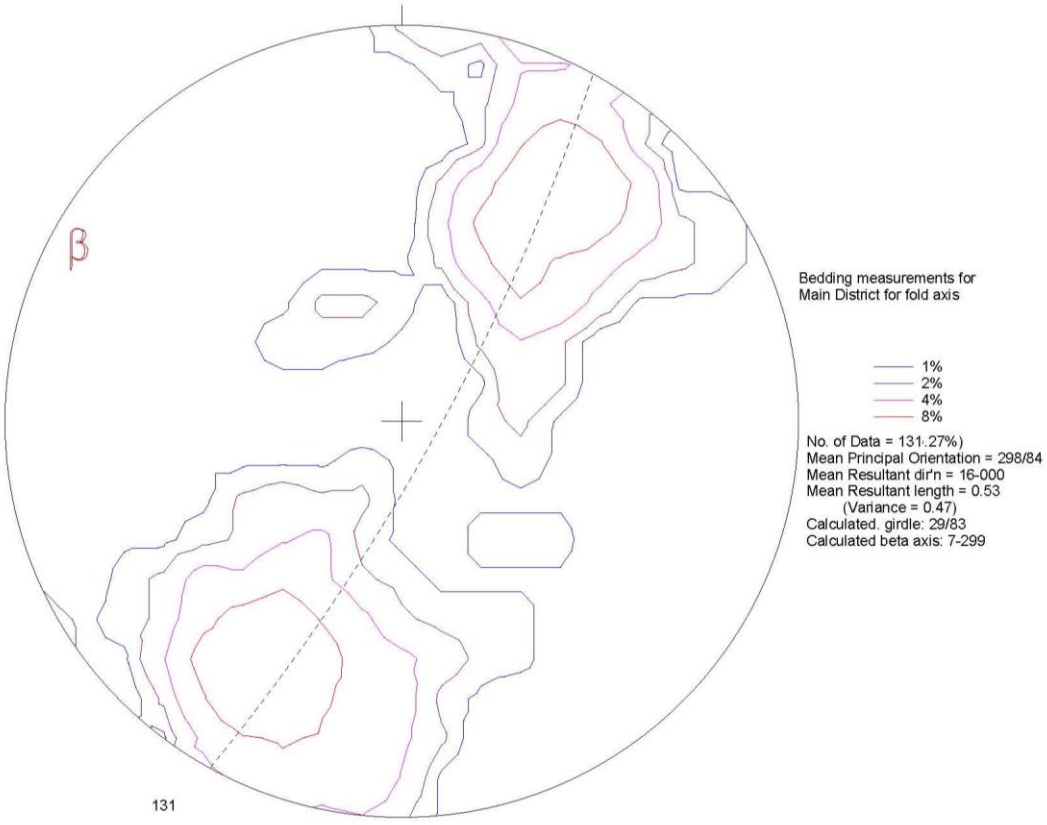

Figure 2-32 Contoured lower hemisphere, equal area plot of poles to bedding (S_0) of the Gregorio syncline, exposed within the Toro-Gregorio study area. 131 data points. Calculated axis 7°→299.

Combining many of the measurements made by Animas Resources geologists throughout the entire district provides a very similar plot (Figure 2-33). Both plots reveal a shallow-plunging fold, consistent with field observations and with Animas 2008 and 2009 drilling in the Toro-to-Gregorio study area. Gently plunging folds with gently curved hinges can plunge shallowly in opposite directions (NW vs. SE), as is locally observed in the district.

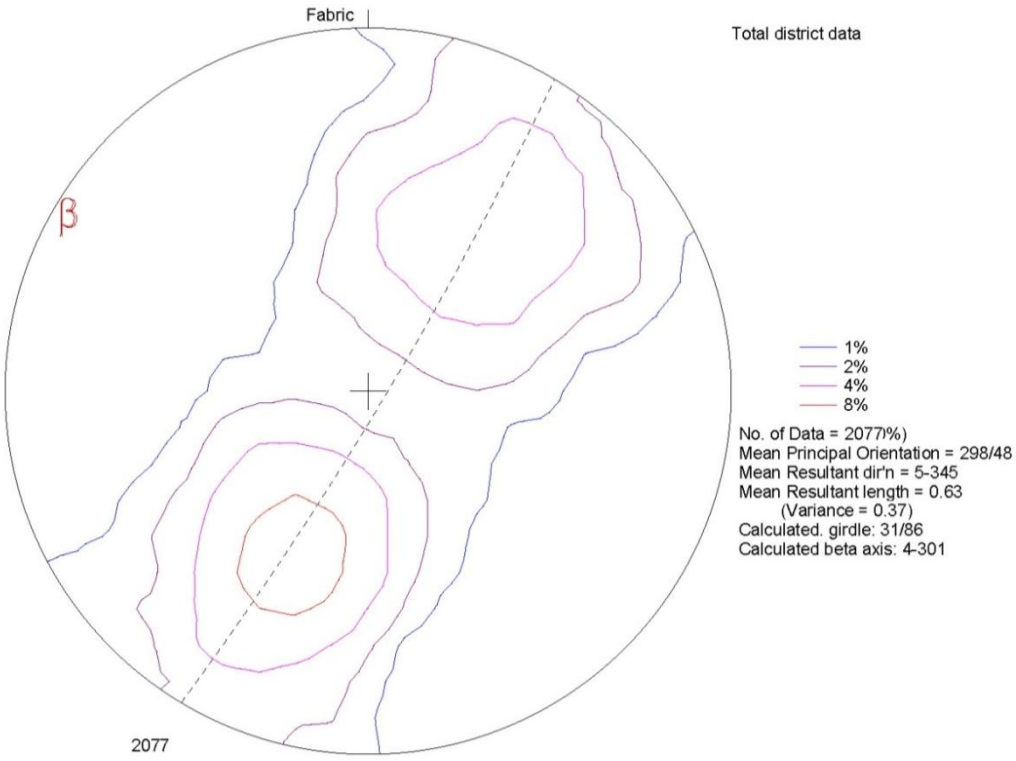

Figure 2-33 Contoured lower hemisphere, equal area plot of poles to bedding (S_0) for the entire district. 2077 data points. Calculated beta axis 4°→301.

Recognition of the overturning and modeling the fold in the subsurface were aided by the exposure of the overturning in and near the Gregorio Mine. Along a high bench on the northwestern wall, the stratigraphy changes over a few meters from moderately southwest-dipping and upright to steeply northeast-dipping and overturned (Figure 2-34). S_1 is folded along with the bedding, yet there is no S_2 cleavage parallel to the axial planar surface within the refolded Ks beds.

Figure 2-34 Overturning of the stratigraphy in Gregorio Mine, looking northwest. Ks bedding rolls over abruptly at mid-picture, from southwest-dipping and upright, to vertical at the top of the outcrop. Note that S_1, which is parallel to bedding, is being folded, and there is a lack of S_2. Outcrop is approximately 4 m thick.

A simplified schematic cross section of the overturning, excluding the older top-to-the-northeast structures, modeled from the field mapping, and Animas 2009 drilling is presented in Figure 2-35. It reveals that the orientation of S_2 cleavage associated with many of the smaller folds is not consistent with the cleavage that would be associated with the F_2b Gregorio syncline.

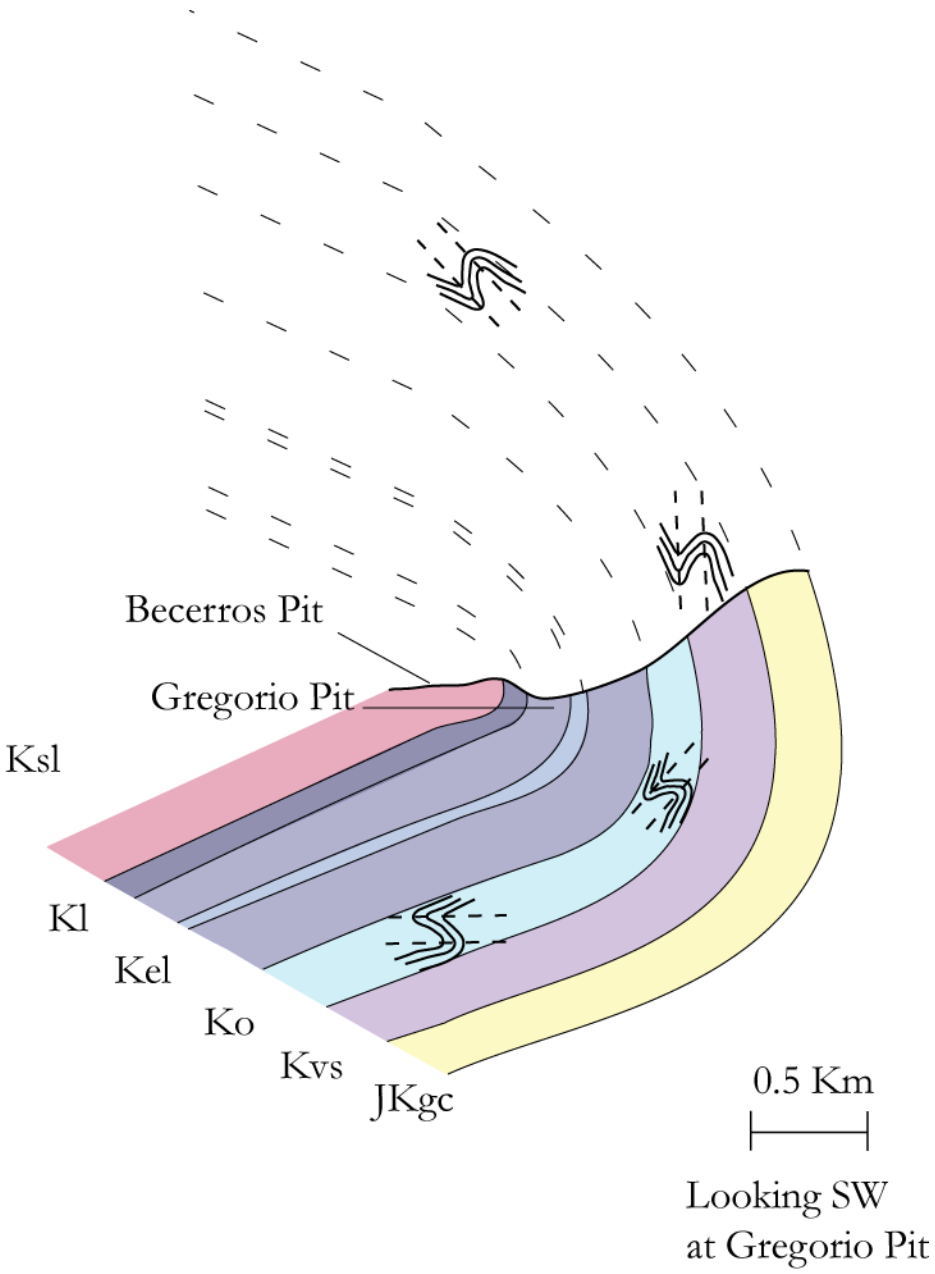

Figure 2-35 Simplified schematic cross section of Main District, Gregorio syncline modeled from exposures at Gregorio Pit, Animas 2009 drilling and field mapping. F_2a folds are overturned by the Gregorio syncline (F_2b).

It is evident that there are complex folds throughout the district, from the outcrop scale to the regional scale. At Amelia Mine, in the extreme northwest portion of the district, folded beds and cleavage in the Kl limestone at M Hill (Figure 2-36) define large, upright folds that have a much tighter inter-limb angle as compared to the stratigraphy-overturning Gregorio syncline. This area also exhibits a near-vertical cleavage that is axial planar to the tight folds. Tight kink folds are also evident in portions of the district, preferentially exposed in the mudstones and siltstones (Figure 2-37).

Figure 2-36 View looking west at Amelia Mine and M Hill. Large-scale folds in Kl limestone are evident at the top of the hill behind the mine waste. Large ridgeline in far background is Sierra Madera, a Tertiary metamorphic core-complex.

Figure 2-37 Tight kink folds (F_2a) in the Ks upper.

Open folds are rarely evident in the field, but do exist, adding another complexity to the geologic history of the district (Figure 2-38). It is not clear whether such folds are F_2a folds or large F_2b folds, such as parasitic folds to the Gregorio syncline. The open folds post-date the shearing, thrusting, and cleavage associated with S_1, but their significance and structural history are poorly understood.

The lack of a strong cleavage or ductile shear fabrics related to the second folding event, combined with the semi-brittle nature of the fold hinge observed in the 2009 Animas drilling of the Gregorio syncline, indicates that the F_2a and F_2b events were much more brittle than the initial thrusting and faulting related to the S_1 cleavage. D_1 and D_2 deformation, with their associated folds, cleavages, and fabrics may be related to the Laramide orogeny.

Figure 2-38 Large-scale open fold in Kl limestone south of Dora Mine.

Low-angle thrust faults

Field mapping and Animas 2009 drilling revealed the presence of low-angle, southwest-dipping, ductile to brittle-ductile thrust faults. Within the Mirador study area, the Gate fault has strong, top-to-the-northeast ductile shear fabrics, bedding offsets, and local southwest-dipping cleavage. These low-angle thrust structures are also present in Dora, Toro Norte, Toro, Ruben, Gregorio, and Camello Mines. The total offset on the structures was never determined, in part due to later brittle, normal reactivation. Presumably, these structures are associated with top-to-the-northeast shortening. They may be most responsible for repetition of the stratigraphy and duplexing seen in Aqua Blanca, Corral, and Sargento and with the generation of S_1 fabric. At Sargento prospect, for example, a gently southwest-dipping, brittle-ductile shear zone carries Mural Limestone in its hanging wall, repeating the section compared to the same units in the Main District. The structure has a clear top-to-the-northeast sense of shear, based on

minor structures. Although they appear to precede mineralization, no significant deposits have been associated with the low-angle structures, but their potential remains largely untested.

Northeast-dipping, brittle to brittle-ductile thrust faults at the Veronica prospect, 1 km north of Mirador Mine cut across the upturned Bisbee Group F_2b fold limb. A weakly to strongly developed cleavage parallels this thrust fault. Sense of shear fabrics indicate the structure has top-to-the-southwest vergence. The fault postdates F_2b, but has a similar vergence direction. It may represent a post-F_2b phase of D_2, or may be related to an undescribed D_3 deformation.

Northeast-trending brittle faults

Northeast-trending, steeply northwest-dipping brittle faults post-date the northwest-trending, bedding-parallel structures and the southwest-verging folds. They are characterized throughout the district as vertical to northwest-dipping brittle structures, striking between N10E and N65E. The northeast-trending faults offset the northwest-trending shear-zones, with highly broken and fractured hanging walls and relatively unaffected footwalls. This had a profound control on future mineralization. Slickensides, both pre-mineral and post-mineral, attest to multiple reactivations and movement orientations. Offset of lamproite dikes in the Enedina study area suggests that latest movement is post-Oligocene. Helmstaedt (1996) and Anderson (1999) proposed that the northeast-striking structures might have originated as conjugate shear faults related to the thrusting in the district (Figure 2-39).

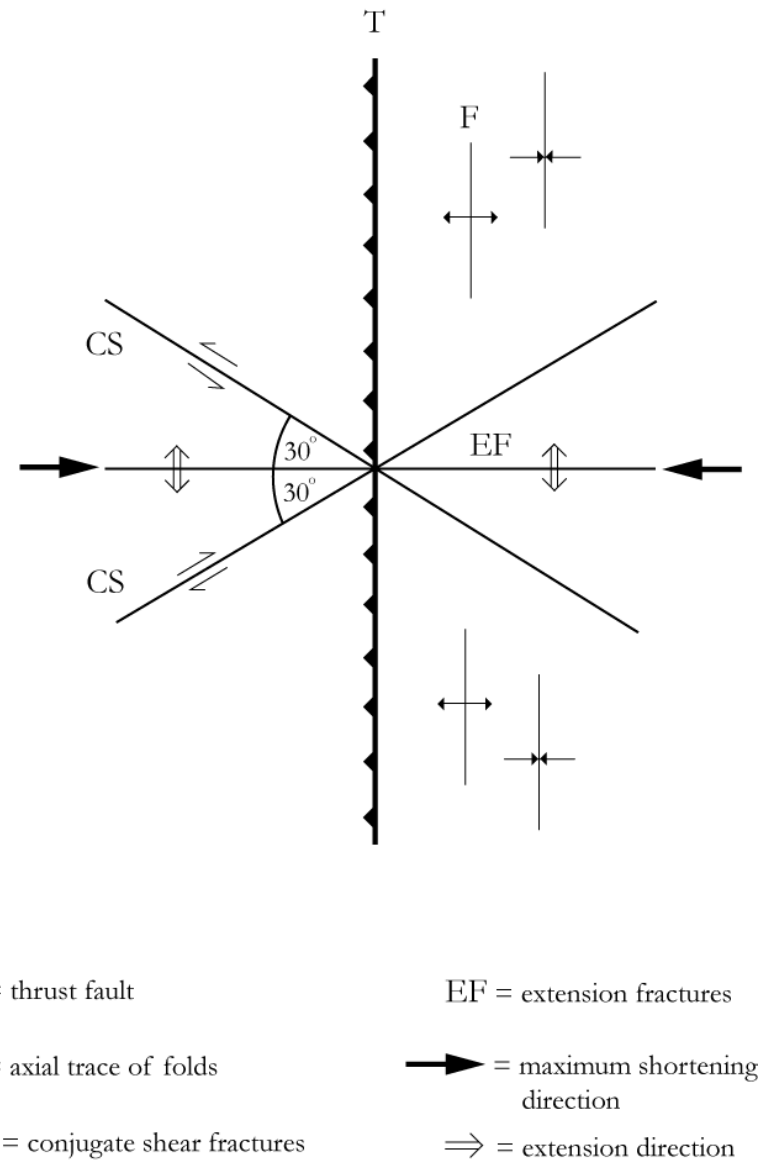

Figure 2-39 Orientations of structures related to thrust faulting, including conjugate shears. Adapted from Sylvester (1988).

Silicification of breccia, limestone replacement, and silicified, decalcified limestone is most commonly associated with the northeast-trending structures. Limestone decalcification, directly tied to northeast structures, and strong mineralization are observable in Toro Norte, Ruben, and several other open pits along strike of the northeast faults in the Main District.

Low-angle normal faults

Southwest-dipping, low-angle brittle faults are evident in multiple exposures in the Main District open pits and in the Animas 2009 drilling. In the southern wall of the Maribel Mine, a mineralized zone is clearly truncated by an overlying low-angle, southwest-dipping normal fault (Figure 2-40; Figure 2-41). Mineralization is abundant in the footwall but is mostly absent in the hanging wall. This same relationship is observed in the Dora Mine and in nearby drilling.

Figure 2-40 Looking south-southwest at Maribel Mine, post-mineral structure 315 40° SW with an unmineralized purplish-green hanging wall and purplish red mineralized footwall. Recent gravel fan at water's edge covers a portion of the fault.

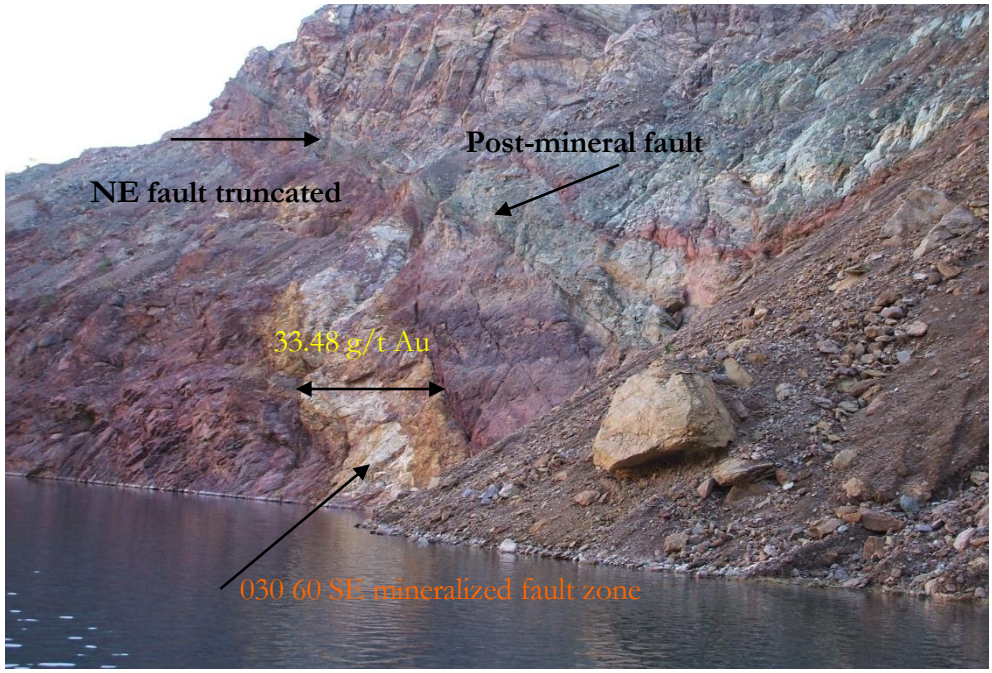

Figure 2-41 View of post-mineral fault in Maribel Mine from the water's edge, looking across the recent gravel fan from Figure 2-71. Intensely leached and altered zone is associated with a 030 60° SE fault and is truncated at the post-mineral fault near the top of the pit.

In the Corral Mine, top-to-the-southwest overturning of the stratigraphy is truncated by a southwest-dipping, low-angle fault. The fault clearly saws through the limbs of F_2a folds exposed along the northwestern benches of the pit (Figure 2-42). These faults locally have a preserved fault parallel cleavage in their hanging walls, so may have an older, thrust-related history, in addition to normal faulting.

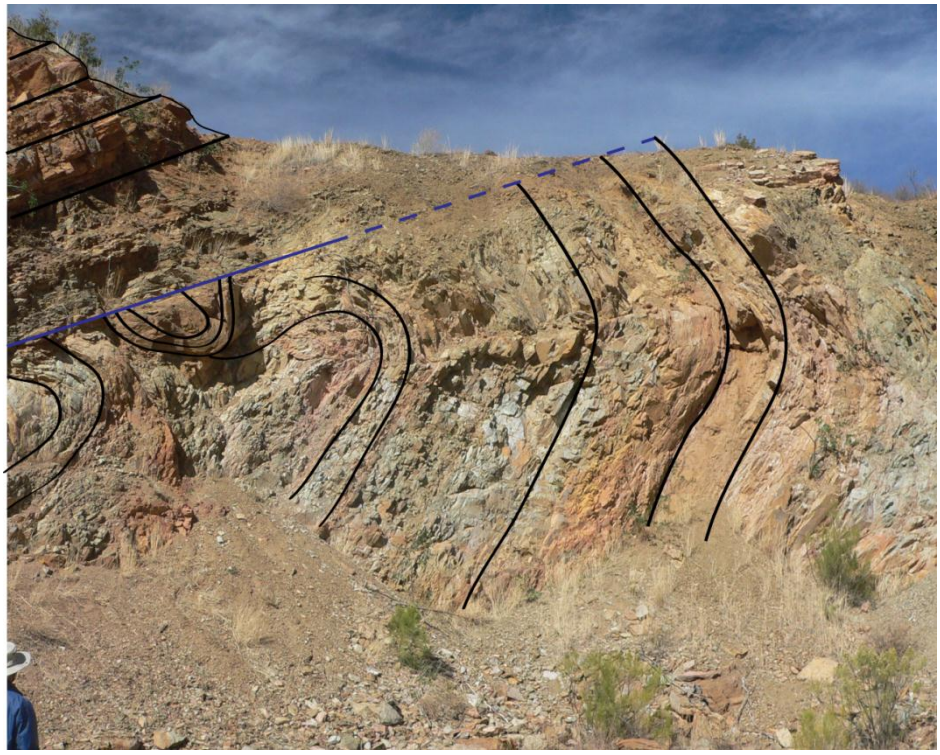

Figure 2-42 Photo of northwestern wall of Corral Mine showing post-folding, post-mineral fault cutting the limbs of the overturning, southwest vergent folds. Hanging wall is unfolded.

In the Mirador area, the Gate fault (Figure 3-36), so named for the excellent exposures at the northbound, gated road at Mirador Mine, is exposed for several hundred meters along the road. It strikes 045 21°SE and reveals a complex movement history including top-to-the-northeast ductile thrusting and later reactivation by brittle normal movement with apparent displacement of the hanging wall to the southwest. The Gate fault has major significance within the district; it separates the Main District, non-hornfels, and structurally controlled distal disseminated gold from the strong hornfels in the Mirador study area (Figure 2-43). The non-hornfelsed, post-mineral hanging wall of the Gate fault represents the bulk of the mined gold within the district, while the underlying hornfels is generally uneconomic. Animas 2009 drilling confirmed that the low-angle structures cut the distal disseminated and quartz-related mineralization associated with hornfels and skarn mineralization.

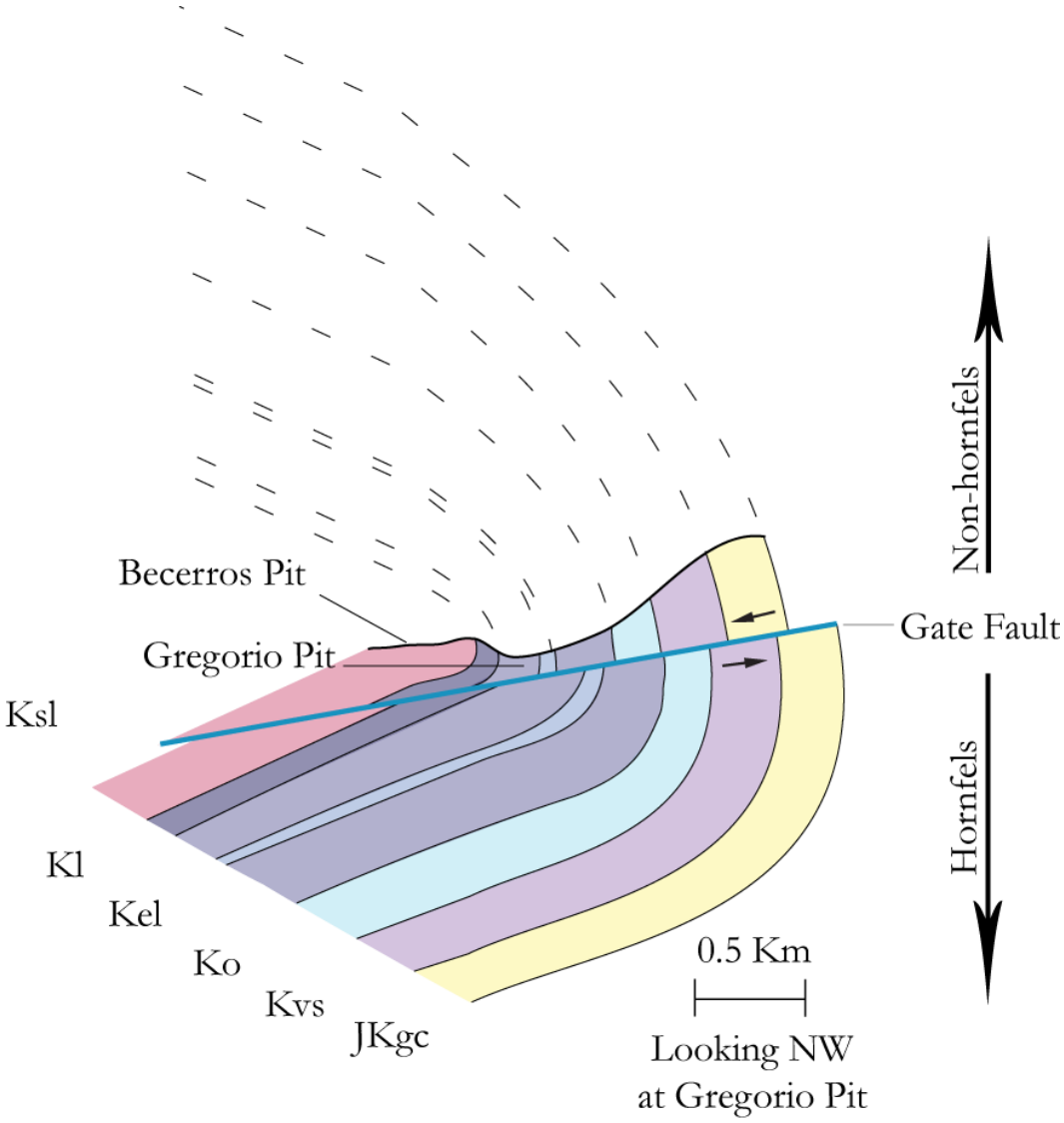

Figure 2-43 Offset of the Main District stratigraphy and mineralization by low-angle faulting. Although the mappable, apparent offset on the Gate fault is less than 50 m, the obvious change in the thermal regime across the fault attests to movement prior to and following the hornfels event.

Figure 2-44 Dramatic faulted contact going down hole from upper left with black calcareous, non-hornfels Ks faulted against strong Ks hornfels with healed breccia extending 10 more meters down the hole. Core from ARTG-005, 486 m depth.

The possibility of large-scale movement along the fault is not obvious in field mapping. Units nearly line up across the fault, yet the change in metamorphic grade dictates that the rocks in the hanging wall had to have been several kilometers separated from the heat source. Below the fault, limestones have been converted to garnet skarn, and the calc-silicates have become brown-biotite hornfels. Two meters away, across the Gate fault, the equivalent limestones are relatively unmetamorphosed and the calc-silicates, mudstones, and shales are nearly pristine (Figure 2-44). In the Mirador Mine, the Red fault (Figure 3-36), is a northwest-trending, brittle-ductile, bedding-parallel structure that hosts mineralization along strike for several kilometers as it cuts through the hornfels footwall of the Gate fault. The Red fault does

not cut the hanging wall of the Gate fault, providing further evidence for post-mineral movement of the Gate fault.

High-angle normal faults

The district is cut by several through-going, northwest-trending, steeply southwest-dipping, brittle normal faults. In the southern end of the Main District, the Santa Nino fault cuts 35° counter to the strike of the stratigraphy, sawing off all of the units. In the north-central portion of the district, the Las Macarias fault, paralleling the Santa Nino fault, down drops and complicates the stratigraphic and tectonic history. The structures cut all rock types, mineralization, alteration styles, and all older structures. The overall effect of the high-angle normal faults is to downdrop the stratigraphy and the mineralization in a normal sense along a northeast to southwest transect of the district. The post-mineral, Las Macarias fault is most evident in the vanadium soils-plot in Figure 2-66 as the linear feature that terminates the circular pattern defined by the La Bonita Hornfels.

Structures within the Bisbee Group

All of the Bisbee Group units experienced varying and overprinting structural deformations. Ductile fabrics are recognized in all of the units in the district. The shales and metapelitic units have anastomosing, bedding parallel, brittle-ductile shear zones, locally in contact with the more competent units. Multiple generations of folds and cleavage formation are present. Younger, brittle faults crosscut folds, cleavage, and mineralization. Crosscutting relationships between fault, folds, and the intrusives, along with the recognition of offset of the local stratigraphy have aided in determining the structural history of the district. The following section summarizes structural observations of the individual Bisbee Group units and several other units in the district.

Deformation of the Glance Conglomerate is most evident as stretched-pebble and stretched-boulder conglomerate. Long axes of pebbles have a general trend of 45°→240 and a 3:1 aspect ratio. This deformation is also recognized in the pebble conglomerates of the Morita Formation. The style and orientation are consistent with top-to-the-northeast shortening.

Deformation is best recognized in the stretched-pebble conglomerates, with aspect ratios and axis orientations comparable to the Glance Conglomerate. Mineralized faults cut the Morita Formation, but gold-grade and rock alteration are weak to non-existent.

Structurally, the massive beds of the Ko reef facies of the Mural Limestone acted as rigid buttresses, against which the overlying Ks siltstones and the interbedded silt and mudstones of the Ko were deformed. Within the most massive reef facies, bedding-parallel shear is nearly absent. Deformation, if present, is most prevalent near the top of the Ko, where the oyster-bearing limestone beds become thinner and the presence of interbeds of siltstone and sandstone become more prevalent. Although intrafolial, bedding-parallel, folds are rare within the massive Ko units, they are present within the less competent interbeds. Northeast-trending faults, in two sites, cut through the facies change from reef facies to siltstone/mudstone facies change, west of Ruben Pit and east of Corral Pit (Figure 3-39). This may be coincidence or it may be related to a change in rock strength controlling faulting.

Thickness variability is a result of bedding-parallel shortening, shearing, and duplexing of the units. Some of the units are also locally structurally attenuated. The deformation predates the hornfelsing event as evident by hornfels preserving pressure shadows on pyrites and isoclinal, bedding-parallel folds.

The Ks upper and lower units exhibit the most dramatic structural deformation, presumably due to rock strength. They were the most selectively altered and mineralized and hosted the greatest concentration of gold within the district, accounting for roughly 58% of the total gold production. The fissile, weak nature and calcareous content of the two Ks units allowed for intense deformation and decalcification of the variable lithologies, creating fluid pathways and sites for chemical reactions that would deposit sulfides and ultimately gold.

Deformation of the Kl Limestone is generally limited to bedding-parallel shear within the siltstones, but shear-zones are also recognized cutting the limestone units (Figure 2-21). Deformation of the interbedded siltstones appears to have been buttressed by the surrounding rigid limestones.

Deformation of the Cintura Formation is consistent with deformation throughout the district in Bisbee Group rocks, with bedding-parallel slip concentrated in the siltstone and mudstones and along the contacts with massive sandstones. Fracture-controlled color leaching of the Cintura Formation is evident throughout the district, associated with various fracture sets and affecting the purplish siltstones dramatically (Figure 2-45).

Figure 2-45 Purplish Cintura Formation with strong cleavage and fracture and irregular color leaching to pale tan. Whitish spots in purple siltstone are micritic calcareous nodules.

Structures associated with other units

The Magdalena Formation represents local basin fill during extension and half graben formation. It overlies deformed rocks along an unconformity and contains clasts of mineralized rock. Given the relative age of the unconformity and the Batamote trachyandesite, uplift of mineralized rock could have begun as early as 42 Ma, and is at least initiated during the Oligocene. This agrees with the onset of extension in Sonora during the Oligocene as proposed by Ferrari (2007). Presumably, the Magdalena Formation is related to mid-Tertiary extension.

The diorite unit, exposed widely across the district, typically intruded as sills in the presently folded and overturned stratigraphy. It primarily intrudes the Cintura Formation throughout the

district. The diorite intrudes the bedding-parallel S_1 cleavage in Becerros Norte and at Maribel. Cleavages are absent in the diorite, and the diorite is cut by the mineralized, northwest-trending shear-zones and lamproite dikes (Figure 2-46). South of Dora Mine, calcite ladder veins and copper oxides are abundant within the diorite (Figure 2-47). The diorite, observed to be cut by the Las Panochas Granite at San Enrique, has abundant disseminated pyrite, chalcopyrite and greisen-bearing quartz veins, which cut from the granite into the diorite.

Figure 2-46 Pyrophyllite alteration of diorite, lower right of photo. Diorite is irregularly cut by lamproite dike in upper middle portion of the photo. South of Dora Mine.

Figure 2-47 Ladder calcite veins cutting diorite and disseminated Cu-oxides. South of Dora.

Given the lack of Laramide fabrics in the district, the configuration of the sill, and the crosscutting and mineralizing Las Panochas Granite, the diorite is older than the 42 Ma Las Panochas Granite and younger than the folding that led to the district stratigraphy being overturned, as discussed in the Structural Geology section of this study. Exposure of the granite is a combination of tectonic denudation and erosion, presumably beginning during the Oligocene and concurrent with initiation of the Magdalena Formation.

The lamproite dikes cut the older fabrics, intrusives, and mineralization, intruded parallel to and within bedding-parallel faults, and along low-angle, southwest-dipping, brittle-ductile faults. Regularly, they are incorporated in the related fault breccia and can show as smeared zones along the fault contact with footwall rocks of the normal faults. A weak, paralleling fabric in the lamproites intruding low-angle faulting in the La Gloria prospect may be tectonic. Low-angle and bedding-parallel structures seem to have been active during intrusion;

northeast-trending structures clearly offset the lamproites during their latest phase of reactivation.

Structural Discussion

Cessation of passive-margin sedimentation by the early Mesozoic in southern Arizona and northern Sonora is ultimately related to the rifting of Pangaea and the initiation of subduction of the oceanic plates in the Pacific ocean beneath the North American continent. Opening of the Gulf of Mexico lead to the formation of the Chihuahua Trough, a northwest-trending terrestrial and marine basin, possibly extending as far northwest as eastern California (Dickinson et al., 1989). Bilodeau (1982) suggested that the trough was similar to an aulacogen extending away from the opening Gulf of Mexico and related to backarc rifting. Evidence for arc volcanism, compressional deformation, oblique crustal translation, and backarc extension are recognized throughout the region, and interpreted to be related to the temporally evolving western North American margin. The Bisbee Basin and smaller, localized basins (Figure 2-1) containing thin basinal limestones represent the extreme edge of platform reef facies of the Chihuahua Trough, with intervening highs dictating facies and unit thickness. Locally, the southwestern flanks of Sierra Azul define the eastern edge of the San Antonio Basin (McKee, 1991; McKee and Anderson, 1998; Figure 2-1), in which were deposited terrestrial and marine units correlative to Bisbee Basin rocks.

The upper limestones of the Bisbee Group, representing the maximum transgression of the Bisbee Sea, were subsequently covered by thick packages of fluvial and alluvial sequences of the Cintura and the Fort Crittenden Formation of Campanian to Santonian age (Hayes and Drewes, 1978; Dickinson, 1989). Schafroth (1965) reported examples of Fort Crittenden Formation sitting unconformably on folded Bisbee Group rocks in the Empire Mountains of

southern Arizona. Dickinson et al (1989) state that the Fort Crittenden Formation "immediately preceded" the Laramide magmatism and was subsequently involved in regional thrusting and folding associated with the Laramide Orogeny. The basins in which the Fort Crittenden Formation were deposited have been inferred to be related to early Laramide deformation (Drewes, 1978; Davis, 1979).

The Santa Gertrudis Mining District has undergone multiple deformations that have had a profound effect on the stratigraphy and mineralization. The oldest fabric (S_1) recognized is associated with top-to-the-northeast shortening and ductile shear. The cleavage is parallel to bedding, or cuts the bedding at low angles. Northeast-verging thrust faults that cut the cleavage and the folded Bisbee Group rocks are interpreted to be associated with progressive (D_1) deformation associated with the Laramide orogeny.

The S_1 cleavage is subsequently folded by northwest-trending, outcrop-scale folds, which are then locally overturned as part of the southwest-vergent, regional-scale, Gregorio syncline. This progressive (D_2) deformation event is also interpreted to be associated with the Laramide orogeny. D_2 lacks a strong cleavage and has a semi-brittle fold hinge, as observed in the 2009 Animas drilling of the Main District fold. D_2 appears to have more brittle deformation than D_1. Animas 2009 drilling revealed that there was no gold mineralization concentrated within the fractures associated with the brittle hinge of the Gregorio syncline.

Laramide deformation, as recognized in southeastern Arizona and south into Sonora, has a component of northeast vergence followed by southwest vergence and overturning (Krantz, 1989). Timing of the Laramide Orogeny in southern Arizona has been constrained by Dickinson et al. (1989) from peak volcanism to span from 77.5 to 57.5 Ma, although the span

has been suggested to last as long as 80 to 40 Ma. (Coney, 1971; 1976). The end of the Laramide Orogeny has been identified by Krantz (1989) as the inception of sweeping volcanism related to shallowing of the dip of the Farallon Plate (Coney, 1976; Coney and Reynolds, 1977; Dickinson and Snyder, 1978; Dickinson, 1981; Spencer and Reynolds, 1989). Reynolds and Keith (1980; 1981) note that by Eocene time, the angle of subduction had shallowed enough to create a gap in volcanism, with minor crustal melting producing peraluminous, two-mica granites.

Southwest-dipping, low-angle normal faults cut the older faults and folds. The faults, associated with D_3, locally reactivate the older, top-to-the-northeast thrust faults. The reactivation may have been related to large-scale extension of the crust and is consistent with regional observations for timing and orientations for extension. Drilling reveals that movement on the fault post-dates the hornfels and the latest movement on the Red fault in Mirador Mine. These faults are important in the district since they appear to dismember the deposits. This hypothesis was first proposed by Anderson (1999).

Basin and Range faulting in southern Arizona and northern Sonora is typified by high-angle, normal faults that trend north, north-northeast, or northwest and that active from the Late Miocene and into the Pliocene (Menges and Pearthree, 1989). Extension and strike-slip motion led to the formation of the Gulf of California, in part accompanying the northward migration of the San Andreas-Farallon triple junction. At Santa Gertrudis, the Basin and Range faults clearly offset mineralization as well as the low-angle structures related to mid-Tertiary extension.

In northern Sonora, Ferrari et al. (2007), suggest that extension starting during the middle Eocene, prior to the emplacement of ignimbrite sequences. Such early extension may be recorded by the formation of the Batamote half graben and deposition of the Magdalena Formation unconformably over the Las Panochas Granite (Smith, 2006). Wholesale extension of the crust and metamorphic core complex formation began in southern Arizona and northern Sonora by 20 Ma (Spencer and Reynolds, 1989; Wong and Gans, 2003). Within the district, emplacement of the lamproite dikes and the presence of southwest-dipping, low-angle structures displacing the Laramide structures may be indicative of mid-Tertiary extension.

This study concludes that the Las Panochas Granite is as old as 42 Ma, but the K-Ar 36 Ma (Bennett, 1993) is also consistent with Ferrari's proposed moderate-angle unconformity and extension prior to emplacement of ignimbrites of the Sierra Madre Occidental (Ferrari et al., 2007), which unconformably top the Las Panochas Granite within the district. The family of low-angle structures cut mineralization in the Santa Gertrudis mining district and have apparently decapitated the deposits in a top-to-the-southwest sense, after emplacement of the Las Panochas Granite, and perhaps in part prior to the 30 Ma ignimbrite event. Geophysics and interpretation by John Reynolds, Durango Geophysics (2009) (Figure 2-48) combined with 2009 drilling revealed the continuity of the low-angle structures and their importance in dissecting the mineralization throughout the district.

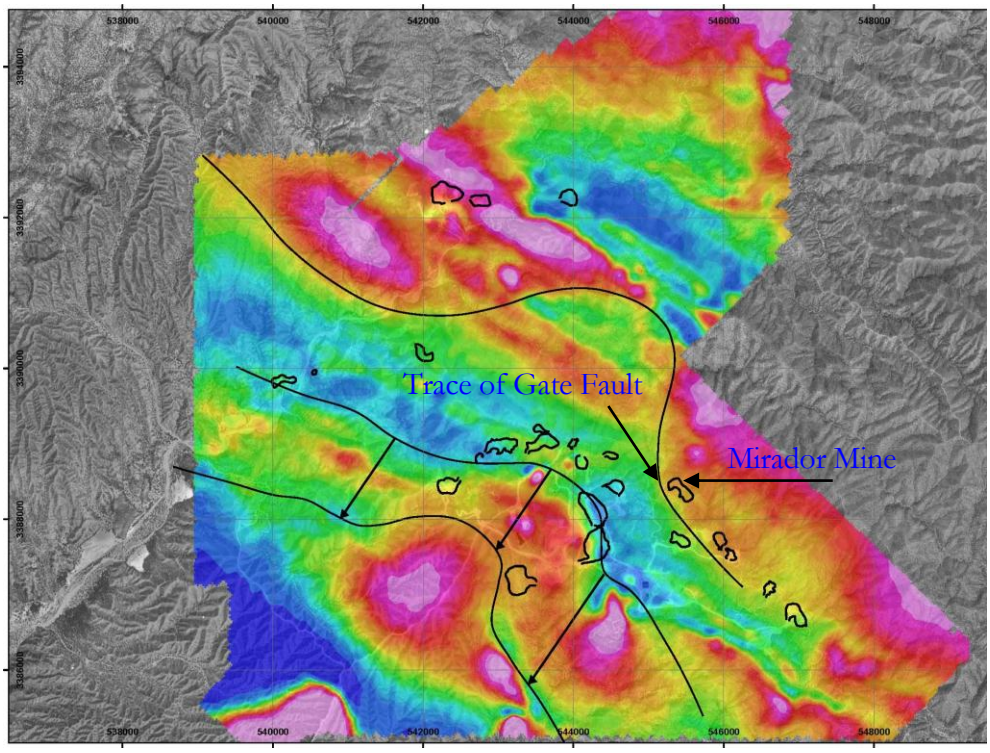

Figure 2-48 Possible geophysical evidence for the dismemberment of the deposits and the Main District mineralization along low-angle faults, implying that the individual deposits may represent tops and roots of continuous mineralization. The southwest-dipping Gate fault in the Mirador study area may be a candidate for a detaching structure; another sliver may exist south of Dora and Maribel Mines, but is covered by gravels. Reduced-to-the-pole airborne magnetics courtesy of Durango Geophysics, 2009.

This structural evolution has implications for original mineralization continuity and zoning based on depth/distance from the mineralizing source prior to low-angle faulting. One possibility for the history of the Gate fault would begin with top-to-the-northeast thrusting cutting bedding-parallel shears, perhaps as progressive deformation. The total displacement on the fault would have to have been several kilometers to separate the rocks from the oncoming thermal alteration. Overturning of the district by top-to-the-southwest thrusting would have stranded much of the original northeast-verging structures, which would have orientations not easily reactivated by later extension. Hornfelsing of the district would have been the next major

event that would have affected the district and the Gate fault. The footwall rocks of the Gate fault have been strongly hornfelsed, implying they were proximal to the source of heat. Following the thermal alteration and mineralization, the Gate fault was reactivated and the hanging wall returned to a stratigraphic position close to the pre-thrust fault orientation, placing two differing alteration styles, but essentially the same rocks, in close conjunction.

An overview of the regional structures in the Santa Gertrudis district by Servicio Geológico Mexicano and from visible features in Landsat imagery reveal several circular features that have been modified by younger structures (Figure 2-49). These features may represent ring faults surrounding buried intrusives. Within the Main District, there is an apparent circular pattern to the mined mineralization (Figure 2-50). Whether the mineralization is associated with deeper, unexposed intrusives or if this is a coincidence is unknown.

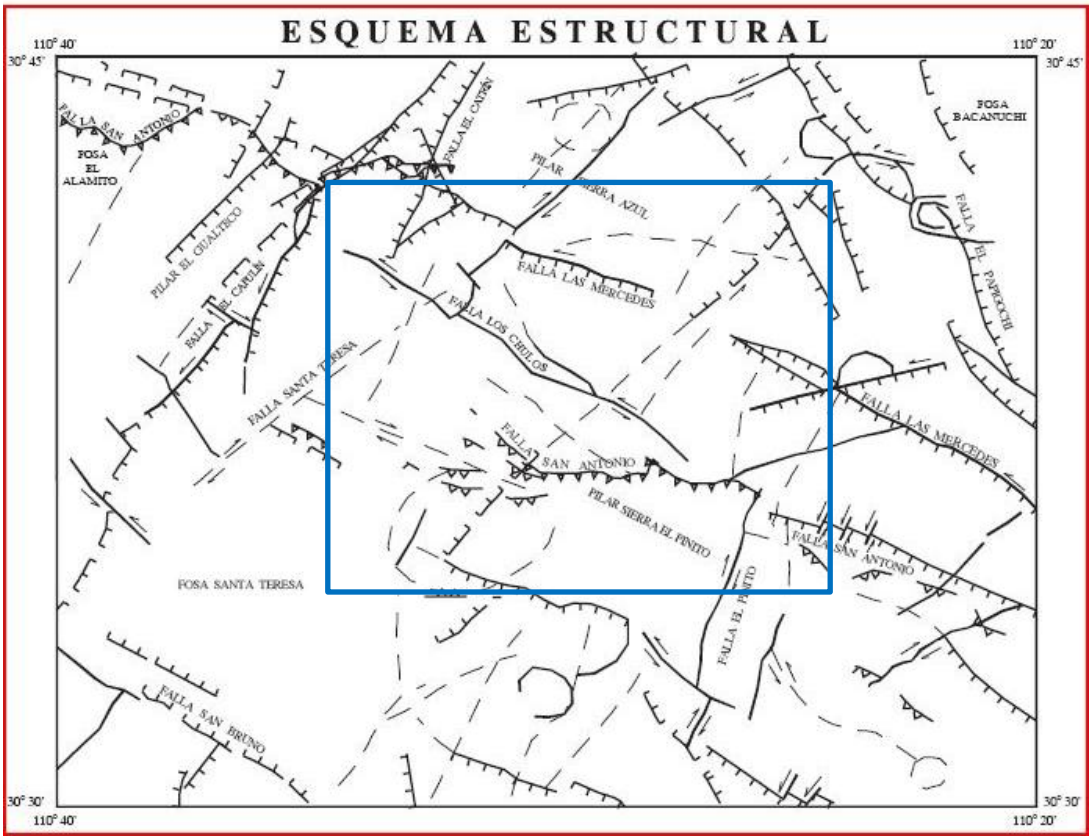

Figure 2-49 Structures identified within the SG region. The district lies within the blue box. Note several circular patterns identified throughout the region. From S.G.M. map "Carta Geologico-Minera Santa Teresa H12-B62, Sonora", 2003.

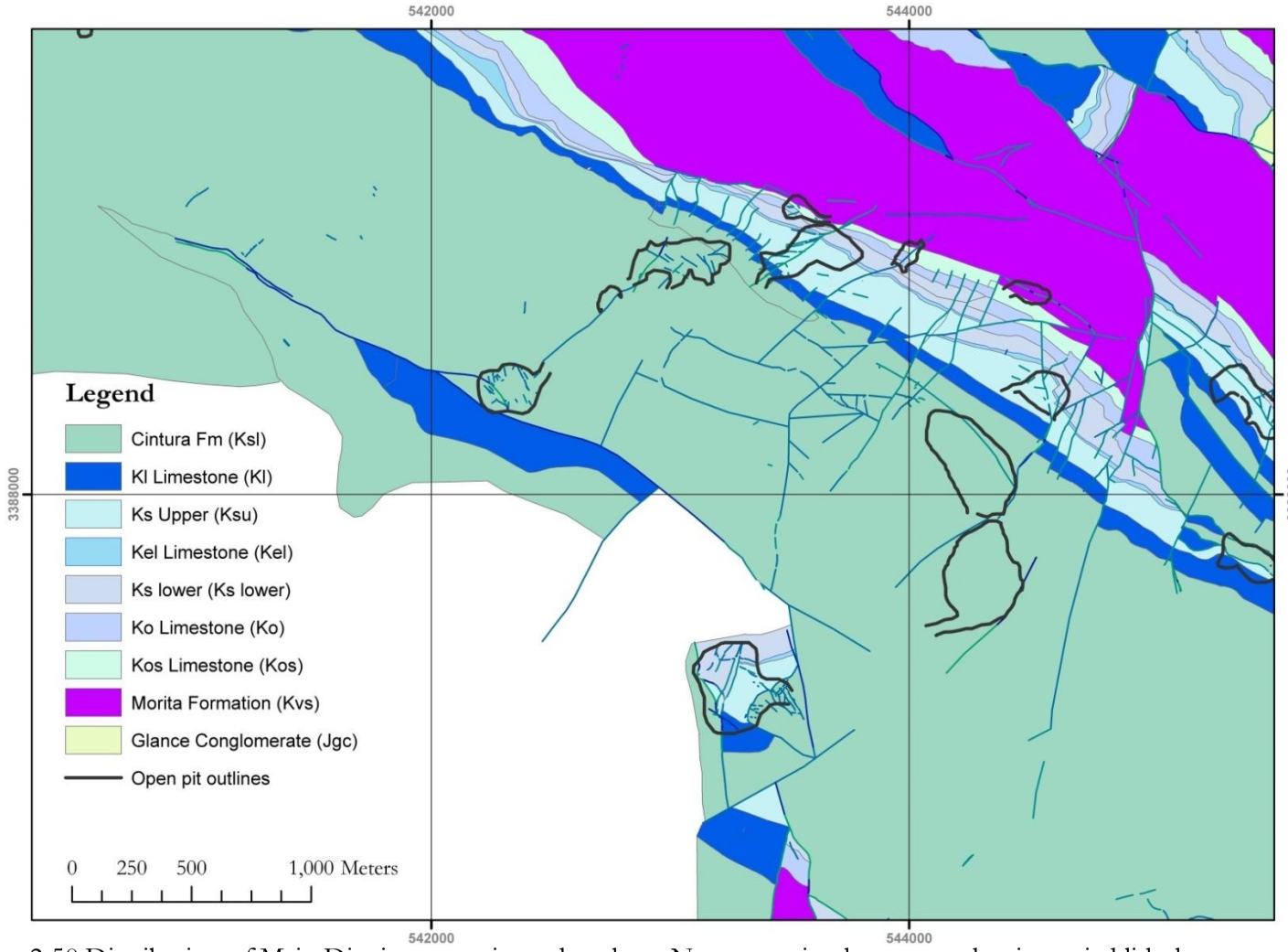

Figure 2-50 Distribution of Main District open pits and geology. Note near circular pattern despite varied lithology.

Mineralization

There are four deposit types in the district: 1) distal disseminated; 2) hornfels and skarn; 3) quartz veins; and 4) poly-metallic veins. The deposit types are identified based on geochemical associations, rock alteration, gold grade, and oxidation. Geochemical associations and rock alteration have served as guides for discovering deposits throughout the district. Post-mineral faulting and oxidation have played a key role in modifying the deposit types and juxtaposing differing types of rocks, alteration, and structures against one another.

Distal Disseminated Deposits

The most widespread deposit type is distal disseminated, sediment-hosted gold associated with structurally prepared, chemically reactive Bisbee Group rocks. This deposit type has been the most productive for gold and is the typical style of mineralization in the Main District. Structural intersections within calcareous siltstones and mudstones, along with carbonaceous, pyritic black shales acted as primary sites for mineralization, with mineralization bleeding along northwest-trending, bedding-parallel shear-zones. Native gold is sub-micron to micron in size and tightly bound to the surface of iron and arsenic sulfides disseminated throughout the non-hornfels, unoxidized calcareous rocks. Pyrite ranges from diagenetic to hydrothermally-introduced through sulfidation, ranges from 0 to 5% of the mineralogy, and is most evident in sandstones due to higher permeability and porosity (Figure 2-51). Arsenopyrite is rare but has been identified in drill core since the Phelps Dodge era.

Figure 2-51 Fine-grained, bedding-controlled pyrite in the Ks upper at Aqua Blanca Pit. Calcite vein incorporates pieces of Ks bedding with pyrite, but the vein contains no pyrite.

Geochemical haloes have been useful for delineating favorable mineralized zones. Visual clues including color leaching and hydrothermal clay formation, strong zones of oxidation of sulfides, and redistribution of iron and zinc oxides along shear-zones. Other characteristics of distal disseminated include the presence of turgite as crustiform coatings on limonites, liesegang banding, and arsenic blooms (Figure 2-52; Figure 2-53).

Figure 2-52 Typical bedding-parallel shear-zone with argillization, bleaching, liesegang banding and gold mineralization. Gregorio Pit, courtesy of S.J. Reynolds.

Arsenic, followed by antimony, silver, and zinc, form excellent geochemical pathway targets, with haloes 10 to 100 times broader than the thin (0.1 to 3 meter wide) fault zones that typically host gold mineralization. Since all of the surface exposures within the Main District are heavily oxidized, surface samples are profoundly influenced by oxidation and element redistribution. These effects can reach as deep as 200 m along structural and fluid pathways, but typically, the oxide/sulfide boundary is within 100 m of the surface. This has serious implications for gold recovery due to the preg-robbing properties of the unoxidized, carbon-rich, calcareous mudstones and siltstones. The gold grades generally decreases to sub-economic grade with depth, typically below the current oxide boundary. Typically, both Phelps

Dodge and Campbell abruptly ceased exploration drilling and mining once they reached the irregular, but ever present oxide/sulfide boundary (Figure 2-54).

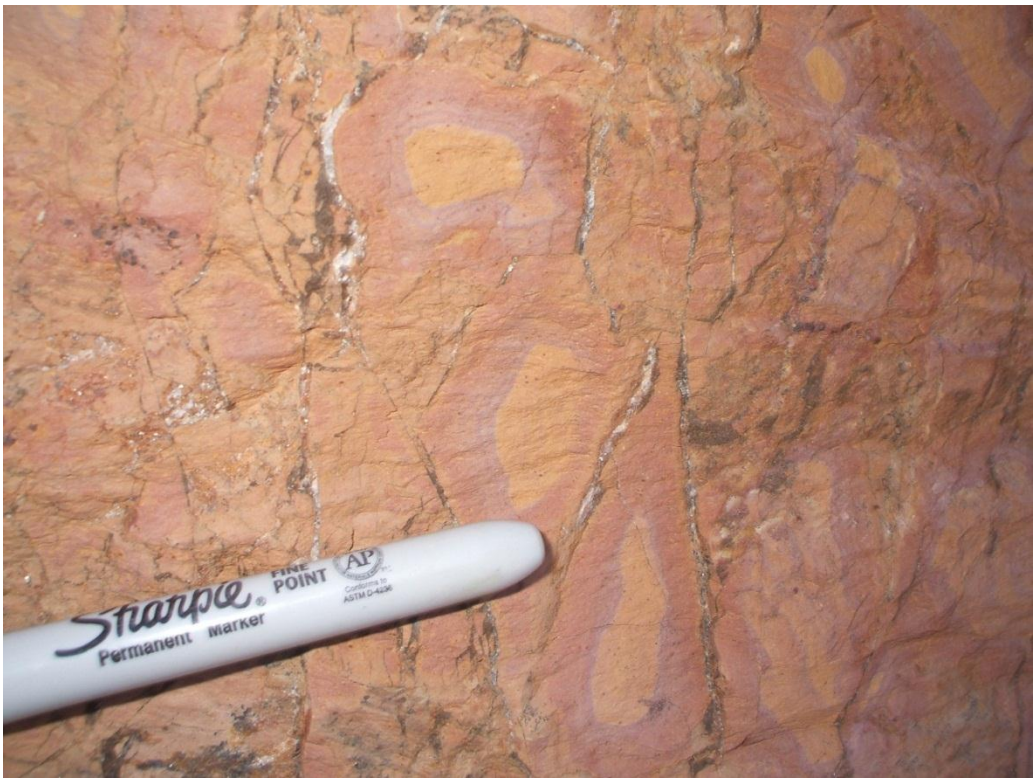

Figure 2-53 Liesegang banding and fine disseminated hematite after pyrite pseudomorphs in leached, then oxide-stained siltstones. Camello Mine. Fractures control oxide distribution; late-stage calcite fills fractures.

Figure 2-54 Oxidation front is typically irregular but has strong fracture and bedding control. A Centavo coin for scale, 100 m depth.

Exposures in Dora Mine show the irregular nature of the oxide/sulfide boundary and the typical mineralogy observed within the unoxidized Ks siltstones (Figure 2-55). At Dora Mine, pyrite is typically 1 to 3% disseminated as 1 mm cubes, arsenic typically forms a greenish bloom within the matrix, sulfo-salts can be observed within open spaces at the surface, and arsenopyrite and arsenian pyrite are locally present.

Figure 2-55 Variable leaching and oxidation of Ks lower carbonaceous mudstone. Alteration is fracture and fault controlled. Pyrite, jarosite and sulfo-salts are dominant in the carbonaceous material; hematite is dominant in the oxidized material. Photo from Dora Mine.

The associations of gold and arsenic have been recognized on the Carlin Trend and elsewhere in sediment-hosted gold deposits. Fleet and Mumin (1997) state that previous studies have found a correlation between invisible gold and arsenic enrichment (Wells and Mullens, 1973; Fleet et al., 1989, 1993; Bakken et al., 1991; Mumin et al., 1994). Fleet (1993) proposed that gold is incorporated into solid solution with arsenian pyrite as arsenic-rich growth surfaces, while Arehart (1993) proposes that gold is deposited as a charged species in coupled substitution with arsenic in pyrite. Bennett cites a very limited data set in 1993 of run-of-the-mill samples from the Main District and concludes that Au, Hg, Sb and Zn were much lower at Santa Gertrudis than at Carlin, while Ag, Pb, Te, and As were significantly higher and Cu about the same as the Carlin District (Bennett 1993; Radtke et al., 1972).

Corral Mine, the southeastern most of the Main District open pits, has an excellent exposure of a high-grade, mineralized fault plane that strikes northwest and dips southwest (Figure 2-56). Gold, associated with arsenic, is focused on the bedding-parallel structures in a highly deformed, gouge matrix, and in the fractured host rocks. Reddish hematite dominates the iron oxides in the gouge, with variable amounts of goethite and jarosite adding an assortment of colors.

Figure 2-56 Mineralized, northwest-trending fault plane in Corral Mine, looking down dip-slope, with dark gray, carbonaceous Ks lower in the foreground footwall, 1.5 m fault gouge in the middle of the picture and slickenlines on the hanging wall showing strike slip motion as a last recorded movement. Slickenlines overprint oxides, indicating reactivation after mineralization. Fault 335 53°SW, slickenlines 50°→305, sample grade 3.75 g/t Au, 945 ppm As, 3.9 ppm Ag.

Decalcification has a close spatial association to distal disseminated mineralization across the district. It variably affects the calcareous units based on proximity to fractures, cleavages, and

bedding planes, and other prior structural preparation. Decalcification is rarely followed by silicification, except with the total decalcification and silicification by replacement of the Kos Limestone and within northeast-trending faults, where fault breccia in the Ko Limestone may be decalcified. The combination of strong decalcification and silicification has been a successful indicator for gold mineralization throughout the district since the earliest exploration began, yet some large zones of silica replacement are barren of gold.

Decalcification is best developed along the edges of the more massive Ko and Kl limestones, leaving the interior intact (Figure 2-57), unless channeled by a pre-existing fluid pathways. In outcrop, the rocks appear hummocky and pitted (Figure 3-5).

Figure 2-57 Initial decalcification of Ko limestone along front, with bedding plane control. A Centavo coin for scale.

Stronger decalcification within the limestones leads to compaction of the matrix, disarticulation of fossils, and development of minor open-space (Figure 2-58). The increase in porosity and permeability evidently allowed later mineralizing fluids to fill the voids easily.

Figure 2-58 Open space decalcification breccia with disarticulated fossils and wispy red hematite deflected around fragments. A Centavo coin for scale.

The strongest decalcification within the limestones leads to collapse breccia and fine-grained matrix infill of terra rosa (Figure 2-59). In outcrop, the rocks have an obvious mottled and dissolved appearance, with clast disarticulation and a reddish matrix surrounding the clasts (Figure 3-6). Typically, the clasts have a sub-rounded nature and are elongated. A few collapse pits are present in the Mirador Mine area. Overall, intense decalcification of the limestones is limited to structural fluid pathways and is not a dominant alteration style encountered

throughout the district. Where it is present, it is commonly associated by high-grade mineralization.

Figure 2-59 Strong decalcification and collapse breccia. A Centavo coin for scale.

Decalcification of the Ks and Ksl lithologies, especially calcareous mudstones to siltstones, and calcareous sandstone, is also dominated by structural controls. Compaction and collapse breccias are present throughout the district, associated with calcareous and carbonaceous rocks (Figure 2-60). Although many meters of decalcified Ks and Ksl were logged in the 2008 and 2009 Animas drilling program, there was a weak association between decalcification and gold deposition within these units. Gold mineralization was observed in rocks that had minor or no decalcification, but typically there was some degree of decalcification within a few meters of the gold in the drill core.

Figure 2-60 Strong decalcification and collapse breccia in calcareous and carbonaceous mudstones of the Ks. A Centavo coin for scale.

Throughout the district, distal disseminated, sediment-hosted gold is associated with non-hornfels, phyllic-altered, weakly metamorphosed calcareous sediments. Base metal associations are interpreted to have been altered due to element mobility during oxidation, but tracer element haloes are still useful for identifying the zones of favorable mineralization. Geochemical associations, in order of presence with gold, include: As, Ag, Sb, Zn, Pb, and Cr. Generally, Bi, W, Mo, and V are at or below detection levels. Figure 2-61 plots averages of the most important trace elements in high-grade gold samples taken throughout the Main District (n = 28).

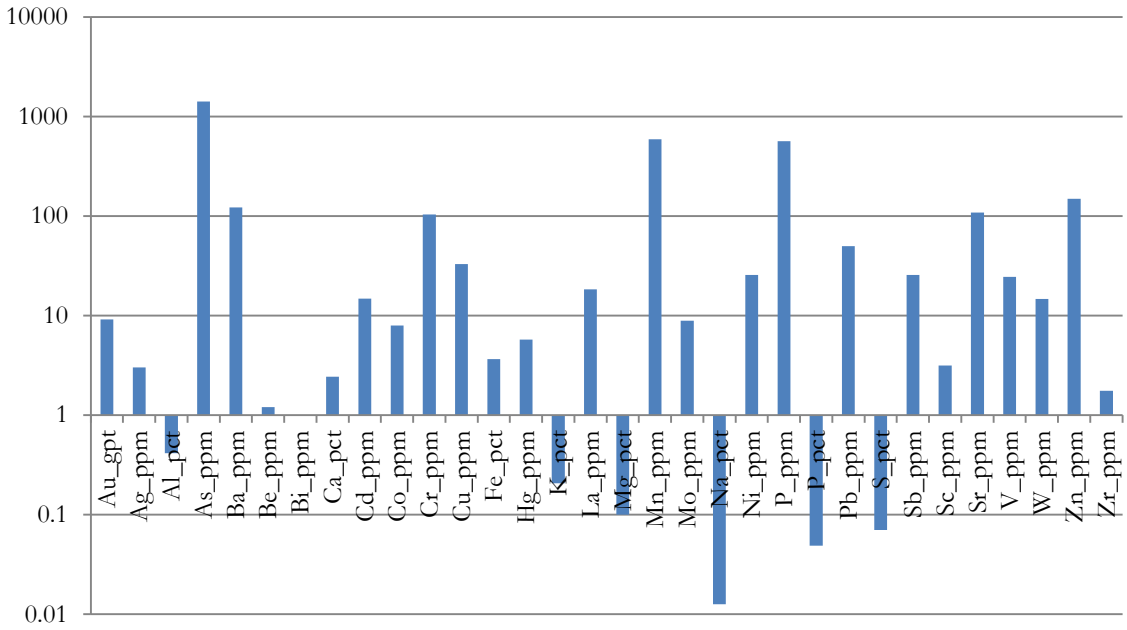

Figure 2-61 Log plot of trace elements of 28 high gold-grade samples from the Main District, sediment-hosted, distal disseminated deposits. 24 of the 28 samples are from northwest and northeast-mineralized structures. Average gold grade is 8.25 ppm. Note the differences in units.

District wide, the effects of thrust faults, folds, and deformation were essential in preparing the rocks for mineralizing fluids along structurally-prepared paths. Rock preparation allowed for increased porosity and permeability, increased surface area through fragmentation, increased chemical reaction rates, and provided conduits for future intrusive and mineralizing fluids. Brittle reactivation of bedding-parallel structures during the formation of the top-to-the-southwest folds and overturning may have played a key role in providing some mineralizing sites, such as the Becerros pits (Figure 2-62).

Figure 2-62 Mineralized breccia along bedding-parallel slip planes in the Ksl, between Becerros Norte and Becerros Sur. Note curved, boudinage surfaces.

Hornfels and Skarn

At least four areas within the district have disseminated, zoned base metals in hornfels and minor skarn, which are interpreted to be related to exposed and hidden igneous intrusive stocks. Hornfels covers vast portions of the district including San Enrique, La Bonita to the north of the Main District (Figure 2-66), Mirador, Enedina, and structurally below the Main District (Animas, 2009). The hornfels, associated with calc-silicate rocks in the Mural Limestone and Cintura Formation, range from albite-epidote to pyroxene hornfels. In San Enrique, the hornfels grades from pyroxene hornfels at the margins of the Las Panochas Granite to brown-biotite hornfels distal to the intrusive. To the northeast, pyroxene hornfels is exposed at Enedina Hill associated with quartz + Mo-V-W mineralization. Surrounding the pyroxene hornfels is a 2.5 km doughnut ring of brown-biotite hornfels. Beyond the central,

zone of hornfels and skarn, disseminated sulfides of Cu, Pb, Zn, and Ag (?) extend away in over-lapping, concentric shells, commonly as visible minerals (Appendix B). Disseminated sulfides, mostly pyrite, range from 0.5 to 3% throughout the hornfels. Zoning within the iron sulfides was recognized in the Enedina study area, with a central pyrrhotite zone surrounded by a diffuse marcasite/pyrite zone, then a km-wide ring of pyrite. Rare boxwork textures reveal the past presence of disseminated sulfides. Vein associations with base metals are less common in the outer zones, but minor examples do exist (Figure 2-63). Flanking the base metal and hornfels zones of Enedina, San Enrique and La Bonita, native gold and electrum are associated with bedding-parallel shear-zones and with decalcified, calcareous rocks as sub-micron thick coatings on iron sulfides, typical of the distal disseminated deposits previously described (Figure 2-33).

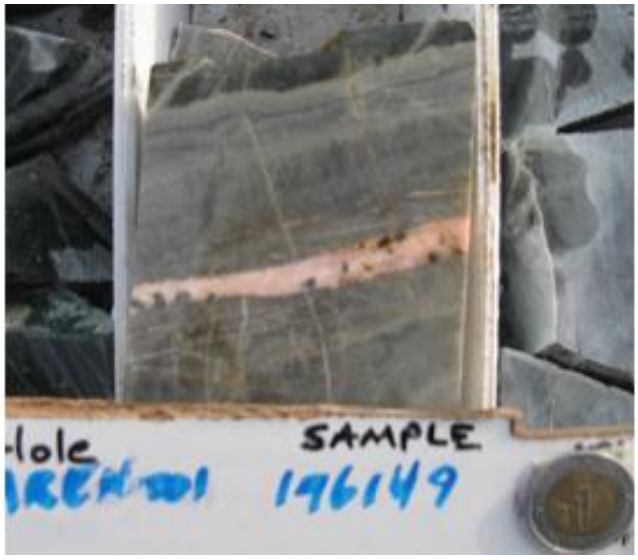

Figure 2-63 Rhodocrosite + pyrite that rapidly oxidized within minutes of cutting. A Centavo coin for scale. Core from AREN-001.

Based on soil and rock-chip sampling, base-metal zoning is distinct in the Enedina study area (Appendix B; Figure 2-66), at La Bonita (Figure 2-66), and surrounding the San Enrique

prospect. Mineralization is observed disseminated throughout the hornfels, in association with structures that were present during mineralization, and related to quartz veins plus base metals cutting the hornfels rocks.

At Enedina, mineralization includes W and Mo associated with quartz + feldspar veins (Figure 2-64; Figure 2-67) and rarely, as disseminated mineralization associated with skarn. Core logs of AREN-001 and ARET-001 (Enedina and El Tigre) reveal the quartz + molybdenite veins consistently cut prograde and retrograde alteration associated with hornfels and propylitization alteration. Smith reported in 2006 that core recovered from Campbell Resource drilling in Enedina, EN-001, showed late-stage quartz plus Mo cutting earlier anhydrous mineralization (Figure 2-64; Figure 2-67). Overall, the frequency of quartz veins with high-temperature mineralization is less than one per forty meters in AREN-001 and other holes collared in the hornfels by Animas. Quartz + magnetite veins are abundant, as are disseminated magnetite and skarn-related, replacement magnetite within the Kl and Kel limestones proximal to Enedina Hill.

Figure 2-64 Quartz stockwork in potassium-altered hornfels. Note the late, nearly core parallel vein with axial molybdenite. Core from EN-001, depth unknown. (Teck Cominco, 2006).

Photomicrographs sulfide mineralization in hornfels were taken by Teck Cominco in 2005 during their drilling program in the San Enrique area. Core from RCSE-5 was examined by J.A. McCloud (Teck Cominco, 2005); with sample 3249 (Figure 2-65) containing:

> Two parallel veinlets of pyrite, 3 cm's apart and 1 mm in width are present. Included in the pyrite and peripheral to it are grains of chalcopyrite up to 0.5 mm in size. Minor amounts of sphalerite are also included in the pyrite and are often composited with chalcopyrite. Rare, tiny flakes and spindles of molybdenite are observed in the outer selvage to the pyrite veinlet.

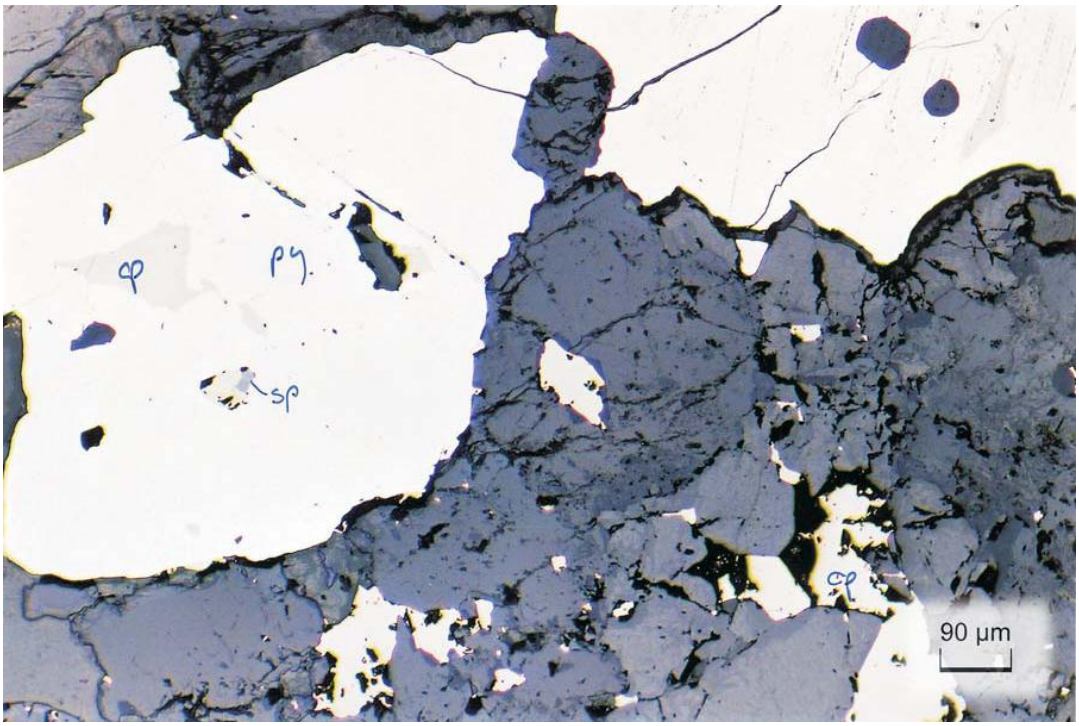

Figure 2-65 Large grains of pyrite (py) in a vein with inclusions of chalcopyrite (cp) and sphalerite (sp) and adjacent chalcopyrite. Vein is a carbonate, plagioclase, epidote vein. Reflected light, magnification 80x. From McCloud, J.A., Teck Cominco, 2005.

According to Misra (2000), many models have been proposed for distinct chemical zoning in ore deposits including: variations in temperature and pressure (Blanchard, 1947), heat of formation of the minerals (White, 1945), relative volatilely of the minerals (Brown, 1948), free energies of formation of solute ions and complexes (Likhachev, 1975), changes in the solvent composition (Spence and de Rosen-Spence, 1975), electrode potential (Govett and Whitehead, 1974), stabilities of metal-chloride complexes (Garrels, 1941; White, 1974), and metal-sulfide complexes (Barnes and Czamanske, 1967), relative metal ion concentrations in the fluid, multiple pulses of fluids, and fluid mixing. It is uncertain which of these factors contributed to zoning in the district, but several were probably important.

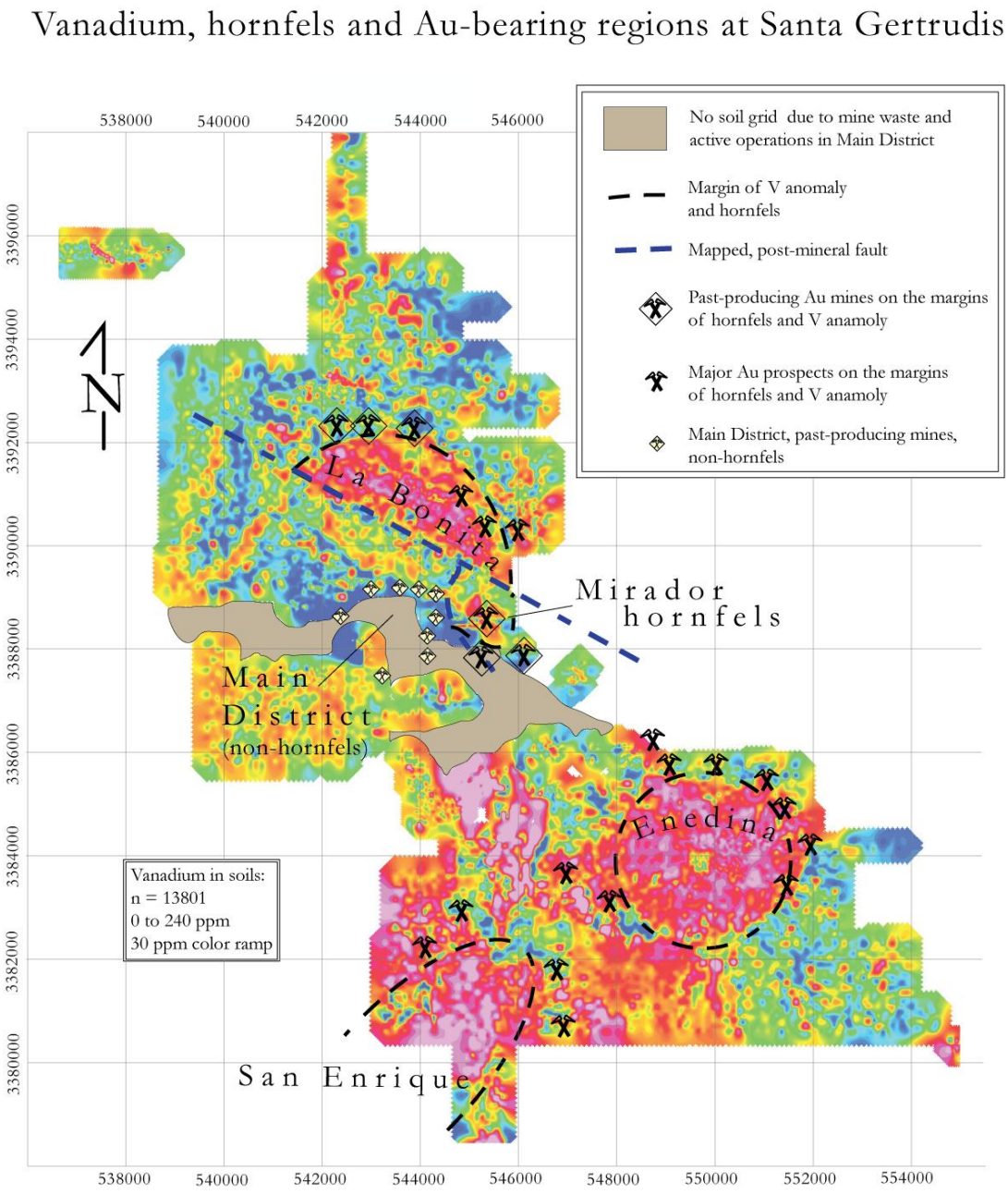

Figure 2-66 Map of vanadium in soils throughout the district. Vanadium defines the brown-biotite hornfels mapped within the four identified hornfels sectors. Gold mineralization flanks the margins of the hornfels and V anomaly throughout the district. Note near circular pattern of Main District open pits. Adapted from John Reynolds, Durango Geophysics.

Figure 2-67 Quartz + feldspar + molybdenite cutting chlorite/epidote alteration. Core from AREN-001, 356 m depth. A Centavo coin for scale. (Animas, 2009)

Animas 2009 Main District drilling program cut several zones of hornfels and skarn-related mineralization and base metals, some accompanying quartz-sericite-pyrite altered felsic dikes (Figure 2-68). The striking geochemical similarities between the Main District and the aureole-related mineralization surrounding the hornfels zones will be discussed in detail in Chapter III.

Figure 2-68 Pyrite and sphalerite in a highly altered felsic dike from 2009, Main District, Animas drilling program. Core from ARTG-001, 474.15 m. Sample assayed at 6.3 ppm Ag, 210 ppm Ba, 39.2 ppm Cd, 1020 ppm Pb and 1715 ppm Zn.

Quartz veins

Although serving a subordinate role in mineralization, the next style of gold mineralization observed in the district is related to quartz veins. Overall, quartz veins are only locally abundant, but the highest abundance of quartz veins accompanies fault breccia and shear-zones in mineralized fault surfaces exposed within the open pits of the Main District (Figure 2-69).

Figure 2-69 Quartz vein fragments in fault breccia in Dora Pit. These fragments can contain gold, or can be barren.

Most quartz veins in the Main District are less than 1 cm wide, discontinuous in strike, and typically in bedding-parallel shear-zones, but otherwise crosscut bedding at relatively low angles (Figure 2-70). Quartz veins can contain calcite associations and generally have limonite after sulfides or open voids where the limonite has weathered away in surface exposures. Animas 2009 Main District drilling revealed minimal quartz veins overall (Figure 2-71).

Figure 2-70 Bedding-parallel shear (pen is parallel to bedding) and quartz veins associated with hematite, goethite, argillization and color leaching. Note that shear in the upper right is localized at the change in rock strength at the sandstone/siltstone interface and crosscuts an older vein set. Photo from Gregorio Mine, courtesy of S.J. Reynolds.

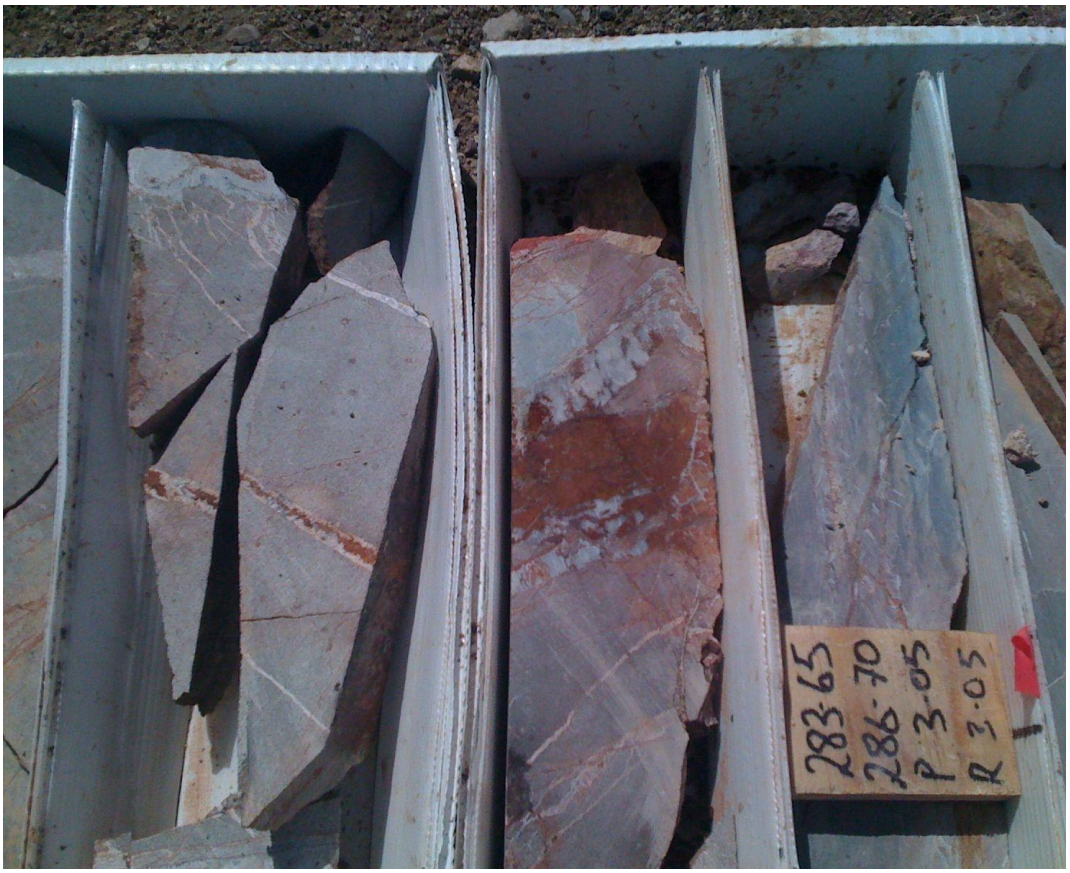

Figure 2-71 Drill core from ARTG-001, 280 m, with oxidation of quartz + sulfides crosscutting older cleavage.

At Gregorio Mine, a 2-m wide open-space quartz-calcite-barite vein bisects the southern wall and is closely associated with a 025 70° NW high-angle fault. It assayed at 1.39 g/t Au, 280 ppm Ag, 377 ppm As, 501 ppm Cu, 44 ppm Hg, 1846 ppm Pb, and 1005 ppm Sb (Figure 2-72). A second sample contained 0.270 ppm Au, 0.900 ppm Ag, 1359 ppm Ba, 200 ppm Pb, and 1076 ppm W. This is the main example of a large-scale quartz vein within the Main District that has economic gold associated with a north-northeast shear-zone. The vein has been removed from the center of the open pit and no maps remain of the association of the vein to northwest-trending, mineralized structures. The vein does not reach the northern wall of the pit, and has presumably been faulted away.

Figure 2-72 Photo at Gregorio Mine, looking southwest at quartz vein in high-angle shear (025 70° NW) with high-grade gold, open-space, euhedral quartz; calcite; barite; and visible copper oxides. Assays reveal abundant As, Ag, Hg, W, Pb and Ba. Scale The base of the vein is 2 m.

High-grade, gold-bearing quartz veins cut fold limbs and axial planar S_1 cleavage and associated with top-to-the-northeast-verging folds. Sample 133853 (Figure 2-73), was a high-grade sample of a quartz vein that intersects a fold in thin sandstone beds of the Ks upper in Dora Mine. The vein assayed at 5.69 g/t Au, 17,000 ppm As, 268 ppm Cr, and 531 ppm Sr.

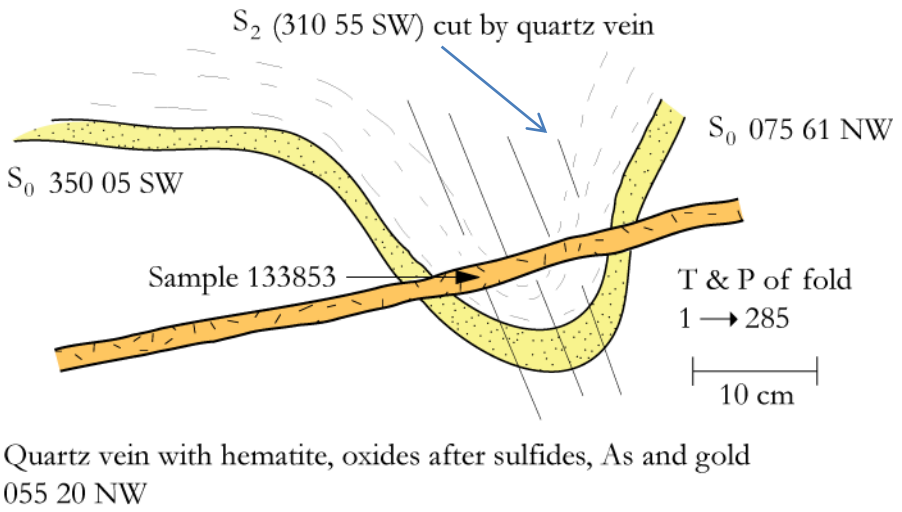

Figure 2-73 Cross section sketch of gold-bearing quartz vein cutting S_1 and S_2 cleavages and folded sandstone in Dora Mine. High-grade sample 133853 of the vein assayed at 5.69 g/t Au, 17,000 ppm As, 268 ppm Cr and 531 ppm Sr.

Throughout the district, quartz veins have geochemical associations similar to the distal disseminated deposits. In addition to gold, silver, and arsenic, the veins typically have elevated levels of Cu, Bi, Sb, Cr, Sr, Pb, Zn, W, Mo, and Mn. A contoured plot of poles to the planes of 100 quartz-vein orientations in the La Bonita hornfels, northwest of the Main District reveals three distinct orientations of mineralized quartz veins. Utilizing the assay data for the quartz veins, Figure 2-74 plots orientation and assay as standard deviations of ppm of bismuth.

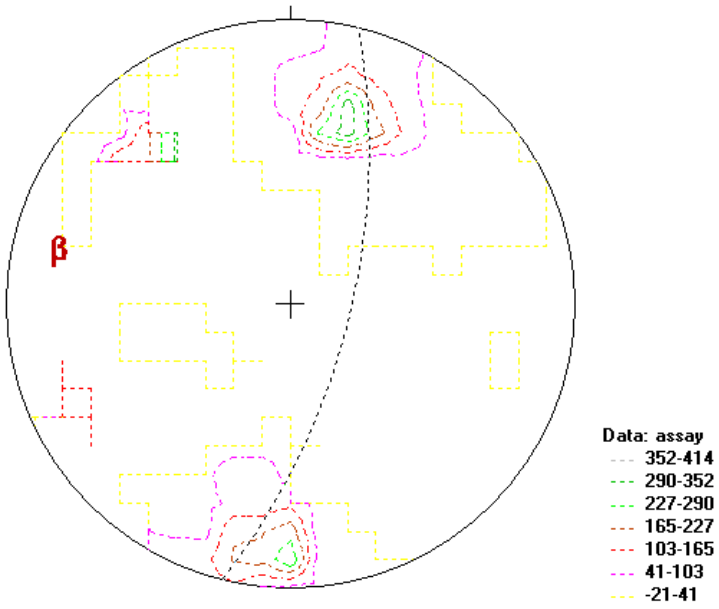

Figure 2-74 Plot of contoured poles to planes of 100 quartz vein orientations from the La Bonita hornfels. Color contours associated with Bi ppm. Calculated beta axis of vein orientations is 17° → 284.

Poly-metallic veins

Poly-metallic veins are at least an order of magnitude less abundant than the quartz veins. They are characterized by 0.5-to-1cm wide, silvery-gray veins crosscutting the S_1 cleavage. Almost all of the examples of poly-metallic veins within the Bisbee Group rocks have been completely oxidized. Examples throughout the district have strong, fracture-controlled haloes of hematite or goethite emanating from the oxidized vein (Figure 2-75).

Figure 2-75 Strong color leaching of Cintura Formation siltstones and later oxidation of poly-metallic veinlet. Oxides disseminated as haloes and fracture controlled. Oxidation may predate minor offset and calcite veins perpendicular to the sulfide veinlet.

The Enedina study area has several poly-metallic veins that flank the hornfels Bisbee Group rocks to the north and northeast. There are old antimony mines on the southeast borders of the hornfels that were visited by Bennett in 1993. A sample taken by this author of a poly-metallic vein that had been mined in the Santiago prospect contained 728 ppb Au, 49 ppm Ag, >10,000 ppm As, 214 ppm Cu, 27.8 % Fe, 204 ppm Pb, 278 ppm Sb, and 9.54 % S. It was in a single, high-angle, northeast-trending, silvery-gray vein that was 3 cm wide.

Relationship of mineralization and structures

Mineralization throughout the district is associated with the intersections of northeast-trending and northwest-trending structures in chemically reactive, structurally prepared Bisbee Group rocks. Within the Main District, this relationship is clearly seen in Maribel, Katman, Toro, Dora, Toro Norte, Ruben and Corral Pits, as wells as in multiple prospects stretching along the whole strike of the Bisbee Group through the district. Gold mineralization is generally focused along the argillized and leached fault gouge and into the hanging wall of the northeast-trending structures, with mineralization bleeding into older, prepared, northwest-trending structures. Figure 2-41, from the water's edge at Maribel Mine, reveals a northeast fault that has strong sericite and clay alteration, quartz veins as fragments, moderate silicification of breccia, disseminated hematite, and liesegang banding. A 2-m skip sample across the leached and oxidized portion of the northeast fault zone featured in Figure 2-41 contained 33.48 gpt Au, 2.3 ppm Ag, 856 ppm As, and relatively low to trace amounts of Zn, Pb, and Sb.

The mineralization does not extend along strike or dip of either the northwest-trending or the northeast-trending structures, nor along the linear, plunging intersections of the two fault planes. Each of these potential structural controls to mineralization pathways have been tested in drilling extensions of multiple open pits within the Main District, all without avail.

Rose diagrams of mean gold grade (ppb) (Figure 2-76) in surface samples in mineralized structures versus the azimuth of the structures reveals that the gold grades are 3-5 times greater in northeast-trending structures than in the northwest-trending structures (n = 112).

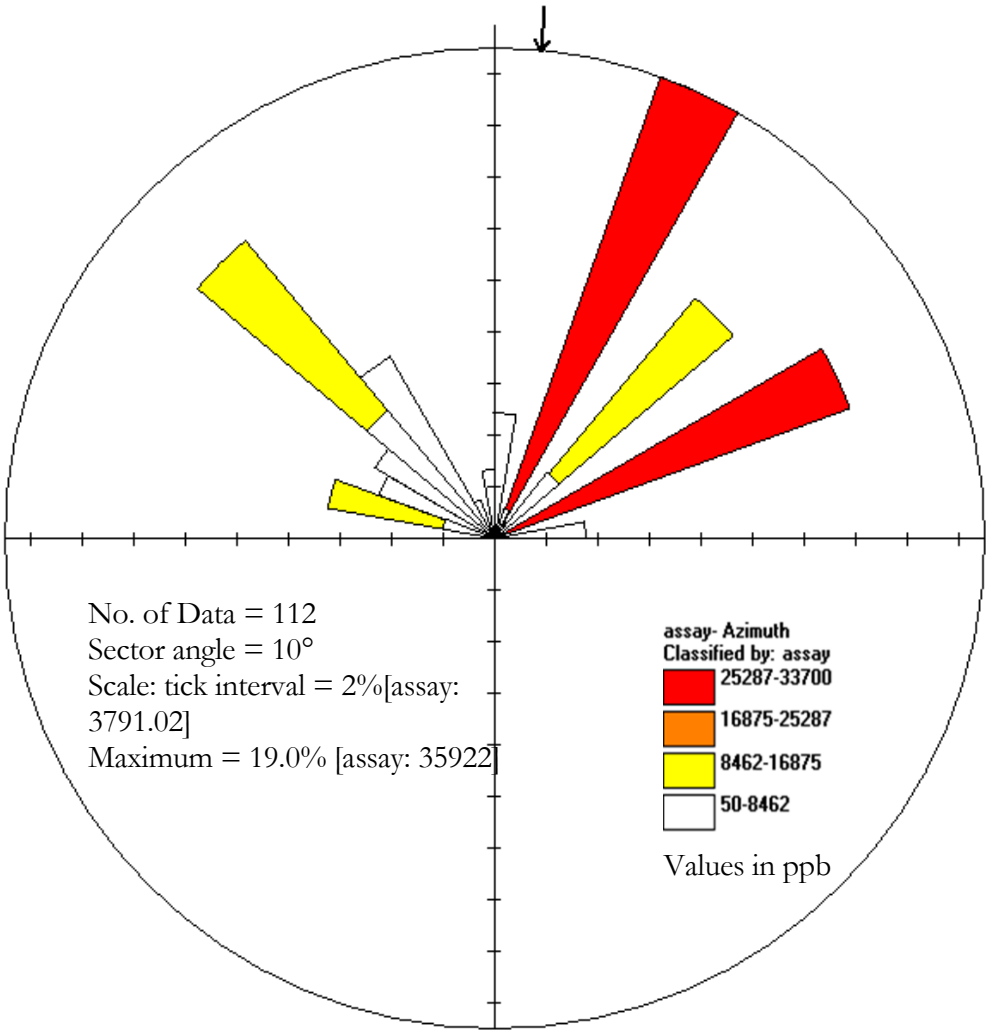

Figure 2-76 Northern hemisphere rose diagram of gold assay in ppb versus the azimuth of the mineralized structure it was sampled from in the Main District.

Within the Enedina study area the northeast-trending structures exhibit a variation of mineralization with zoned geochemistry as a function of distance from Enedina Hill. Continuity of mineralization (Figures 3-19; 3-20; 3-21; 3-22; 3-23) along the northeast-trending structures and geochemical zoning reveals a potential cause for irregular, discontinuous gold mineralization observed elsewhere in the district. As is the case in the Main District, the

intersections of northwest-striking and northeast-striking structures on the periphery of the hornfels act as the sites that host the most gold mineralization, but only in the preferred lithologies and in the gold-geochemical zones. These include La Gloria, Esperanza, Lupita, Greta, Nelly, Jabali, and El Tigre prospects. Silicification styles are identical to the Main District silicification and are abundant on the periphery of the hornfels, as observed within the aforementioned prospects. Decalcification is strong throughout the Enedina study area, focused along the northeast-striking structures distal to the center of the hornfels.

Although the northwest-trending and northeast-trending structures and their intersections have been reactivated in a brittle manner, evidence suggests they each originated under higher confining pressure and ductile conditions. Relative timing reveals that the northeast-trending structures postdate the northwest-trending structures and acted as primary conduits for later mineralization. The highest gold grades are observed in conjunction with the northeast-trending structures at or near to the sites of intersections with mineralized northwest-trending faults.

Rock Reactivity

Mineralization styles and gold grades vary within the terrestrial Glance, Morita, and Cintura Formations and the marine Mural Limestone. Mechanical factors, chemical factors, and the degree of metamorphism may have played a role in concentrating economic gold.

Mineralogy, matrix composition, low porosity, and low reactivity within the Glance Conglomerate generally limited mineralization within the formation. Minor sulfidation of diagenetic iron produced scattered pyrite, but the sparse concentrations are reflected in the limited porosity and reactivity of the mineralogy. Annealing of the sand grains and hornfelsing

throughout the Glance Conglomerate, possibly related to thrust burial and later contact metamorphism, further reduced porosity and permeability.

The non-calcareous, continental clastic sediments that comprise the majority of the Morita Formation limit reactivity to mineralization. The Trinidad Mine, mined by Campbell in 2000, produced 15,380 ounces from a mineralized lens of the calcareous lowermost Morita Formation and upper Glance Conglomerate. Here, mineralization was concentrated along a bedding-parallel shear-zone.

Alteration and mineralization of Kos (along the Morita – Mural contact) in prospects and mined areas include typically stratiform silicification of the unit, including druzzy quartz in the fossil molds, as a process of total replacement of the unit. It is the only unit in the district to experience wholesale replacement by silica. Gold grades in Kos in mineralized areas are typically higher than in the rest of the district, leading to several mines within the Kos, with higher grades and lower strip ratios, including San Ignacio and Toro Norte. The minimal thickness of the Kos limits the economic potential of deposits centered within the Kos.

Alteration and mineralization within the Ko are varied, but the consensus is that the unit is not a favorable host for gold mineralization. Typically, the massive beds are not cut by any hydrothermal veins nor do they contain abundant hydrothermal pyrite. Evidence of pre-mineral shearing with bedding-parallel slip is typically absent within the massive beds. Mineralization in close association with the contact of the Ko and the Kos reflects a change from massive bedding to more fissile and weaker bedding. This is evident in San Ignacio, Toro Norte, and Ruben Pits (Figure 2-77).

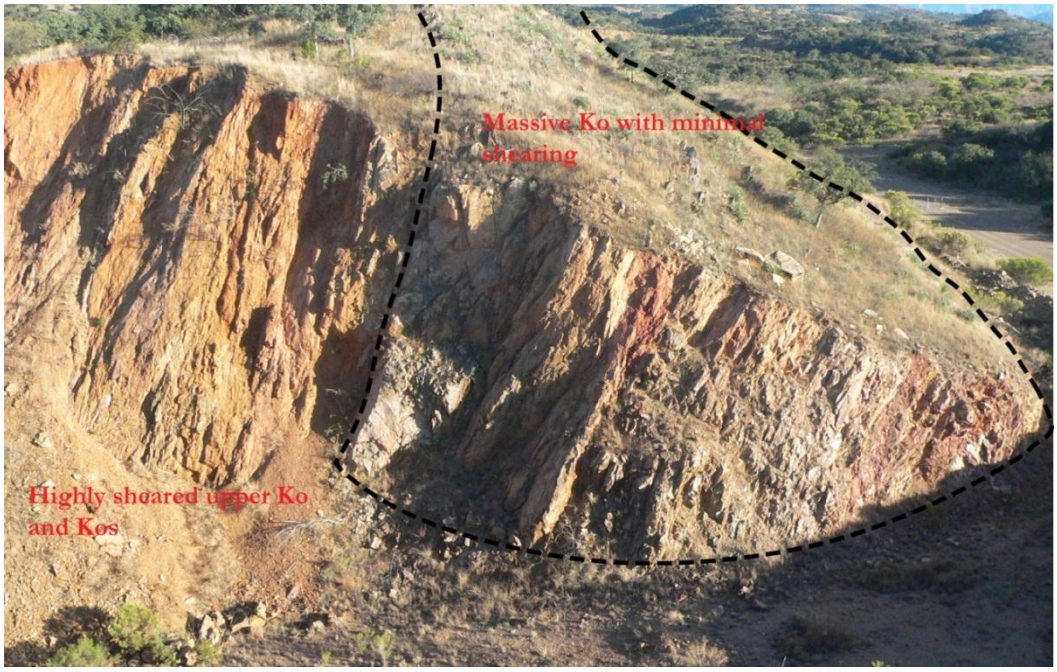

Figure 2-77 Photo into Ruben Pit, looking southeast down strike of overturned bedding and bedding-parallel shear zones. Note extreme difference in alteration and shearing in the massive Ko limestone bedding versus the weaker Kos, which has the bulk of the deformation and mineralization.

Silicification in the Ko typically is in fault breccia incorporating angular clasts of Ko limestone in silica-rich, locally gold-bearing matrix. This character is exclusively observed in association with select northeast-trending faults and spawned many prospects throughout the district due to the ease of identification and to high-grade gold samples observed in the silicified breccias. Typically the silicification and the gold grades were absent in the subsurface in subsequent drilling of the northeast-trending structures. Several gold-bearing, silicified breccias remain in the Santiago, Greta, and La Gloria prospects, closely associated with northeast-trending structures. They display pod-like, lenticular, shapes, ranging from several meters to tens of meters along the long axis, and discordant to the Ko bedding. They also

typically have overprinting slickensides, evidence for multiple fault movements recorded since mineralization.

The thinly bedded Kel Limestone is typically a poor host to mineralization. Decalcification of the Kel limestone is minor, but present in the Main District and the Enedina study area. No deposits were ever located on the Kel exclusively, perhaps due to the lack of reactivity to mineralizing fluids.

The Ks-upper and Ks-lower units locally host mineralization. They exhibit variable decalcification and subsequent compaction. Gold mineralization mined from the Ks units was typical, distal disseminated gold, associated with brittle to brittle-ductile shear zones sub-parallel to the strike of the units.

The Kl unit, a limestone-dominated unit at the top of the Mural Limestone, is not a favorable host to mineralization. Decalcification of the Kl limestone is limited to the periphery of the Enedina and San Enrique hornfels and exposed in the Main District open pits. Replacement skarn of the Kl Limestone is observed flanking the Enedina hornfels, but is generally uneconomic andradite garnet-after-magnetite with minor, localized disseminated 1% Mo and Zn. No major deposits were ever located within the Kl Limestone; perhaps it may have resisted chemical alteration during mineralization.

The Cintura Formation (Ksl) is the most productive unit in the district. The lowermost 100 m of the Cintura Formation is highly calcareous and contains abundant beds of coarse-grained, weakly calcareous sandstone. Main District mining, accomplished by Phelps Dodge, recovered 215,000 ounces of gold at an average grade of 2.1 g/t Au from the lower Ksl in Becerros Norte, Becerros Sur, Maribel, Katman and Manueles Sur Mines. This accounts for 38% of all

of the gold that was recovered from Santa Gertrudis. More importantly, the gold mineralization is highly compartmentalized by structures and only represents 3 km^2 of the entire district. Elsewhere in the district, the Cintura Formation is not considered a productive host, except in select, structural-controlled sites surrounding the Enedina hornfels study area discussed in Chapter III. The calcareous nature of the lower portions of the unit and the coarse-grained sandstones with a calcareous matrix may have increased porosity and permeability, allowing for concentration of mineralization.

Although spatially associated with mineralization in Becerros Norte and Sur, the diorite was not a host for mineralization. Field inspection, drill-hole data, and 3-D visualization reveal that the diorite is in structural contact with the mineralized hanging wall and contains none of the alteration typically associated with Santa Gertrudis mineralization. In Becerros Sur Mine, a felsic dike, presumed to be related to the Las Panochas Granite, cuts the diorite. The felsic dike is highly altered by quartz-sericite-pyrite, and the diorite has disseminated pyrite when in contact with the felsic dike.

Mineralization associated with the Las Panochas Granite includes skarn, mostly localized along marble/hornfels contacts, and quartz-stockwork-hosted chalcopyrite and molybdenite, which cut the granite and the surrounding metamorphosed host rocks. The stockwork zone is the primary economic target according to Smith (2006). Alteration styles are similar to a porphyry system, including weak to strong phyllic alteration and geochemical evidence of potassic alteration, but the system lacks widespread disseminated mineralization. Based on limited soil data from Teck Cominco, weak base-metal zoning has a central Mo core, followed outward by Cu, Pb and Ag/Au, which extend 2.5 km from the central portion of the intrusive

stock as distal disseminated and vein-hosted mineralization in variably metamorphosed Bisbee Group.

The lamproite dikes have been proposed as the causative intrusive for gold mineralization in the district. Multiple samples of the dikes and the rocks they intrude have been encountered during the multiple drill programs and rock-chip sampling. There is no clear relationship to gold mineralization and lamproite dikes based on identifiable geochemical associations. One example of a lamproite sampled with gold was along the La Gloria Shear, north of the Tracy prospect in the Enedina study area. A wide lamproite sill is offset several meters by the northeast-striking shear-zone. This offset of the dike is a reactivation of the fault, based on the larger offset in the Bisbee Group. Multiple overprinting slickensides along strike of the fault, and overprinting mineralization, imply movement on the fault after mineralization. Within the hanging wall of the shear zone, the lamproite has abundant fracturing, thin calcite veins and iron-oxide infiltration from the surrounding ore-bearing rocks. The sample was taken within the fractured and supergene enriched 2-m wide lamproite section directly adjacent to the fault. Subsequent sampling by the author revealed that the zone of mineralization extended a few meters from the fault, and that the fractured, non-oxide-bearing lamproite was below detection for gold. It is possible that the faulting, as reactivation, assisted in grinding the lamproite and mineralized rocks, allowing for element redistribution into the lamproite as a surficial process, post-mineralization and post-lamproite intrusion.

Much speculation has been made about the spatial and temporal associations between gold mineralization and lamprophyre intrusions (Boyle, 1979; Rock and Groves, 1988; Rock, 1991). However, Müller and Groves (2000) state that lamproites (Group I and II of Foley et al., 1987) are rare and are not associated with gold or base-metal mineralization. Crosscutting

relationships reveal that the lamproites cut the Cu-Mo-Au mineralization related to Las Panochas Granite.

There is a weak spatial correlation to mineralization and an assortment of post-mineral dikes, but the relative lack of mineralized zones within the dikes precludes any association gold mineralization. It is clear that the dikes cut the alteration associated with gold mineralization within the district, commonly along the structural weaknesses that the mineralization previously utilized. Like the lamproites, the undifferentiated dikes cut the chloritized diorites, Las Panochas Granite, and the hornfels. In Ruben Pit, an andesite intrudes parallel and adjacent to a high-grade zone of northeast, fault-controlled gold mineralization. The dike post-dates the tectonic brecciation along the fault, as well as the intense leaching and silicification indicative of high-grade mineralization along the fault.

Within the Enedina study area, the bedding-parallel shear structures and associated fabrics have been overprinted by later thermal alteration and hornfelsing, effectively locking the structures and preserving the older deformation. This differs from the Main District since reactivation of these structures played a key role in providing host sites for future mineralization; hornfelsing had an opposite effect at Enedina by reducing permeability, porosity, and resisting fault reactivation. This led the exploration geologists with Animas Resources to conclude that the hornfels rocks acted as a poor host for gold mineralization. Two exceptions to this conclusion are the Red fault at the Mirador study area and the El Tigre fault in the Enedina study area, which were faulted in a brittle fashion through the hornfels and thus host mineralization.

Mineralization models

Although many possibilities exist for the cause(s) of mineralization, four models have some agreement with observed spatial and crosscutting relationships, alteration styles, and geochemical signatures. The four proposed models for gold mineralization in the district are: 1) intrusive-related gold associated with the lamproites or undifferentiated dikes, 2) recycling of sediment-derived, detrital gold in the local Bisbee Basin rocks (heat-engine model), 3) intrusive-related to a Las Panochas Granite-style stock, and 4) mineralization associated with mid-Tertiary extension. There is always the distinct possibility that several of the models are correct, but determining if the gold is sediment-derived (Kirk, et. al, 2001) is beyond the focus of this study.

Although volumetrically insignificant, the lamproites and undifferentiated dikes are present throughout the district. They are mapped in most of the open pits, locally intruding parallel to structures identified as ore-bearing. In these cases, the dikes crosscut the mineralization. Geochemical studies of the dikes and the units they intrude do not reveal any spatial or geochemical associations with gold. The lamproites are anomalous in Ni and Cr, but an average of 15 lamproite dikes contains less than 20 ppb Au. The lamproites cut the mineralization present in the Las Panochas Granite, therefore they are older that that style of mineralization. The potential for the lamproites to have provided a heat engine to drive hydrothermal fluids preceding or during emplacement of the dikes is one scenario that would involve the lamproites and gold mineralization, yet post-dates the mineralization at San Enrique. The gold-bearing fluids could have been derived from the lamproites or driven from the surrounding rocks. Although this hypothesis has merit, it does not explain the association of gold prospects, margins of the hornfels, and the vanadium soil anomaly illustrated in Figure

2-66. Gold is associated with Ag, As, Mo, Cd, Mo, Bi, Zn, S, and Pb (Figure 3-50) in the deep drilling by Animas (2009, Main District). If the Main District mineralization is purely associated with the lamproite and undifferentiated dikes, then an assumption is that the other elements are also being supplied / driven by the lamproites. Gold is associated with Ag, As, Cu, Mo, Cd, Zn, and Pb in the San Enrique, hornfels and skarn mineralization (Figure 3-29). Gold is associated with Ag, As, Cu, Mo, Mn, Sb, Bi, Zn, and Pb at Enedina Hill (Figure 3-26). The similarities in gold associations in the three areas are striking, yet the suggestion at Enedina and San Enrique is that the hornfels and skarn are older than the lamproites. The lamproite hypothesis also fails to address the background gold found in the hornfels, locally in excess of 100 ppb.

Deriving the gold directly from the sedimentary rocks has merit, but the aforementioned geochemical associations would also have to be explained. In the heat-engine model, the combination of magmatic, base-metal-bearing and acidic fluids may have liberated the gold from the Bisbee Basin rocks. In this scenario, either, or both of the intrusive suites could have driven mineralization. Alternatively, the melting of continental crust may have supplied the source for the gold and the formation of the peraluminous, S-type Las Panochas. This may address the issues with S-type granites and gold mineralization (Reynolds, 2010; John Wilson 2008, per. comm.). Although this idea has merit, determining if it is a viable hypothesis is beyond the scope of this study. Whether gold is igneous- or sediment-host-derived has been an ongoing scientific argument in the world's largest gold deposits for decades (Carlin, NV; Witwatersrand, South Africa). Multiple tests of the igneous- or sediment-host-derived hypotheses in those areas have proven contrary.

Gold mineralization derived from the Las Panochas Granite is discussed in Chapter III, Enedina study area. The hypothesis focuses on the base-metal zoning and hornfels and skarn possibly related to felsic intrusives.

The final alternative is that some of the gold mineralization occurred in association with mid-Tertiary extension. Some mid-Tertiary normal faults have been silicified and perhaps mineralized, but subsequent movement reactivated these fault zones, forming fault surfaces and striations that cut the silicified fault breccias. Also, the main movement of these normal faults postdates mineralization, cutting off ore grades in several pits. This author concludes that this model has viability, but lacks data generated from testing this model. Further exploration of this model is warranted.

III. CASE STUDIES

Enedina Study Area

The Enedina study area, located 14 km southeast of the Main District (Figure 3-1; Figure 3-2), is 15-km^2 zone of hornfels and garnet skarn developed from the Bisbee Group. The area was chosen due to the excellent exposures of hornfels and skarn, proven-gold mineralization, and the abundant historical data. Within the Enedina study area, four probable gold reserves have been historically identified since the Phelps Dodge era: La Gloria, Greta, El Tigre, and Tracy prospects (Figure 3-2; Figure 3-4).

Enedina Geology

The Enedina study area is centered on a belt of northwest-striking Mural Limestone, flanked to the northeast by Morita Formation and to the southwest by the Cintura Formation (Figure 3-4). The units generally strike northwest, dip moderately southwest, and are upright. The area has a large, open, southwest-plunging syncline that causes the units to deflect out of their typical northwest trend. Northwest of the syncline is the northeast-trending La Gloria shear zone, with similar-trending faults present to the east of the syncline., Southwest-dipping, low-angle faults are present throughout the study area, several of which contain sheared lamproite dikes. Felsic dikes are present to the east, northwest, and west of Enedina Hill.

The majority of the study area is hornfels of varying metamorphic grade. The hornfels defines a circle of metamorphism 2.5 km in diameter and with increasing metamorphic grade towards the center. The geographic center of highest-grade metamorphism is named Enedina Hill, and will be used to define a location and the center of high-grade hornfels.

Enedina Structures

The latest movement along the northeast-trending structures is recorded as slightly oblique, strike-slip slickenlines on the silicified breccias and on the limestones of the Ko. This movement is post-mineral, adds some degree of offset to the stratigraphy and most importantly, offsets northwest-trending, bedding-parallel, mineralized shear-zones. This relationship occurs throughout the district and is interpreted as reactivation of older structures, possibly as accommodation structures during low-angle extension or during Basin and Range high-angle extension. Helmstaedt (1996) concluded that the structures were purely pre-mineral or inactive post-mineral, and acted only as channel sites for mineralization along the intersections of northwest-and northeast-trending structures. He cited the lack of offset of northwest-trending mineralization by northeast-trending structures as evidence for lack of movement, but northwest-trending mineralization is clearly offset by northeast-trending structures in several places within the district including southeast of Mirador and at El Tigre. Despite this late movement, mineralization is strongly associated with northeast-trending structures in the Enedina area and in other parts of the district. Reactivation of faulting within the district is not surprising given the complex tectonic history of Sonora, and the potential for the faults to have existed before the Eocene.

Silicification of breccia in 060-trending faults and bedding-parallel silicification/replacement at fault intersections are abundant. Fracturing and faulting are abundant. Fracturing has no obvious preferred orientation and affects all of the rocks in the mapped area, including the limestones. Fracturing seems most prevalent around northeast-trending fault planes. Northeast-trending fault planes are the dominant orientation, with minimal apparent left-lateral offset. Silicification of the northeast-trending fault planes and of the surrounding fractured and

brecciated rocks, and bedding-parallel silica replacement occurs independent of rock type. The structures may be partly related to emplacement of an unexplored pluton hypothesized to exist below Enedina Hill. Legacy drilling in El Tigre, Nadia, La Gloria and Greta focused on the northeast shear-zones and their associated mineralization.

Enedina Mineralization

Mineralization within La Gloria, Greta, and Tracy are associated with the northeast-trending, steeply northwest-dipping La Gloria shear zone. Disseminated and invisible gold associated with arsenic is the dominant deposit type, with strong structural controls and secondary lithological controls. Sigmoidal tension gashes associated with the northeast-trending structures host discontinuous silicified breccia pods, which are tens of square meters in surficial exposure, are highly resistant to erosion, and locally contain gold. Polymetallic veins in the La Gloria and Greta prospects and in other areas peripheral to the proposed hidden intrusion include arsenopyrite with 0.7 g/t gold, stibnite veins, and löllingite veins. Polymetallic veins are uncommon within the entire district.

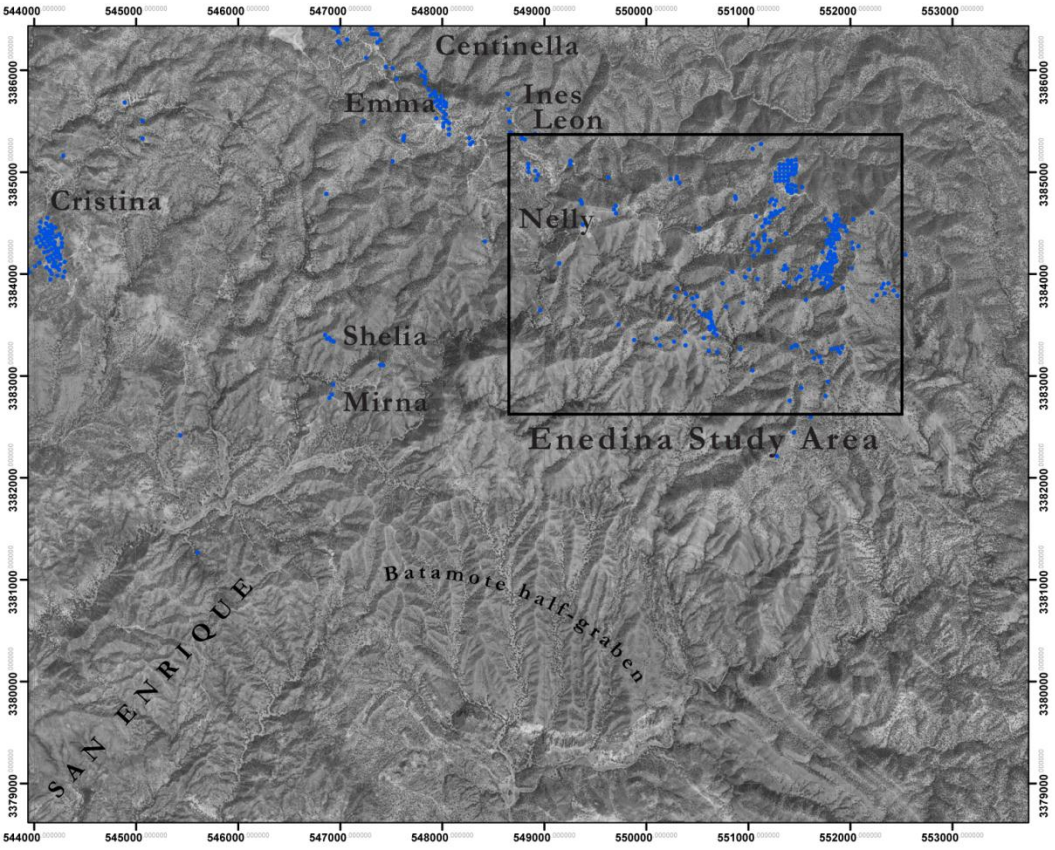

Figure 3-1 INEGI air photo of Enedina study area and surrounding prospects, 14 km southeast of the Main District. Blue dots represent drill collars.

Mineralization within the hornfels area is strongly zoned, both from the soil geochemistry and from the changes in mineralogy evident in the field. The zoned base-metal system is approximately 4 kilometers in diameter with the strongest zonation evident in the calcareous units of the Bisbee Group. Proximal to the center and extending up to 800 m, magnetite is dominant as disseminations, veins, bedding replacements, and associated with quartz. The central portion of the base metal shell is anomalous in V, W, and Mo, with 100 ppb gold associated with a central stockwork of high-temperature quartz veins. Scheelite and molybdenite are associated with quartz veins and rarely as disseminations. Beyond the magnetite zone is a narrow sulfide + sphalerite/galena/stibnite zone, both as disseminations of

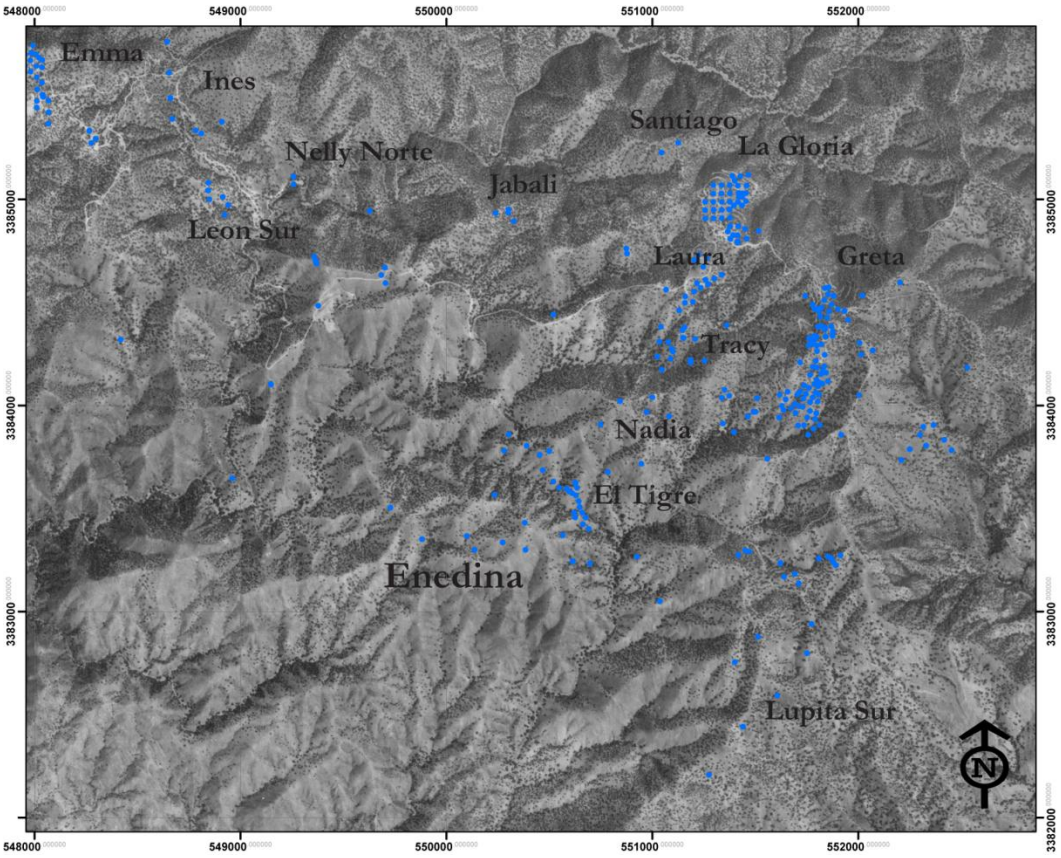

Figure 3-2 INEGI airphoto of Enedina study area with prospect names and drill collars (blue dots).

sulfides and within quartz veins and quartz + specular hematite. Next is a pyrrhotite/ pyrite/arsenopyrite zone, approximately 500 m thick, ranging from a background of 0.5% disseminated sulfide to nearly complete sulfide fractures filling and sigmoidal voids. Quartz + sulfides veins are present as 1 mm-to-1cm-wide veins. Surficial oxidation of sulfide and polymetallic veins is most evident within this zone as seen in Figure 3-3. Drilling by Animas into this zone revealed multiple generations of unoxidized, crosscutting sulfide and polymetallic veins, but with limited vein density.

Figure 3-3 Multiple generations of oxidized sulfide veinlets in a marbled Kl limestone. Goethite is the most common oxide seen in this zone, with jarosite concentrated on freshly oxidizing, sulfide-rich hornfels and skarn.

There is a zoning within the sulfide-mineral zone. There appears to be an increase in the percentage of sulfides moving outward toward the sulfide + sphalerite/galena/stibnite zone. Finally, a pyrite zone extends for hundreds of meters, but it is difficult to distinguish from the background diagenetic sulfides and hydrothermal sulfides present beyond the hornfels zone. Mineralization within the limestone/marble/skarn is limited to an average of less than 2% pyrite, with minor arsenopyrite and pyrrhotite and magnetite when in the magnetite zone. Botroydial smithsonite and sphalerite are prevalent within the Zn soil anomaly, stibnite is within the Sb soil anomaly, and galena is within the Pb soil anomaly. Oxidation of the sulfides is limited to fractures and faults in the skarn. Rarely are the rocks oxidized more than a few

centimeters below the weathering surface. Goethite is dominant, followed by jarosite and finally by limited hematite. Hematite does not become the dominant oxide until 2 km from the center. Reduced-To-the-Pole (RTP) airborne magnetic data of the Enedina area reveal a strong magnetic anomaly coincident with the pyroxene hornfels and the presence of magnetite as replacement skarn and quartz plus magnetite veins (Appendix C).

Quartz, quartz-calcite, quartz-sericite, and quartz-magnetite stockwork increases toward the center of the hornfels zone. Zoning of the quartz veins includes distal quartz/pyrite, medial quartz/calcite and quartz/pyrrhotite/arsenopyrite/pyrite, and proximal quartz/magnetite, quartz/chlorite, and quartz/hematite/sericite.

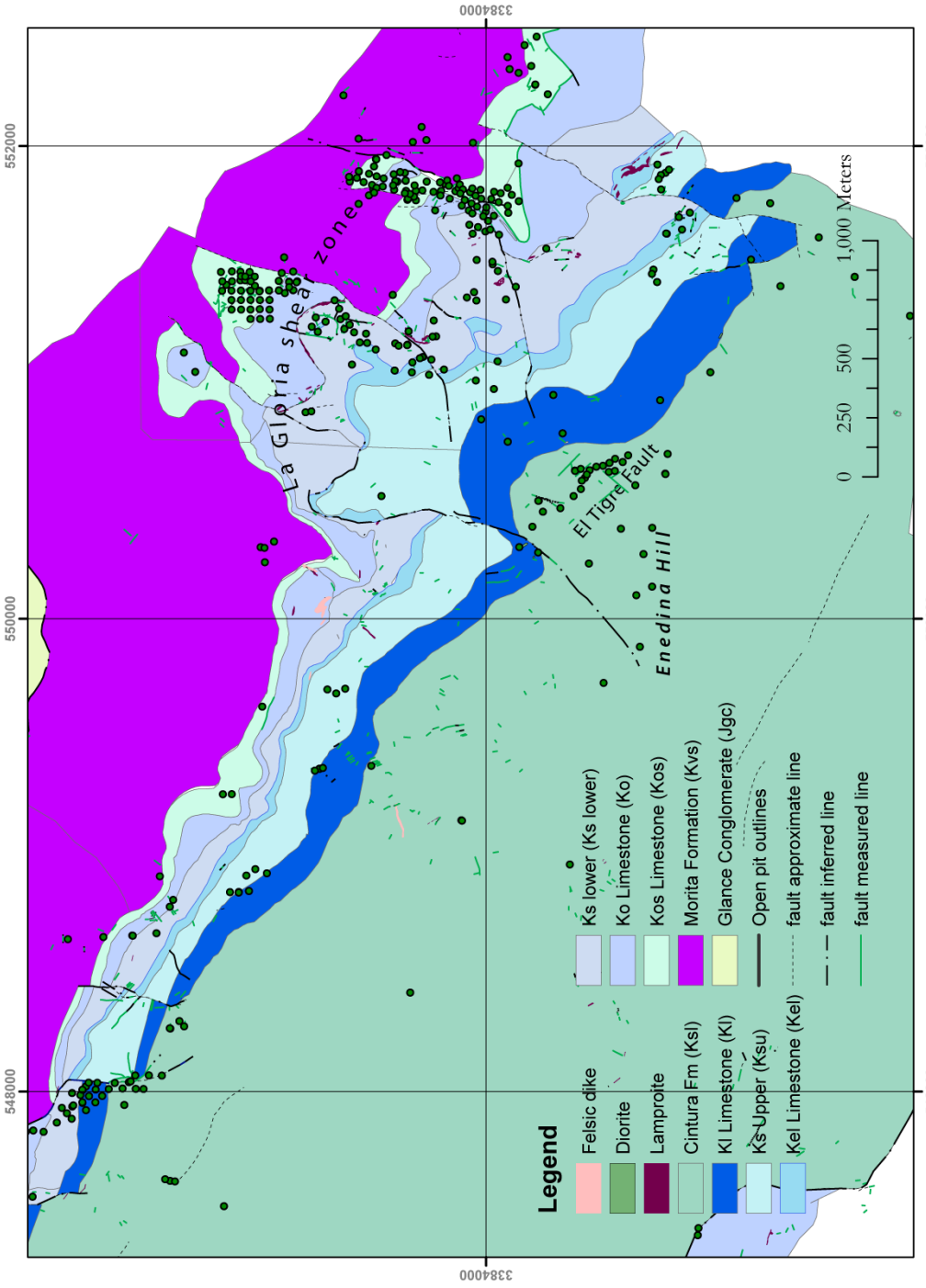

Figure 3-4 Geologic map of the Enedina study area and surrounding geology. Green dots are drill collars.

To illustrate the changes associated within the hornfels zone, I will describe a transect from the least hornfels rocks in the northwest (Ines prospect), toward more hornfelsed rocks in the southeast (Enedina Hill). The transect begins southeast of the Ines prospect (Figure 3-2), where a weak metamorphic overprint is exposed in the calcareous siltstones of the lower Ks unit. A phyllitic texture is observed, especially in the tan and black shales, along with a minor tannish weathering rind. This phyllitic aspect could represent the results of D_1 deformation rather than effects related to the hornfels. A slight hardening and loss of fissility in the siltstones and shales is observed in the washes. Sandstones show minor recrystallization, but still have a sandy texture; limestones are competent and show no recrystallization. Minor decalcification is present within the limestones but is not necessarily associated with mineralization (Figure 3-5; Figure 3-6).

Figure 3-5 Decalcification and goethite staining in Kl limestones peripheral to the central zone of most intense hornfels at Enedina Hill.

Figure 3-6 Strong decalcification and goethite/clay infill peripheral to Enedina Hill. Note the unaffected siltstone/hornfels interbeds in the lower right hand corner.

Continuing to the southeast, the first identifiable signs of true hornfels are observed in the shales and siltstones of the Ks, Ksl, and interbedded siltstones of Kel, Kl, and Ko units. Hornfels was identified by a hardening of the rock, accompanied by concoidal fracture, grain-size reduction, color change, loss of fissility, and a brownish-tan surface weathering rind all of which were used to identify hornfels rock. Although the intensity of metamorphism increases to the southeast toward Enedina Hill, variability in lithologies dictate the degree of hornfelsing. Quartzite is observed in the road to the south of La Gloria Camp, and is prevalent in the Cintura Formation. Recrystallization of the Kl to marble is observed south of La Gloria Camp.

A strong hornfels is present in the Cintura Formation, with albite-brown-biotite hornfels as the dominant alteration (Figure 3-7); these rocks are similar to rocks observed in the Mirador drill holes. The hornfels is dark gray to gray-green, harder than steel, has concoidal fracturing, and is chloritically altered. Where present, the micritic nodules of the Ksl have been completely replaced by epidote and chlorite, appearing as light green nodules in a fine-grained, dark gray to black hornfels matrix. The transect finishes at the "center", an intriguing area at Enedina Hill. The Cintura sandstone at Enedina Hill has been altered to quartzite, the siltstones are pyroxene hornfels, and the limestones are magnetite skarn. The rocks have been highly fractured and sericitized. Quartz veins, 5-cm-to-1-m-thick, crosscut the entire area, commonly at densities exceeding 10 per meter. The quartz can contain > 0.5% sulfides, 2% sericite books (5 mm) and pockets of hematite greater than goethite. The central portion of the mineralized shell is anomalous in V, W, and Mo, with 100 ppb gold associated with the central stockwork of high-temperature quartz veins. In 2000, Anderson proposed the idea of the Enedina Hill quartz swarm as a quartz cupola capping a magmatic stock (Figure 3-24). Mapping in the Enedina prospect reveals that the stratigraphy deflects around high-grade hornfels (Figure 3-4).

Photo 3-7 Distal alteration of brown-biotite hornfels northwest of El Tigre similar to drill core from Mirador and El Tigre. Note albite-epidote hornfels alteration along fractures.

Enedina Hornfels

Since the majority of the protolith was weakly to non-calcareous siltstone and sandstone, much of the Enedina study area is now brown-biotite hornfels and quartzite. Thin sections reveal that there are three varieties, and generations, of hornfels; the highest grade is associated to dark green pyroxene calc-silicate hornfels that is cut by biotite hornfels, which is then cut by a late-stage epidote hornfels (Figure 3-8). Presumably, the pyroxene hornfels represents the maximum temperatures and the albite-epidote hornfels represents the waning stages of isochemical alteration due to decreasing temperatures.

Rock block (left) and thin section (right) of ARTG-004 424 meters. The rock is pyroxene calc-silicate hornfels (dark green) cut by quartz veins with alteration zones of epidote hornfels (pale) and biotite hornfels (brown) Thin section slide is 27 x 46 mm.

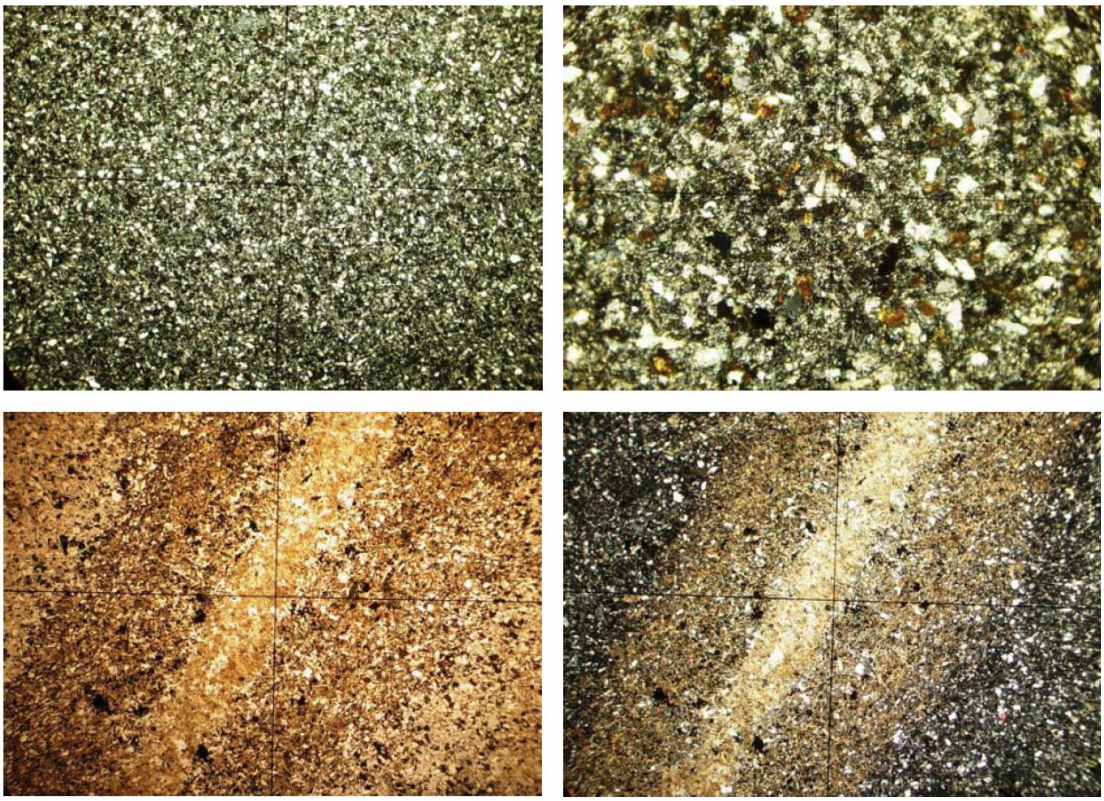

Figure 3-8 Photomicrographs of ARTG-004 at 424 m. Upper left photo, 5.7 mm wide, shows fine hornfels texture; upper right photo 2.6 mm wide, shows same tight interlocking hornfels texture. Birefringent grains are augite. Both top photos XP. Lower photos in PP left and XP right, 5.7 mm wide, show a quartz-biotite vein cutting the rock with the alteration selvage of brown biotite. The pale outer alteration selvage is epidote hornfels. (Burnham Petrographics, 2009).

Carbonaceous mudstones were not isochemically altered to hornfels, but carbon mobilization was evident in the Enedina and El Tigre drill-holes and in surficial leaching that is

commonly associated with fractures and pre-mineral faulting. The micritic nodules common in the non-hornfelsed Ksl siltstones are replaced by quartz and chlorite on the fringe of the zone, and by an arsenopyrite/pyrite/pyrrhotite + quartz/chlorite mineralogy near the center of the zone. Based on geochemistry anomalies and the increase in grade of hornfels, the "center" is designated as being located at drill-hole EN-101 (Figure 3-9).

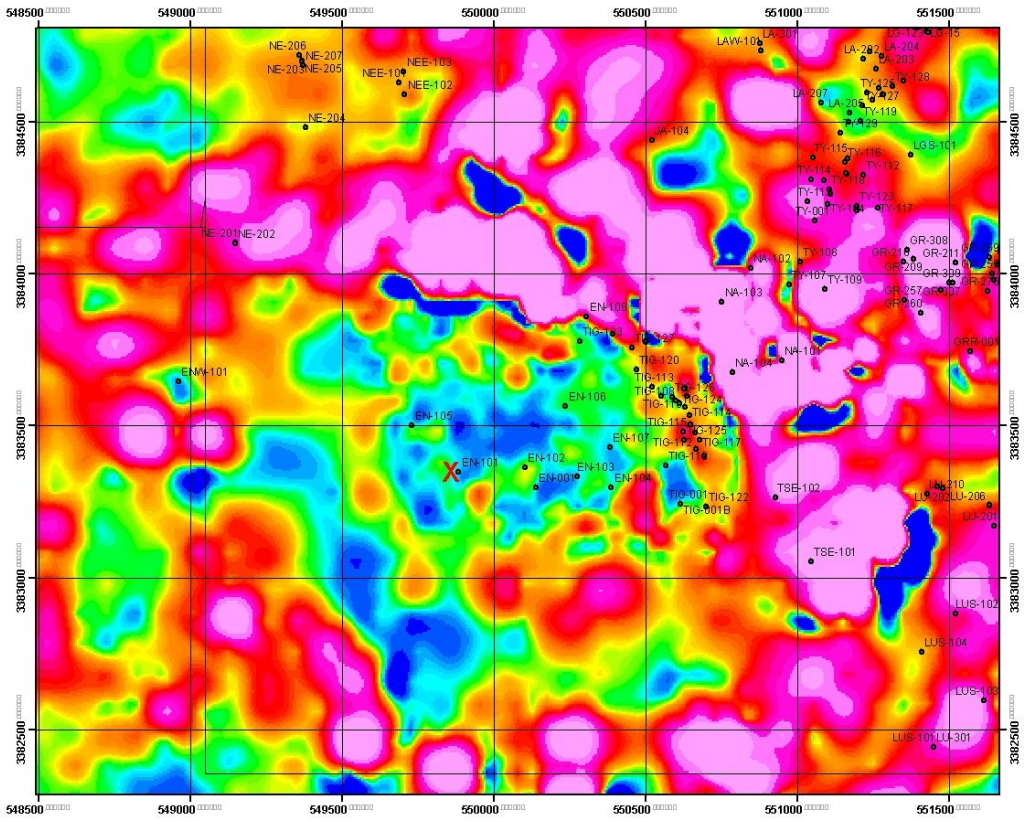

Figure 3-9 Zn soil anomaly surrounding "center" point. Red "X" marks the spot. Scale 1:12,800. All of the rocks in this view are hornfelsed/thermally altered.

Field evidence for retrograde metamorphism includes epidote and chlorite overprinting the hornfels, along with quartz and calcite pseudomorphs, calcite veins, quartz-calcite veins, quartz-chlorite veins, quartz-magnetite veins, and quartz-sulfide veins.

Enedina Skarn

Three typical types of skarn have been identified within the Enedina study area. The distal skarn consists of patchy, 1-to-10-cm-thick, bedding-parallel or structurally controlled andradite garnet skarn. This grades into massive, bedding-parallel andradite garnet skarn in calcareous rocks interbedded within calc-silicate hornfels (Figure 3-11). Stringer zones of garnet skarn are present up to 3 km away from the central Enedina prospect; massive garnet skarns are limited to 0.5 km from Enedina Hill and coincide with the impure limestones of the Kl and Kel of the Bisbee Group. Hornfels or skarn with a variety of mineralogies were identified including: biotite-sericite-quartz hornfels; andradite-garnet skarn; garnet-idocrase-diopside skarn (Figure 3-10); quartz-calcite-diopside hornfels; magnetite-garnet skarn; and amphibole skarn. By volume, the andradite garnet skarn is the most abundant of the skarns at the surface and in the Animas 2009 drilling, followed by magnetite-andradite skarn and minor amounts of amphibole skarn.

The second skarn style observed is a magnetite skarn, exposed 500 m to 200 m from the central Enedina Hill. The magnetite is associated with the andradite skarn and crosscuts the older garnet skarn. Magnetite skarn zones range from 1% magnetite to 100% magnetite (Figure 3-12) and are dominantly bedding controlled. Magnetite skarn is mostly within the upper portions of the Kl limestone, close to the Cintura Formation, and within the 300 m zone of Enedina Hill. Magnetite is associated with quartz veins crosscutting the less calcareous quartzite beds of the Cintura Formation, within the same 300-m radius zone. A zone of total replacement of Ksl limestone up to 30 cm thick is exposed on the southern flanks of Enedina Hill.

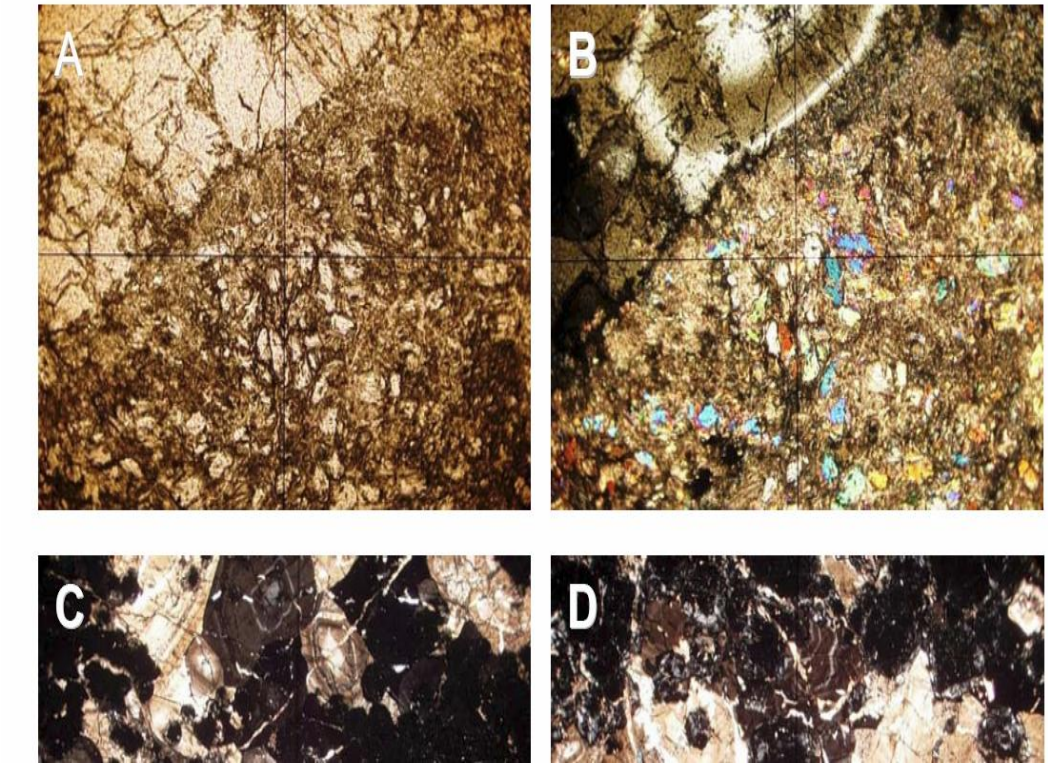

Figure 3-10 ARET-001, Garnet-idocrase-diopside skarn (A and B) at 286 m showing birefringent diopside in calcite matrix on lower left and idocrase on upper left. A is PP, B is XP. 1.6 mm wide. Idocrase has anomalous brown birefringence and compositional zoning. (C) Diopside and calcite at bottom; black equant grains are extinct garnet. Brown zoned crystals are idocrase. XP 5.7 mm wide. (D) Equant garnet grains: isotropic cores with rims showing anomalous birefringence. Zoned grains are idocrase. XP 5.7 mm wide (Burnham Petrographics, 2009).

Figure 3-11 Bedding-parallel and stringer andradite skarn replacing limestone bed in Kl. Erosion resistant stringers of skarn are cutting the greenish hornfels.

Figure 3-12 Bedding-parallel, massive magnetite skarn in the El Tigre prospect. This bed is over a meter thick and contains accessory greenish muscovite.

The third style of skarn is an amphibole skarn zone that overprints the garnet and garnet + magnetite zones, first as patchy zones less than 1 km away from Enedina Hill, then as wider zones within the garnet skarn. Within the El Tigre and Enedina prospects and further to the southeast, there locally are larger, amphibole-dominant skarns. The central pyroxene hornfels (Figure 3-24) within the Cintura has patchy to bedding-parallel amphibole skarns, probably related to the more calcareous nature of the lower portions of the Cintura. Amphibole skarns are dominantly bedding controlled, but several zones have definite structural control. Large, bladed sprays of actinolite-tremolite are common within the amphibole skarn (Figure 3-24), along with elevated base-metal and precious-metal contents, including Cu, Au, Ag, Co, Pb, Zn, Te, Bi, As, Hg, W, and Sb.

Approximately 700 m south of La Gloria Camp, or 1.1 km from Enedina Hill, the Kl and Kel limestones show minor recrystallization. No skarn mineralization is noted in the limestones in this area, despite the presence of hornfels interbedded within the limestones. Within 800 m of the center, the Kel limestone has no evident skarn mineralization and only minor recrystallization. Within 600 m of the center, the Kl is dramatically skarnified, with 2 cm to fist-sized, masses of pale, brownish lime green andradite garnet (Figure 3-13; Figure 3-15), which is zoned. The Kl also contains zones of andradite-magnetite plus chalcopyrite and pyrite, grading into 2 m-thick bedding replacement zones of pure magnetite within the Kl. Magnetite skarn, along with andradite-magnetite skarn, alternate with amphibole skarn toward the central point, presumably dependent on the distance from the heat source, the impurity of the limestones, and structural pathways for fluid and heat flow.

The garnets indicate that the temperature was > 400ºC. Actinolite-tremolite is observed at the contacts between limestone and hornfels. Wollastonite is not evident in the field, but may be present or may indicate that the temperature or X_{CO2} did not reach the stability field for wollastonite (Figure 3-27). Drill core from Teck Cominco in the San Enrique revealed wollastonite in conjunction with marble and skarn associated with the Las Panochas Granite (Figure 3-14).

Meinert (Figure 3-16) illustrates the distribution of mineral assemblages and alteration based on lithology in a skarn environment, with attention drawn to the metasomatic reaction accompanying the formation of a reaction skarn at the contact of hornfels and marble.

Figure 3-13 Zoned andradite garnet skarn from the lower Kl, 500 m north of Enedina Hill.

Figure 3-14 Core photo of drill-hole SE-15-5, Teck Cominco, from San Enrique reveals wollastonite-garnet skarn with quartz/chalcopyrite/moly veins postdating the formation of skarn.

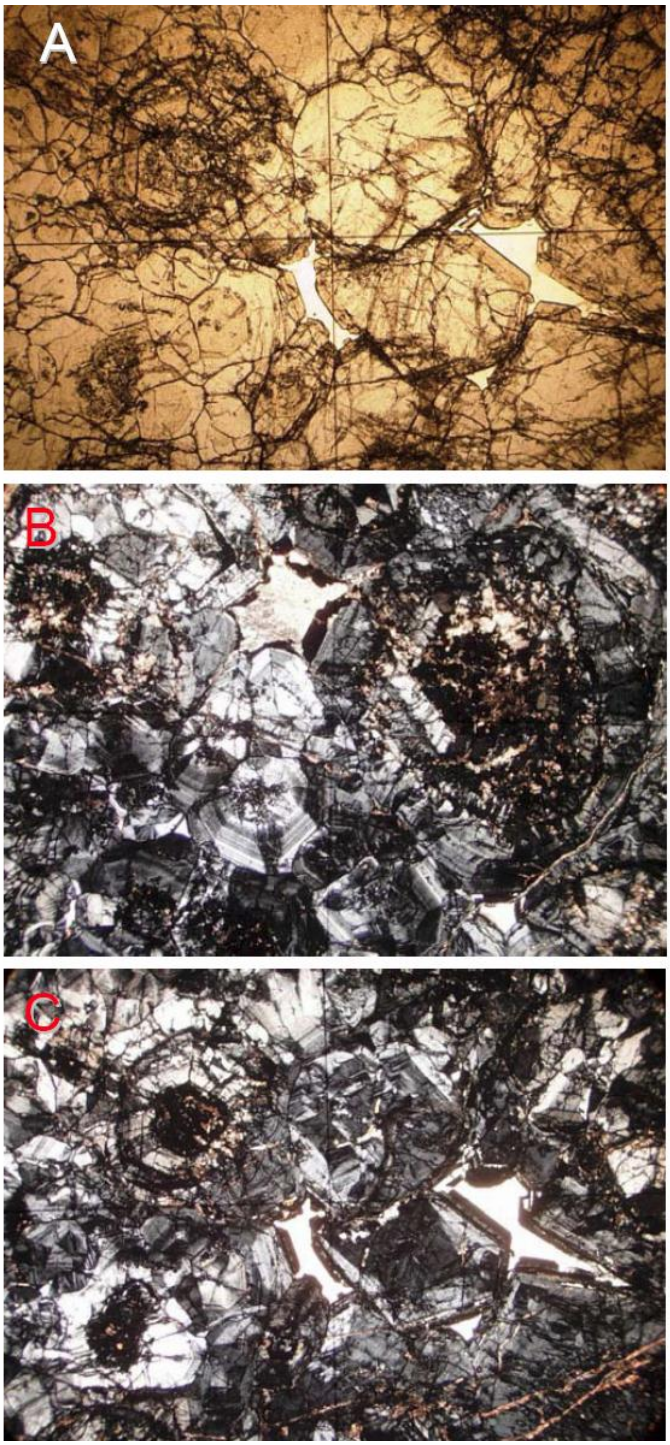

Figure 3-15 ARET-001, 277 m. Zoned andradite garnet skarn (A) shows light brown equant garnet with colorless calcite in PP light, 5.7 mm wide. (B and C) show the garnet in XP, with anomalous birefringence (Burnham Petrographics, 2009).

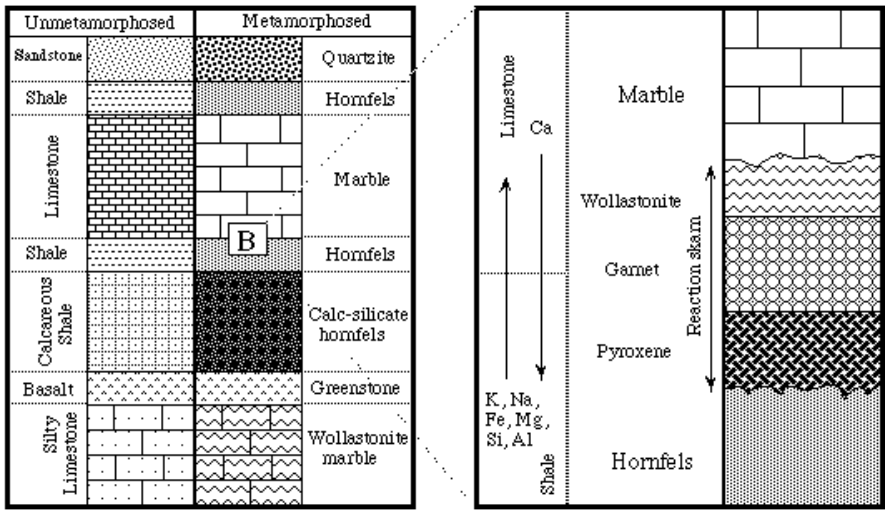

Figure 3-16 Zoning of alteration and formation of marble front and reaction skarn in metasomatic skarn systems. From Meinert, 1997.

Zoning within the skarn is evident from field mapping and from drill core from El Tigre prospect during the 2009 Animas drill program. Outer zones of magnetite skarn were generally in contact with marble or pyroxene hornfels, locally with abundant actinolite and tremolite in the transitions from skarn to hornfels. These zones graded into andradite garnet skarn zones followed by marble zones, which generally were in contact with hornfels (Figure 3-17).

At El Tigre, a northwest-trending fault system, the El Tigre shear-zone, intersects the skarnified Kl. Along with apple-green andradite, a red garnet is present, possibly showing an increase in temperature or change in chemistry along the fault plane. Very little of the Kl and none of the Kel fall within the intense skarn zone, since the units are left laterally offset at El Tigre by the northeast-trending La Gloria shear zone (Figure 3-4). The offset and differing skarn styles in the limestones may imply that the northeast-trending fault predates the skarn. It appears as though the Kl was intensely skarnified within this zone, while the Kel was nearly unaffected.

Figure 3-17 2.40 m of core from ARET-001, El Tigre with gradation from pyroxene hornfels in upper left grading to magnetite skarn then grading to andradite garnet skarn in the middle two rows, and marble as pure white at end of third row and most of fourth row.

Within the study area, a geochemical comparison was made of four general skarn types: andradite garnet skarn, mixed andradite-magnetite skarn, pure magnetite skarn, and amphibole skarn (Table 3-1). Base-metal values are highest in the amphibole skarn, as is the precious-metal concentration. The calculated silver-to-gold ratio in the amphibole skarn is 588:1, indicative of an intrusive source for silver mineralization.

	Skarn type				
	Garnet	Mag/Gar	Magnetite	Amphibole	
Au ppb	27.5	10.0	12.5	144.0	Au ppb
Ag ppm	1.1	0.1	0.8	84.7	Ag ppm
Al %	1.8	1.6	0.7	2.2	Al %
As ppm	76.0	74.0	45.5	1345.5	As ppm
Ba ppm	60.0	20.0	52.0	7.5	Ba ppm
Be ppm	0.8	0.5	0.7	0.7	Be ppm
Bi ppm	2.8	4.0	13.5	565.0	Bi ppm
Ca %	7.0	7.0	1.6	6.4	Ca %
Cd ppm	4.0	<0.5	2.0	39.6	Cd ppm
Co ppm	6.3	7.0	28.5	14.5	Co ppm
Cr ppm	72.0	7.0	59.0	11.0	Cr ppm
Cu ppm	30.5	111.0	159.5	8255.0	Cu ppm
Fe %	7.0	16.2	28.6	6.7	Fe %
Ga ppm	10.0	10.0	20.0	10.0	Ga ppm
Hg ppm	1.8	0.5	1.0	0.8	Hg ppm
K %	0.1	0.0	0.2	0.1	K %
La ppm	8.0	5.0	12.0	5.0	La ppm
Mg %	0.3	0.9	0.9	0.9	Mg %
Mn ppm	2630.0	2330.0	5054.5	3435.0	Mn ppm
Mo ppm	1.5	2.0	45.0	4.5	Mo ppm
Ni ppm	9.3	11.0	21.0	9.5	Ni ppm
P ppm	445.5	270.0	345.5	500.0	P ppm
Pb ppm	3.6	0.1	1.0	8.0	Pb ppm
S %	0.1	0.1	0.2	0.9	S %
Sb ppm	4.5	1.0	3.0	4.5	Sb ppm
Sc ppm	5.5	3.0	2.5	3.5	Sc ppm
Sr ppm	38.5	89.0	215.0	69.5	Sr ppm
Th ppm	11.0	10.0	16.0	10.0	Th ppm
Ti %	0.1	0.1	0.0	0.0	Ti %
Tl ppm	11.5	5.0	5.0	5.0	Tl ppm
V ppm	34.0	22.0	27.5	17.0	V ppm
Zn ppm	197.5	105.0	399.0	2068.0	Zn ppm

Table 3-1 Comparison of averaged samples of four skarn types from the Enedina study area. Note strong base and precious metal associations within the amphibole skarn. Au in ppb.

Overprinting the initial hornfels and retrograde metamorphism is a central zone of sericite alteration extending less than 500 m out from the center. The sericite is overlapped by a propyllitic zone extending out an additional several hundred meters and a distal argillized zone

up to 3 km from the center. Sericite and chlorite alteration is focused along abundant fractures. The K soil and chip anomaly plot done by John Reynolds of Durango Geophysics (Figure 3-18) best defines the potassium anomaly. Potassium alteration is nearly one-to-one with the mapped extent of the hornfels, but it is a minor component of the overall alteration within the system. Potassium feldspar was present in quartz + Mo veins in the core from ARET-001 and AREN-001. Visible feldspar is associated with sulfide-bearing quartz veins bearing sulfides and as irregular replacement zones in the hornfels and skarn. This association was recognized within the higher grade, pyroxene-hornfels zones

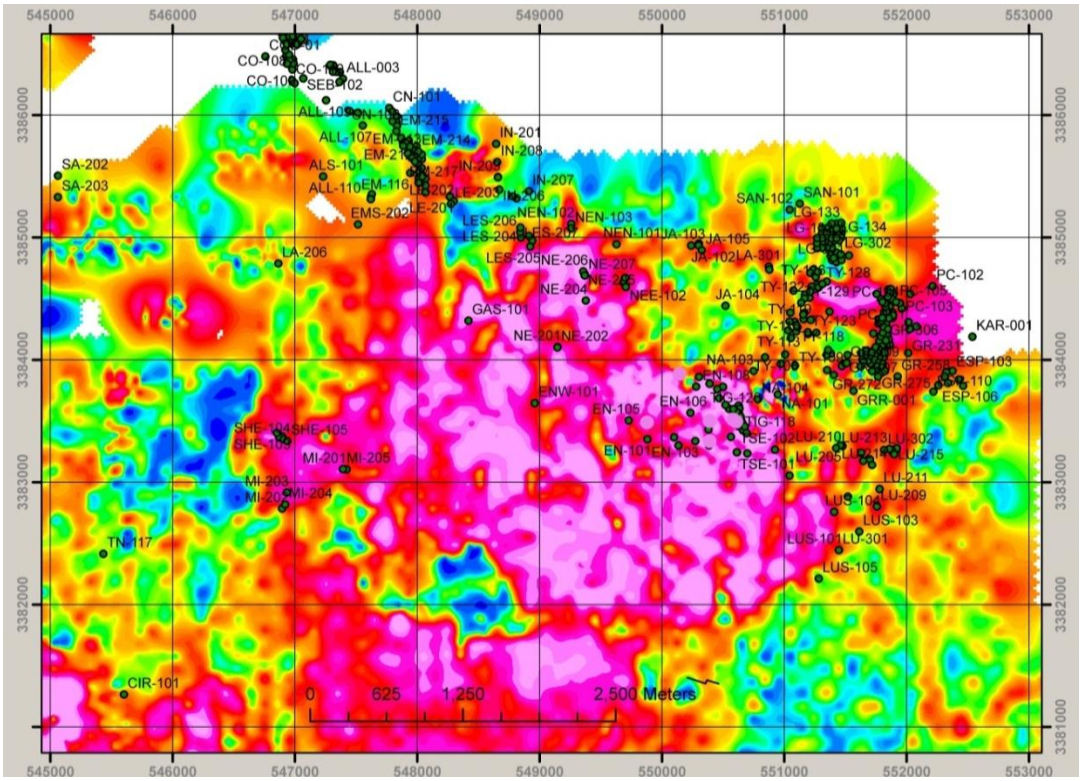

Figure 3-18 Potassium anomaly associated with the soils sampling accomplished in the Enedina area by Campbell and Phelps Dodge. Unit less color range of K in soils, with blue representing relative lows and pink representing relative highs. Kreiging by John Reynolds, Durango Geophysics, 2007.

Enedina Discussion

Gold mineralization, magnetics and soil anomalies reveal that the strongest mineralization seems to be focused along the northeast-trending fault planes, with the La Gloria and El Tigre fault zones acting as primary conduits (Figures 3-19; 3-20; 3-21; 3-22; 3-23).

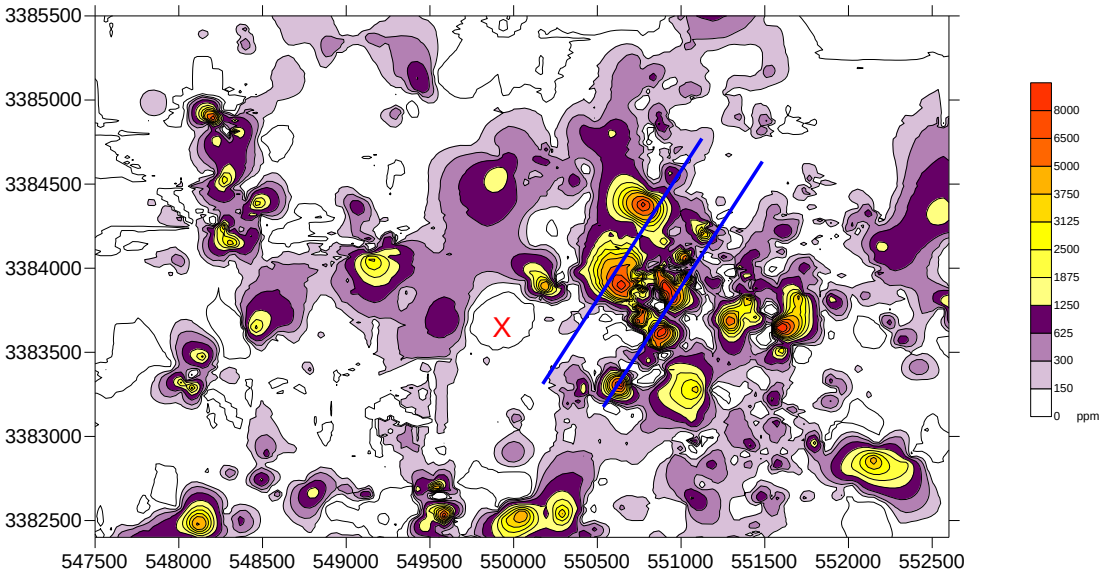

Figure 3-19 Zn in soils and rocks in the hornfels area. X marks the "center". Blue lines show general trend of NE faulting and Zn anomalies. Also note the near circular pattern of the zinc around the central peak. The void in the southwest portion is related to lack of samples. Approx. 3 X 5 km.

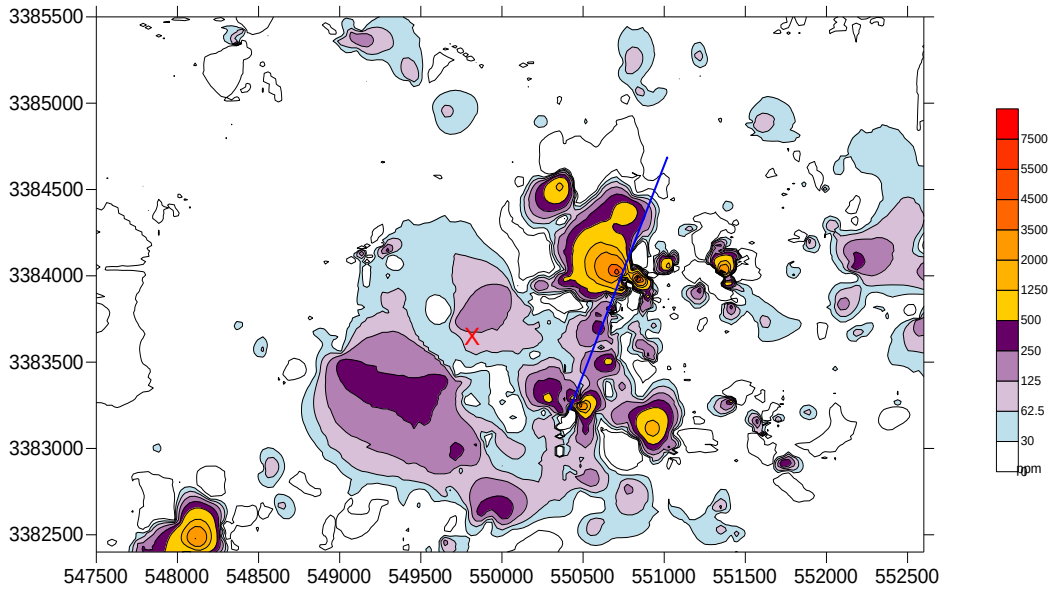

Figure 3-20 Mo in soils and rocks in the hornfels area. X marks the "center". Blue line shows general trend of NE faulting and Mo anomalies. Approx. 3 X 5 km.

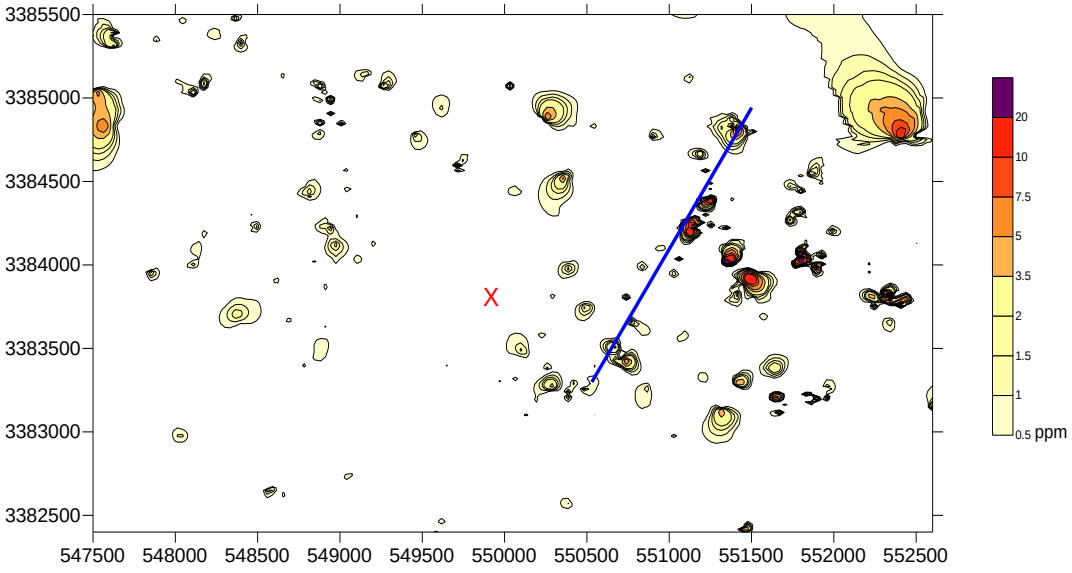

Figure 3-21 Au in soils and rocks in the hornfels area. X marks the "center". Blue line shows general trend of NE faulting and Au anomalies. Approx. 3 X 5 km.

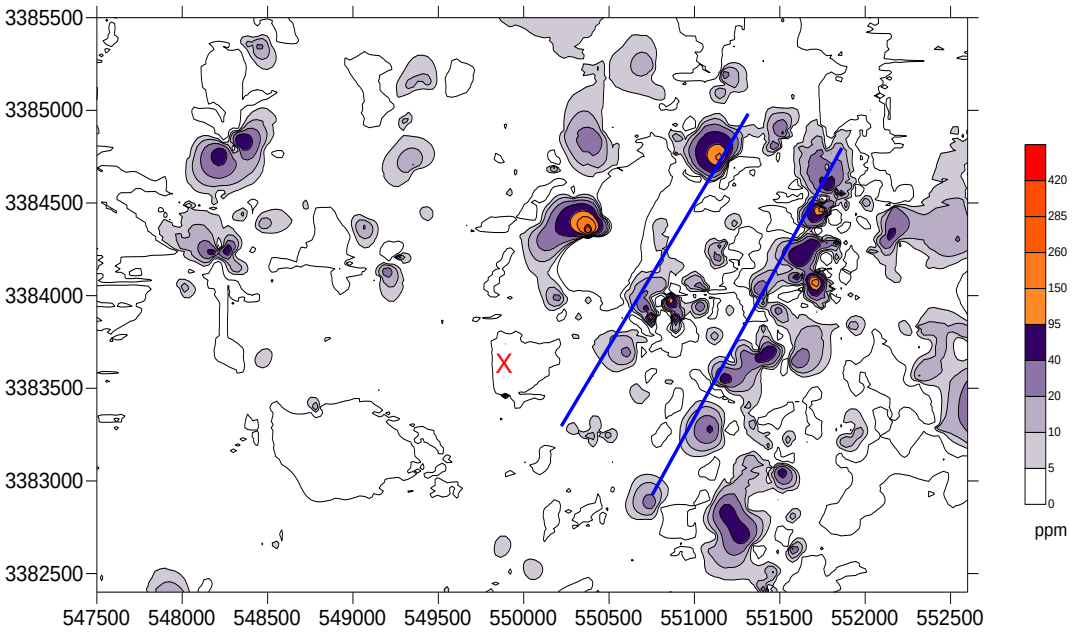

Figure 3-22 Ag in soils and rocks in the hornfels area. X marks the "center". Blue lines show general trend of NE faulting and Ag anomalies. Approx. 3 X 5 km.

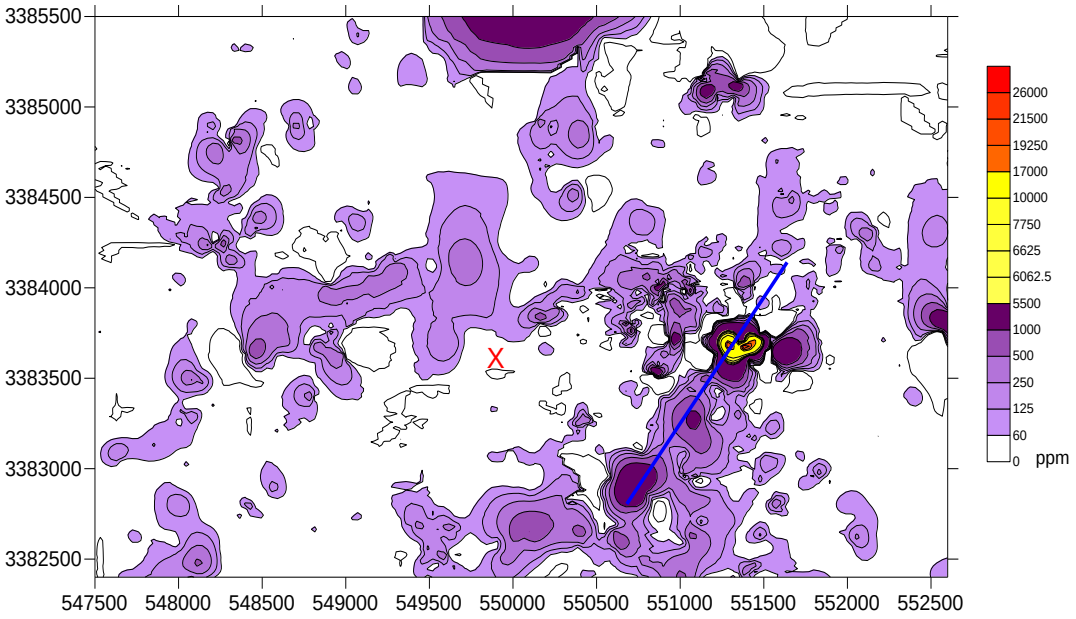

Figure 3-23 Cu in soils and rocks in the hornfels area. X marks the "center". Blue lines show general trend of NE faulting and Cu anomalies. Approx. 3 X 5 km.

In 2009, Animas began a limited, deep-drilling program in the Enedina study area with the intent of discovering precious-metal or base-metal deposits associated with the proposed hidden intrusive and its interaction with the surrounding chemically reactive Bisbee Group and northeast-trending structures. Two initial sites were selected based on the proximity to the proposed central heat source and the intersection of northeast-trending, gold-bearing faults cutting favorable lithology (Figure 3-24).

Surface and shallow gold mineralization has been recognized in the Enedina study area since the Phelps Dodge era and several proven resources have been associated to the La Gloria and El Tigre shear-zones as they cut through and beyond the hornfels and into more phyllitic rocks beyond La Gloria. ARET-001 was sited by the author to intersect favorable lithology and the La Gloria shear several hundred meters below the surface, with the possibility of higher-grade, structurally controlled skarn mineralization and perhaps the causative intrusive.

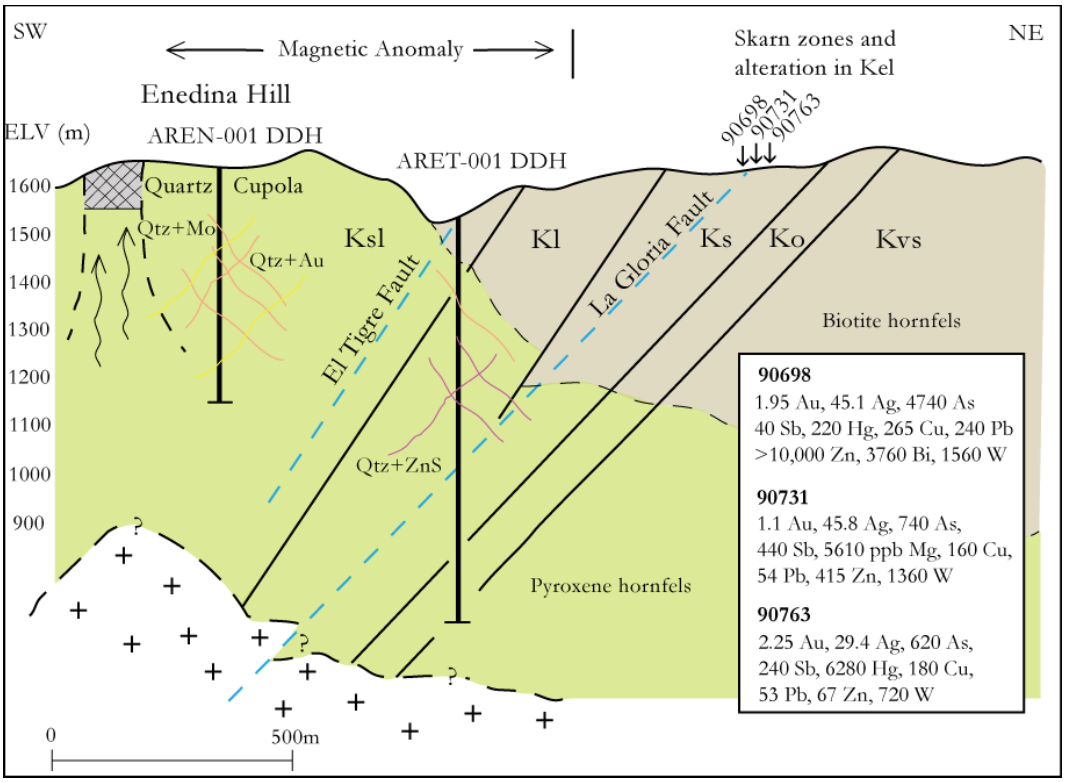

Figure 3-24 Schematic of La Gloria and El Tigre faults and their interaction with stratigraphy and the proposed intrusive. Stratigraphy, pyroxene hornfels (green), biotite hornfels (gray) and quartz veins plus metal are based on AREN-001 and ARET-001 diamond drill-holes. Surface samples in ppm in amphibole skarn. Adapted from Anderson, 2000. Looking northwest.

AREN-001 was designed to test the high-temperature quartz veins plus Mo and W and pyroxene hornfels. Drilling of AREN-001 revealed the typical pyroxene hornfels with minor garnet skarn associated with the more calcareous portions of the Cintura Formation. High-temperature quartz veins with medial-line molybdenite were a minor presence in the core of AREN-001, but insignificant in ARET-001. ARET-001 had an increasing quantity of quartz plus sphalerite veins, also reflected in the soil geochemical zoning. Although both holes were successful in intersecting the proposed structural controls and favorable lithology, neither intersected significant mineralization nor the proposed buried intrusive. Amphibole skarn was not present in either hole, mirroring its scattered and minor presence on the surface. ARET-

001 intersected the Bisbee Group within the favorable skarn zones, at depth, and within the presence of the major northeast-trending La Gloria structure. Skarn styles changed throughout the hole, reflecting lithological variations. Skarn mineralization was typical of the surface skarn. Base-metal mineralization was most associated with quartz veins in the form of sulfides and only locally was disseminated. Plots of correlations coefficients of the downhole assay of ARET-001 and AREN-001 reveal strong clustering of base-metal associations (Figure 3-25; Figure 3-26). The figures are generated by calculating the first two factors in a Principal Component Analysis (PCA) and plotting them on a correlation coefficient scatter plot. The uses of PCA include: 1) reduce the number of variables in a data set, and 2) distinguish structure in the relationships between variables. The plots reveal the clustering of data in the 31-element analysis of the core. Figures 3-25, 3-26, and 3-29 reveal a tight clustering of the same base metals and precious metals in the core from Enedina Hill and San Enrique. This implies that the Las Panochas Granite and the proposed buried intrusive at Enedina Hill have similar mineralization styles, geochemical associations and perhaps parent intrusive chemistries.

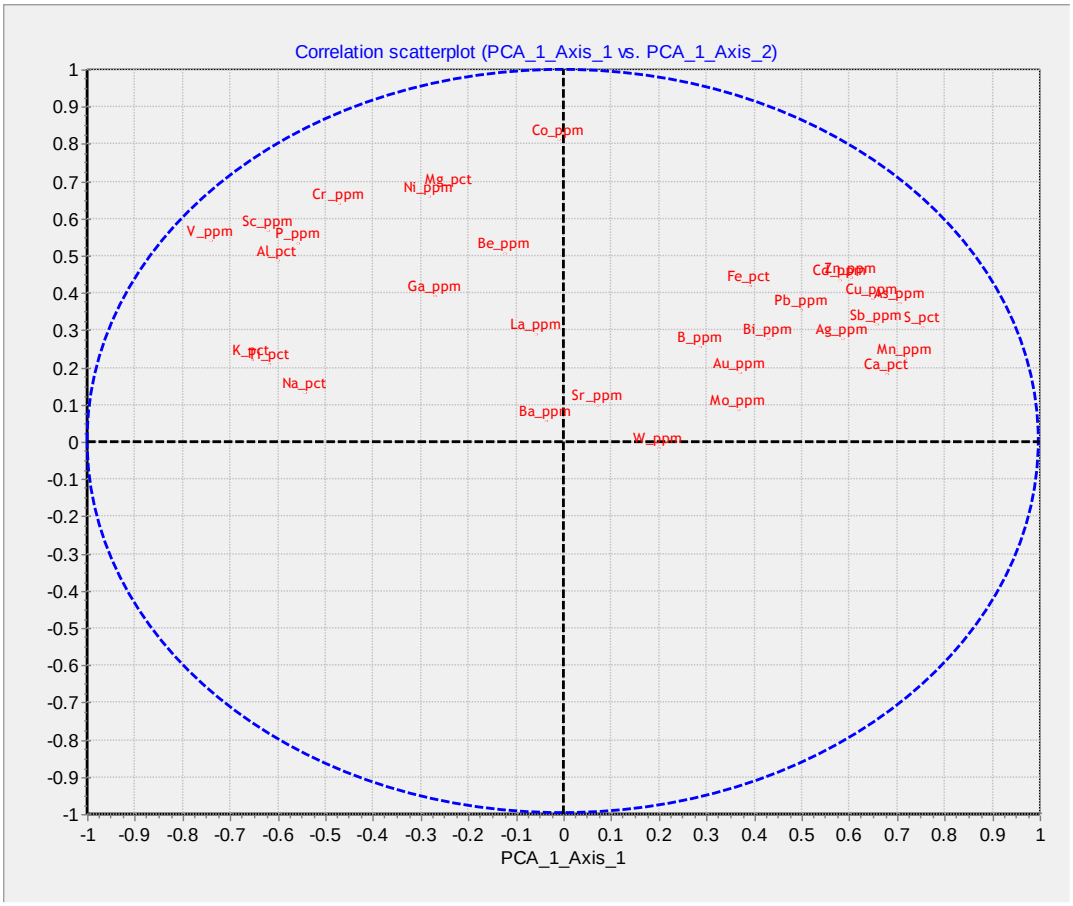

Figure 3-25 Correlation coefficient scatter plot of ARET-001, n = 426, with strong clustering of Mo, Au, Bi, Pb, Ag, Mn, As, Sb, Cu and Zn. The plot relates the degree of similarity among the data set. Strong clustering is evident and may infer a correlation among associated elements. The axes of the plot are the calculated (r) values from the PCA calculation.

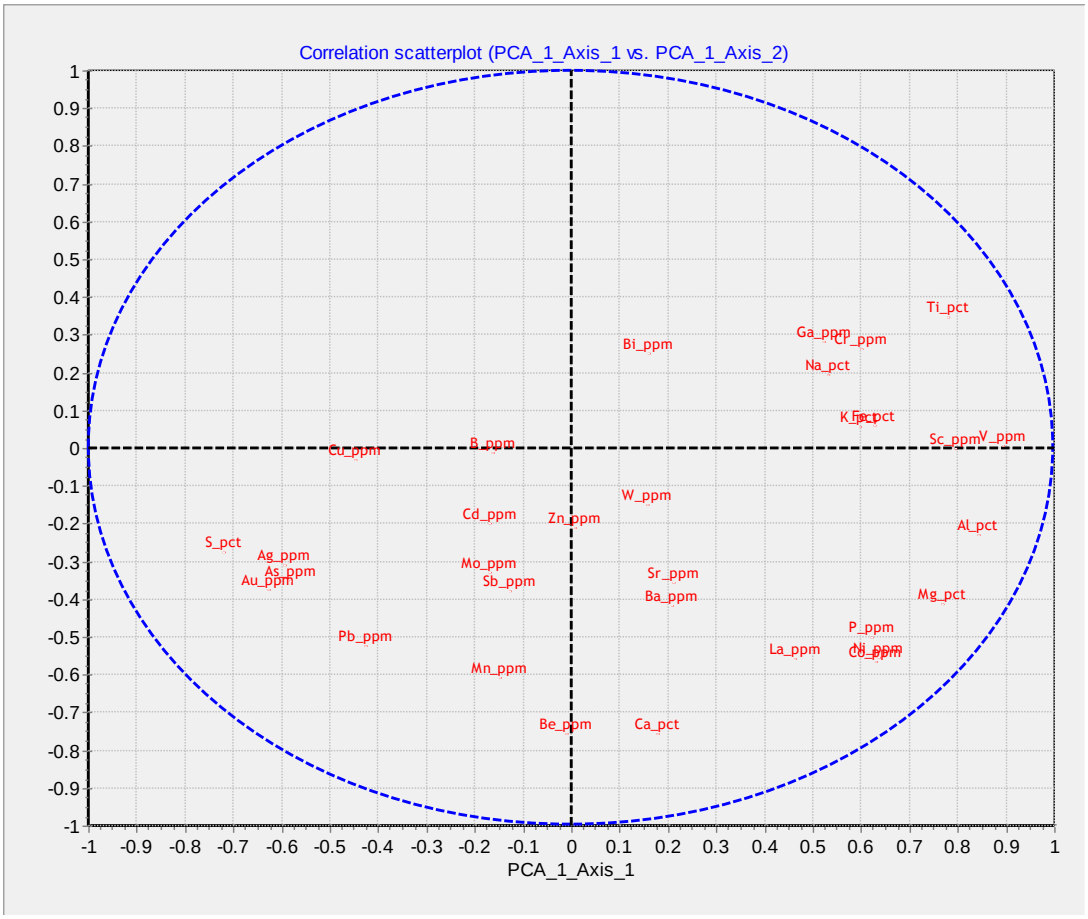

Figure 3-26 Correlation of AREN-001, n = 290, with a less clustered base metal correlation, possibly due to the central location of the collaring of the drill-hole.

Base-metal zoning in the study area is typical of intrusive-related porphyry deposits (Guilbert and Parks, 1986), with overlapping shells of base-metal zoning, reflecting temperature and chemical gradients. High-temperature metals, including tungsten, molybdenite, and vanadium are present in the inner thermal zone, followed by a shell of Cu, then Sb and Pb/Zn (Appendix B). The outermost zones include shells of gold and silver overlapping the Zn shell. Gold prospects including La Gloria, Greta, Lupita, Santiago, Nelly, and Jabali lie along the gold shell where it intersects favorable lithology and structural preparation.

Zoning within the hornfels and skarn types is dictated by lithology and proximity to heat, with the majority of the alteration being isochemical hornfels and recrystallization of sandstones and limestones several kilometers from Enedina.

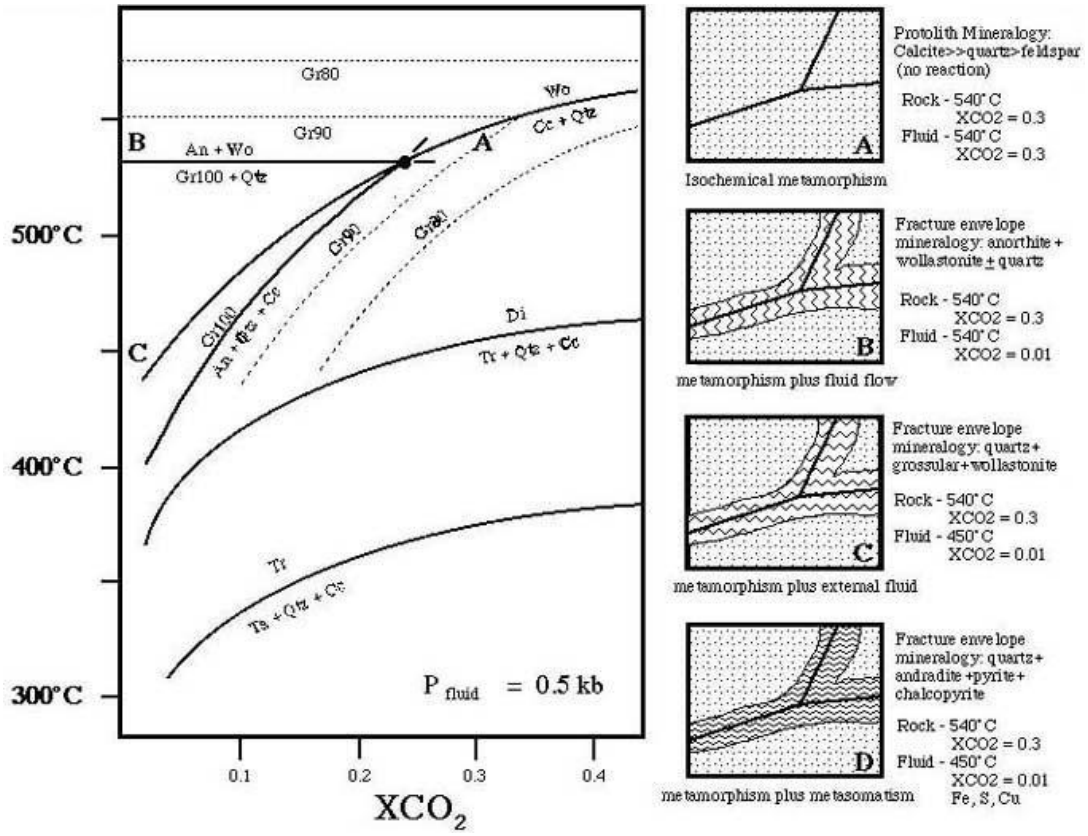

Figure 3-27 Illustration of metamorphic phase equilibria for selected reactions in the system Ca-Mg-Al-Si-H2O-CO_2. Modified from Greenwood (1967) and Kerrick (1974). Examples of four fracture controlled alteration events: A) Fluid in fracture is same temperature and composition as surrounding rocks at high XCO_2. B) Fluid in fracture is same temperature as surrounding rocks but has flushed some CO_2 out of the system. C) Fluid in fracture is cooler than surrounding rocks and has flushed some CO_2 out of the system. D) Fluid in fracture is a concentrated metasomatic fluid with magmatic components including Fe, Cu and S. (Meinert, 1997)

A possible scenario for the Enedina hornfels zone would begin with an increase in surrounding rock temperature as the geothermal gradient increased due to regional intrusive centers. Shallow intrusions and small-scale stocks caused the fracturing of rocks, which were being isochemically metamorphosed to hornfels prior to any fluid introduction or metasomatic reactions. Fractures would have then provided primary fluid pathways for skarn mineralization and increased temperature along the pathways. The northeast-trending fault planes acted as conduits for heat, mineralization, and alteration, providing favorable zones through mechanical and chemical preparation for the deposition of ore. Figure 3-28 shows the progressive development of hornfels, introduction of silica, and, introduction of sulfides.

Figure 3-28 Enedina hornfels and quartzite cut by high temperature quartz vein, all of which are then cut by the now-oxidized sulfide veinlets.

Four kilometers southwest of the Enedina study area, the San Enrique prospect and the Las Panochas Granite are interpreted to be equivalent to the proposed buried intrusive at Enedina. Evidence for this includes similar thermal alteration of the country rocks, geochemical associations including Mo, Cu, Au, Ag, Pb and Zn in zoned patterns (Figure 3-29), skarn geochemistry, and location along the northeastern La Gloria structure. Greisen alteration, a common constituent of the Las Panochas Granite, occurs on the top of Enedina Hill, associated with the quartz-stockwork cupola (Anderson, 2000; current study).

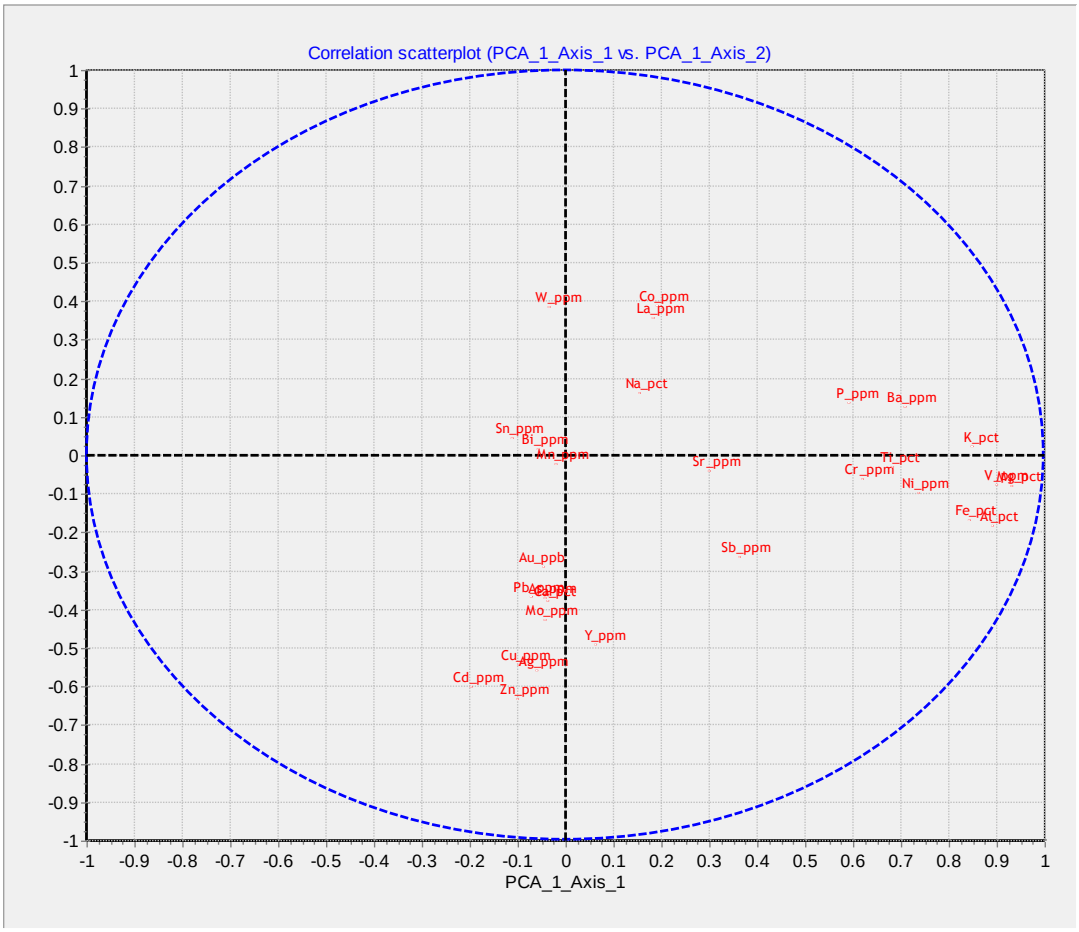

Figure 3-29 Plot of correlation of Teck Cominco's RSE 1-5 drilling results at San Enrique n = 648. These holes are collared in hornfels Bisbee Group rocks on the margins of the exposed Las Panochas Granite. Note the strong correlations to Au, Pb, Mo, Cu, Zn, Cd, Ag and As. This is the same clustering seen in ARET-001 (Figure 3-26).

Enedina is classifiable as a small-scale W (Mo,Cu,Au) polymetallic skarn deposit with a central Mo-W anomaly, ringed by a zone of Cu-Zn, then an outer disseminated, structurally controlled Au-Ag-Pb zone. The silicate textures in the rocks all appear to represent prograde mineral assemblages, with alteration halos probably being due to removal of iron to form pyrite through the process of sulfidation (Christensen, 2010) (Figure 3-30).

Figure 3-30 Greenish alteration with banding and diffuse margin to pyroxene hornfels, banded fine-grained sulfides and quartz + pyrite cutting across retrograde alteration. Linear quartz + molybdenite at 50° to axis of core. Base metals appear to post-date isochemical event and retrograde alteration seems to be associated with the quartz + molybdenite veins. A Centavo coin for scale.

Retrograde alteration is limited in scale and intensity, reflecting the lack of interaction with meteoric water, perhaps as a function of depth of the exposed rocks during emplacement of the parent intrusive. The metamorphism appears to have been mostly isochemical for the major-element chemistry, and perhaps most rocks are better called hornfels rather than skarn - the result of thermal processes rather than hydrothermal processes (Christensen, per comm., 2010). Drilling in the area since the Phelps Dodge era has been unsuccessful in uncovering large-scale skarn emplacement and base-metal concentrations typical of economic deposits.

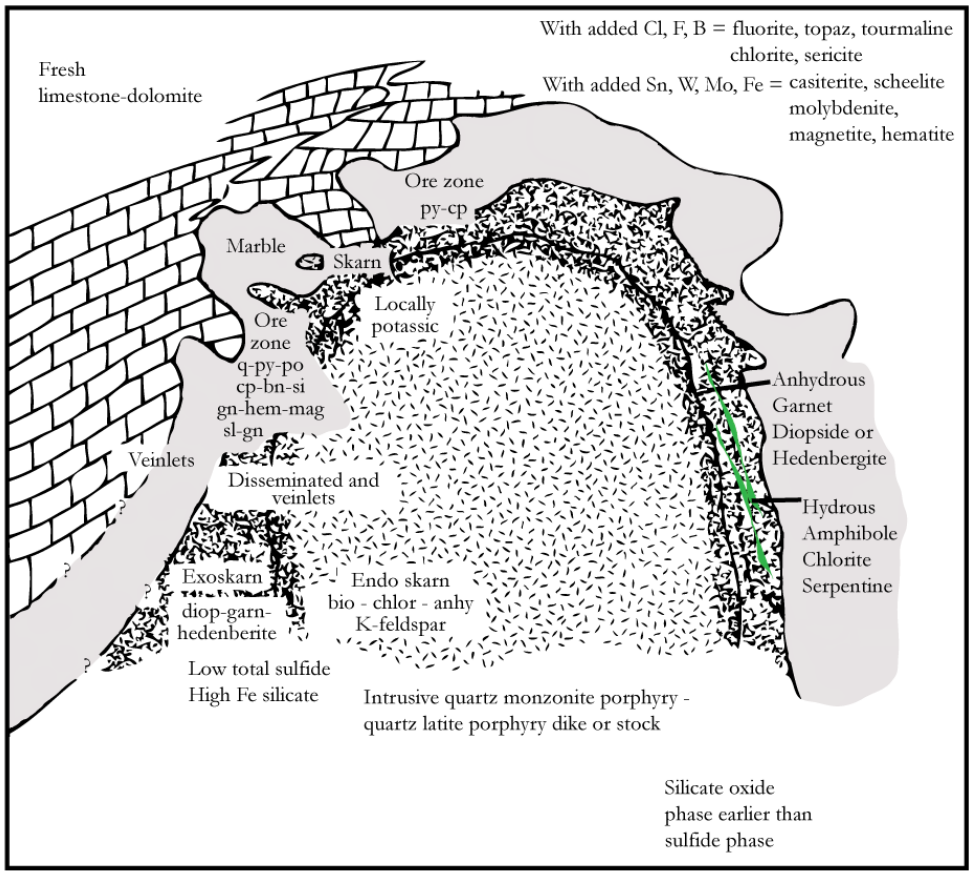

Figure 3-31 Schematic of stock with a skarn contact zone. The skarn is subdivided on the right side, the ore zone generalized on the left (After Guilbert and Lowell, 1974; modified from Guilbert and Parks, 2007).

Within in the study area and the district, there is little evidence for large-scale, hydrous phase minerals replacing anhydrous skarn minerals. This is also reflected in the minor distribution of sulfide veinlets. Furthermore, all of the primary rocks contained very little diagenetic iron and consequently the amount of pyrite formed by sulfidation was minor. If sulfidation of available iron was an important reaction for the deposition of gold in this system, the rocks served as poor hosts (Christensen, per comm., 2010). Guilbert and Park (2007) state that pyroxenes in skarns are typically diopsidic; therefore most anhydrous skarns contain andradite and diopside in metasomatic reactions with rocks containing silica, magnesium, aluminum, and iron. They go on to state that veinlets and masses of hydrous equivalents of the calco-magnesian, anhydrous minerals, and sulfide veinlets tend to cut the anhydrous garnet skarn (Figure 3-31). The skarn assemblages at Enedina are consistent with a relatively dry environment during their formation.

There is a clear spatial relationship between the widespread thermal alteration centered on Enedina Hill, the zoned geochemical halo, the quartz cupola, 150 ppb background average Au in the hornfels, the presence of Te, Bi, V, and W, and silver-to-gold ratios. This spatial pattern is repeated at San Enrique, with the Las Panochas granite and its associated hornfels, skarns, greisen alteration, quartz veins bearing (Mo, W, V, Cu, Ag, Au), and disseminated gold. Fluorine and tin are anomalously high in the rock-chip and drill core in the central zone of Enedina Hill and at San Enrique, where it is associated with greisen alteration of the Las Panochas Granite. Smith (2006) reported:

> Overall, the system appears to be very sulphide poor. The peraluminous and leucocratic nature of the host pluton are not typical of rich copper porphyry systems, but are more typical of Mo, Au, Sn or W systems…The Greta (Enedina) Cu-Mo anomaly appears to be another system virtually identical in many respects to the San Enrique system, although the causative intrusion is not exposed on surface. The hornfelsed and skarn altered carapace contains significant magnetite, such that it produces a profound aeromagnetic response. There is more sulphide (i.e. pyrite) related to this system than at San Enrique. Overall, the system appears to be more moly and gold rich relative to San Enrique, and relatively copper poor.

In August 2010, Animas reported that the results of the most recent drilling at Enedina revealed a large porphyry molybdenum target with elevated levels of fluorine and tin and potassic alteration. (Animas Resources website August, 2010).

Interestingly, a comparison of the Las Panochas Granite to molybdenite-bearing granites of Henderson, Colorado (Wallace, 1995) reveals that the values of Ni and Cr are greatly elevated in the Las Panochas Granite (Figure 3-32). The abundance of basic elements in the peraluminous Las Panochas Granite implies that there is a deep-seated, basic rock source for the crustal melting (Xinxiang et al., 1996).

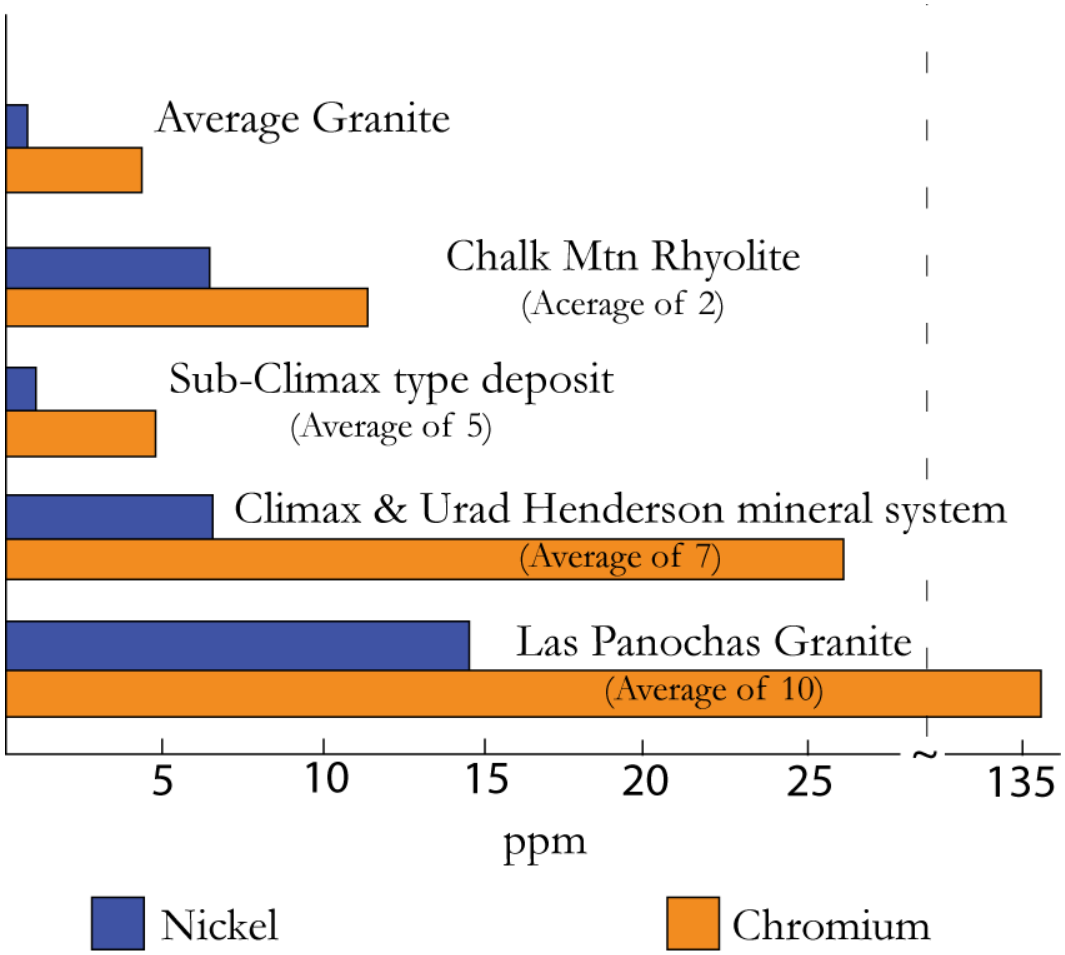

Figure 3-32 Comparison of Ni and Cr in average granite, Climax-related intrusions, and Las Panochas Granite. Note large break in scale needed to accommodate Cr in the Las Panochas Granite. Modified from Wallace, 1995.

Phelps Dodge proposed a model in 1992 (Annual Report) referred to as the "British Columbia Epithermal Model" (Figure 3-33) to explain the mineralization observed in geographically separate areas within the district.

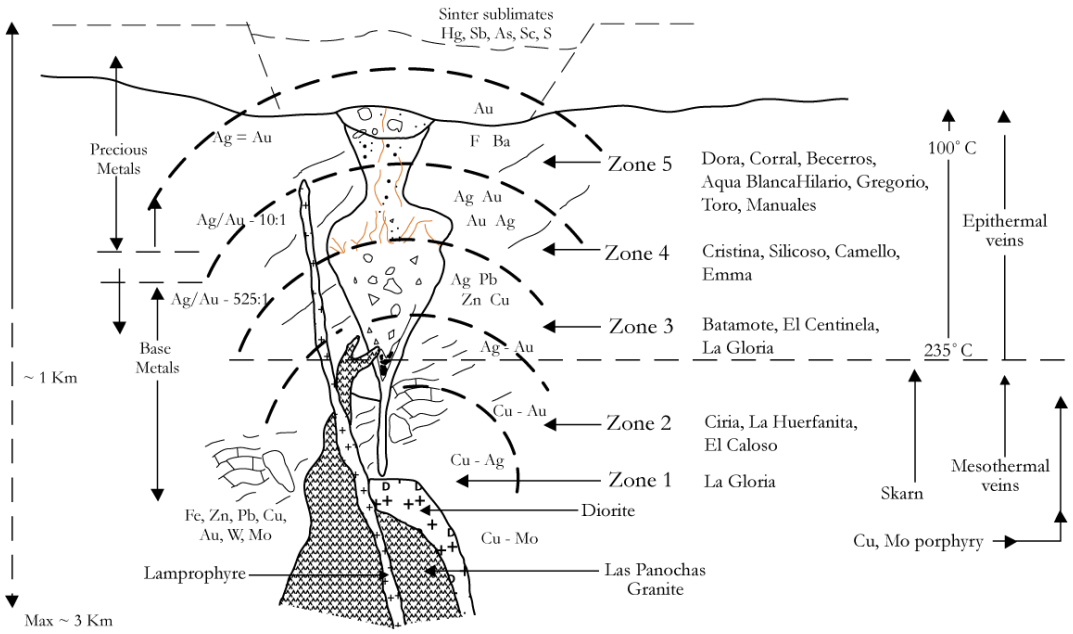

Figure 3-33 Schematic of Phelps Dodge' British Columbia Epithermal Model with zoning of base metals and precious metals, skarn and disseminated mineralization and varying Ag/Au ratios. Deposit/prospect names associated with zones. Modified from Phelps Dodge, 1992.

Phelps Dodge's model allowed for multiple styles of mineralization, and classifications of mineral deposit types often not observed in relative close relation. Post-mineral faulting in the area would have dissected the stack of alteration, mineralization, and deposit types, juxtaposing differing crustal levels and dissimilar deposit types. This would help to explain the lack of easily correlatable element associations with precious metals and the close association of differing deposit types over a relatively small area. Phelps Dodge attributed all of the discovered deposits at that time to the causative Las Panochas Granite, but the possibility of multiple intrusive stocks, currently at various structurally controlled levels, may better explain mineralization spread throughout the district, including Enedina, Mirador, and several other thermally altered areas in the district.

Within the district, there are five distinct areas with widespread brown-biotite hornfels and associated gold mineralization, including Enedina and San Enrique (Figure 2-66). In the northwest corner of the district, southwest of and adjacent to the Amelia Mine, La Bonita hornfels covers 5 km², flanked by several gold-producing open pits. Drilling by Animas (2009) extended the La Bonita hornfels eastward for several more kilometers. The drilling, at the Escondida/Vibora area, revealed unmapped, strong hornfels. In the Mirador study area, brown biotite and minor skarn are exposed in the Mirador open pit and to the southwest of the pit, extending for several kilometers. The margins of this hornfels were never fully explored, but it does extend to the north, east of the haul road for several kilometers. It is truncated and overlain by a low-angle fault and weakly phyllitic altered rocks to the west of the pit. This low-angle structure was intersected several times by Animas deep drilling in 2009, up to 1.5 km west of Mirador Pit, each time passing from weak phyllitic alteration in the hanging wall into strong hornfels in the footwall of the structure. This implies that the surface expression of the Mirador hornfels is quite small in comparison to the subsurface extent. The structural complications and juxtaposition of low-grade to high-grade hornfels rocks has complicated visualizing the district as a single thermally altered regime, where distinct stocks caused zoned thermal mineral assemblages and associated base and precious metals. Finally, Anderson (2000) and this author noted brown biotite and pyroxene hornfels associated with Woolfolk/La Verde, on the extreme western edge of the district. The area had been archaically surface-stripped mined in the past, perhaps for copper oxides associated with an endoskarn from an undated granodiorite intruding into the Bisbee Group. Only a few days were spent in the Woolfolk/La Verde area, but the similarities to the rest of the district were striking.

Tight structural controls for economic mineralization and associated trace elements are most notable in the higher grade hornfels in the Enedina study area, with minor, non-economic outcrops of base metal plus precious metal bearing amphibole skarn. Potentially economic mineralization blossoms on the periphery of the high-grade thermal hardening, especially in the northeastern quadrant of the hornfels zone, coincident with 1) the northeast structures that acted as conduits for mineralization and 2) the chemically reactive calcareous rocks of the middle and lower Bisbee Group. This is also noted by Smith (2006) at San Enrique in association with the Las Panochas Granite. Of the 162 highest gold grade rock-chip samples taken throughout the entire district since the earliest Phelps Dodge days, 119 of them are on the periphery of the Enedina hornfels, with an average grade for the richest samples of 25.59 g/t. This implies that over the approximately 750 km^2 of the district, 74% of the highest grade samples come from less than 10 km^2, or 1% of the entire district, surrounding the northeastern flank of a proposed mineralizing intrusive. Thermal hardening and sulfidation seem to have preceded the main pulse of mineralization, but background anomalous gold and trace elements distributed throughout the hornfels dictate that early fluid flow introduced the elements or they were pre-existing in the sediments. The structurally controlled mineralization cuts the hornfels, with discontinuous prospects scattered along the faults at the intersections with chemically reactive rocks. Along zones of non-reactive, broken rock and fault gouge within the hornfels, mineralization and trace element geochemistry are much lower than in the more reactive calcareous rocks along the fault planes in the hornfels and beyond the hornfels. Beyond the thermal hardening, silicification of fault breccias, formation of silica-filled tension gashes, and silica replacement of limestone are more common along with polymetallic veins and the more typical "Santa Gertrudis type" fine-grained, disseminated gold and arsenic. Is there a coincidence between the multiple hornfels in the district, their associated geochemistry, and the

number of deposits that are in units that are less altered and that flank or may have flanked a hornfels? Is there a coincidence in the geochemical associations for gold and the trace elements, across both the hornfels and the less thermally altered rocks that flank the hornfels? Is there a coincidence to the association of high gold grade, northeast-trending fault control, and gold peripheral to the proposed intrusive centers? Unfortunately, some of these questions remain unanswered by the currently available data.

Mirador Study Area

Located within the main zone of mined mineralization within the district, the Mirador study area covers 1.5 km^2 (Figure 3-34). Within the study area, several prospects follow the southeast extension of a sub-bedding-parallel, northwest-trending, brittle structure called the "Red fault" (Figure 3-36). The name is due to its association with hematitic rocks. The area was chosen due to the similarities to the Enedina study area and the complex structural history, but is 7 km to the northwest of Enedina.

Mirador Geology

Much of the northern portion of the study area, including the Mirador Mine, exposes moderately to steeply dipping, upright Bisbee units, which include, from northeast to southwest, Glance Conglomerate, Mural Limestone, and Cintura Formation. The units in the northern portion of the study area are hornfels. The northwest-striking, southwest-dipping Red fault cuts through the hornfels Ks-upper. The southern portion of the study area includes repeated Kl stratigraphy and the Agua Blanca Mine. Structural complexities and non-hornfels rocks dominate the southern portion. The north-striking, vertical Ortega Fault is along the western margin of the Mirador study area.

Brown-biotite hornfels is prevalent in the northern portion of the Mirador study area, with the highest exposed metamorphic grades in and around the Mirador Mine. The hornfels resembles the hornfels elsewhere in the district, including the selvages of albite-epidote hornfels cutting the brown biotite. Pyroxene hornfels was not identified in the Mirador study area. Skarns are bedding and lithologically controlled, but are an insignificant part of the thermal alteration. They are generally less than 1 cm thick, consisting of 1-mm-diameter, lime green to brownish andradite garnets that replace impure calcareous interbeds within the upper and lower Ks. Skarn stringers locally cut the Kel and Ko along the back wall of Mirador, but in general, the limestones are strongly recrystallized, but not skarn. Non-hornfels Bisbee Group units that are in structural contact with the hornfels define the western and southern portions of the study area. The weakly phyllitic rocks in the hanging wall of the Gate Fault represent the lithologies hosting gold mineralization in the Main District.

Mirador Structures

Three named structures are present in the Mirador study area. Based on crosscutting relationships, the oldest fault is the northwest-trending, southwest-dipping, sub-bedding parallel Red fault (Figure 3-36). It is best exposed in the Mirador Mine, where it cuts hornfels Ks and extends to the southwest for more than 2 km. Truncating the Red fault is the low-angle, southwest-dipping Gate fault, exposed northwest and west of the Mirador Mine. The structure has experienced a complex movement history based on overprinting types of brittle-ductile and brittle fabrics shear indicators, locally with conflicting sense of shear. In the western portion of the study area, the vertical, north-trending, Ortega fault (Figure 3-36) cuts the older Red and Gate faults with apparent left-lateral offset.

Ductile fabrics and complex folds (Figure 3-35) associated with the Red fault reveal a complex movement history with an early thrusting and ductile folds followed by later reactivation and brittle deformation of the hanging wall and footwall. Anderson (1998) describes the structure, prior to mining, as a dextral-reverse shear-zone. The structure cuts the brittle hornfels without any obvious folding, but less than 2 km to the southwest, complex folding is present along the fault in the weak, phylitic Ks-upper unit.

To the northwest, mineralization is truncated by the east-northeast-trending, southeast-dipping, low-angle Gate fault. The trace of the Red fault disappears under the hanging wall of the Gate fault. The Gate fault strikes 045, dips 25°SE, and is associated with S-C fabrics, stretching lineations, imbricated stratigraphy and ductile fabrics. These structural fabrics imply that the structure has experienced early ductile to brittle-ductile deformation, and reverse movement. Sense of shear and strain indicators record early deformation that included bedding-parallel compression. Brecciation observed along the structure indicates reactivation, perhaps in a normal sense. These multiple offsets in opposite directions, have complicated determining total offset by each phase of faulting. The hanging wall contains the Main District package of weakly phyllite-altered Bisbee Group rocks, and represents the bulk of the ore-bearing rocks mined in the district. The footwall contains brown-biotite hornfels represented at Mirador Mine, and extends several kilometers to the west in the subsurface based on drill-holes ARTG 005-007 (Animas Resources, 2009). Three-point problems on the fault intersections in ARTG drill-holes yield a 038 21°SE orientation to the fault plane. Down-dip projection of the Gate fault from outcrops to the westernmost drill hole of the ARTG series predicts that the structure was too deep for intersection by the drilling; yet the fault was intersected.

Restoring the stratigraphy from the post-mineral high-angle, north-trending Ortega fault allows for the restoration of the projection of the Gate fault to be intersected by the ARTG drill-holes, therefore, the Ortega fault postdates the-Gate fault and mineralization (Figure 3-36). Latest movement on the low-angle Gate fault also cuts and offsets the Main District fold hinge, which assists in the prediction of the relative timing of folding, faulting, and mineralization.

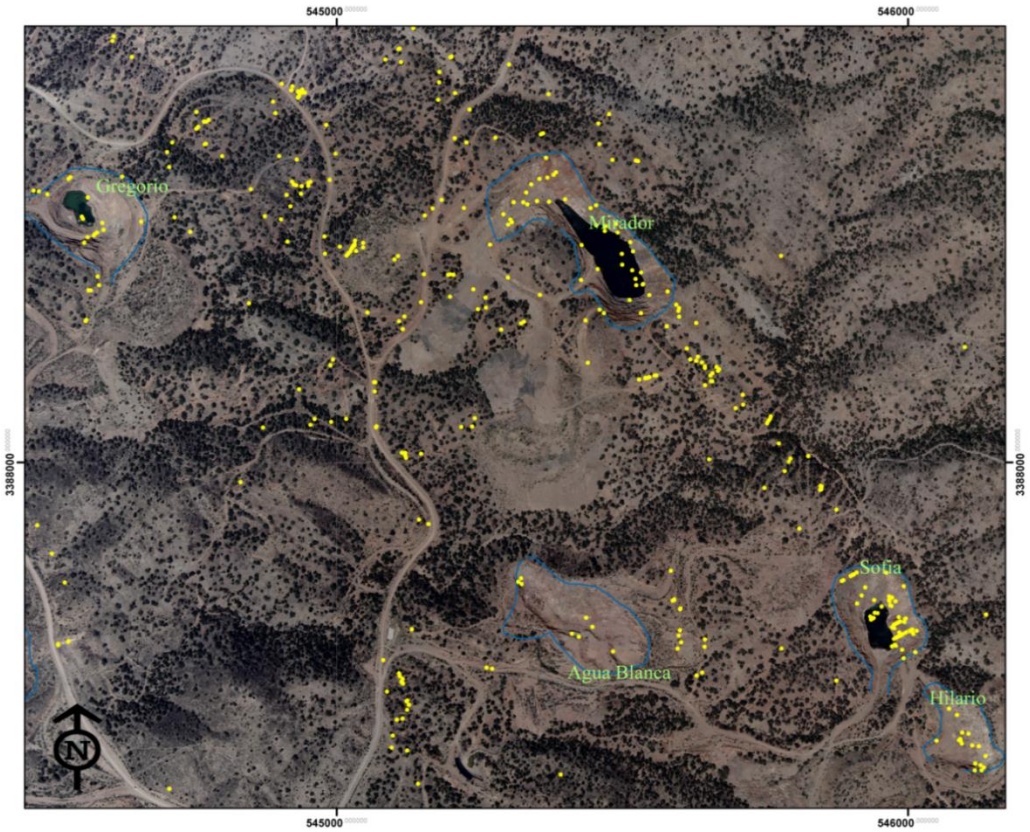

Figure 3-34 Mirador study area includes the Mirador, Aqua Blanca, and Sofia Mines. Yellow dots represent rock-chip samples greater than 0.5 g/t gold.

Figure 3-35 Box fold along the southwest extension of the Red fault. Looking southeast.

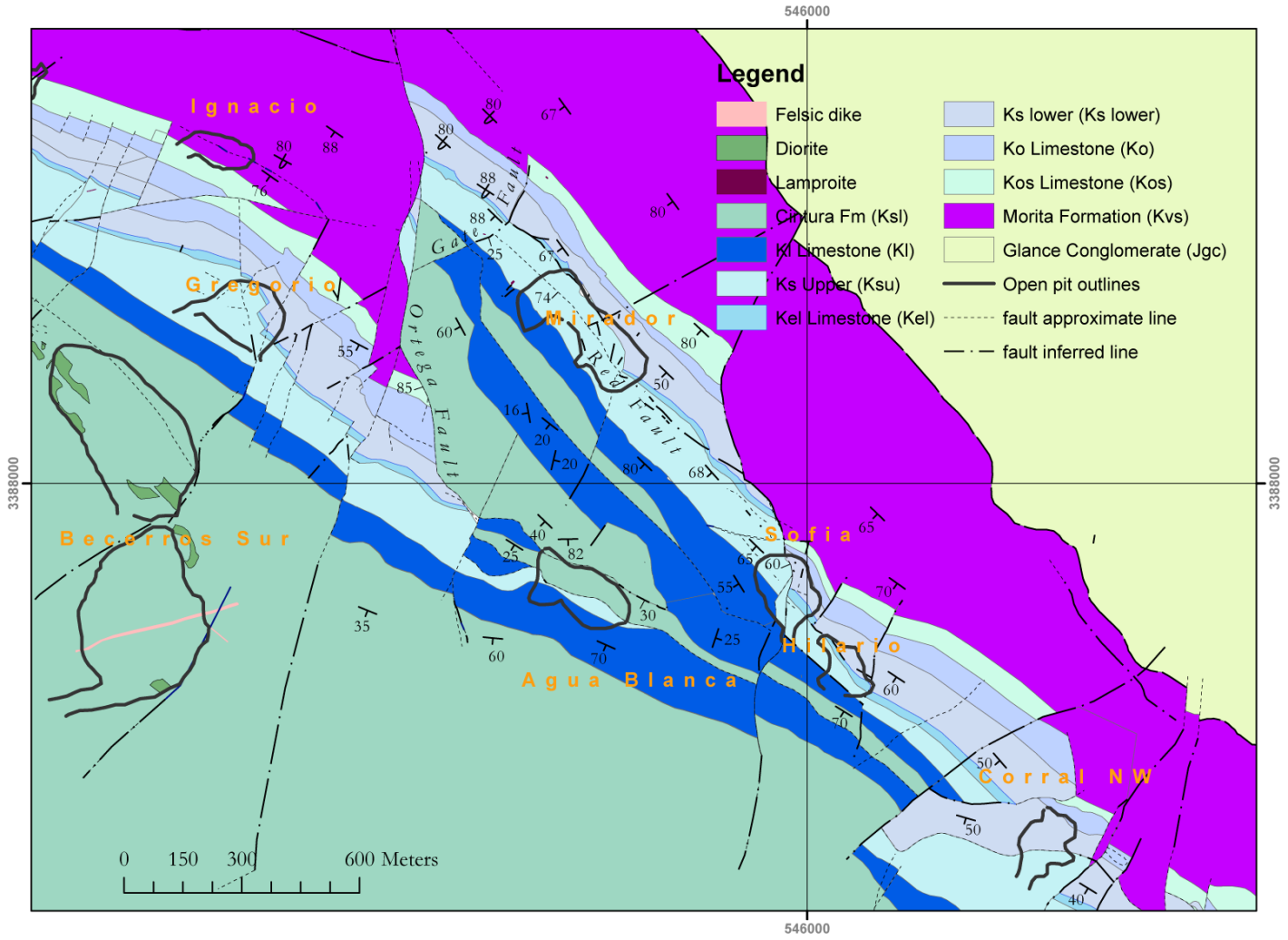

Figure 3-36 Geologic map of the Mirador study area

Mirador Mineralization

Mineralization in the Mirador Mine is focused along the Red fault, aptly named due to the abundance of hematite and goethite present along the surface expression and mined exposures. Mineralization is typical of the Main District mineralization, with fracture-dominant pseudomorphs of oxides after sulfide, with micron to sub-micron native gold. As is common throughout the district, fractures control mineralization. Gold mineralization along the fault is in a brittle-ductile shear-zone less than 6 m wide and is discontinuous along strike with several mineralization blossoms occurring at the Mirador and Melissa prospects. Campbell drilled 54 DDH and 1 RC hole, directed to intersect the Red fault orthogonally, revealing a zone 1.5-km in length with an average gold grade of 313 ppb (n = 3182). Drilling revealed a the highest gold grades at approximately 45 m below the surface (Figure 3-37), with a slope on the graph of gold grade increasing at a rate of 4 meters of depth per ppm Au (Figure 3-37, red line) and decreasing at a depth of 45 m at a rate of -4.9 m per ppm Au, nearly symmetrically mirroring the rise in grade with depth above 45 m (Figure 3-37, purple line). The symmetry of grade to depth, independent of lateral extent over 1.5 km along strike of the Red fault, is not typical of most hydrothermal deposits. The structure is parallel to the nearly vertical beds; so the lithology does not vary with depth. Interestingly though, 45 m is approximately the depth to the current water table exposed at Mirador Pit.

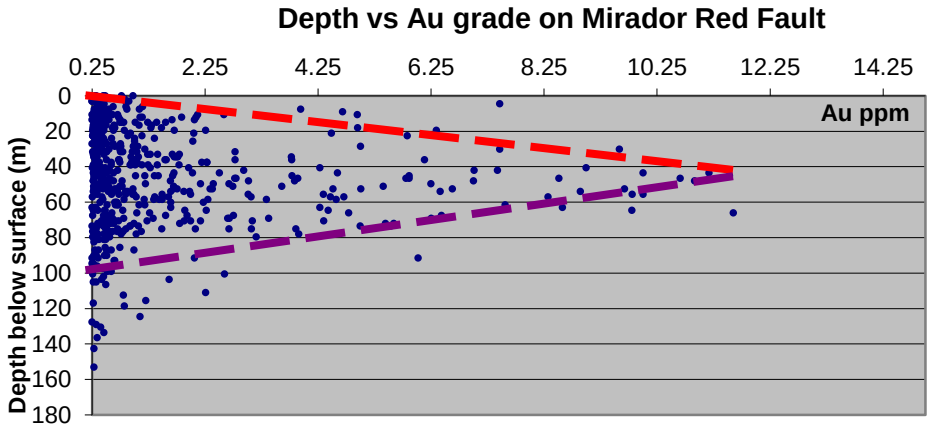

Figure 3-37 Plot of gold grade (ppm) versus depth for 55 holes drilled orthogonal to the Red fault in the Mirador study area. Red line is approximation of slope of increase in gold grade with depth at 4 m/ppm Au, purple line plots at -4.9 m/ppm Au.

Although there is a direct correlation to economic gold mineralization and the Red fault, rock chip surface samples reveal that background gold mineralization within the hornfels averages 215 ppb (n = 55). This is the same relationship seen in Enedina and San Enrique; background gold-bearing hornfels, economic gold associated with brittle structures cutting through the hornfels, and base-metal zoning with structural controls (Appendix B). Zoning of base metals at Mirador is not as well recognized due to 1) structural complications that limit the aerial extent of the full hornfels extent, 2) limited soil surveys due to previous mining, 3) leaching and waste storage in the Main District, and 4) the unsampled northeastern portion of the Mirador area, which is underlain by the unfavorable Morita and Glance Conglomerate. In the same Mirador hornfels sample subset-set (n = 55) background Cu is 369 ppm, Zn is high at 1173 ppm, Mo is low at 6 ppm, As is 800 ppm; this is a recognized association throughout the district.

Mirador is an enigma in the district for several reasons. It is one of only a few places where distal disseminated gold is hosted within hornfels, the other being at El Tigre prospect in the Enedina study area. This fact may be reflected in the very poor overall gold grades mined from the pit, with structures acting as the primary sites to host mineralization in the otherwise hardened and tightened rock. The Mirador Mine produced 10,202 ounces of gold from 221,865 tons of ore mined, with a grade of 1.43 g Au/t and a strip ratio of 8.8 ore to waste. A logical conclusion is that the gold-bearing fluids postdate the isochemical annealing of the rock that formed the hornfels. Furthermore, the Mirador study area lacks structural intersections observed elsewhere in the district. Offset of mineralization along the Red fault is observed southeast of Mirador Mine by a northeast-striking, northwest-dipping strike-slip fault. There are no significant gold values along this northeast-trending structure, nor any blossoming of mineralization at the structural intersection.

Agua Blanca

Stratigraphy is complex south of Mirador Mine, complicated by large-scale imbricate thrusts and related folds repeating the stratigraphy of the Ksl and Kl four or more times between Aqua Blanca and Mirador Mines (Figure 3-36). The Cintura and Kl limestones are not as strongly metamorphosed, and multiple, short, shear-zones host economic grade gold in the highly sheared and structurally prepared calcareous-siltstone interbeds of the Kl unit. Varying porosity and permeability within the structures and the surrounding broken and fractured rocks permitted fluid dissipation, creating a much wider geochemical halo around Aqua Blanca Mine as compared to Mirador. This is the same relationship seen at the distal La Gloria Prospect as compared to the tighter structural controls seen in the proximal northeastern structures cutting through the hornfels. Despite the post-mineral extensional faulting at Aqua

Blanca, which preclude a direct relationship of zoned hornfels to less thermally altered, mineralized, peripheral gold deposits, the potential for Aqua Blanca representing a "gold zone" on the periphery of the Mirador hornfels is intriguing. Mineralization within Aqua Blanca follows a strong ENE control (Figure 3-38) (Bennett, 1993), crosscutting the older structural fabric and bedding.

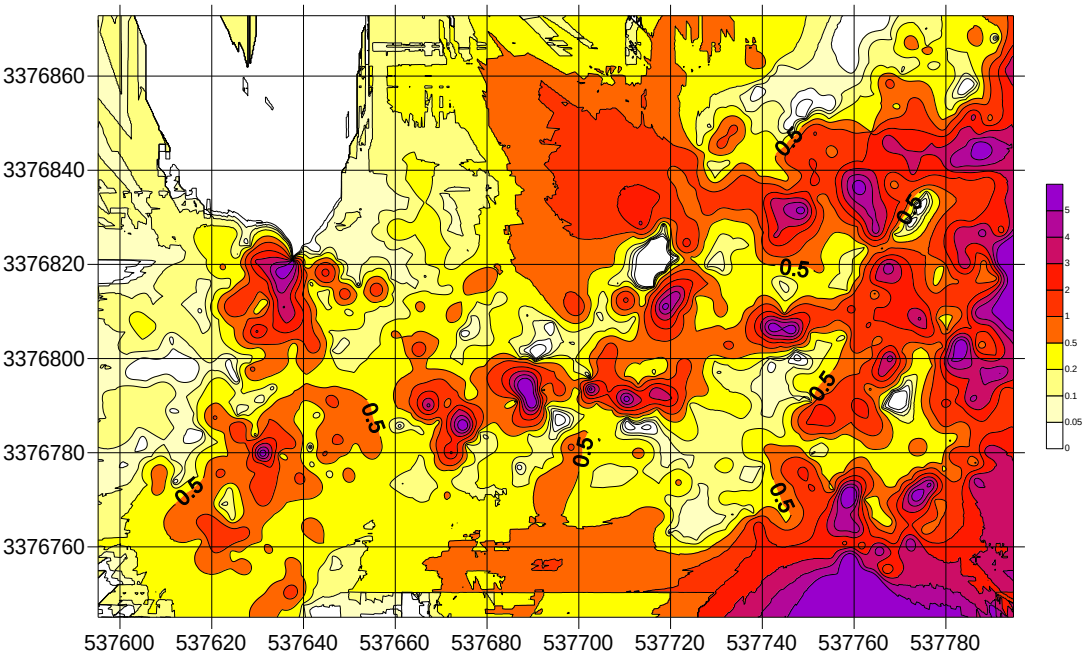

Figure 3-38 Surfer plot of the 1495 m elevation, bench blast data for the Aqua Blanca Mine. Scale 0 to 5 ppm gold. Note strong ENE trend to mineralization, counter to the northwest-trending bedding.

Toro-to-Gregorio Study Area

The Toro-to-Gregorio study area lies within the heart of the Main District, and represents the main strike belt of the Mural Limestone. The Toro-to-Gregorio study area covers 2.5 km^2, incorporating the full suite of Bisbee Group units and containing eight open pits including the Toro Norte, El Toro, Ruben, Camello, San Ignacio, Becerros Norte, Becerros Sur, and Gregorio mines (Figure 3-39; 3-41). The study area is centered on steeply dipping, upright to

overturned Morita and Glance Formations to the northeast and overturned to upright Cintura to the southwest (Appendix D). The units strike northwest and are involved with the overturning, Gregorio syncline.

Toro-to-Gregorio Geology

The locus of mining and the highest concentration of mineralization are within the Main District, which includes the earliest discovered and mined deposits, the mine office site, the majority of the legacy leaching facilities, and most waste piles from previous operations. Mining focused on intersections of northwest-trending, southwest-dipping to northeast-dipping, bedding-parallel shear zones and northeast-trending, high-angle, northwest-dipping brittle faults. Mineralization, originally associated with pyrite, is characterized as micron to sub-micron native gold liberated by the oxidation of gold-bearing sulfides. Mineralization is localized along structurally prepared and chemically reactive rocks (Figure 3-40). Recognition of the controls for mineralization within the study area was aided by detailed pit mapping, often from the bow of a rowboat in the water-filled pits. Very few legacy, pit-production, geologic maps remain. Phelps Dodge recognized northeast-trending, northwest-dipping, high-angle faults and northeast trends to mineralization, and this recognition directed exploration and drilling throughout the district. Despite a strong northwest trend to mineralization, it is clear in many of the pits that the intersections of northwest-striking and northeast-striking faults played a key role in concentrating mineralization. This implies that the intersections, and the northeast-striking faults existed during or prior to mineralization. There is evidence, however, for post-mineral movement on both the northeast-trending structures and perhaps the northwest-trending faults. Bench data for the 1446 m bench of Campbell's Toro Norte Mine (Figure 3-42) clearly shows the intersection of high gold grades in northwest and

northeast orientations, which correlate to mapped structures in the pit. The northeast-trending structure has strong decalcification and collapse of the Ko and Kos limestones associated with elevated As and Au grades. The northeast-northwest structural intersections create several rich zones, blossoming southwest along the strike of the northeast-trending structure, leading to Toro Norte, Katman, Manueles Sur, and Maribel open pits (Figure 3-42; Figure 3-43). The intersection relationship is also recognized in Ruben, Toro, Camello, Gregorio, and Corral Mines.

Seven of the eight deposits were discovered and mined by Phelps Dodge with an estimated 59,000 ounces of gold recovered. Legacy and Animas sampling, mapping, and 2008 drilling focused on proving structural extensions of shallow, high-grade mineralization beyond the pits, along the northwest-trending and northeast-trending structures. Animas began a deep drilling program in 2009 with the goal of extending mineralization below the sulfide/oxide boundary, along structurally prepared rocks and with the intent of discovering a master feeder system of faults. The following discussion will focus on the field and pit mapping, combined with drill core logging completed by the author.

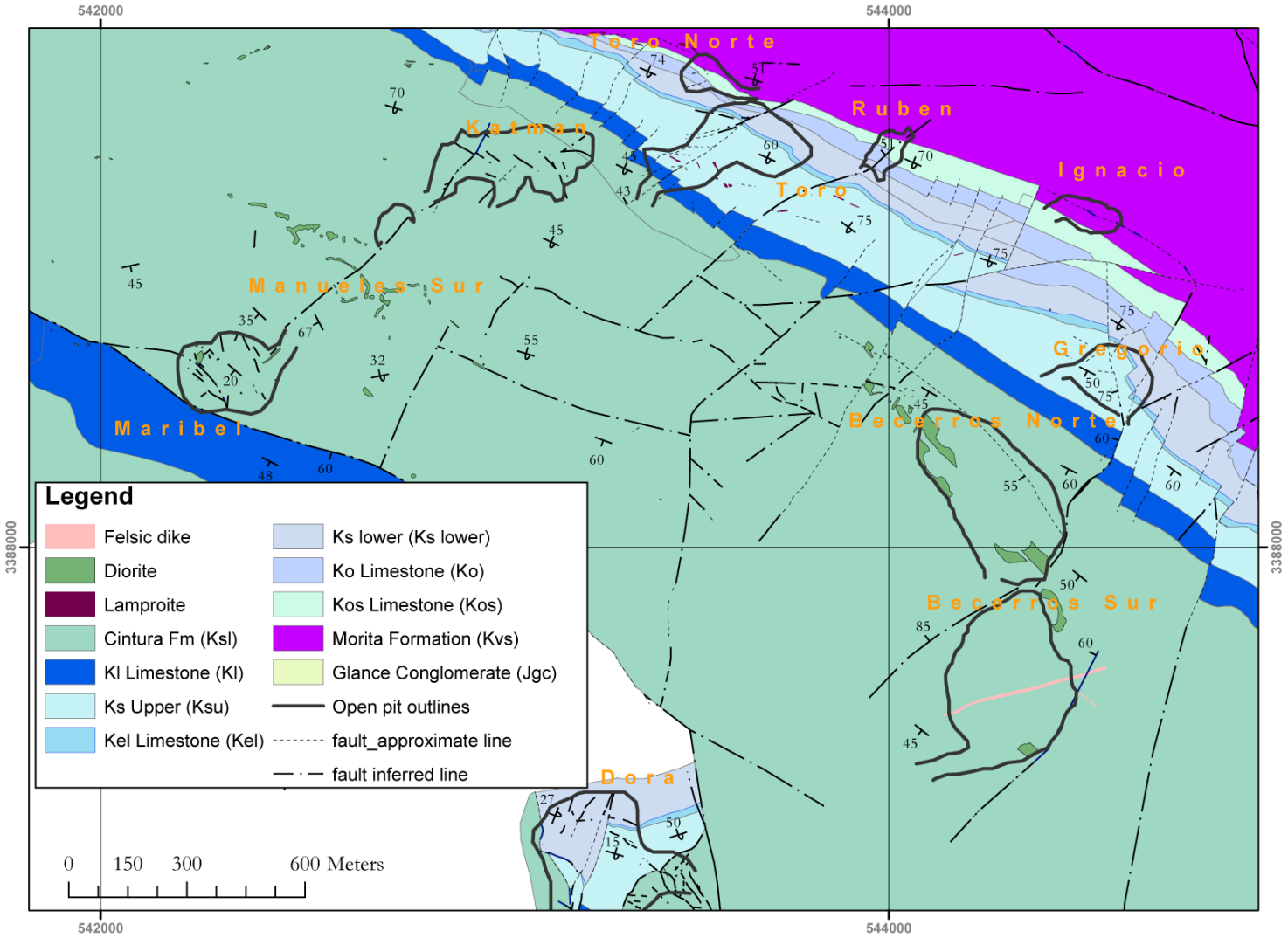

Figure 3-39 Geologic map of the Toro-to-Gregorio study area

Figure 3-40 Bedding-parallel shear-zone with associated structural preparation and mineralization. Camello Mine. Scale is 12 X 18 inches.

The combined production from the Becerros Norte and Becerros Sur Mines (Figure 3-41) represent the greatest amount of recovered gold in the entire Santa Gertrudis mining district, and these pits are hosted entirely in Cintura Formation. Strong structural control is evident, with mineralization sited in the hanging wall of a family of southwest-dipping, brittle structures that are cut by a highly quartz-sericite-pyrite altered felsic dike that locally hosted gold in Becerros Sur (Onsite, Phelps Dodge pit maps). The felsic dike was clearly of interest to Phelps Dodge; they bulldozed, trenched and drilled it along the strike for nearly a kilometer. Bennett noted a N70°E structural control to mineralization at Aqua Blanca (Figure 3-39) and Becerros Sur, parallel to the felsic dike. Becerros Norte has abundant northwest-trending, shear-zone-hosted mineralization, which dictates the orientation of the pit but the source was most likely the northeast structure evident in the bench blast maps at 1410 m (Figure 3-44) and in mapping by this author.

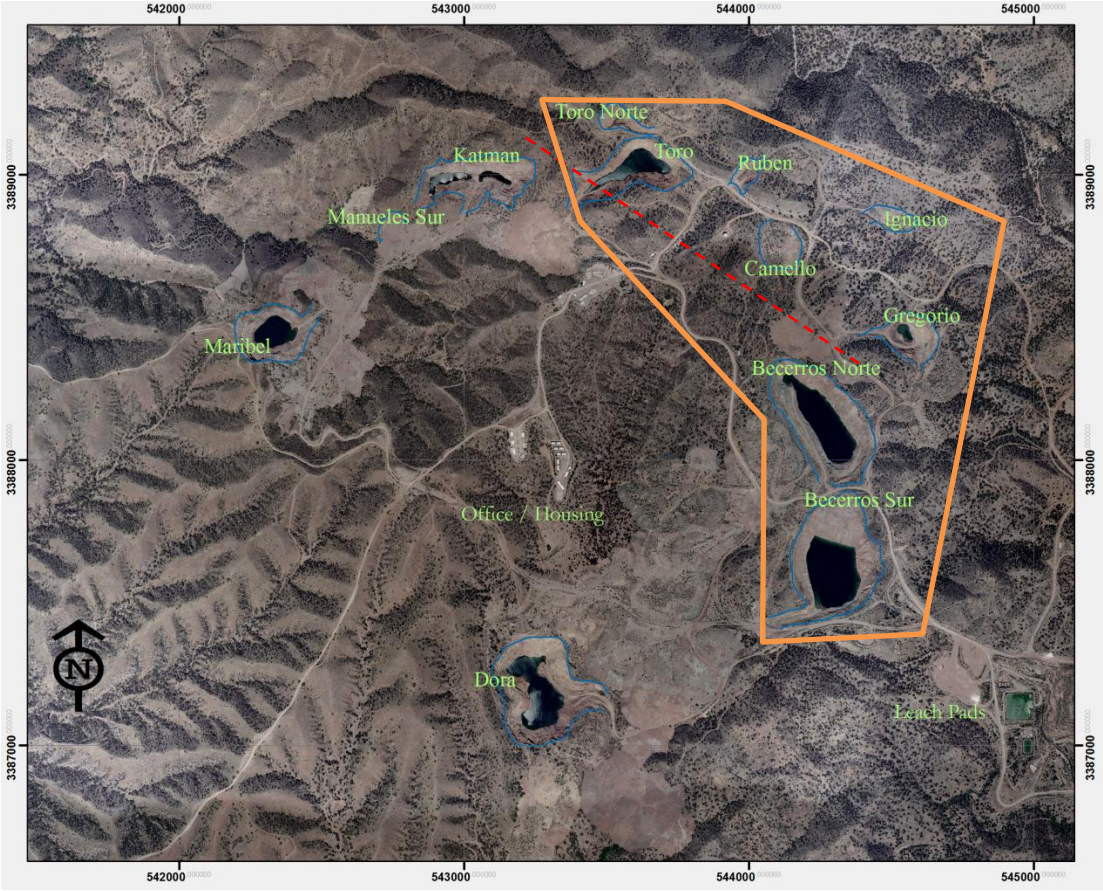

Figure 3-41 Toro-to-Gregorio study area (orange box), all mines southwest of a line drawn from Katman to Becerros Norte are in Cintura Formation, excluding Dora. All mines northeast of that same line are in the Ks through Ko units. Note strong circular pattern independent of stratigraphy and dominant, northwest-trending structural fabric.

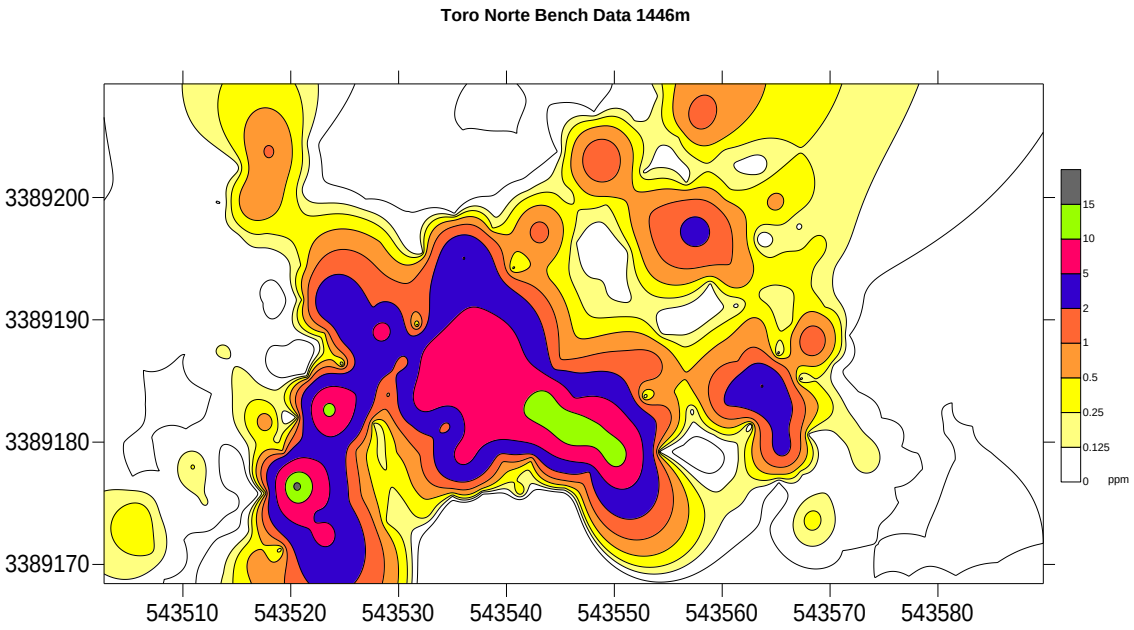

Figure 3-42 Surfer plot of bench blast data at Toro Norte Mine, at 1446 m elevation. Note NNE and NW structural controls to mineralization. Units range from 0 to 15 ppm gold.

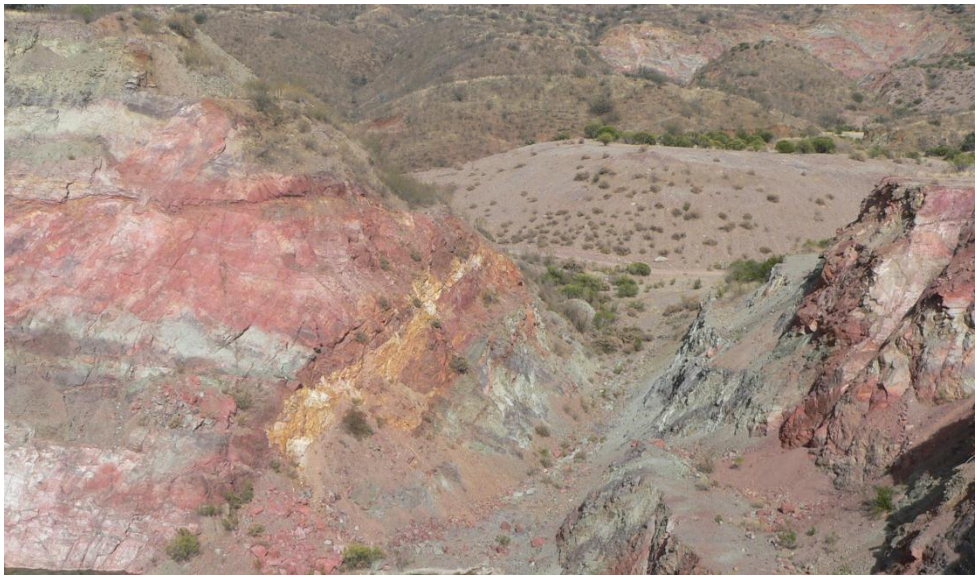

Figure 3-43 Northeast-trending mineralization and alteration associated with a northeast-trending fault in Maribel Mine, Manueles Sur lies beneath the tailings pile in mid-picture and Katman Mine is in the background. Looking northeast.

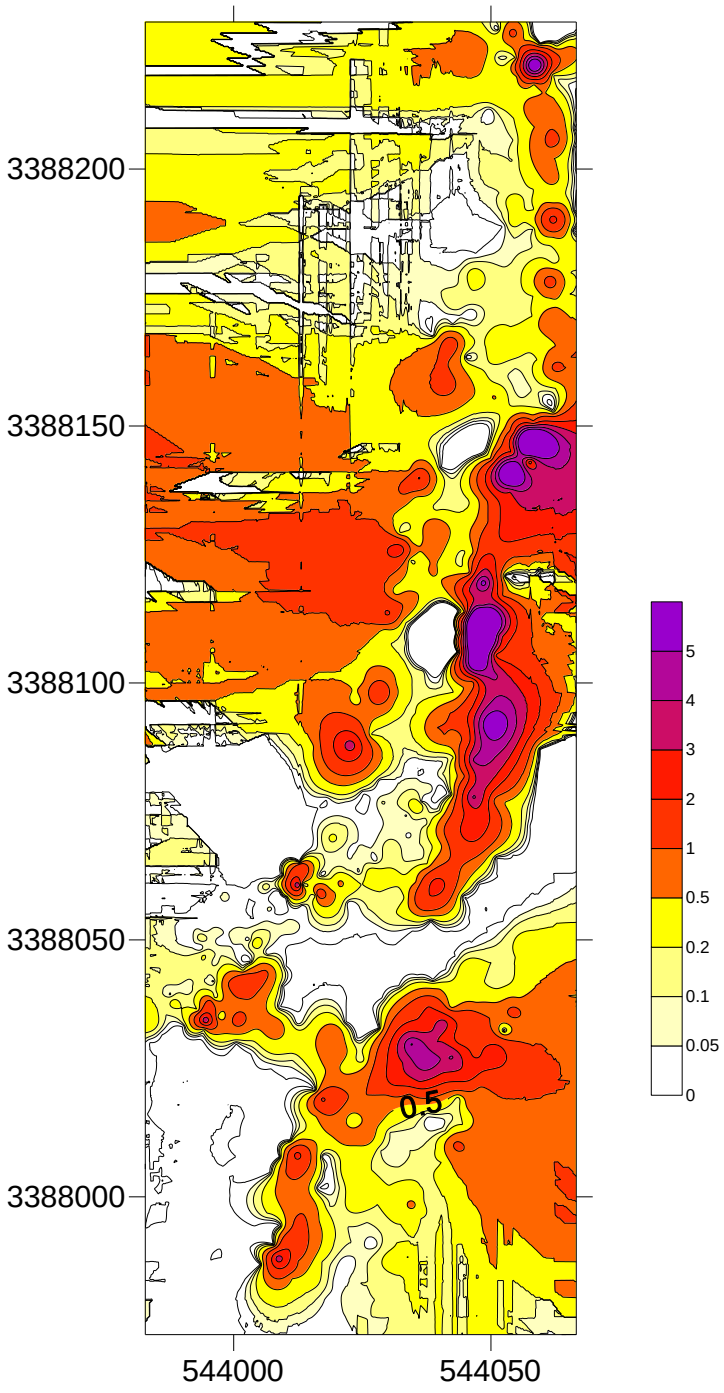

Figure 3-44 Surfer plots of bench blast maps at 1410 m elevation at Becerros Norte Mine, southwest corner of the pit. Note NNE control of the gold mineralization. The felsic dike exposed in Becerros Sur cuts the structure that controls mineralization and also cuts a similar structure at Becerros Sur.

Along the northwestern and southeastern walls of Becerros Norte, in the hanging wall of the northeast-trending structure, there is an excellent exposure of the pre-mineral diorite and associated local hornfels in shear contact with the mineralized hanging-wall rocks (Figure 3-45). The diorite was a non-receptive host within either of the Becerros pits and may have acted as a barrier to the mineralizing fluids.

Figure 3-45 View looking 330° at Becerros Norte. At left, dark grayish green rock is pre-mineral diorite with hornfels associated with local, contact metamorphism. Reddish area on right is the mineralized shear-zone that was the primary mined ore zone.

Shear-zone mineralization in Becerros Norte is typical of the Main District, sediment-hosted distal disseminated gold with sulfide and arsenic associations. Drilling along all of the obvious extensions of mineralized structures extending away from Becerros Norte and Sur have

revealed the pinch-and-swell nature of the structures, as well as the compartmentalized shallow gold observed throughout the Main District.

Geochemical observations

A comparison was attempted between legacy drilling and Animas 2008 and 2009 drilling in the Toro-to-Gregorio study area, to quantify the primary association and to identify recognizable patterns of element redistribution utilizing Principal Component Analysis (PCA). Data were split into less than 200 m drill depth and greater than 200 m drill depth and PCA was run utilizing Tanagra 1.4.36. PCA is a mathematical transformation of possibly correlatable variables into a smaller number of uncorrelated principal components, with the first component accounting for the largest amount of variability within the data and the following components accounting for a portion of the remaining variability. This allows for the calculation of correlation coefficients within the individual principal components, with the first two components generally serving as the best representation of correlation and variability within the data.

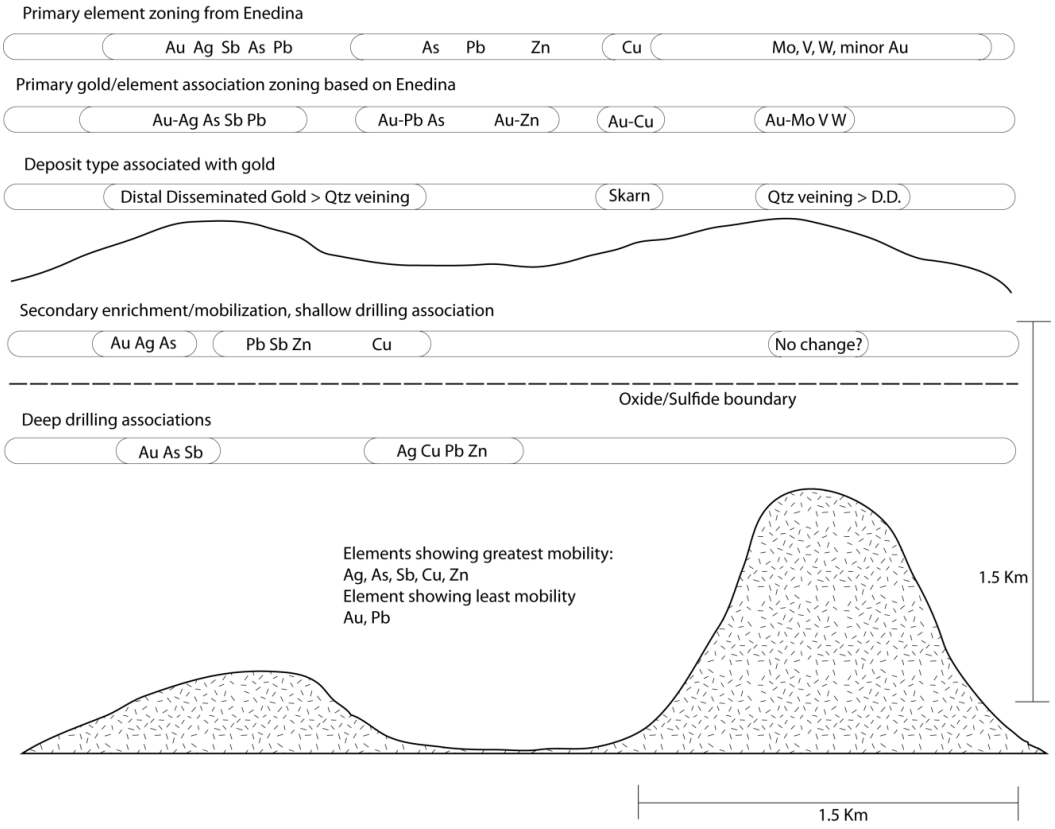

Figure 3-46 Schematic of element distribution and association in Enedina based on drill core, rock chip, and soil sampling (above topography) and as compared to Main District shallow and deep drill core (below topography).

The data analyzed represents the bulk of the collection of legacy and Animas multi-chemical assays within the Toro-to-Gregorio study area, has been parsed to gold > 0.05 ppm and run in an eigenvector-based multivariate analyses, with a seven-matrix trace that emphasizes on element correlation. The depth of legacy drilling was largely dictated by the oxide/sulfide boundary and rarely exceeded 200 m, due to the preg-robbing properties of the sulfide ore encountered below the oxide zone. Animas drilled more than a dozen holes deeper than 200 m during their exploration of the Main District.

The first two principal component axes account for 57.68% of the data within the shallow-drilling data, and 53.42% of the deep data. Covariance and correlation within the data are evident and correlations vary with depth (Figure 3-47; Figure 3-48).

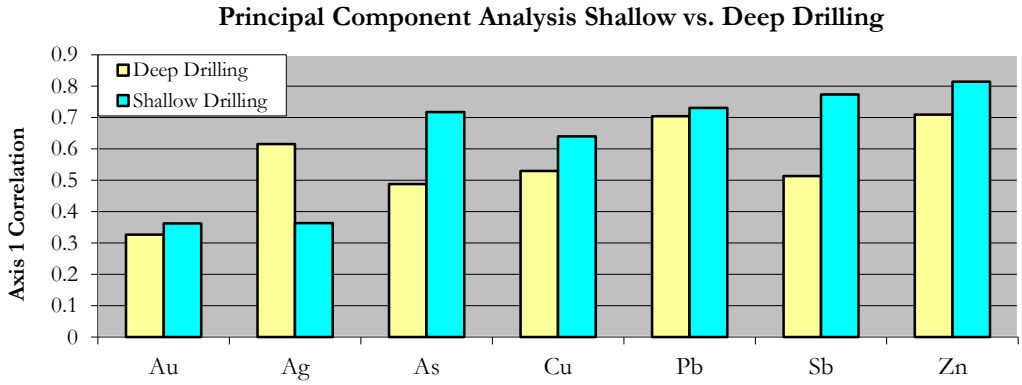

Figure 3-47 Plot of values of Axis 1 correlation coefficients from Principal Component Analysis of Toro-to-Gregorio study area shallow (>200 m, n = 701) and deep (<200 m, n = 488) multi-element, drill core data.

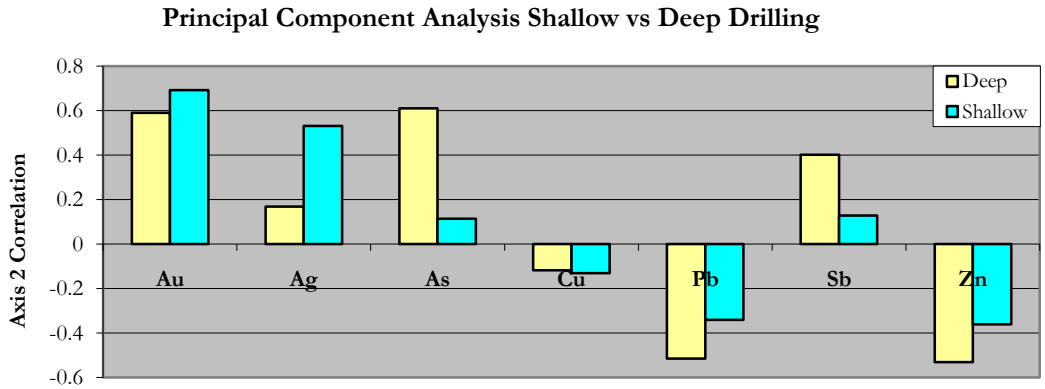

Figure 3-48 Plot values of Axis 2 correlation coefficients from Principal Component Analysis of Toro-to-Gregorio study area shallow (>200 m, n = 701) and deep (<200 m, n = 488) multi-element, drill-hole data.

There is a strong correlation between As, Cu, Pb, Zn, and Sb in the shallow drilling. There is also a close correlation of silver to gold, which is less than half the average correlation of the base metals (Figure 3-49).

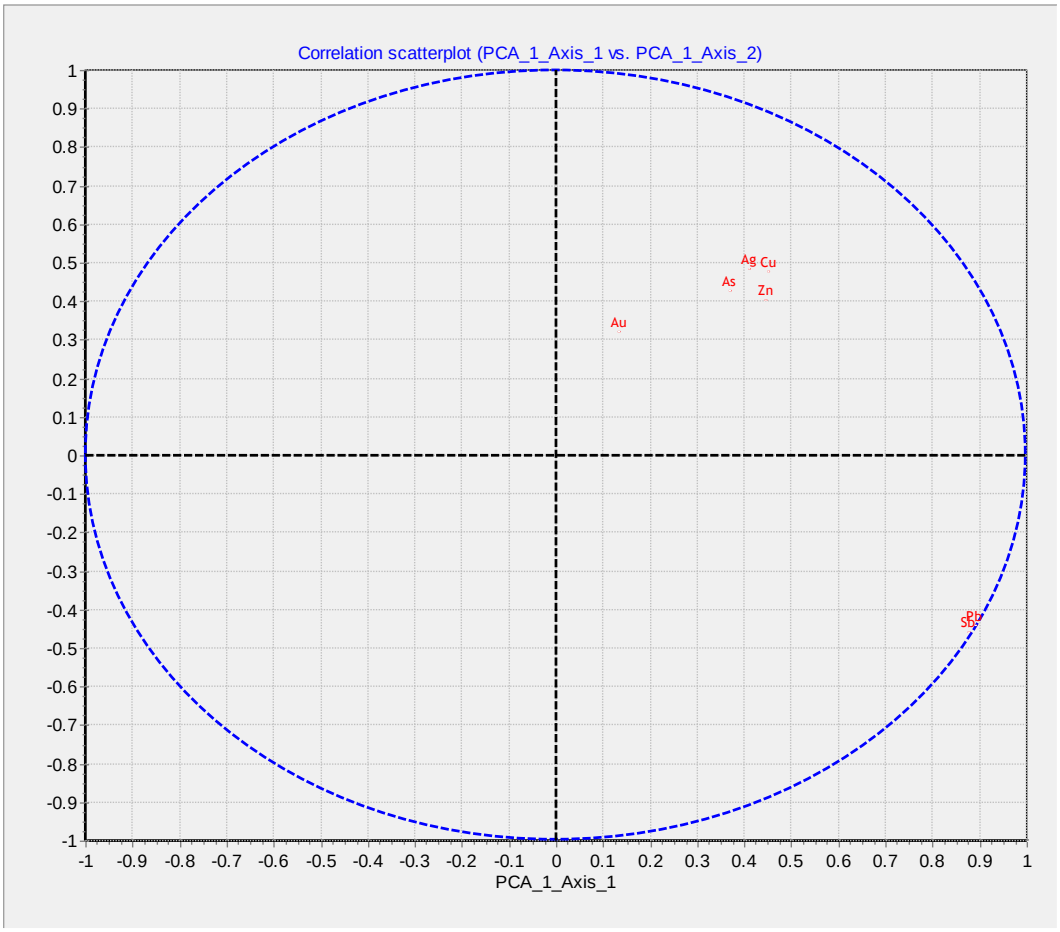

Figure 3-49 Shallow drilling (> 200m), Toro-to-Gregorio study area, n = 6761 reveals a strong correlation to Ag, Cu, As and Zn, with a lesser association to gold.

In the deep drilling, there is a correlation between Zn and Pb, with lesser correlation to Ag (Figure 3-50).

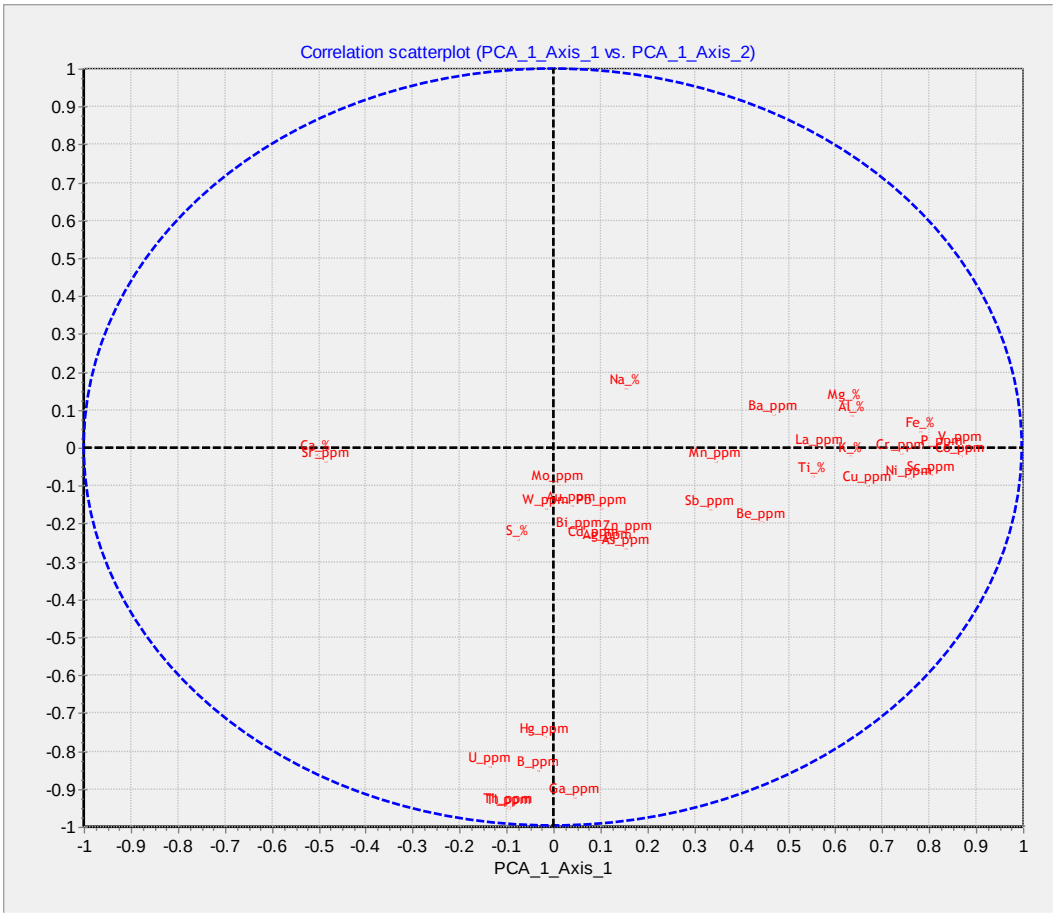

Figure 3-50 Drilling deeper than 200 m, Toro-to-Gregorio study area, n = 1226, with tight clustering of Mo, W, S, Bi, Cd, As, Au, Ag and Zn.

The primary distribution of mineralization by hydrothermal fluids is dependent on temperature, pressure, pH, redox potential, rock reactivity, and other factors. Groups of elements that have similar geochemical behavior during hydrothermal transport and deposition will exhibit spatial correlation based on the factors that dictate their distribution. Following the initial mineralizing event, oxidation and redistribution of mobile elements and enrichment of less mobile elements through chemical-erosional lag will alter the initial spatial distribution of the elements. This redistribution of like elements that have similar geochemical behavior in the oxidizing environment will exhibit similar modification of their distributions. Quantifying the

primary element associations to mineralization and recognizing geochemical associations that identify element redistribution are important to the understanding of the paragenesis and modification of the mineralization (Figure 3-46).

Interestingly, the overall change in the correlation between elements for deep versus shallow sites is the least for gold and lead, and with the largest change occurring in antimony, arsenic, zinc, and silver. Silver becomes less correlatable to gold at depth, whereas arsenic, antimony, and zinc become more correlatable with depth (Figure 3-47; Figure 3-48). This seems to match the assertion by Roslyakov (1972) that Zn > Cd = Hg> Ag > Cu = Mo > Co = Ni > Au > Pb > Sn = W = Bi in relation to element mobility in non-humic complexing, supergene environments. It also implies that gold and lead correlations are not changing by the same processes that are altering the other, more mobile elements. The wild variation in Ag-to-Au ratio values in surface, soil, and shallow drill-hole data (Bennett, 1993 and this study) appears negated by the correlation of Au-Ag in the shallow drilling versus the lack of correlation of Au-Ag at depth. This may be the best evidence for secondary element mobility in the system. The correlation comparisons also help to explain the surficial dispersion halos associated with the gold-bearing structures, implying that the halos are not primary mineralization features, but the result of element mobility and enrichment in the oxide zone. The halos may represent the oxidation of Au-As-Sb-Ag-bearing sulfides and dispersion of the more mobile elements. This will be discussed in further detail in Chapter IV.

IV. FINDINGS AND DISCUSSION

Structural Observations

Following the deposition of the Bisbee Group, the Bisbee Basin was closed by uplift of the region and tectonic events. The oldest recorded fabrics in the district include bedding-parallel shear zones and isoclinal folds with S_1 axial planar cleavage roughly parallel to bedding (S_0). The fabrics consistently indicate top-to-the-northeast shortening in sections that are still upright. They pre-date the thermal event associated with the Enedina hornfels, with F_1 isoclinal folds preserved within the hornfels and the S_1 fabric being annealed by the hornfels event. The bedding-parallel shear-zones were later locally overturned along with the bedding in the large, outcrop-scale, northwest-trending, southwest-vergent folds. Large-scale top-to-the-southwest deformation ductilely deformed the rocks, folding and overturning the stratigraphy of the Bisbee Group in the Gregorio syncline. Flexure slip and shearing related to folds reactivated the bedding-parallel slip planes, further preparing open spaces for future mineralizing fluids. Mineralization, focused along brittle-ductile fault structures and intersections, post-dates the main overturning event. The best local evidence for a timing constraint on the cessation of Laramide ductile deformation is the lack of ductile fabrics in the 42 Ma Las Panochas Granite. Mineralized structures are then dismembered by reactivated low-angle, southwest-dipping structures, with extensional movement as a last recorded movement. Basin and Range-related structures then cut through the low-angle structures and the mineralization, uplifting northeast blocks relative to southwest ones.

Although there are many structural complexities and reactivated structures within the district, the generalized field relationships of crosscutting structures is consistent with the

regional geologic history of northern Sonora and southern Arizona. Compressive deformation, related to Laramide orogeny is evident in many sites within the area, including all three of the study areas. Early bedding-parallel slip is later overturned as the thrusting progressed and the folds became more complex. Thrust directions switch from early, northeast directed to a later, southwest directed, as is common in the region (Krantz. 1989). Wholesale extension of the crust began approximately at the onset of Eocene and Oligocene magmatism recorded in the Sierra Madre Occidental. Decapitation of Laramide fold structures and pre-existing mineralization would be an expected outcome of the extension of the crust, as is evident at Santa Gertrudis at the Gate fault near Mirador, Maribel Mine (Figure 2-40), Corral Mine (Figure 2-42) and Toro Norte Mine. Finally, Basin and Range normal faulting, recognized throughout the district, cuts all of the aforementioned structures and mineralization.

This sequence of events, based on field and drill core evidence, places the timing of gold mineralization after Laramide deformation, but prior to extension. The earliest recorded extension in Sonora is Eocene in age (Ferrari et al., 2007), with three pulses of extension occurring from the Eocene to the late Miocene. Therefore, mineralization at Santa Gertrudis can be constrained between the end of Laramide compression and the extensional faults that cut the mineralization. Broadly, this could be from 50-23 Ma, but it could be as early as 50-40 Ma, depending on the age of the mineral-truncating Gate fault in the Mirador study area and similar faults in the district.

Another constraint lies in the Batamote graben and in uplift that was associated with basin formation. Mineralization does not cut into the Oligocene Magdalena Formation or the underlying trachyandesite. Exposures of conglomerate in the Batamote graben, interpreted to be Magdalena Formation, unconformably overly the mineralized and sheared Bisbee Group at

San Enrique and may preserve the first exposure of mineralization to the surface. This constrains the minimum age of mineralization to older than 23 Ma based on the age of the Magdalena Formation.

Geochemical Observations

Geochemistry within the district varies, with broad correlations or associations to mineralization, trace elements, alteration, and deposit types. This has led some to the conclusion that there have been multiple pulses of mineralization, temporally spaced and within widely varying ore-forming environments. This study has shown that there is 1) a clear relationship between the base metal and precious metal zoning and the proposed intrusive beneath Enedina, and 2) a correlation to central-hornfels-zones and peripheral mineralization elsewhere in the district (La Bonita). Geochemical signatures of San Enrique and the Las Panochas Granite are nearly identical to the Enedina study area: from the initial, nearly isochemical metamorphism, to the structurally controlled emplacement of intrusives, and finally to mineralization and the zoned base-metal systems. Peripheral, disseminated gold is found in the Enedina study area at La Gloria, Greta, Nelly, Tracy and Laura prospects. Peripheral, disseminated gold is found flanking San Enrique at La Gotera, El Grasero, San Rafael, Rebbeca, Ciria, and Don Enrique prospects (Figure 4-1).

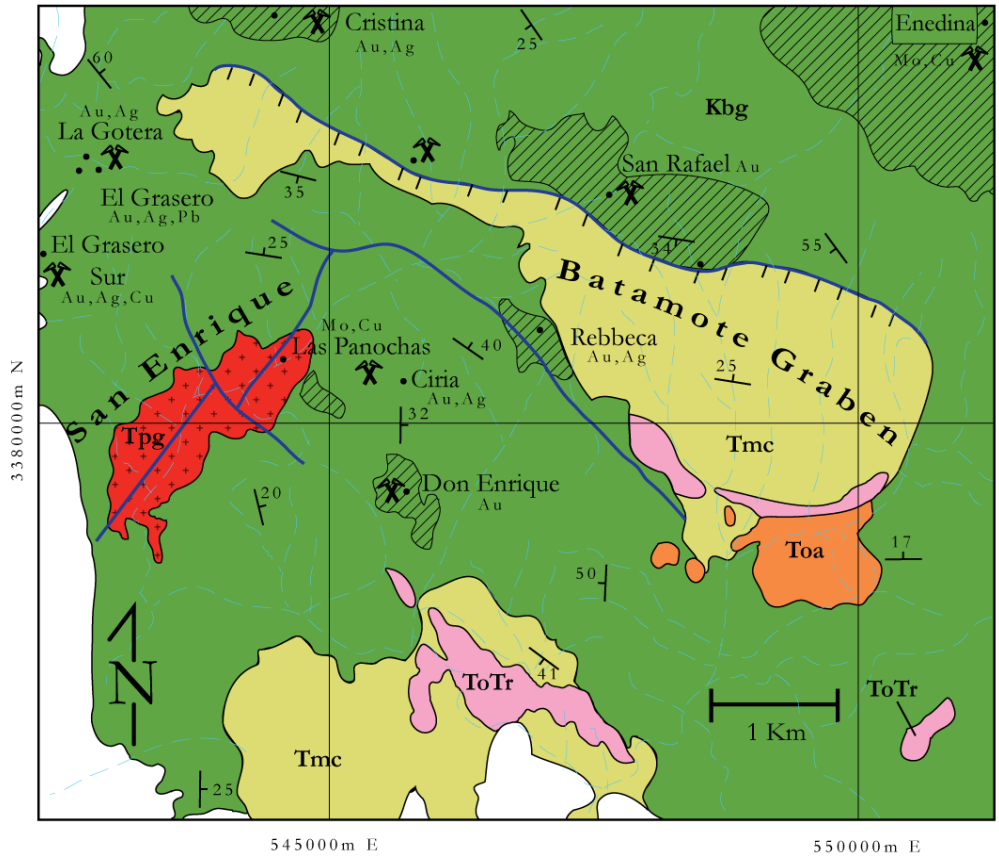

Figure 4-1 General geology and prospects associated with San Enrique and the Las Panochas Granite. Stippled areas are oxidized units. Kbg is Bisbee Group undifferentiated. Adapted from SGM, 2003.

The distances from the intrusive center to the flanking prospects at San Enrique are 2.5 to 3.4 km; it is 2.5 km from the center of Enedina Hill to the La Gloria prospect and similar distances to the other prospects. Similar types of deposits and alteration styles flank San Enrique, with the strongest mineralization focused in the northeastern corner, another intriguing similarity to the Enedina study area. This spatial relationship hints at structural control for emplacement of the mineralization and possibly the causative intrusive. Alternatively, it could indicate post-mineral, northeast-side down tilting.

Zoning within the gold mineralization is evident in the Enedina study area, from proximal, high-temperature quartz plus Au/Mo to the distal, disseminated, higher-grade Au/As/Sb associations. This may be evidence for an evolution in hydrothermal fluids and in the type of Au-complexing during mineralization. Mirsa (2000) states that although the solubility of both chloride and bisulfide complexes increases with increasing temperature (Henley, 1973; Seward, 1973; Wood et al., 1994), thermal effects on natural systems are more difficult to predict due to varying temperature-affecting parameters (such as oxygen and sulfur fugacities), that have a greater influence on the solubility of gold. Complexing and deposition of gold within natural systems are closely tied to changes in the activities of hydrogen, oxygen, and chlorine in chloride complexes. A potential Au-chloride complex reaction is:

$$4\ AuCl_2^- + 2\ H_2O = 4\ Au^0(s) + 8\ Cl^- + 4\ H^+(aq) + O_2$$

This reveals that gold precipitation will be caused by an increase in pH or a decrease in either the activities of chlorine or oxygen. Utilizing thermodynamic data, Huston and Large (1989) proposed that gold precipitation in chloride complexes would be initiated by a simple decrease in temperature, and to a lesser extent, by a rise in pH or decrease in the activity of oxygen. This is easily achievable during fluid mixing, diluting the saline fluids and lowering the activity of chlorine or during boiling of the hydrothermal fluids during depressurization. An increase in pH is likely when acidic fluids encounter calcareous rocks, like those in the Mural and basal Cintura Formation.

In contrast, Au-bisulfide complexes have a wide temperature range of stability from 150-350°C (Seward, 1973; Hayashi and Ohmoto, 1991), negating a simple temperature relation to deposition (Mirsa, 2000). Several reactions (Huston and Large, 1989; Hannington et al., 1991;

Hayashi and Ohmoto, 1991) have been proposed for the deposition of gold from bisulfide complexes including:

$$4\ Au(HS)_2^- + 2\ H_2O + 4\ H^+(aq) = 4\ Au^0\ (s) + 8\ H_2S\ (aq) + O_2$$

$$HAu(HS)_2^0 + \tfrac{1}{2}\ H_2\ (aq) = 4\ Au^0\ (s) + 2\ H_2S\ (aq)$$

The bisulfide reactions imply that gold precipitation can be caused by a decrease in aH_2S and by either a decrease in aO_2, or an increase in aH_2, depending on the bisulfide complexes (Mirsa, 2000). Changes in the hydrothermal fluids may be brought about by the interaction of the gold-bearing fluids with wall rocks, with the most efficient method of precipitating gold achieved by decreasing the activity of reduced sulfur. This is due to a two orders of magnitude decrease in solubility of gold with each order of magnitude decrease in the activity of reduced sulfur (Huston and Large, 1989). Proposed methods for reducing the activity of reduced sulfur include 1) dilution of S_2^- species in the hydrothermal fluid; 2) oxidation of H_2S and HS^- to sulfate and sulfur, perhaps by mixing with meteoric water; 3) boiling of hydrothermal fluids; 4) sulfidation through Fe-rich wall rock interaction (Christensen, 2010; Phillips and Groves, 1984); or 5) precipitation from the residual fluids after boiling (Drummond and Ohmoto, 1985). Phillips and Groves (1984) propose that sulfidation of the wall rocks and gold deposition could be achieved in iron-rich sediments under greenschist metamorphic facies by the following process:

$$FeO + HAu(HS)_2 + \tfrac{1}{4}\ O_2 \rightarrow FeS_2 + 3/2H_2O + Au$$

They state that many gold deposits can be attributed to the sulfidation process in hydrothermal fluids at temperatures of less than 300°C (Phillips and Groves, 1984).

Sillitoe (1989) proposed a genetic model linking differing gold-enriched porphyry copper deposits to various intrusion-related and epithermal gold deposit types based on interdependent fluid regimes in porphyry, intrusion-related deposits. Sillitoe recognizes three interdependent fluids: 1) dense, high salinity (30 to >75 wt% NaCl equivalent), high-temperature (400 to >700°C) magmatic, hydrothermal brines; 2) ascending plumes of lower density, sulfur-rich, magmatic volatiles that condense upwards and mix with meteoric fluids; and 3) meteoric-water convection cells on the margins of the intrusive. Sillitoe proposes that these fluid regimes, with magma and/or country rocks acting as the source of gold, are capable of producing a variety of gold deposit types from fluids of varying temperature and salinity and at various distances from the intrusion. Sillitoe adds that proximal, high-temperature, magmatic hydrothermal fluids that are oxidizing and saline could introduce gold and copper as chloride complexes. Gold and copper would be precipitated with decreasing temperature or increasing pH. This contrasts with lower temperature, distal, fluids that are less oxidized and more dilute, formed from the mixing of magmatic hydrothermal fluids and convecting meteoric waters. Such fluids are likely to carry bisulfide complexes to be associated with decalcification and/or silicification in carbonate host rocks (Sillitoe 1989), with a spatial distribution consistent with stratigraphic and structural control.

Beyond the zones of visibly hornfelsed rocks, with their tight structural controls on economic mineralization, there lie large zones of weakly phyllitic altered rocks. Bennett attributed this to regional metamorphism related to early burial and ductile deformation (Bennett, 1993), but this could be instead be associated with elevated geotherms related to multiple intrusive stocks throughout the district. The planar deformational fabrics, including cleavage, in the phyllitic rocks, as opposed to structureless hornfels, suggests a close tie to

deformation-related processes. Mineralization within these phyllitic zones represents the bulk of the mined and recognized gold.

One of the earliest models proposed for mineralization at Santa Gertrudis was based on the Carlin model of far-removed, distal disseminated gold. Two of the geochemical characteristics of Carlin-like deposits is a ratio of Ag < Au (10 Au:1 Ag) and very low base metal contents in the deep deposits (Christensen, 2010). Phelps Dodge published early reports that touted the possibility of a Carlin-like deposit, and Bennett (1993) pointed out that the district had a variable, but overall average Au-to-Ag ratio, of greater than 1:1. Since the early Phelps Dodge and Bennett studies, an enormous geochemical database has been amassed and this study reveals the Ag:Au ratio is high throughout the Main District (Figure 4-2, n = 21,085). This suggests that the intrusive geochemical signature recognized in the zoned base metal systems is being continued out into favorable stratigraphy that has structural preparation, perhaps kilometers away from the central stock that supplied the mineralizing fluids. Although no studies have ever been undertaken on the paragenetic nature of the silver, electrum has been identified by electron microprobe and has been noted as a source of ore in several Phelps Dodge studies and in Bennett's (1993) thesis.

Animas 2008 and 2009 drilling has revealed a primary correlation to gold and Zn, Pb, As, Cu, and Sb, unlike the geochemical signature at Carlin. Bennett had recognized this association with only nine samples in 1993. The base metal association with gold (Figure 4-3), present in the Main District and kilometers away from the closest intrusive center exposed at the surface, mimics the associations seen on the periphery of the Enedina and San Enrique hornfels. It is unlike the patterns at Carlin.

Geochemical zoning and element association are most easily recognized in the Enedina study area, presumably due to less structural perturbations than in the Main District and the lack of strong oxidation within the Enedina hornfels. The geochemical associations are still recognized in the Main District deep drilling. Guilbert and Park (1986) state that ore body zoning is nonexistent in deposits and districts that have persistent, temporally spaced mineralization. Although there is always the possibility of multiple, temporal-spaced mineralizing events bringing gold and base metals to the Main District, the easiest explanation would be to associate the Main District gold to one mineralizing event based on field and geochemical evidence. Quartz and poly-metallic veins with similar geochemical associations at Enedina and the Main District reveal a plausible temporal association. The high-angle, fault-bounded quartz vein described in the Gregorio Mine (Figure 2-72) has geochemical associations similar to that at Enedina.

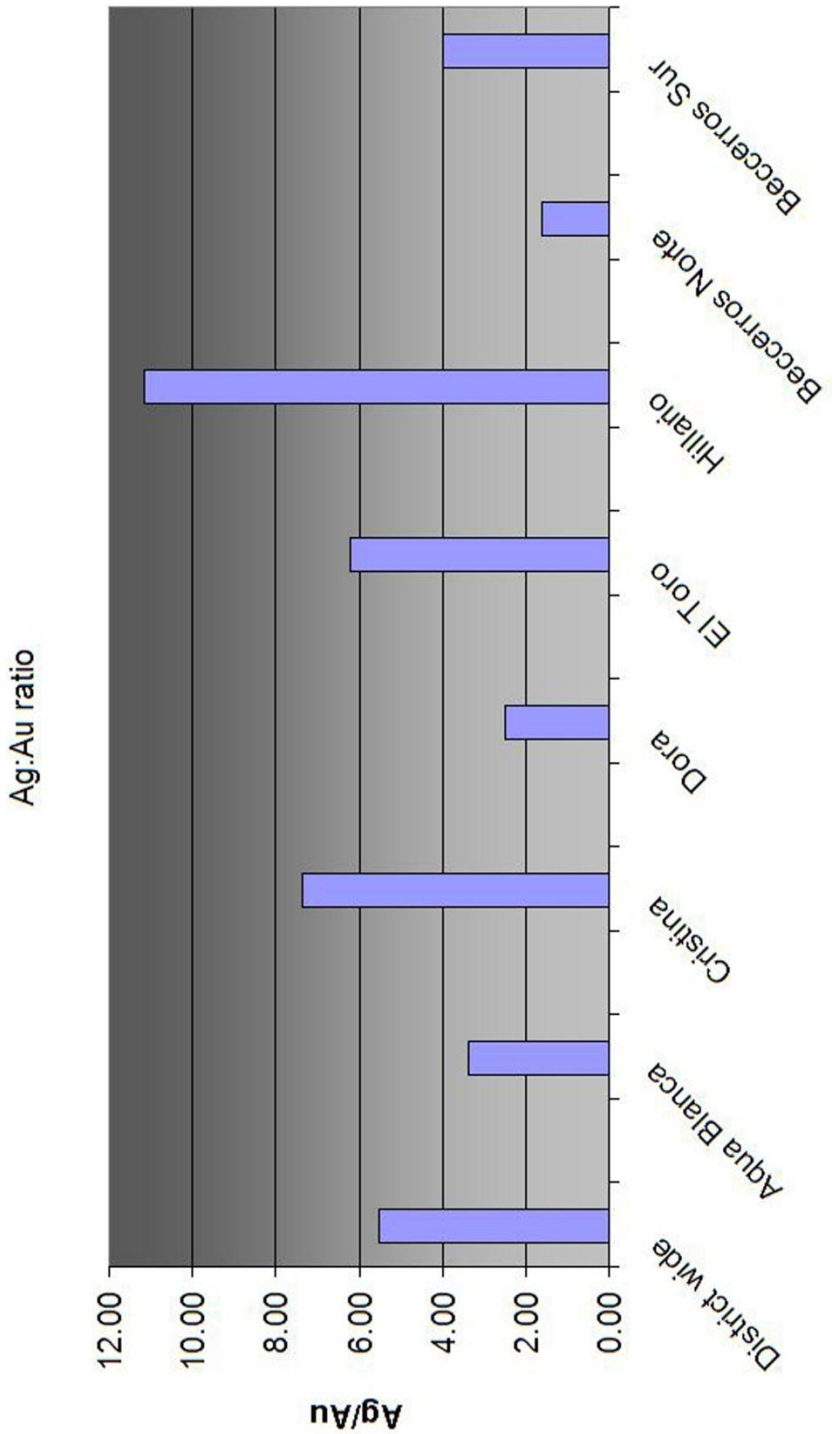

Figure 4-2 Ag:Au ratios for individual mines and district wide data (n = 21,085)

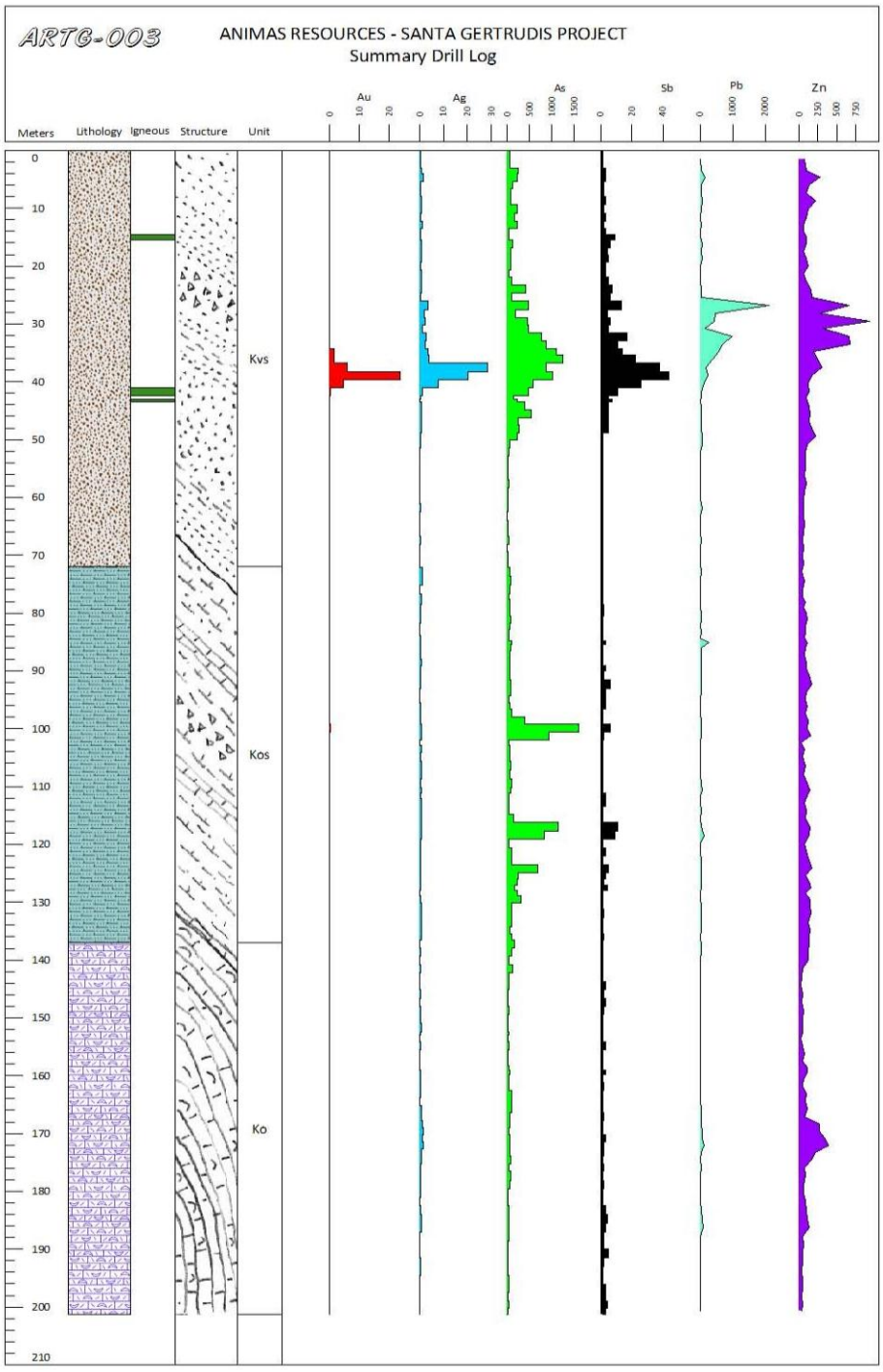

Figure 4-3 Strater log of ARTG-003, Main District, combined with structural oriented cross section showing strong association of gold to base metals. All elements in ppm. (Christensen, Geier, MacFarlane, 2009)

A possible analog to Santa Gertrudis is the Toqui district located in southern Chile. The district has a total resource of 20 million tons at 8.2% Zn and 1.5 g/t Au contained in skarn and replacement ore bodies within 24 km^2 (Bussey et al., 2010). Within Toqui, Fe, As, Au, Bi, and Co are associated with garnet, pyroxene, and amphibole alteration, whereas Pb and Ag are associated with chlorite and sericite; Zn grades are uniform across the district.

> According to Bussey et al., 2010, economically significant gold mineralization was superimposed on earlier base metal-rich skarn in the southeastern part of the district. Late hydrothermal fluids entered the skarn system along preexisting northwest-trending structures. Gold occurs as electrum associated with native bismuth, cobaltite and a variety of sulfosalts. Gold-rich ore generally contains abundant arsenopyrite, but arsenopyrite-rich ores are not necessarily gold rich.

They add that deep drilling has revealed two sub-economic pyrite-chalcopyrite-molybdenite stockworks beneath the skarn and the sericitized mineralization, associating the district to a large porphyry-skarn with multiple pulses of intrusives and alteration (Bussey et al., 2010).

Many similarities exist between the Toqui District and the Enedina study area and the San Enrique prospect. Skarn associations and rock types, including oyster-bearing limestone are accompanied by geochemical signatures including Cu, Au, Ag, Co, Pb, Zn, Te, Bi, As, Hg, W. and Sb and older anhydrous skarn overprinted by amphibole skarns as base and precious metal hosts (This study, Table 3-1). Gold occurs as electrum (Bennett, 1993, Phelps Dodge, 1992), and cobalt is anomalous in many samples from the Enedina study area, as is bismuth. The scale of the areas are similar, with Enedina coming up slightly smaller in area; mineral potentials appear to differ by orders of magnitude.

Supergene Enrichment

One of the largest distinctions between the hornfels versus the phyllitic-altered rocks in the district is the large amount of surficial oxidation that has occurred in the weakly metamorphosed, iron-sulfide-bearing phyllitic rocks. Fluid flow and oxidation have altered the phyllitic rocks much more dramatically than the sealed hornfels. Remobilization of elements and potential concentration of sub-economic gold into small, shallow, porous structural intersections would be much more likely in the phyllitic rocks. The abundant exposures of iron oxides in the Main District, similar to a gossan, are non-existent in the Enedina and San Enrique areas. Abundant hematite and goethite are not present at Enedina except along the La Gloria shear-zone and near the periphery gold deposits (La Gloria on the northeast and Leon and Emma on the northwest). Instead, the sulfides have avoided oxidation by being associated with hornfels rocks that lack fissility and other types of permeability. In contrast, the Main District has strong hematite and goethite associated with fractures, joints, faults, shear-zones and fold-flexure brecciation in non-hornfels rock. The structural perturbations have allowed for the influx of meteoric waters and oxidation of sulfides of Cu, Zn, Pb, As, Ag, and Au, redistributing the mobile elements and concentrating the less mobile ones. This is evident in the shallow-versus-deep drilling results in the Main District discussed in Chapter III. Haloes of tracer elements are much larger and volumetrically more abundant than gold at the surface, but seem to narrow with depth, becoming more closely tied to the mineralized structure at depth. This is also the case for gold associations with base metals at depth, as evident in Figure 4-4.

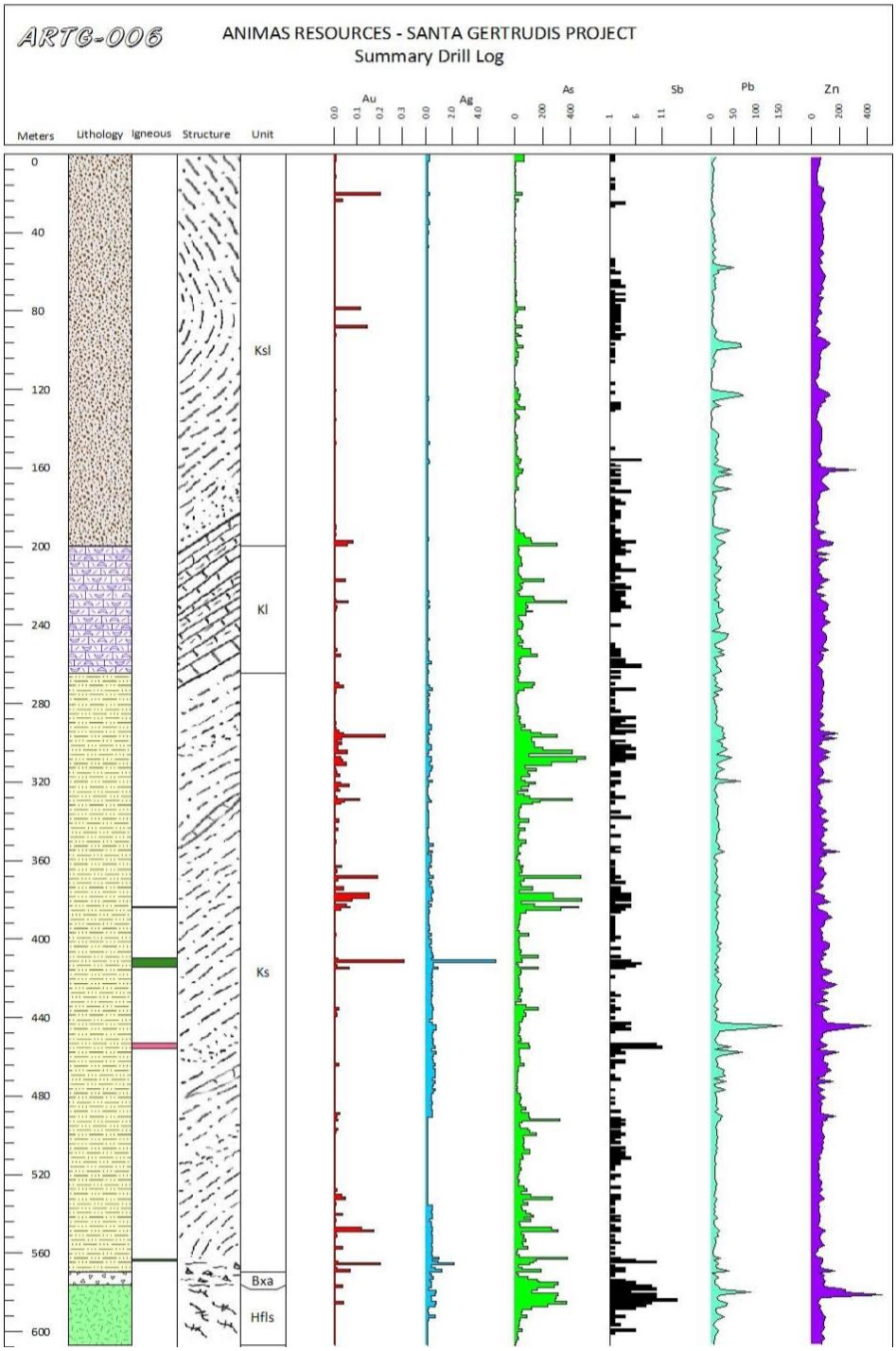

Figure 4-4 Strater log of Animas ARTG-006. Gold association with base metals increases with depth, the oxide/sulfide boundary is approximately 200 m depth. All elements in ppm. Silver scale 10X gold. (Christensen, Geier, MacFarlane, 2009).

It is conceivable that the higher grades of gold mineralization at the surface, the redistribution of mobile elements, and the decreasing grade with depth may be attributed to supergene enrichment and residual lag of gold at the surface. The possibility that mineralization has been intermittently exposed to the near surface since the Late Oligocene has been proposed in this study, allowing ample time for element redistribution and supergene enrichment.

Listova et al. (1966) performed experiments utilizing solutions created during the oxidation of lead, zinc, and iron sulfides, finding that gold was dissolved in these solutions. They noted a marked increase in gold solubility when $CaCO_3$ was present and concluded that the gold was complexing with thiosulphates and polythionates under the alkaline conditions created by oxidizing sulfides and then reacting the products with carbonates. Furthermore, the presence of Fe^{3+} or similar oxidants and chloride in solution increases the solubility and mobility of gold by forming stable, chloride-based complexes based on the reaction:

$$2Au^{o} + 2H^{+} + 4Cl^{-} \rightarrow 2[AuCl_2]^{-} + H_2$$

It has also been suggested (Al'bov, 1952) that gold solubility increases in oxidation zones as the size of the particle decreases below 100 microns. Given the presence of oxidizing sulfides, carbonate rocks, micron to sub-micron gold particles and iron sulfides, it is possible that gold mobility and enrichment focused widespread, lower grade gold along pre-existing structural weaknesses at the near-surface. This may help to explain the decrease in grade with depth, and the lack of continuity to mineralization.

Finally, one of the largest Au-Ag open pit mines in the world, Pueblo Viejo, Dominican Republic has 27 Mt grading at 4.23 g/t Au and 21.6 g/t Ag. It is hosted in an oxidized, sulfide

protore and ore is attributed to supergene enrichment (Kesler et al., 1981). Interestingly, the 5:1 silver to gold ratio noted at Pueblo Viejo is the same 5:1 silver to gold ratio observed in the Main District at Santa Gertrudis.

Conclusion

Tectonism, volcanism and structural-controlled mineralization related to the subduction of oceanic plates in the Pacific played a key role in shaping the economic deposits of Mexico since the Jurassic Period (Figure 4-5).

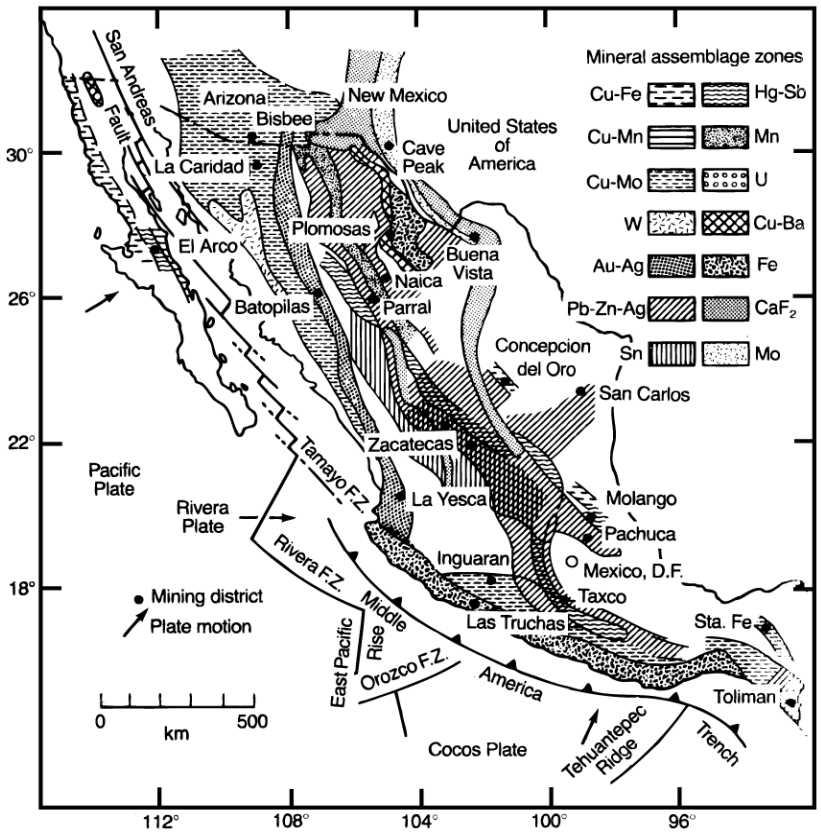

Figure 4-5 Proposed mineral zoning in Mexico paralleling the subducting margin. Santa Gertrudis lies in the Cu-Mo belt, just west of La Caridad. From Guilbert and Park (1986) by Damon, Shafiqullah and Clark (1981).

District wide, Santa Gertrudis has experienced various structural deformations, related to its proximity to the actively evolving western margin of the North America Plate. The earliest recorded deformation in the district is the opening of the Bisbee Basin and the deposition of the Glance Conglomerate. The conformable transition from Glance Conglomerate to Morita Formation marks the cessation of rifting and the switch to passive subsidence and from terrestrial to marine sedimentation. Deposition of the Cintura and El Tuli Formations marks the return to terrestrial-dominated sedimentation, potentially related to structural perturbations beyond the scope of this study. Within the district, the closure of the Bisbee Basin and the onset of crustal shortening are recorded in two distinct events; an older, ductile to brittle-ductile top-to-the-northeast thrust and penetrative shearing, followed by a younger, brittle-ductile top-to-the-southwest thrusting. These shortening orientations and the related fabrics are consistent with Laramide compression. Folding, overturning, and repetition of the units occur throughout the district, along with ductile fabrics and abundant shear indicators. Presumably, the formation of the north-northeast-trending and northeast-trending, high-angle faults is related to the thrusting event as tear faults. This hypothesis has been put forth since the earliest Phelps Dodge era. Field evidence is clear that the northeast-trending faults have experienced multiple episodes of reactivation. Cessation of shortening and fabric formation is best estimated by the age of the Las Panochas Granite (42 Ma). The lack of shear fabrics and shortening within the granite and associated felsic dikes precludes the intrusions presence during compression.

By the end of the Laramide Orogeny, the combined effects of sedimentation and deformation resulted in a thick sequence of clastic to siliciclastic to calc-silicate to marine deposits, cut by multiple generations of faults and structural fabrics. Within the district, this

deformation structurally prepared the rocks for the onset of mineralization by creating sinuous, tapered, bedding-parallel fluid pathways produced by shearing and by bedding-parallel slip, during thrusting and during fold-flexure (Figure 2-62). The brittle-ductile nature of the faults and shear zones, and the tapered, pinch-and swell profile of their fault breccias, dictated future sites of mineralizing fluid flow and mineral deposition. Field evidence to support this interpretation is abundant throughout the district including exposures in El Toro, Ruben, Becerros Norte, and Amelia, as well as the multitude of drill-holes that attempted to track mineralization along northwest-trending, bedding-parallel shear-zones.

Field evidence, drilling, core inspection, and rock-chip assays indicate that the gold mineralization postdates the shortening and overturning of the district and is related to a magmatic event that delivered the gold along with base metals. Gold, throughout the district, has been most often characterized as being associated with iron, arsenic, and lead sulfides as surficial coatings. Drill core from AREN-001 and ARET-001 both reveal an initial, disseminated sulfidation event associated with early retrograde metamorphism, but prior to base metal sulfides plus quartz veins, which also produced abundant pyrite.

Although the drilling at El Tigre and Enedina was unsuccessful in penetrating the causative intrusive in the Enedina study area, the geochemistry of the holes and the overlying geochemical halo are consistent with the proposal that the causative intrusive is very similar in nature to the Las Panochas Granite. The geochemical associations at Enedina and San Enrique are nearly identical; only the levels of exposure differ. Most of the upper geochemical halo at San Enrique has been eroded away or tectonically stripped off during the uplift of the intrusion. Most of the possibly gold-enriched areas on the northeastern corner of San Enrique

lie under a post-mineral normal fault, of which the entire Santa Gertrudis District is the hanging wall.

This study concludes that the causative intrusives for the gold emplacement are chemically and temporally associated to the Las Panochas Granite, as a series of related stocks that are distributed throughout the district at differing emplacement levels and at different post-mineral structural levels. Therefore, the timing for a pulse gold mineralization is well correlated to the age of molybdenite mineralization at San Enrique, radiometrically dated at 42 Ma. Bennett's 36 Ma K-Ar age on greisen alteration in the Las Panochas Granite is likely reset due to Ar loss, or is a cooling age and may not a viable date for mineral emplacement. Mineralizing fluids were most concentrated along pre-existing and syn-kinematic structures, and gold mineralization was concentrated on the periphery of the intensely hardened hornfels and zoned base metals in chemically reactive, calcareous to calc-silicate rocks, especially within the intersections of northwest, bedding-parallel shear-zones and north-to northeast-trending, high-angle structures. Although dissemination of the gold is widespread, the concentration was most limited to pre-mineral fault gouge, syn-kinematic gouge, and rarely as quartz vein fragments plus gold in syn-kinematic fault gouge, such as Gregorio Pit. Disseminated gold haloes flanking the brittle, mineralized faults that cut hornfels, including at Mirador Pit and El Tigre prospect, reveal that pervasive, yet localized fluids postdate the hornfelsing event. Presumably, the gold was deposited on the surfaces of diagenetic and hydrothermal pyrite present in the hornfels as the hydrothermal fluids permeated through fractures or late-stage faults.

Reduced-to-Pole magnetics reveals that there is a highly anomalous magnetic halo associated with the Enedina hornfels and skarn intrusive-related mineralization (Appendix C, C-1). RTP magnetics of the entire district Figure C-2 (Appendix C) hint that there may be magnetic highs

associated with the gold deposits within the district. Beyond Enedina, the Main District has a nearly 1:1 correlation to magnetic highs associated with gold, but the anomaly is weaker (deeper?) than at Enedina. Amelia and Trinidad are also associated with magnetic highs. The magnetic signatures may be reflecting the underlying, deeper stocks associated with the gold mineralization and the hornfelsing event. At Enedina, it seems clear that the magnetic signature is associated with the magnetite observed at the surface, and should not be attributed to unseen, intermediate to mafic intrusives. Given the similarities in geophysical, geochemical and alteration styles to the different deposits throughout the district, this study concludes that there is no need to evoke younger, differing mineralization events to explain the district.

Northeast-trending structures played a key role in channeling gold-bearing hydrothermal fluids to more reactive, less thermally altered rocks on the periphery of Enedina and San Enrique. In the Enedina study area, gold-bearing silicified breccias are associated with northeast-trending structures as they cut through the less metamorphosed and highly reactive Ks, Ko, and Kos in the La Gloria, Greta, Nelly, Lupita, and Esperanza prospects. Each prospect is approximately 2.5 to 3 km away from the inferred central heat source and all are associated with northeast-trending structures. Silicification is strongest along the fault zones and dwindles tens of meters from the fault zones. The most intense silicification is in the footwalls of the northeast-trending, northwest-dipping faults. Decalcification is also strongest within the aforementioned prospects, presumably a product of acidic fluids utilizing the faults and attacking the calcareous units prior to, or during silicification. Within the Main District, the association of northeast-trending and northwest-trending structures has been recognized for over 30 years. It is clear in Toro Norte Pit that the two faults have very differing alteration styles, even though they cut through the same lithologies. The northwest-trending faults have

the typical bedding-parallel shear fabrics and gouge, with disseminated gold and iron oxides. In contrast, the northeast-trending faults have strong decalcification and silicification of the Ko beds, also with elevated gold values. Field evidence in Toro Norte and Ruben Pits shows a clear relationship of mineralization apparently bleeding out of the northeast-trending faults and into the northwest, bedding-parallel shear-zones.

The Batamote graben has basal Oligocene volcanics and conglomerates with fanning dips. Presumably, these units and the active basin they filled represent the uplift and exposure of the Las Panochas Granite during extension and prior to the emplacement of the Late Oligocene to Miocene ash-fall tuffs of the Sierra Madre Occidental. Although this event is not well understood within the district, it is an important detail, since it may be the timing for first exposure of mineralized rocks at the surface. Subsequently, the sediments in the graben were covered by the Miocene tuffs.

Although not present within the three study areas, the next important event is the deposition of ash-fall tuffs and pyroclastic deposits related to the Sierra Madre Occidental. The tuffs probably blanketed the Batamote graben and currently flank the district to the northeast, east, southeast and south. They occur as thick, continuous sheets that are fault bounded on the edges of the sheet. These units would have covered the district at some time, given their thickness and lateral continuity, but have been stripped off by erosion or tectonics, or some combination. The volcanism is 36 to 26 Ma based on crosscutting relationships with younger dikes and their unconformable contact with the Las Panochas Granite in the western portion of the San Enrique prospect area (Smith, 2006). No mineralization or alteration is present within the tuffs, and their unconformable contact on mineralized rocks solidifies the hypothesis that mineralization near the granite is older than the unconformity that exposes the

Las Panochas Granite Although the lack of evidence is never a compelling argument, no alteration related to gold mineralization is present in any unit younger than Eocene.

Regionally, Miocene extension was the next major deformational event to affect the mining district. This study was unable to directly correlate the low-angle normal faults or any other structures to core-complex formation, nor were any detachment-style faults or fabrics recognized within the Main District or the three study areas. Within the San Enrique area, there are reported extensional shear fabrics (Smith, 2006), but this study was unable to establish any link of these with core-complex formation. Although the extensional effects of core complex formation are an intriguing idea to evoke for uplift, exposure, heat generation, intrusives, and subsequent mineralization, the geochemical and structural evidence presented in this study, along with the pre-detachment, Late Oligocene to Early Miocene unconformity, indicates that mineralization pre-dates Late Miocene detachment faulting and core-complex formation. Drilling and field mapping throughout the district have revealed several post-mineral, low-angle structures that clearly displace the Laramide folds, the Eocene hornfels and the northwest-trending, bedding-parallel mineralized structures (i.e. Main District, San Enrique and Mirador). The low-angle, post-mineral normal faulting was perhaps most successful at unroofing the underlying mineralized rocks from the capping, Miocene ash-fall tuffs and in decapitating the deposits.

Abundant intermediate to ultramafic dikes and sills intruded the district during the onset of regional extension. They are post-mineral, although they can accompany anomalous gold. Except where shattered by younger faulting, they appear fresh and unaltered by mineralizing fluids throughout the district and in the Animas 2008 and 2009 drilling program. Although

Rock et al. (1988) hint at a relationship to lamprophyre intrusives and gold mineralization, no geochemical or spatial evidence exists for this being the case at Santa Gertrudis.

Basin and Range, high-angle faults are the youngest recorded tectonic event, cutting all other structures and rock types. Several northwest-trending Basin and Range faults have been identified within the district; all are clearly post-mineral. Maximum offset along these faults can exceed 1 km, placing weakly phyllite-altered rocks adjacent to strong hornfels.

Element enrichment through chemical precipitation and as mechanical lag has been an important process in the concentration of gold within the highly oxidized, weakly metamorphosed sedimentary rocks since their exposure to the surface. This may have begun as early as the Late Oligocene with the uplift and exposure of the Las Panochas Granite and the surrounding mineralized Bisbee Group. The unconformity seen in Maribel Pit, with mineralized Bisbee rocks topped with unmineralized conglomerates, reveals the opportunity for enrichment began prior to present generation of erosion. Subsequent exposure by unroofing would have allowed for continued enrichment, mostly focused in fractured, faulted, and chemically reactive rocks. Depending on the age of unroofing of the district, mineralized rocks may have been exposed to the surface for more than 25 Ma, allowing surficial oxidation to penetrate to average depths of 150 m and up to 250 m deep along fault planes. This oxidation liberated the gold as native grains, some of which may have been dissolved and transported, and some of which remained as grains that could be concentrated as lag, more mobile elements were transported away. Erosion of the surrounding topography would have lowered the mineralized rock level, but erosional lag of gold grains may have remained, further enriching the oxidized ground. Finally, there is tentative evidence that the current or past position of the water table may have played a role in concentrating the gold, such as in the drill

results along strike of the Red fault at Mirador Pit. The role of supergene enrichment is poorly understood in the district, but the Animas geologists and this author suspect it is important (John Wilson, per comm.). It has been invoked to explain gold anomalies in very localized, surficial samples that appear to counter, otherwise salient field and drill evidence, such as the minor presence of gold in lamproite dikes. This interpretation is founded on the strong effects of oxidation on the host rocks and on the mineralization, and the results of the geochemical studies undertaken during this study. Further studies in the area would benefit from exploring the role of supergene enrichment.

BIBLIOGRAPHY

Allmendinger, R., 2006, Stereonet v. 1.2.0 software, http://www.geo.cornell.edu/geology/faculty/RWA/programs.html.

Al'bov, M.N., 1952: Forms of the migration of gold in the oxidized zone of mineral deposits; Akad. Nauk SSSR, Izv., Ser. Geol., no. 4, p. 41-52.

Anderson, T.A., Nourse, 2005, J.A., Pull-apart basins at releasing bends of the sinistral Late Jurassic Mojave-Sonora fault system, Geological Society of America Special Paper 393, p. 97-122.

Anderson, S.D., Monthly Reports for Campbell Resources, May 1997 to Mach 2000, Campbell Resources.

Anderson, S.D and Oro de Sotula staff., 2000. The Santa Gertrudis Property, Northeast Sonora, Mexico: Geology, Structure, Exploration Model, and targets for Deep Drilling, for Campbell Resources Inc., internal report, October 1, 2000, 12 pp.

Anderson, S.D., Hamilton, 2000, W.S., Summary report of exploration on the Santa Gertrudis property, northeast Sonora, Mexico, Campbell Resources, p. 150.

Archibald, L.E., 1987, Stratigraphy and sedimentology of the Bisbee Group in the Whetstone Mountains, southeastern Arizona, Mesozoic Rocks of Southern Arizona and Adjacent Areas, Dickinson, W.R., Klute, M.A., eds., Arizona Geological Society Digest 18, p. 273-282.

Arehart, G.B., Chryssoulis, S.L., and Kesler, S.E., 1993, Gold and arsenic in iron sulfides from sediment-hosted disseminated gold deposits: Implications for depositional processes. Economic Geology, 88, 171-185.

Asmerom, Y., Zatrman, R., Damon, P.E., and Shafiqullah**,** M., Zircon U-Th-Pb and whole-rock Rb-Sr age patterns of lower Mesozoic igneous rocks in the Santa Rita Mountains, southeast Arizona. *GSA Bulletin*; July 1990; v. 102; no. 7; p. 961-968.

Bakken, B.M., Hochella, M.F., Jr., Marshall, A.F., and Turner A.M., 1989, High-resolution microscopy of gold in unoxidized ore from the Carlin mine, Nevada. Economic Geology, 84, 171-179.

Bakken, B.M., Fleming, R.H., and Hochella, M.F., Jr., 1991, High-resolution microscopy of auriferous pyrite from the Post deposit, Carlin district, Nevada. In D.M. Hausen, W Petruk, RD. Hagni, and A. Vassiliou, eds., Process Mineralogy XI: Characterization of metallurgical and recyclable products, p. 13-23. The Minerals, Metals, and Materials Society, Warrendale, Pennsylvania.

Barnes, H.L., Czmanske, G.K., 1967, Solubilities and transport of ore minerals, *in* Geochemistry of Hydrothermal Ore Deposits, H.L. Barnes, ed., New York: Holt, Rinehart and Winston, p 334-381.

Bennett, S. Santa Teresa District, Sonora, Mexico: A Gold Exploration Study Aided by Lithologic Mapping, Remote Sensing, and Geographic Information System Compilation. [M.S. Thesis]: University of Colorado at Boulder, 1993.

Bergman, S.E., 1987, Lamproites and other potassium rich igneous rocks, *in* Fitton, J.G., and Upton, RG.J., eds., Alkaline igneous rocks: Geological Society of London Special Publication 30, p. 103-190.

Blanchard, R., 1947, Some pipe deposits of Eastern Australia. Econ. Geol., 42, p. 265-304.

Blatt, H., Tracy, R.J., Petrology (2nd ed.). New York: Freeman. p. 66. (1997).

Bilodeau, W.L., 1979, Early Cretaceous tectonics and deposition of the Glance Conglomerate, southeastern Arizona [Ph.D. dissertation]: Stanford, Stanford University, 145 p.

Bilodeau, W.L., 1982, Tectonic models for Early Cretaceous rifting in southeastern Arizona, Geology, Vol. 10, p. 466-470.

Bilodeau, W.L., Lindberg, F.A., 1983, Early Cretaceous tectonics and sedimentation in southern Arizona, southwestern New Mexico and northern Sonora, Mexico, Mesozoic Paleogeography of the West-Central United States, Reynolds, M.W., Dolly, E.D., eds., Rocky Mountain Section (SEPM) Rocky Mountain Paleogeography Symposium 2, p. 173-188.

Bilodeau, W.L., Kluth, C.F., Vedder, L.K., 1987. Regional stratigraphic, sedimentologic, and tectonic relationships of the Glance Conglomerate in Southern Arizona. Mesozoic Rocks of Southern Arizona and Adjacent Areas, Dickinson, W.R., Klute, M.A. (Eds.). Arizona Geological Society Digest 18, 229-256.

Boyle, R.W., 1979, The geochemistry of gold and its deposits: Geological Survey of Canada Bulletin, v. 280, 584 p.

Burnham Petrographics, 2010, Petrographic Report, Santa Gertrudis Project, Sonora Mexico, for: Animas Resources Ltd.

Bussey, S.D., Kakarieka, A., Meinert, L.D. 2010 Society of Economic Geologists, Inc. *Special Publication* 15, p. 399–420.

Compton, R. R., 1985, Geology in the Field, Wiley, New York, 387 pp.

Coney, P.J., 1971, Cordilleran tectonic transitions and motion of the North American plate, Nature,
233, p. 462-465.

Coney, P.J., 1976, Plate tectonics and the Laramide orogeny: in Woodward, L.A., and Northrop, S.A., eds., Tectonics and mineral resources of southwestern North America: New Mexico Geological Society, Special Publication, No.6, pp. 5-10.

Coney, P.J., and Reynolds, S.J., 1977, Cordilleran Benioff zones: Nature, v. 270, p. 403-406.

Corona, F.V., 1979, Preliminary reconnaissance geology of Sierra La Gloria and Cerro Basura, northwestern Sonora, Mexico, *in* Anderson, T.H., and Roldán-Quintana, J., eds., Geology of northern Sonora: Boulder, Colorado, Annual Meeting of the Geological Society of America, Field Trip (#27) Guidebook, p. 32-48.

Corona, F.V., 1980, Reconnaissance geology of Sierra La Gloria and Cerro Basura, northwestern Sonora, Mexico [M.S. thesis]: Pittsburg, Pennsylvania, University of Pittsburg, 232 p.

Cox, K. G., Bell, J. D., Pankhurst, R. J., 1979, The Interpretation of Igneous Rocks, George Allen & Unwin.

Christensen, O., 2010, personal communications.

.

Damon, P.E., Shafiqullah, M., Clark, K.F., 1983, Geochronology of the porphyry copper deposits and related mineralization of Mexico, Canadian Journal of Earth Sciences, v. 20, p. 1052-1071.

Davis, G.H., 1979, Laramide folding and faulting in southeastern Arizona: American Journal of Science, v. 279, p. 543-569.

Dickinson, W.R., 1981, Plate tectonic evolution of the southern Cordillera: in Dickinson, W.R., and Payne, W.D., eds., Relation of tectonics to ore deposits in the southern Cordillera: Arizona Geological Society Digest, v. 14, pp. 113-135.

Dickinson, W.R., Fiorillo, A.R., Hall, D.L., Monreal, R., Potochnik, A.R., Swift, P.N., 1989, Cretaceous stratigraphy of southern Arizona. In Jenny, J.P., Reynolds, S.J., eds., Geologic evolution of Arizona: Arizona Geological Society Digest, v. 17, p. 447-461.

Dickinson, W.R., Klute, M.A., Swift, P.N. 1986, The Bisbee Basin and its bearing on late Mesozoic paleographic and paleotectonic relations between the Cordilleran and Caribbean regions, *in*: Abbot, P.L., ed., Cretaceous Stratigraphy, Western North America: Los Angeles, Pacific Section. SEPM, Book 46, p. 51-62.

Dickinson, W.R., Lawton, T.F., 2001, Carboniferous to Cretaceous assembly and fragmentation of Mexico: Geological Society of America Bulletin, v. 113, no. 9, p. 1142-1160.

Dickinson, W.R., Snyder, W.S., 1978, Plate tectonics of the Laramide orogeny, Geologic Society of
America Memorandum, 151, p. 355-366.

Drewes, H., and Thorman, C.H., 1978, Major geologic structures between Lordsburg, New Mexico, and Douglas and Tucson, Arizona, *in* Callender, J.F., Wilt, J.C., and Clemons, R.E., eds., Land of Cochise, southeastern Arizona: Twenty-Ninth Field Conference Guidebook, New Mexico Geological Society, p. 291-295.

Dumble, E.T., 1900, Notes on the geology of Sonora, Mexico: Geological Society of America Bulletin, v. 11, p. 10-14.

Einaudi, M.T., Meinert, L.D., Newberry, R.J., 1981, Skarn deposits: Econ. Geol., 75th Anniv. Vol., p. 317-391.

Fergusson, W.B., 1959, The Cretaceous system of southeastern Arizona: Arizona Geological Society Guidebook II, Geological Society of America, pp. 43-47.

Ferrari, L., Valencia-Moreno, M., Bryan, S., 2007, Magmatism and Tectonics of the Sierra Madre Occidental and its Relation with the Evolution of the Western Margin of North America. In: (eds.) Alaniz-Álvarez, S.A., Nieto-Samaniego, Á.F. Sociedad Geológica Mexicana. Geology of Mexico: celebrating the centenary of the Geological Society of Mexico. GSA, Special Bulletin 422.

Ferrari, L., Rosas-Elguera, J., 2000, Late Miocene to Quaternary Extension at the Northern Boundary of the Jalisco Block, western Mexico: The Tepic-Zacoalco rift revised, *in* Delgado-Granados, H., Aguirre- Díaz, G.J., and Stock, J.M., eds., Cenozoic Tectonics and Volcanism of Mexico: Geological Society of America Special Paper 334, p. 41–64.

Ferrari, L., López-Martínez, M., and Rosas-Elguera, J., 2002, Ignimbrite flareup and deformation in the southern Sierra Madre Occidental, western Mexico—implications for the late subduction history of the Farallon Plate: Tectonics, v. 21.

Fleet, M.E., Minum, A.H., 1997, Gold-bearing arsenian pyrite and marcasite and arsenopyrite from Carlin Trend gold deposits and laboratory synthesis, American Mineralogist, v. 82, p. 182-193.

Fleet, M.E., MacLean, PJ., Barbier, J., 1989, Oscillatory-zoned As-bearing pyrite from strata-bound and stratiform gold deposits: An indicator of ore fluid evolution. Economic Geology Monograph 6, p. 356- 362.

Fleet, M.E., Chryssoulis, S.L., MacLean, PJ., Davidson, R, Weisener, C.G., 1993, Arsenian pyrite fom gold deposits: Au and As distribution investigated by SIMS and EMF, and color staining and surface oxidation by XPS and LIMS. Canadian Mineralogist, 31, p. 1-17.

Foley, S.F., Venturelli, G., Green, D.H., Toscani, L., 1987, The ultrapotassic rocks: characteristics, classification, and constraints for petrogenetic models. *Earth-Sci.* Rev. 24, p. 81-134.

Gans, P.B., MacMillan, I., Roldán-Quintana, J., 2003, Late Miocene (Proto Gulf) extension and magmatism on the Sonoran margin: EOS, Transactions AGU, v. 84(46), Fall Meeting Supplement, p. F1405.

Garcia y Barragan, J.C., 2003, Stratigraphy, sedimentology and tectonic model for the origin of the Late Cretaceous El Tuli Formation in northern Sonora, Mexico, *ETD Collection for University of Texas, El Paso.* Paper AAI3146480. http://digitalcommons.utep.edu/dissertations/AAI3146480

Garcia y Barragan, J. C., 1975, Estudio geologico-radiometrico en el area de EI Picacho, Municipio de Arizpe, Estado de Sonora [B. S. thesis]: Ciudad de Mexico, Universidad Nacional Autonoma de Mexico.

García y Barragán, J. C., Rodríguez-Castañeda, J. L. y Arellano-González, L. C., 2008, Relaciones estratigráficas y tectónicas entre conglomerados del Jurásico en el noroeste de Sonora, en Valencia-Moreno, M. y Vega-Granillo, E. L., 1er. Congreso sobre la Evolución Geológica y Ecológica del Noroeste de México, Universidad Nacional Autónoma de México, Instituto de Geología, Estación Regional del Noroeste, Libro de Resúmenes, p. 114-115.

Garrels, R. M., 1941, The Mississippi Valley type lead-zinc deposits and the problem of mineral zoning: Econ. Geol., 36, p. 729-744.

Geier, J.J., MacFarlane, B.J., 2011, Preliminary inspection of the Papago project, Santa Ana, Sonora, for: Rosemont Copper.

Geospec Consultants, 2006, Re-Os isotopic analyses and age dating of molybdenite, report for: Teck Cominco.

González-León, C.M., Jacques-Ayala, C., 1988, La secuencia del Cretacico Temprano del area de Cerro de Oro, Sonora-implicaciones paleogeográficas: Universidad Nacional Autónoma de México, Instituto de Geologia, Simposio de Geologia y Mineria de Sonora, 2nd. Hermosillo, Sonora, Resúmenes, p. 23-25 (abstract).

González-León, C.M., Lucas, S.G., 1995, Stratigraphy and paleontology of the Early Cretaceous Cerro de Oro Formation, central Sonora, *in* Jacques-Ayala, González-León,

C.M., Roldán-Quintana, J., eds., Studies on the Mesozoic of Sonora and adjacent areas: Boulder, Colorado, Geological Society of America Special Paper 301, p. 41-47.

Govett, G.J.S., Whitehead, R.E.S., 1974, Origin of metal zoning in stratiform sulfides; a hypothesis, Economic Geology; 1 July 1974; v. 69; no. 4; p. 551-556.

Guilbert, J.M., Parks, C.F., 1986, The Geology of Ore Deposits, Waveland Press, Long Grove, Illinois, 985 pp.

Hamilton, W.S., 2003, Technical report of the Santa Gertrudis project, Santa Teresa District, for: International Coromandel Resources Ltd.

Hannington, M., Herzig, P., Scott, S., Thompson, G., Rona, P., 1991, Comparative mineralogy and geochemistry of gold-bearing sulfide deposits on the mid-ocean ridges, Marine Geology, Vol. 101, Issues 1-4, October-November 1991, p. 217-248.

Hardy, L.R., 1973, Geology of an allochthonous sequence in the Sierra de Santa Rosa, northwest Sonora, Mexico [M.S. thesis]: San Diego, San Diego State University, 92 p.

Hayes, P.T., 1970, Mesozoic stratigraphy of the Mule and Huachuca Mountains, Arizona: U.S. Geological Survey Professional Paper 658-A, 28 p.

Hayes, P.T., Drewes, H., 1978, Mesozoic depositional history of southeastern Arizona, *in* Callender, J.F., Wilt, J.C., Clemons, R., eds., Land of Cochise: New MexicoGeological Society 29th Field Conference Guidebook, p. 201-207.

Hayashi, K.I., Ohmoto, H., 1991, Solubility of gold in $NaCl^-$ and H_2S-bearing aqueous solution at 259-350°C, Geochim. Cosmochim. Acta 55, 2111-2126.

Helmstaedt, H., 1996, Structural observations at the gold deposits of the Santa Gertrudis Mine, Santa Teresa District, northeast Sonora, for: Campbell Resources.

Henley, R.W., 1973, Solubility of gold in hydrothermal chloride solutions. Chemical Geology, 11, p. 73–87.

Henry, C.D., Aranda-Gómez, J.J., 2000, Plate interactions control middle-late Miocene proto-Gulf and Basin and Range extension in the southern Basin and Range: Tectonophysics, v. 318, p. 1–26.

Holcombe, R., 2010, GEOrient v. 9, http://www.holcombe.net.au/software/rodh_software_georient.htm.

Huppert, H.E., Sparks, R.S.J., 1988, The generation of granitic magmas by intrusion of basalt into continental crust, Journal of Petrology, v. 29, p. 599–642.

Huston, L., Large, R., 1989, A chemical model for the concentration of gold in volcanogenic massive sulfide deposits, *in* Ore Geology Reviews 4, p. 171-200.

Inman, K. F., 1987, Depositional environments and sandstone petrography of Cretaceous sedimentary rocks, Adobe Canyon, Santa Rita Mountains, southeastern Arizona: Arizona Geological Society Digest, v. 18, p. 301-314.

Instituto Nacional de Estadistica y Geografia, 1:2000 ortho-airphotos. http://www.inegi.org.mx/default.aspx.

Jacques-Ayala, C., 1995, Paleogeography and provenance of the Lower Cretaceous Bisbee Group in the Caborca-Santa Ana area, northwestern Sonora, *in in* Jacques-Ayala, González-León, C.M., Roldán-Quintana, J., eds., Studies on the Mesozoic of Sonora and adjacent areas: Boulder, Colorado, Geological Society of America Special Paper 301, p. 79-98.

Jacques-Ayala, C., 1983, Sierra EI Chanate, NW Sonora, Mexico: Stratigraphy, sedimentology and structure: Cincinnati, Ohio, University of Cincinnati, M. Sc. thesis, 148 p. (unpublished).

Jamison, K., 1987, Petrofacies of Morita Formation (Bisbee Group), southeastern Arizona and northern Sonora, Mexico, *in* Dickinson, W. R. and Klute, M. A., eds., Mesozoic rocks of southern Arizona and adjacent areas: Arizona Geological Society Digest v. 18, p. 257-262.

Keith, S.B., Reynolds, S.J., Damon, P.E., Shafiqullah, M., Livingston, D.E., and Pushkar, P.D., 1980, Evidence for multiple intrusion and deformation within the Santa Catalina-Rincon-Tortolita crystalline complex, in Crittenden, M.D., Coney, P.J., and Davis, G.H., eds., Cordilleran Metamorphic core complexes: Geological Society of America Memoir 153, p. 217-266.

Kern, R.R., Sibthorpe, R.A., NI 43-101 Technical Report on the Santa Gertrudis Property, Sonora, Mexico. Deal Capital unpublished report for: Sonora Gold, 2007.

Kesler, S.E., Russel, N., Seaward, M., Rivera, J., McCurdy, K., Cumming, G.L., Sutter, J.F., 1981, Geology and geochemistry of sulfide mineralization underlying the Pueblo Viejo gold-silver oxide deposit, Dominican Republic, Economic Geology, 1 August 1981, v. 76, no. 5, p. 1096-1117

King, R.E., 1939, Geologic reconnaissance in the northern Sierra Madre Occidental of Mexico: Geological Society of America Bulletin, v. 50, p. 1625-1722.

Kirk, J., Ruiz, J., Chesley, J., Titley, S., Walshe, J., 2001, A detrital model for the origin of gold and sulfides in the Witwatersrand basin recorded on Re-Os isotopes, Geochemica et Cosmochimica Acta, Vol 65, Issue 13, p. 2149-2159.

Krantz, R.W., 1989, Laramide structures of Arizona, *in* Jenny, J.P., Reynolds, S.J., eds., Geologic Evolution of Arizona, Arizona Geological Society Digest 17, p. 463-483.

Lindberg, F.A., 1987, Cretaceous sedimentary geology of Rucker Canyon area, Cochise County, Arizona, Mesozoic Rocks of Southern Arizona and Adjacent Areas, Dickinson, W.R., Klute, M.A., eds., Arizona Geological Society Digest 18, p. 283-299.

Likhachev, A.P., 1975, Redeposition of ore-producing and petrogenic components by aqueous solutions, Geochemistry International, 12, p. 101-113.

Listova, L.P. et al., 1966, Dissolution of gold in media forming during oxidation of some sulphides; Metallogen. Osad. Metamorf. Porod. Akad. nauk SSSR, Lab. Osad. Polez. Iskop., p. 189-199. (Chem. Abstr., v. 68, 88967h.)

Longoria, J.F., Perez, V.A., 1979, Bosquejo geológico de los cerros Chino y Rajon, cuadrangulo Pitiquito-La Primavera (NW de Sonora): Universidad de Sonora, Boletin Departamento de Geologia, v. 1, p. 119-144.

McKee, M. B., 1991, Deformation and stratigraphic relationships of mid-Cretaceous to early Tertiary mass gravity slides in a marine basin in Sonora, Mexico [Ph. D. Dissertation]: Pittsburgh, Pennsylvania, University of Pittsburgh, p. 286.

McKee, M. B., Anderson, T. H., 1998, Mass-gravity deposits and structures in theLower Cretaceous of Sonora, Mexico: Geological Society of America Bulletin, v. 110, p. 1516-1529.

Menges, C. M., and P. A. Pearthree, 1989, Late Cenozoic tectonism in Arizona and its impact on regional landscape evolution, in Geologic Evolution of Arizona, edited by J. P. Jenney and S. J. Reynolds, Ariz. Geol. Soc. Dig., 17, 649-680.

McCloud, J.A., 2005, Memo to Manager, Teck Cominco Mexico Exploration (N.P. O'Brien)-San Enrique samples: #33310-33313, Teck Cominco Ltd., Vancouver, Canada.

Meinert, L.D., 1997, Application of skarn deposit zonation models to mineral exploration. Exploration and Mining Geology 6, p. 185-208.

Misra, K.C., 2000. *Understanding Mineral Deposits*. Kluwer Academic Pulishers, Netherlands.

Mitchell, R.H., Bergman, S.C., 1991. Petrology of Lamproites. 447 p. New York, London: Plenum Press.

Monreal, R., Longoria, J.F., 2000, Stratigraphy and structure of the Lower Cretaceous of Lampazos, Sonora, (northwest Mexico) and its relationship to the Gulf Coast succession: American Association of Petroleum Geologists Bulletin, v. 84, no. 11, p. 1811-1831.

Müller, D., Groves, D.I. 2000. Potassic Igneous Rocks and Associated Gold–Copper Mineralization, 3rd ed. xiii+252 pp. Berlin, Heidelberg, New York, London, Paris, Tokyo, Hong Kong: Springer-Verlag.

Mumin, A.H., Fleet, M.E., and Chryssoulis, S.L., 1994, Gold mineralization in As-rich mesothermal gold ores of the Bogosu-Prestea mining district of the Ashanti Gold Belt, Ghana: Remobilization of "invisible" gold. Mineralium Deposita, 29, p. 445-460.

Nations, J. D., 1989, Cretaceous history of northeastern and east-central Arizona, *in* Jenney, J. P. and Reynolds, S. J., eds., Geologic evolution of Arizona: Arizona Geological Society Digest 17, p. 435-446.

Nourse, J.A., Anderson, T.H., Silver, L.T., 1994, Tertiary Metamorphic Core Complexes in Sonora, northwestern Mexico, Tectonics, v.13, p. 1161-1182.

Pattern Chart, 2006, FGDC Digital Cartographic Standard for Geologic Map Symbolization, FGDC Document Number FGDC-STD-013-2006 http://ngmdb.usgs.gov/fgdc_gds/,.

Peccerillo, A., Taylor, S. R. 1976, Geochemistry of Eocene calc-alkaline volcanic rocks from the Kastamonu area, Northern Turkey. Contributions to Mineralogy and Petrology 58, p. 63–81.

Pérez-Ramos, O., 1988, Estudio bioestratigrafico de algunos rudistas de Sonora, Departamento de Geologia, UNISON, Hermosillo, Mexico, Boletin de Departamento de Geologia, v. 5, p. 41-51.

Phelps Dodge, 1992, Annual Report , 130 pp.

Phillips, G.N., Groves, D.I., 1984, Fluid access and fluid-wallrock interaction in the genesis of the Archean gold-quartz vein deposit at Hunt Mine, Kambalda, Western Australia, *in* Foster, R.P., ed., Gold '82, The geology, geochemistry and genesis of gold deposits, Balkema, Rotterdam, p. 389-416.

Radtke, A.S., Taylor, C.M., Erd, R.C., Dickinson, F.W., 1974, Occurrence of lorandite $TlAsS_2$, at the Carlin gold deposit, Nevada**,** Economic Geology; v. 69; no. 1; p. 121-123

Ransome, F.L., 1904, The geology and ore deposits of the Bisbee Quadrangle, Arizona: United States Geological Survey Professional Paper 21, p.168.

Reynolds, J., 2008, Durango Geophysics K-soil anomaly at Santa Gertrudis, for: Animas Resources.

Reynolds, S.J., Keith, S.B., and Coney, P.J., 1980, Stacked overthrusts of Precambrian crystalline
basement and inverted Paleozoic sections emplaced over Mesozoic strata, west-central Arizona, in

Jenney, J.P., and Stone, Claudia, eds., Studies in western Arizona: Arizona Geological Society Digest, v. 12, p. 45-51.

Reynolds, S.J., Keith, S.B., 1982, Chemistry and mineral potential of peraluminous granitoids, Arizona
Bureau of Geology and Mineral Technology Fieldnotes, v. 12. No. 4, p. 4-6.

Ristorcelli, S., Ronning, P., Bradbury, J., Steininger, R.C., Teitz, P., Hanks, J., 2009, NI 43-101 Technical Report Update on the Santa Gertrudis Gold Project, Sonora, Mexico, for:
Animas Resources.

Roemer, Ferdinand, 1852, Die Kreidebildungen von Texas und ihre organischen Einschlusse, 100 pp., illus., Bonn.

Rock, N.M.S., Lamprophyres. Blackie, Glasgow, UK, 1991.

Rock, N.M.S., and Groves, D.I., Do lamprophyres carry gold as well as diamonds?, Nature, 1988.

Rodriguez, J., Lopez, J., 1992, Geology of the Santa Gertrudis Mining District, Sonora, Mexico, Phelps Dodge Corporation.

Rodriguez-Castaneda, J. L., 1994, Geologia del area EI Teguachi, Estado de Sonora, Mexico: Revista Mexicana de Ciencias Geológicas, v. 11, p. 11-28.

Rodriguez-Castaneda, J. L., 2002, Tectonica cretacica y terciaria en la margen suroeste del Alto Cananea, Sonora norte-central [Ph. D. dissertation]: Ciudad de Mexico, Distrito Federal, Universidad Nacional Autonoma de Mexico, p. 217.

Roldán-Quintana, J., 1991, Geology and chemical composition of the Jaralito and Aconchi batholiths of
east-central Sonora, Mexico, Geological Society of America, Special Paper 254, p. 69-80.

Roslyakov, N.A. et al., 1972: Form of deposition and migration of gold in the weathering crust of gold-sulphide deposits; Tr. Inst. Geol. Geofiz., Akad. Nauk SSSR, Sib. Otd., v. 149, p. 125-138.

Sillitoe, R.H., 1991, Gold metallogeny of Chile-An introduction, Economic Geology 86, p. 1187-1205.

Schafroth, D.W., 1968, Stratigraphy of some Cretaceous formations of southeastern Arizona, Arizona Geological Society Guidebook III, Geological Society of America, Cordilleran Meeting, pp. 59-67.

Scott, B.H., 1979, Petrogenesis of kimberlites and associated potassic lamprophyres from central west Greenland, in Kimberlites, diatremes and diamonds: their geology, petrology, and geochemistry, AGU.

Scott, R.W., 1987, Stratigraphy and correlation of the Cretaceous Mural Limestone, Arizona and Sonora, Mesozoic Rocks of Southern Arizona and Adjacent Areas, Dickinson, W.R., Klute, M.A., eds., Arizona Gological Society Digest 18, p. 327-334.

Scott, R.W., Gonzeilez-Leon, 1991, Paleontology and biostratigraphy of Cretaceous rocks, Lampazos area, Sonora, Mexico: in Perez-Segura, E., and Jacques-Ayala, C, eds., Studies of Sonoran geology*:* Geological Society of America *Special* Paper 254, pp. 51-67. Economic Geology, 68, p. 187-201.

Servicio Geológico Mexicano, 2003, Carta Geológico-Minera, Santa Teresa 1:50,000 geologic map,http://www.sgm.gob.mx/index.php?option=com_content&task=view&id=59&seccion=Productos&Itemid=88, site visited 2/08/2011.

Seward, T.M., 1973, Thio complexes of gold and the transport of gold in hydrothermal ore solutions, Geochim. Cosmochim. Acta 37, p. 379-399.

Smith, M., 2006, Report of Investigations of the San Enrique property, Sonora, Mexico, for: Teck Cominco Limited.

Sosson, M., Calmus, T., 1990, Early Cretaceous overthrusting in northern Sonora responsible for large-scale displacement of the Nevadian Belt, *in* Auboin, J., Bourgois, J., eds., Tectonics of circum-Pacific continental margins, Proceedings, 28th International Geological Congress, 1989, Utrecht, The Netherlands, VSP, p. 37-50.

Spence, C. D., De Rosen-Spence, A. F., 1975, The place of sulfide mineralization in the volcanic sequence at Noranda, Quebec. Econ. Geol. 70, p. 90-101.

Spencer, J.E., and Reynolds, S.J., 1989, Middle Tertiary tectonics of Arizona and adjacent areas, in Jenney, J.P., and Reynolds, S.J., eds., Geologic evolution of Arizona: Arizona Geological Society Digest 17, p. 539-573.

Sylvester, A.G., 1988, Strike-slip faults, GSA Bulletin; November 1988; v. 100; no. 11; p. 1666-1703.

Stern, R.J., Dickinson, W.R., 2010, The Gulf of Mexico is a Jurassic backarc basin, Geosphere, Dec 2010; 6: p. 739-754.

Suzuki, K., Shimizu, H., Masuda, A., 1996, Re-Os dating of molybdenites from ore deposits in Japan:
Implication for the closure temperature of the Re-Os system for molybdenite and the cooling
history of molybdenum ore deposits, Geochimica et Cosmochimica Acta, Volume 60, Issue 16,
August 1996, p. 3151-3159.

Thalenhorst, H., 1994, Strathcona Mineral Services Limited, Ore Reserve Review, Santa Gertrudis Mine, Mexico, for: Campbell Resources Inc.

Turner, R.L., Raines, G.L., and Kleinkopf, M.D. ,1982, Regional northeast-trending structural control of mineralization, northern Sonora, Mexico: Econ. Geol., v. 77, p. 25-37.

Tyrrell, W.W., Jr., 1957, Geology of the Whetstone Mountain area, Cochise and Pima Counties, Arizona, [Ph.D. dissertation]: New Haven, Conn., Yale University, 236 p.

Vedder, L.K., 1984, Stratigraphic relationships between the Late Jurassic Canelo Hills volcanics and the Glance Conglomerate, southeastern Arizona [M.S. thesis]: Tucson, University of Arizona, 129 p.

Vega-Granillo, R., Calmus, T., 2003, Mazatán metamorphic core complex (Sonora, Mexico): Structures along the detachment fault and its exhumation evolution, Journal of South American Earth Sciences, v. 16, p. 193-204.

Wallace, S.R., 1991, Model Development: Porphyry Molybdenum Deposits, Economic Geology, Monograph 8, p. 207-224.

Warzeski, E. R., 1987, Revised stratigraphy of the Mural Limestone: A Lower Cretaceous carbonate shelf in Arizona and Sonora, *in* W. R. Dickinson and M. F. Klute, eds., Mesozoic rocks of southern Arizona and adjacent areas: Arizona Geological Society Digest 18, Tucson, p. 335-363.

Wells, J.D., and Mullens, TE., 1973, Gold-bearing arsenian pyrite determined by microprobe analysis, Cortez and Carlin gold mines, Nevada.

Wendt C.L., Inc., Evaluation of the Santa Gertrudis Mine for deep Carlin potential. Behre Dolbear & Company, unpublished report for: Campbell Resources Inc., 1997.

White, C.H., 1945, The abyssal versus the magmatic theory of ore genesis, Economic Geology;; v. 40; no. 5; p. 336-344

White D E., 1974, Diverse origins of hydrothermal ore fluids. Econ. Geol. 69:954-73.

Winter, J.D., 2001, An Introduction to Igneous and Metamorphic Petrology, Prentice Hall: Up Saddle River, New Jersey.

Wong, M., Gans, P.B., 2003, Tectonic implications of early Miocene extensional unroofing of the Sierra Mazatán metamorphic core complex, Sonora, Mexico: Geology, v. 31, p. 953–956.

Wood, S.A., Pan, P., Zhang, Y., Mucci, A., 1994, The solubility of Pt and Pd sulfides and Au metal in aqueous bisulfide solutions. Results at 25°-90°C and 1 bar pressure. Mineral. Dep. 29, p. 309-317.

Xinxiang, L.U., You, D., Quiling, C., Qinghui, X., Xiaobo, L., Xiaoxia, W., Guowei, Z., 1996 Indosinian Shahewan rapakivi granite in Qinling and its dynamic significance, Science in China, Series D, Vol. 39, No. 3.

Yan, M.Z., K. Hu,. Geological characteristics of the Dexing porphyry copper deposits, Jiangxi, China, *in* S. Ishihara and Takenouchi, eds., Granitic Magmatism and Related Mineralization. Soc. Min. Geol. Jap., Spec. Issue 8, 1980, p. 197-204.

APPENDIX A
METHODOLOGY

In order to assign any control and to constrain the relative timing of mineralization, numerous sources of historic and new data were utilized. Foremost, three areas of interest were identified and field mapped at a scale of 1:2,000, with an emphasis placed on differentiating lithologies, structures, alteration and mineralization. All mapping was done on Mylar overlays on black and white air photos from the Instituto Nacional de Estadistica y Geografia (I.N.E.G.I.) or color air photos from Cooper Aerial, Tucson, Arizona. Phelps Dodge and Campbell had previously mapped the three field sites at various scales, and their newly digitized maps were useful as a reference. Higher detail mapping was attempted in the flooded open pits utilizing a small rowboat to navigate the pit lakes (Figure A-1).

During the mapping phase, digitization of the field sheets was accomplished using ESRI ArcMap 9.3. All field sheets were scanned and georectified, based on the printed grid lines and digitized as points, lines, and polygons according to their attributes. Bryan MacFarlane, Francisco Carrillo, and Ivonne Olivarez Miranda accomplished most of the digitization, including portions of the current study areas.

Figure A-1 Mapping the pit lakes utilizing a small rowboat. José Louis, in the bow, acted as my field assistant for many months during the fieldwork. Photo courtesy of S.J. Reynolds.

Structural controls to mineralization and crosscutting relationships were examined and interpreted during the field mapping, compilation, and digitizing phases. Structures categorized based on whether they were pre-, syn- or post-mineralization, their orientations, the geochemical tracer elements present, and the structural style. Analysis of fold data was accomplished utilizing Stereonet (Allmendinger, 2006) and GEOrient (Holcombe, 2010).

Finding deposits of micron to sub-micron "invisible" gold is only made possible by the collection and analysis of multitudes of soil and rock-chip samples. Thanks to the efforts of multiple generations of exploration companies, over 40,000 rock-chip samples and 100,000 soil samples (randomly scattered and gridded throughout the district) have been taken over the entire district. This geochemical data varies from gold-only assays to 31-element analysis. Much of the older Phelps Dodge data consists of gold-only assays, gold-arsenic assays, or newer generations of paper-only graphical representations of the data. Much of the Campbell, Teck Cominco and all of the Animas Resources geochemical data are 31-element analysis in an Excel spreadsheet format.

Rock-chip sampling was used to explore surface geochemical trends; legacy and Animas Resources down-hole drilling geochemical data were used for the subsurface needs. An assistant, or myself, collected all rock-chip samples, either as a channel sample no less than 0.5 m in length and no more than 3 m in length or as high-grade samples. The samples were immediately bagged onsite and labeled with the location, sample-size, sample type, geology, structural orientation and description of the sample recorded and later digitized. The samples were shipped to, processed and assayed, by ALS Chemex or Skyline Laboratories, both of Tucson, Arizona, with chain-of-command and custody being transferred to the labs after importation into the United States from Mexico. The preferred assay method was Aqua Regia

leach analyzed with ICP/OES for multi-element and Fire Assay AA for gold less than 1 g/t Au. Assays greater than 1 g/t Au and quality control were accomplished with Gravimetric Fire Assays. All geochemical results were digitized and added to the sample description database. The frequency of gold to sample count is illustrated by (Figure A-2).

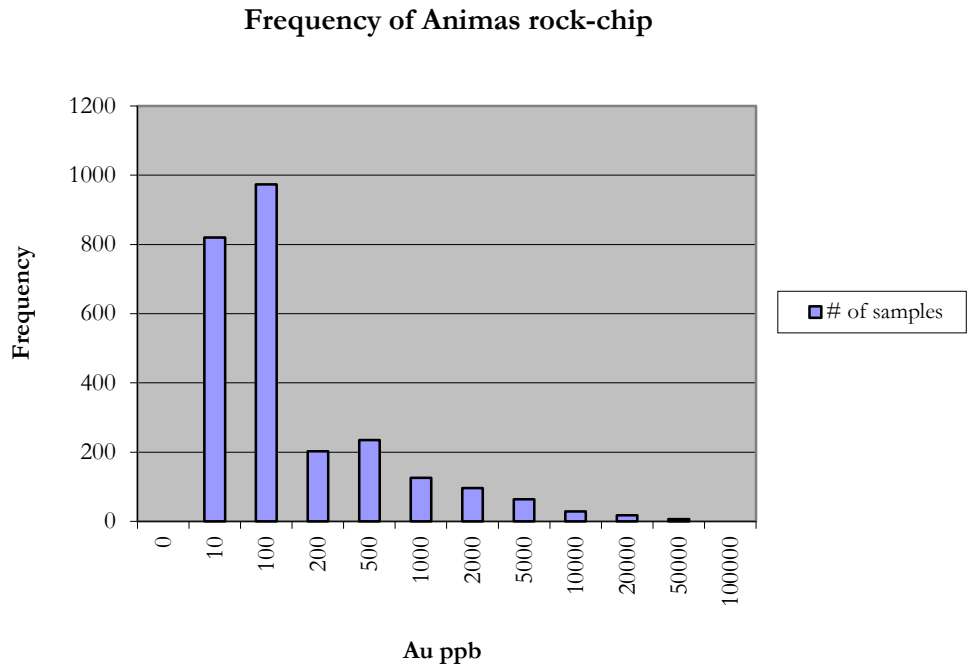

Figure A-2 Frequency of samples plotted against the gold grade (n = 2690).

The rock-chip samples represent the spectrum of primary alteration, mineralization, and surficial oxidation. They were focused on structural settings and areas with primary alteration and mineralization associated with the structures. Sampling in the Enedina area also focused on the possible role of a causative intrusive by comparing the zoned, base-metal geochemistry observed within the hornfels and skarns to the rest of the district and to other intrusive-related mining districts. A subset of intrusive-related quartz veins was sampled in an attempt to establish mineralization vectors.

Spanning 25 years, the collective soil and rock-chip sample database has been utilized in a number of ways. Visualization of geochemical trends, tracer-element haloes, grade distribution, and element associations, integrated into the ArcMap database, allow for interpretation of the interconnectivity of structural and geochemical associations. Statistically, correlation coefficients have been calculated for common element pairing in intrusive-related deposits, and silver/gold ratios have been calculated for surficial and subsurface samples, including the study areas.

Down-hole drilling geochemical data from the Phelps Dodge era are nearly always gold-only, with some arsenic and silver data. Drill-hole data from Campbell are predominantly gold and arsenic only, with some 31 multi-element data. All of the down-hole data from Teck Cominco and Animas Resources are 31 multi-element assays. Despite more than 1,000 drill-holes within the district, much of the multi-element data was lost, poorly collected and stored, or never taken. The current collective database has less than 200 drill-holes with multi-element data. When the mine was in active production during the Phelps Dodge and Campbell eras, sample assaying was done in-house and was generally limited to gold, silver, and arsenic. Paper drill logs and assays were not always reunited, leading to voids in the data, particularly from the Phelps Dodge era.

Most of the legacy drill core, particularly the Phelps Dodge core, was destroyed when a building that was housing it was abandoned for several years and collapsed. Local ranchers used the core to pave portions of the roads. Animas Resources spent considerable time collecting the remaining useable core from the collapsed building, and has it properly stored onsite along with their own core. The loss of the legacy core has been a hindrance to this study and to the exploration of the district.

Golden Software's Strater 1.03 assists in visualization of the drill-hole data, establishing geochemical associations with depth in the drill-holes that have multi-element data. Given the poor spatial distribution of multi-element drill-hole data, establishing subsurface geochemical patterns throughout the district has proven less than reliable and is complicated by post-mineral fault movement. Animas Resources drilled 22 core holes in the three study areas, with a linear, double-spaced pattern in the Toro-to-Gregorio area, structural and mineral tests in the Mirador area, and a buckshot distribution of drill-holes in the Enedina area that tested for precious and base metals associated with structural and intrusive-related targets. All of these drill-holes have 31-element data. A few of the legacy holes in the study areas have multi-element data and are utilized in this study.

Whole-rock studies have focused on the suite of intrusives observed within the district, with 38 legacy and Animas Resources data points utilized to produce IUGS and Cox classification charts (Figure 2-18).

Geophysics has been an important part of exploration in the district since the Phelps Dodge era. Induced-polarization (I.P.) and resistivity studies, along with ground-based and airborne magnetics, have been utilized to establish geologic structures, sulfide/oxide boundaries, buried intrusives, structural domains, rock rheology, and lithology. Within the three study areas, multiple geophysical studies have been undertaken over the years, with several of the recent studies being accomplished by John Reynolds of Durango Geophysics (Durango, Colorado). He is also responsible for the digitization and georectification of the legacy and Animas Resources geophysical data. Pseudo-sections/model-sections of I.P. and resistivity lines run across the Toro-to-Gregorio, and the Mirador areas are matched with surface geology and projected into cross sections that reveal the subsurface structural complexities observed in

those areas. Within the Enedina area, airborne and ground-based magnetics hint at the presence of a buried intrusive coincident with a zoned geochemical base metal halo and directly beneath a quartz cupola with veins of quartz-bearing tungsten, molybdenite and magnetite. Animas Resources 2009 drilling revealed that the intrusive must be deeper than 600 m.

Radiometric dating within the district has been limited to a few academic studies and Teck Cominco's 2006 (Geospec Consultants, 2006) rhenium/osmium date from molybdenite (42.3 Ma +/- 0.3 Ma) in the southern part of the district related to the Las Panochas Granite. A peraluminous, two-mica granite with skarn and stockwork-hosted Cu-Mo-Au mineralization (Smith, 2006), the Las Panochas is weakly greisen altered. Bennett (1993) used K-Ar from muscovite (36.1 ± 0.9 Ma) within the greisen alteration to obtain an age for late-stage alteration of the granite. Bennett also used K-Ar radiometric dating to establish 26.1 ± 0.7 Ma on a biotite-rich diorite.

Data compilation, parsing and interpretation were a difficult and slow task. Very little of the Phelps Dodge data was digital, and most needed mid-1980's software and hardware to access it. Scanning and OCR of all of the remaining Phelps Dodge and Campbell reports, maps, assays, drill logs and other miscellaneous items was accomplished. Most of the Phelps Dodge data is contained in a searchable database managed by LaserFische software. Most of the Campbell reports have been converted to Adobe PDF format with OCR. Campbell's field and compilation maps have been scanned and georeferenced. Conversions of geographic coordinate systems was accomplished through ground and aerial surveys, uniting local mine grid coordinates and NAD27 to UTM WGS 84 12 N coordinates. Legacy data was updated

with the new coordinate system and integrated into ESRI ArcMap. The digital collection exceeds 100 GB of data and will not be included in this thesis.

Issues with misplaced and errant digital data were mitigated by numerous quality control checks of the paper originals when dealing with grade or position critical data. Ground-truthing of legacy drill pads and sample locations allowed for precise correction of the positional data. All assay data were compiled and parsed to equalize the unit conventions, and lower limit thresholds were established for the data and filtered accordingly. Software used in this study to manage the data includes: Golden Software's Strater and Surfer, ESRI ArcMap, Stereonet, GEOrient, GCDKit for R, Microsoft's Access and Excel, LaserFische, and Adobe Acrobat.

The compilation and filtering of the mountain of data received by Animas Resources was a tireless task that included myself; Greg McKelvey, President of Animas Resources; John Wilson, V.P. Exploration of Animas Resources; John Reynolds of Durango Geophysics; Bryan MacFarlane, Exploration Geologist; the staff at MDA, Reno, Nevada and many others who assisted in scanning and organizing the data.

During the compilation of the legacy data and in conjunction with the collection of new data and field mapping, In 2008, Animas began a series of drilling programs to define any possible extensions to known mineralization. This was followed by deep drilling in 2009 to test down-dip extensions, structural complications, and undiscovered sulfide feeders or roots. Finally drilling in the Enedina area was accomplished to define structural data, and intrusive-related mineralization. Each of the selected field sites have multiple new holes drilled since 2008. Each hole was hand-logged with digital core logs, photos, stratigraphic/structural and multi-element

data. The majority of Animas Resources drilling was diamond drill core, completed by Major Drilling Group International Inc., Mexico from September 2008 to January 2010. All core was recovered from the drill pad, boxed, washed and placed on tables for inspection. Core logging was accomplished by Bryan MacFarlane, Fransico Javier Carillo, Ivonne Olivarez Miranda, Miguel Angel Fernandez and myself, and overseen by John Wilson, Greg McKelvey, Odin Christensen, and Jefferson Chambers. All data were immediately entered into an Excel spreadsheet. Attention to stratigraphy and structures, along with mineralization, alteration and veins was stressed throughout the logging process. Sample locations and lengths were determined by the logging geologists and were bracketed between 0.5 and 1.5 m. Sample breaks were determined based on changes in lithology, alteration, structure, or mineralization. Following logging, the core was wetted and photographed, and was then sent to the saw to be split and bagged for shipping. One-half of the core was sent to the assay lab; one-half was boxed and stored on-site. Re-inspection of the cut core was completed when time permitted, with gold-bearing zones garnering extra attention. Cross sections related to the drill-holes were generated based on the drill log results, with emphasis placed on structures, mineralization, and lithology. Within the three selected study sites, this author personally mapped the ground, planned, designed and logged 13 diamond drill-holes during more than two years of study and employment.

Most of the legacy petrographic work was lost; therefore, Animas Resources conducted several petrographic studies while in the drilling phases. During logging, core that was deemed interesting was cut into thin, circular pucks and sent to Dr. Efrén Pérez Segura, Hermosillo, Mexico or to Burnham Petrographics of Rathdrum, Idaho. Digital notes on the petrography were generated and some photomicrographs were taken of the thin sections. This study will

utilize the petrography generated during the Animas Resources studies since most are directly related to drill-holes planned and logged by the author during the course of the study.

APPENDIX B
ENEDINA STUDY AREA SOIL GEOCHEMISTRY

All plots are produced from kriged soil data based on 100 m sampling grids with additional data collected over areas of interest on 25 m grids. All samples were collected by Campbell and Phelps Dodge. Scales are unit-less and range from blue lows to pink highs. Maps are approximately 3.5 km by 5 km. Green circles represent legacy drill-holes. Abbreviations as follows : LE(S)-Leon (Sur), NE(N)-Nelly (Norte), JA-Jabali, SAN-Santiago, LG-La Gloria, TY-Tracy, GR-Greta, NA-Nadia, LA-Laura, TIG-El Tigre, EN-Enedina, LU(S)-Lupita (Sur), ESP-Esperanza. Green dots represent drill collars. All plots produced by John Reynolds of Durango Geophysics (2008). Grid lines are WGS 84 UTM Zone 12N.

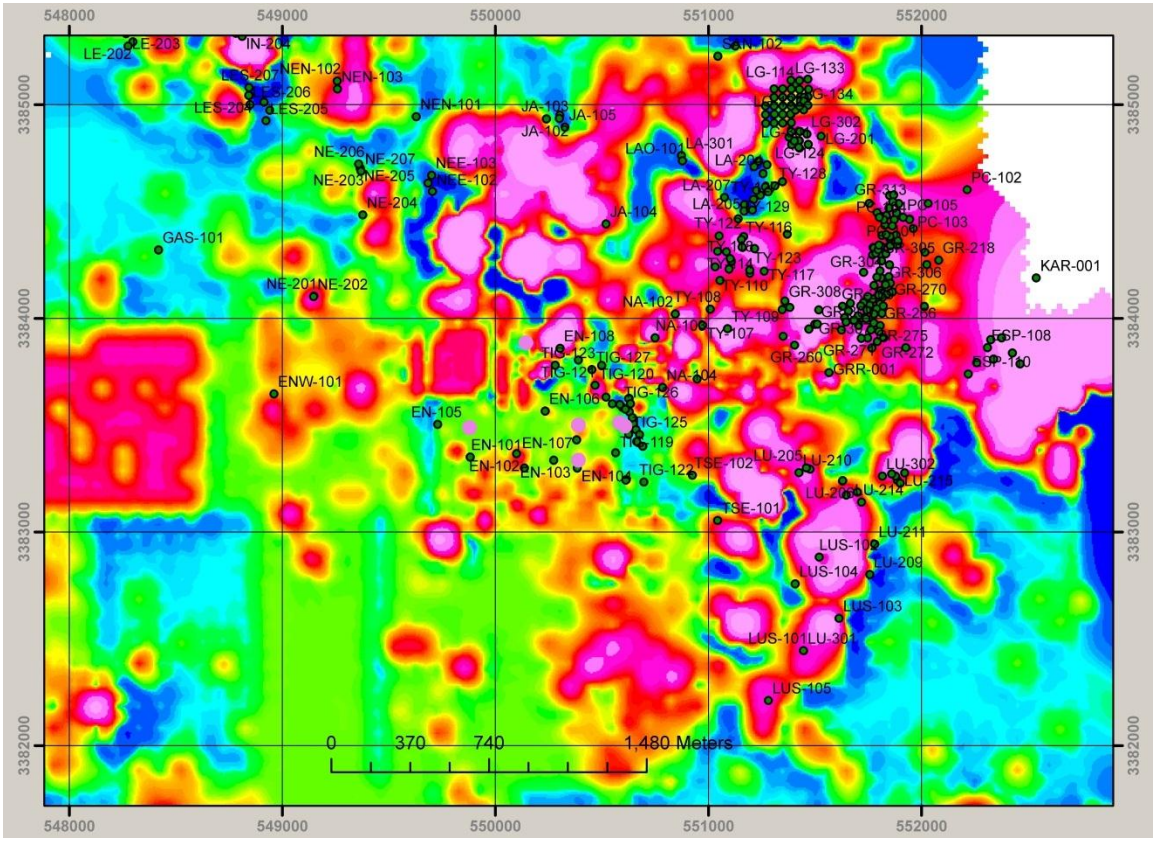

Figure B-1 Ag soil anomaly, blocky and missing data in lower left due to lack of data.

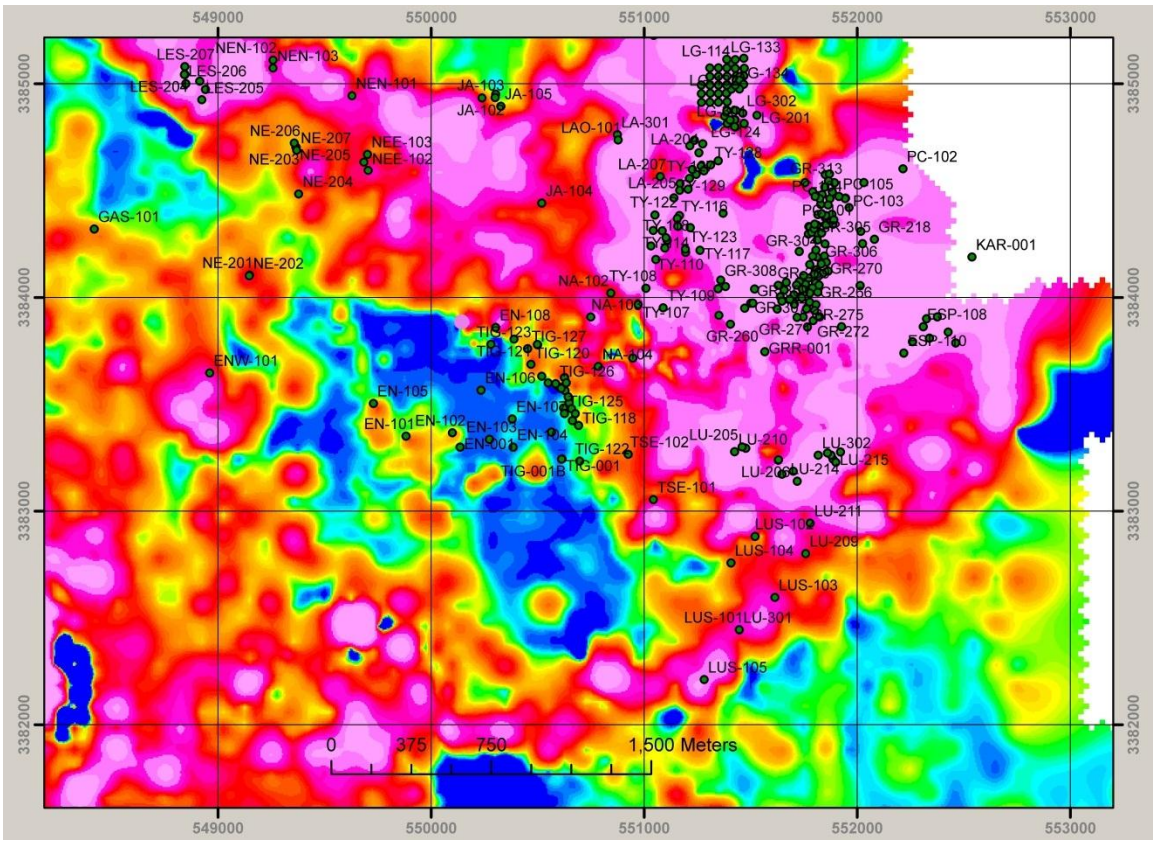

Figure B-2 As soil geochemistry. Note northeast trend in Lupita Sur (LUS), corresponding to northeast family of faults of the La Gloria shear-zone.

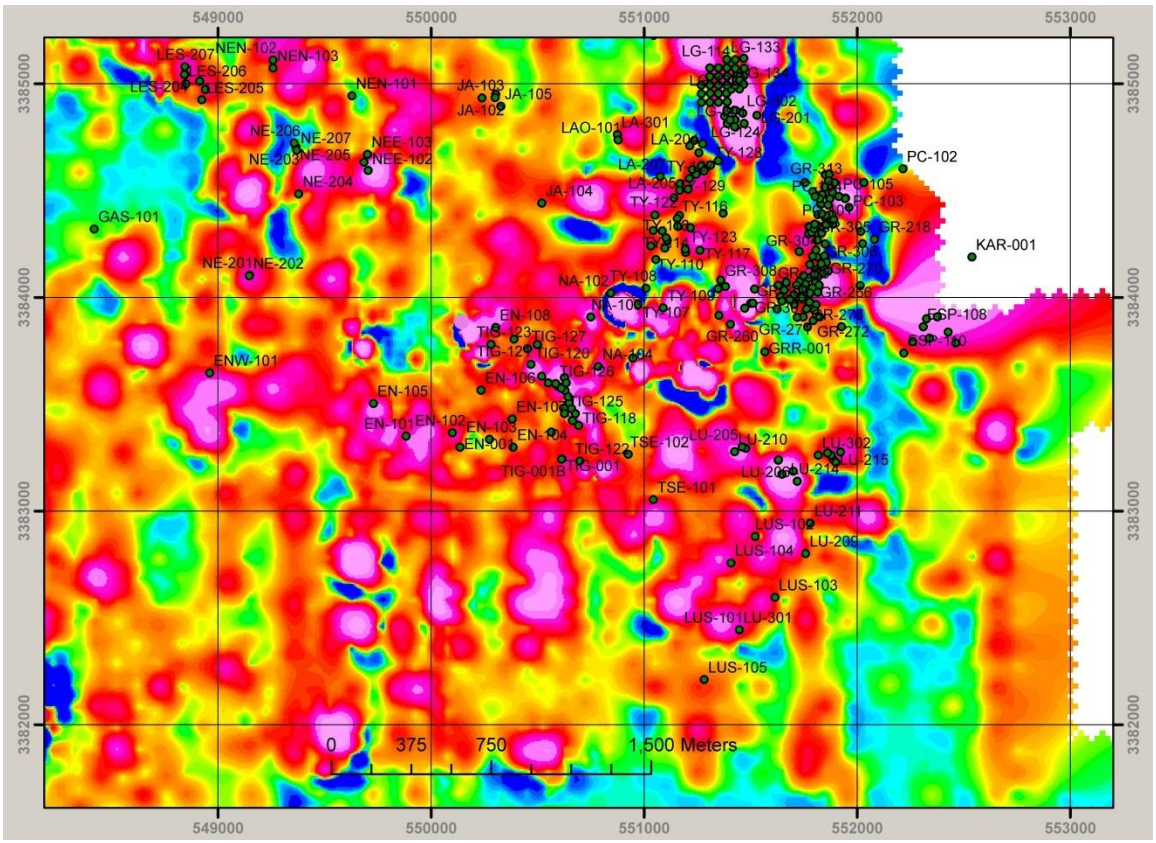

Figure B-3 Au soil geochemistry. Note northeast trend in Lupita Sur (LUS), corresponding to northeast family of faults of the La Gloria Shear-zone.

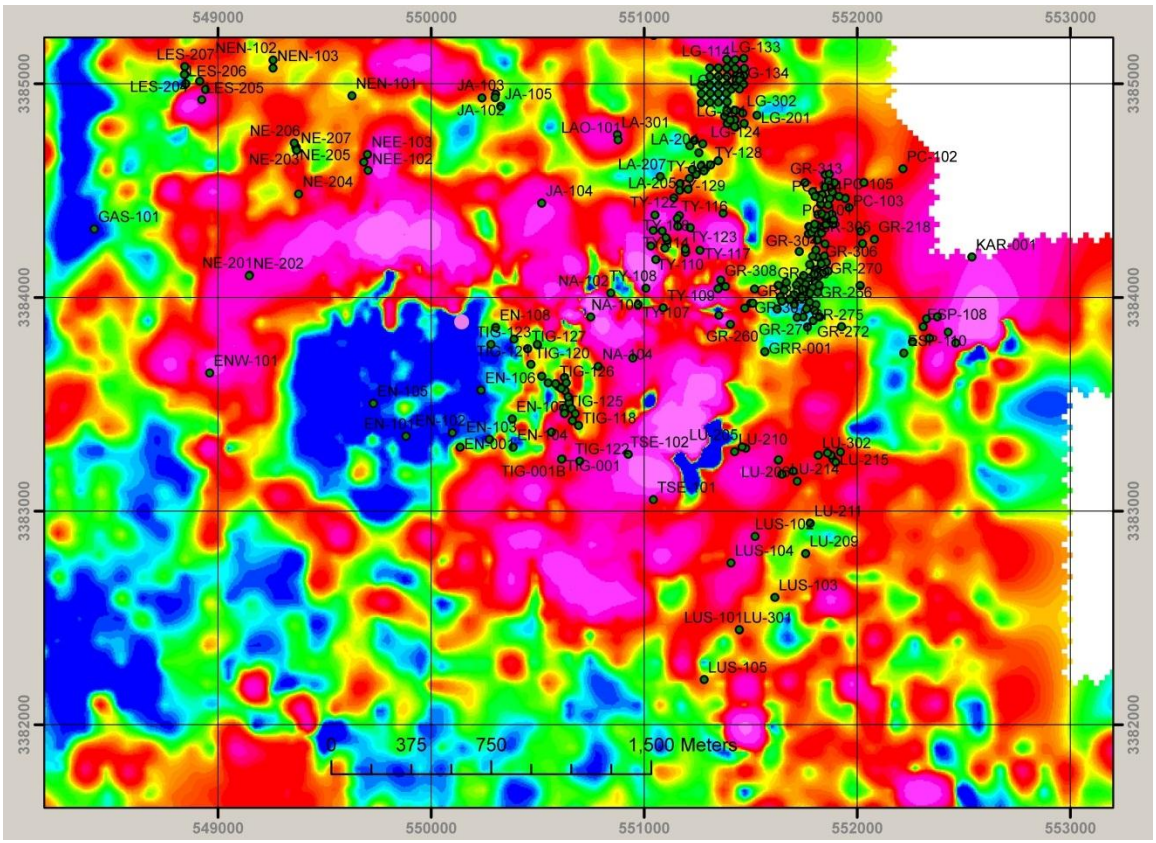

Figure B-4 Cu soil geochemistry. Note the near circular pattern and the bulls eye around the proposed center of mineralization and thermal alteration and northeast trend in Lupita Sur (LUS), corresponding to northeast family of faults of the La Gloria Shear-zone.

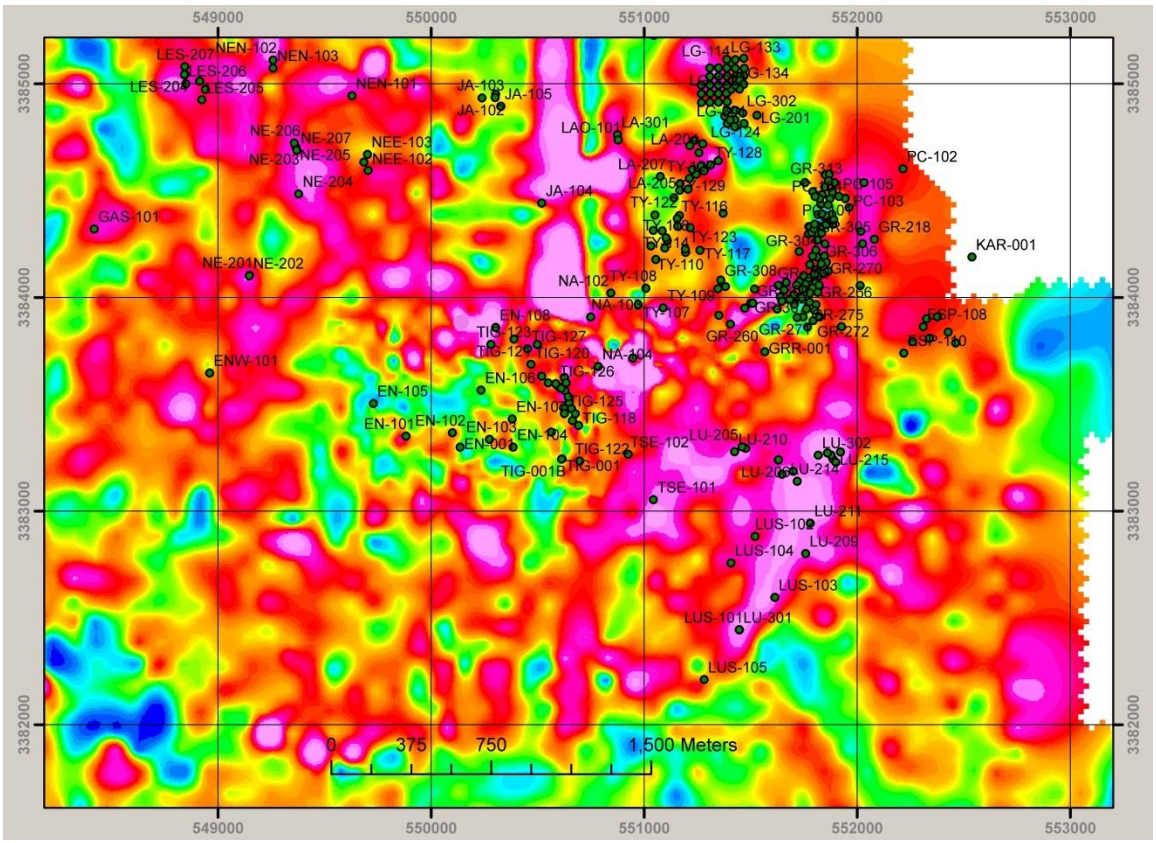

Figure B-5 Fe in soil geochemistry. Note near circular pattern and northeast trend in Lupita Sur (LUS), corresponding to northeast family of faults of the La Gloria Shear-zone.

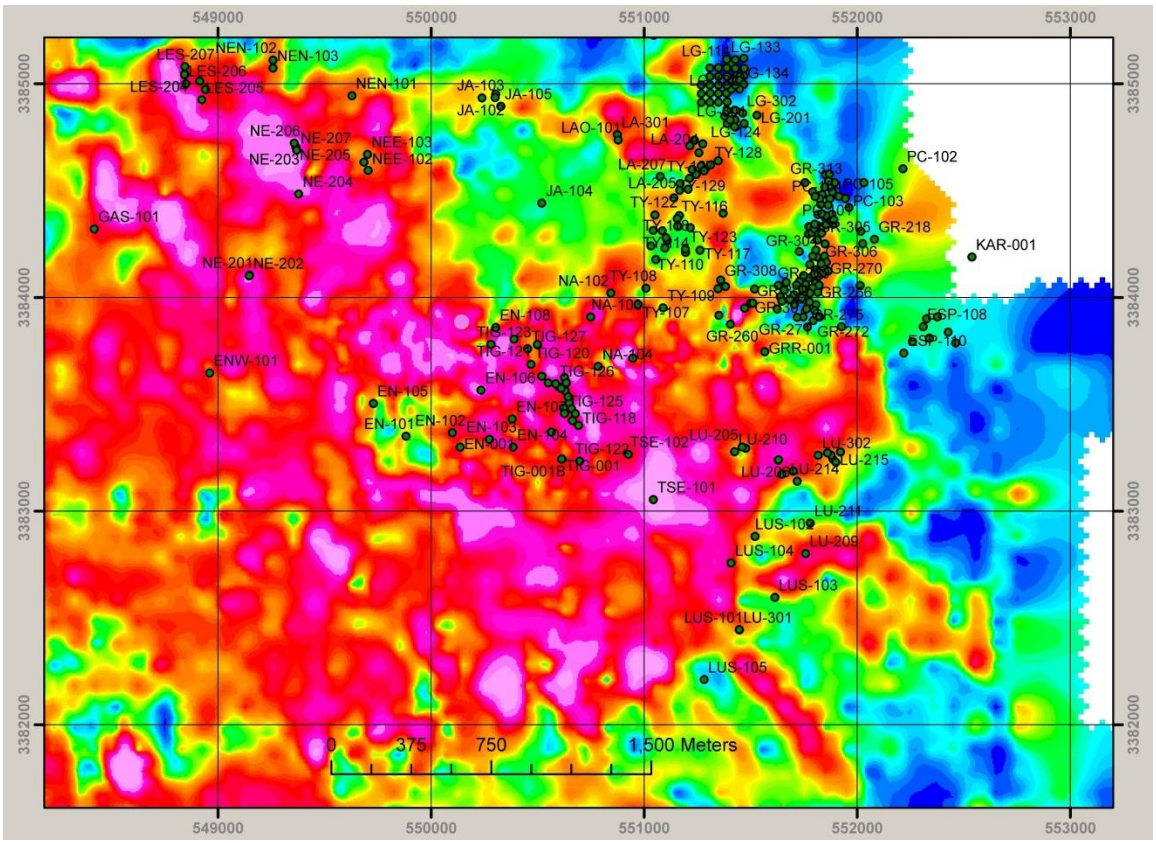

Figure B-6 Mg in soil geochemistry.

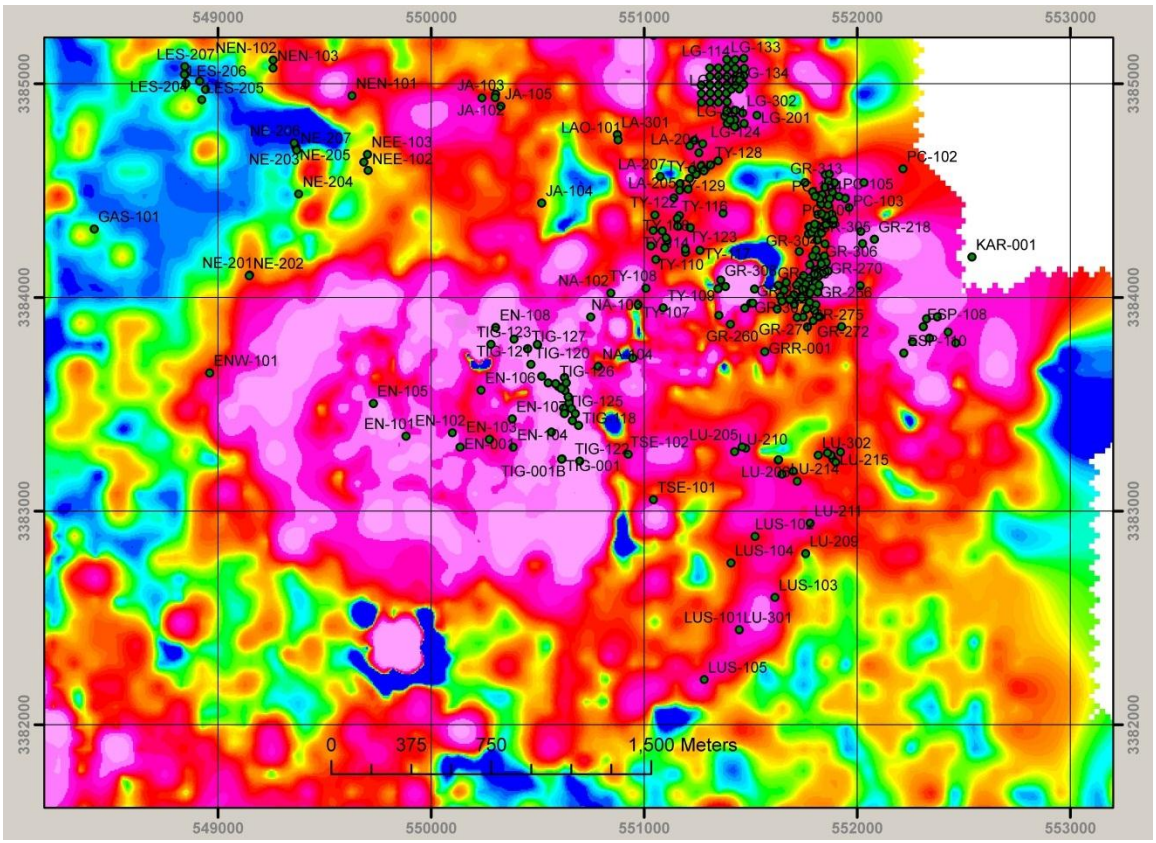

Figure B-7 Mo soil anomaly. Note near circular pattern and centering on the alteration and mineralization bulls eye, and northeast trend in Lupita Sur (LUS), corresponding to northeast family of faults of the La Gloria Shear-zone.

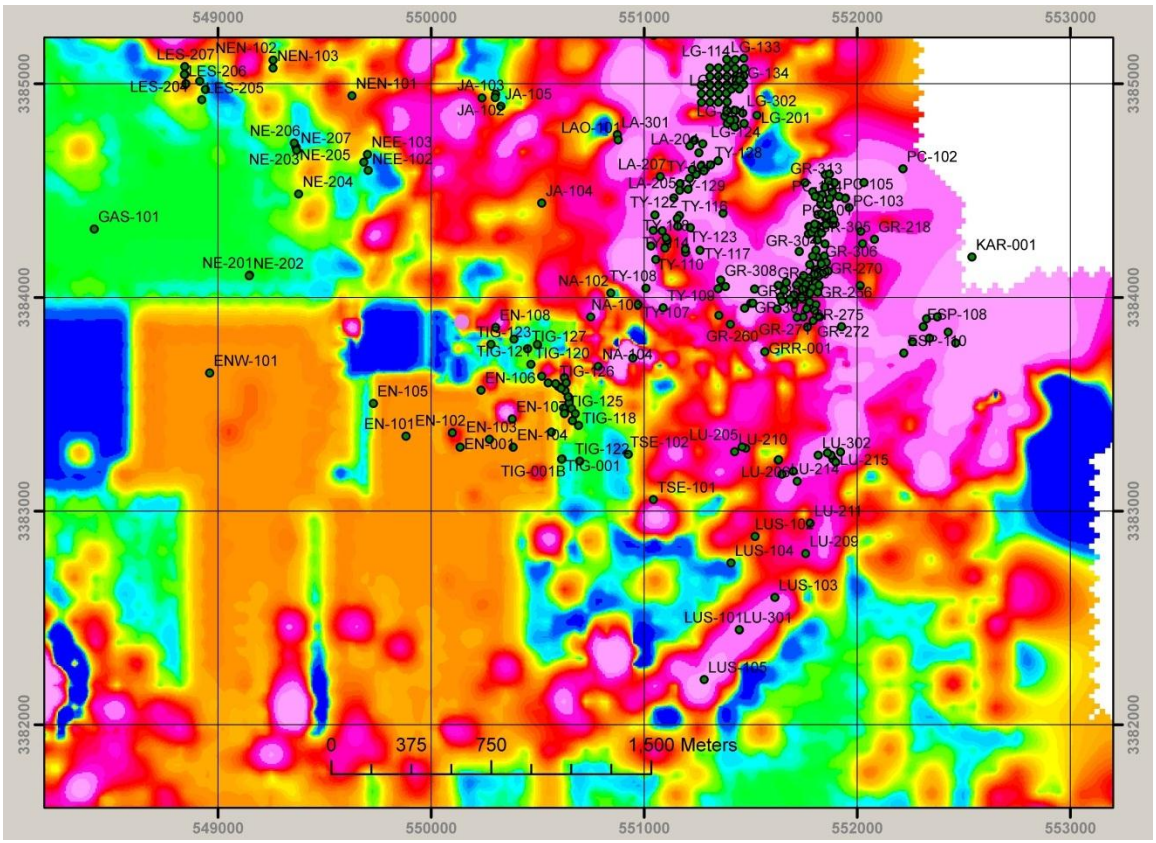

Figure B-8 Pb soil geochemistry. Blocky and missing data in southwest corner is due to lack of Pb data collected in this area. Note northeast trend in Lupita Sur (LUS), corresponding to northeast family of faults of the La Gloria Shear-zone.

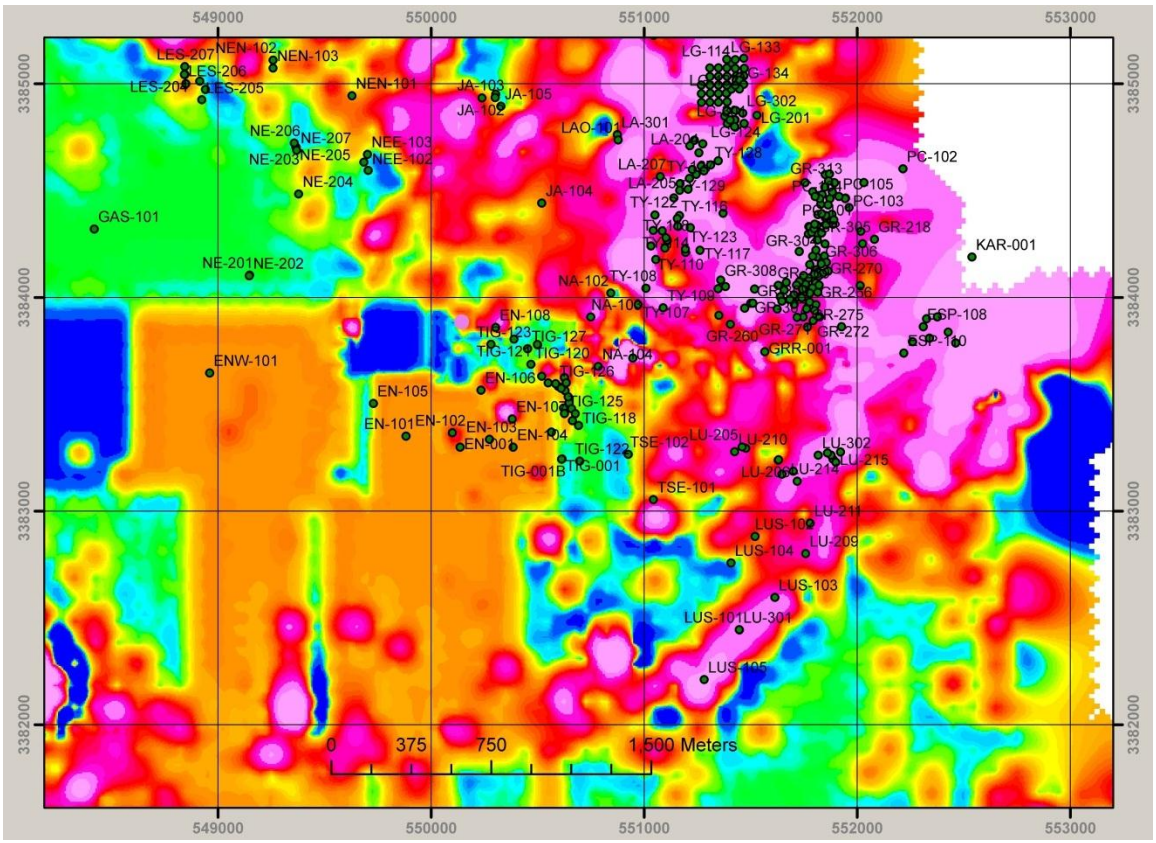

Figure B-9 Sb soil anomaly. Blocky and missing data due to lack of sampling. Note northeast trend in Lupita Sur (LUS), corresponding to northeast family of faults of the La Gloria Shear-zone.

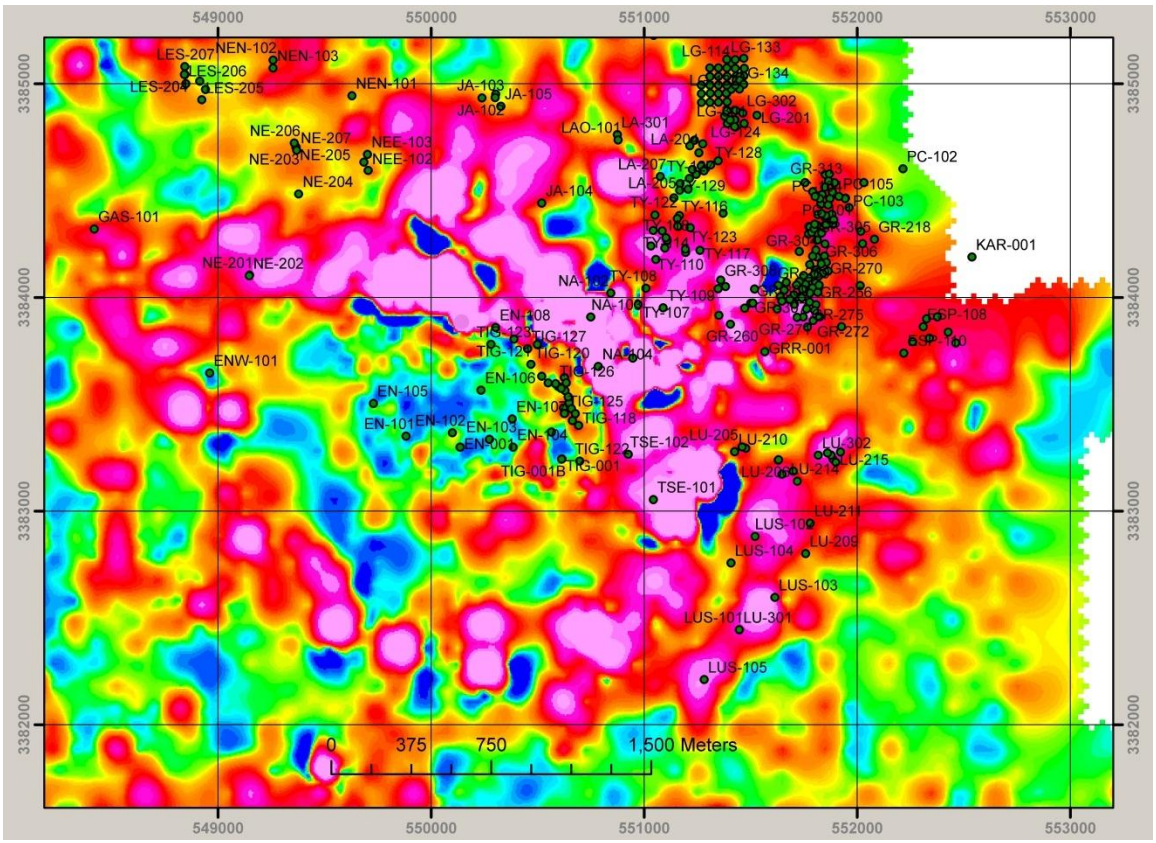

Figure B-10 Zn soil anomaly. Note near circular pattern and bulls eye around the center of mineralization and thermal alteration. Also, note northeast trend in Lupita Sur (LUS), corresponding to northeast family of faults of the La Gloria Shear-zone.

APPENDIX C
REDUCED-TO-THE-POLE (RTP) AIRBORNE MAGNETICS

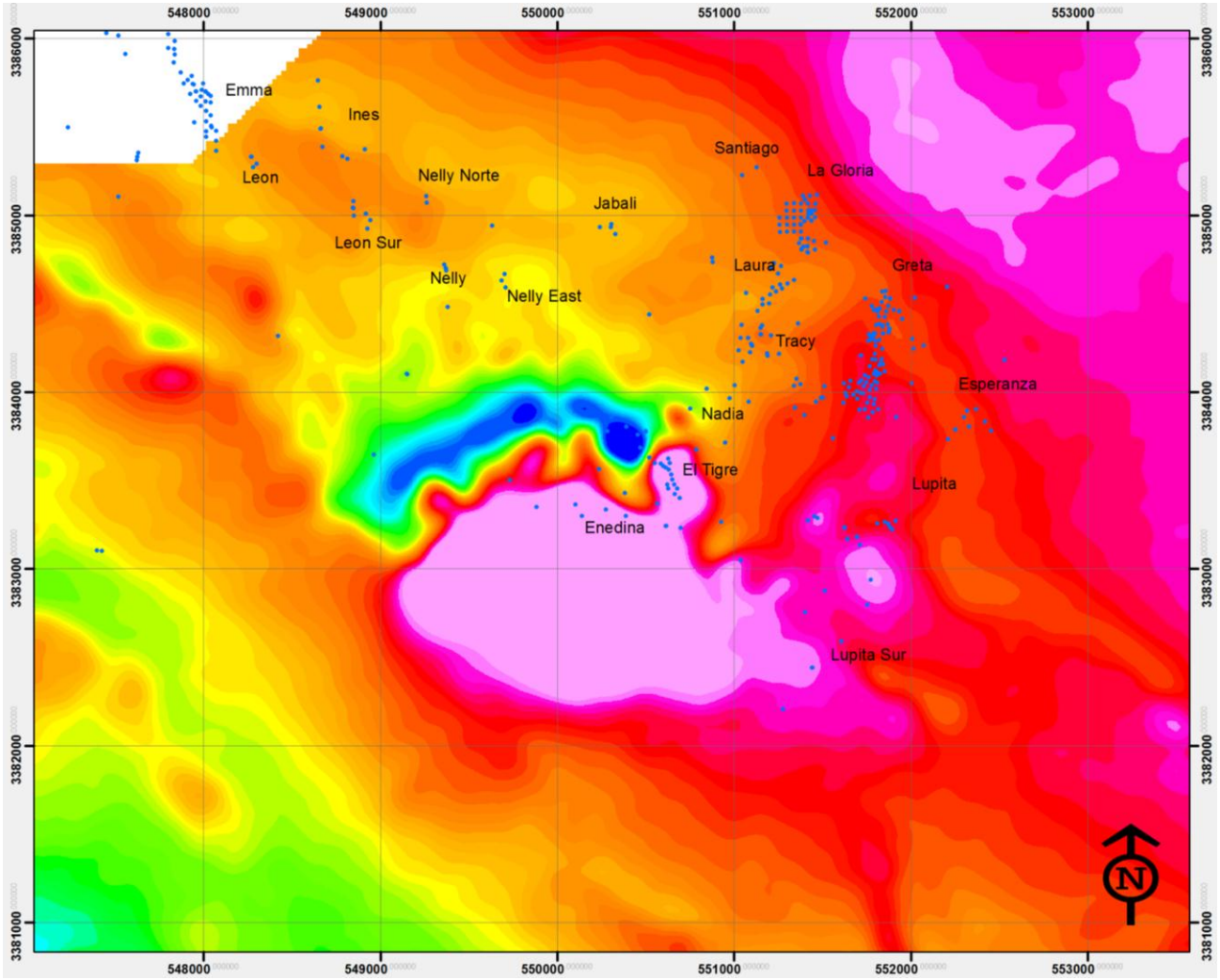

Figure C-1 RTP of the Enedina study area and drill collars. Strong magnetic anomaly coincides with strongest hornfels and magnetite as replacement skarn and vein associations. Courtesy of Durango Geophysics, 2008.

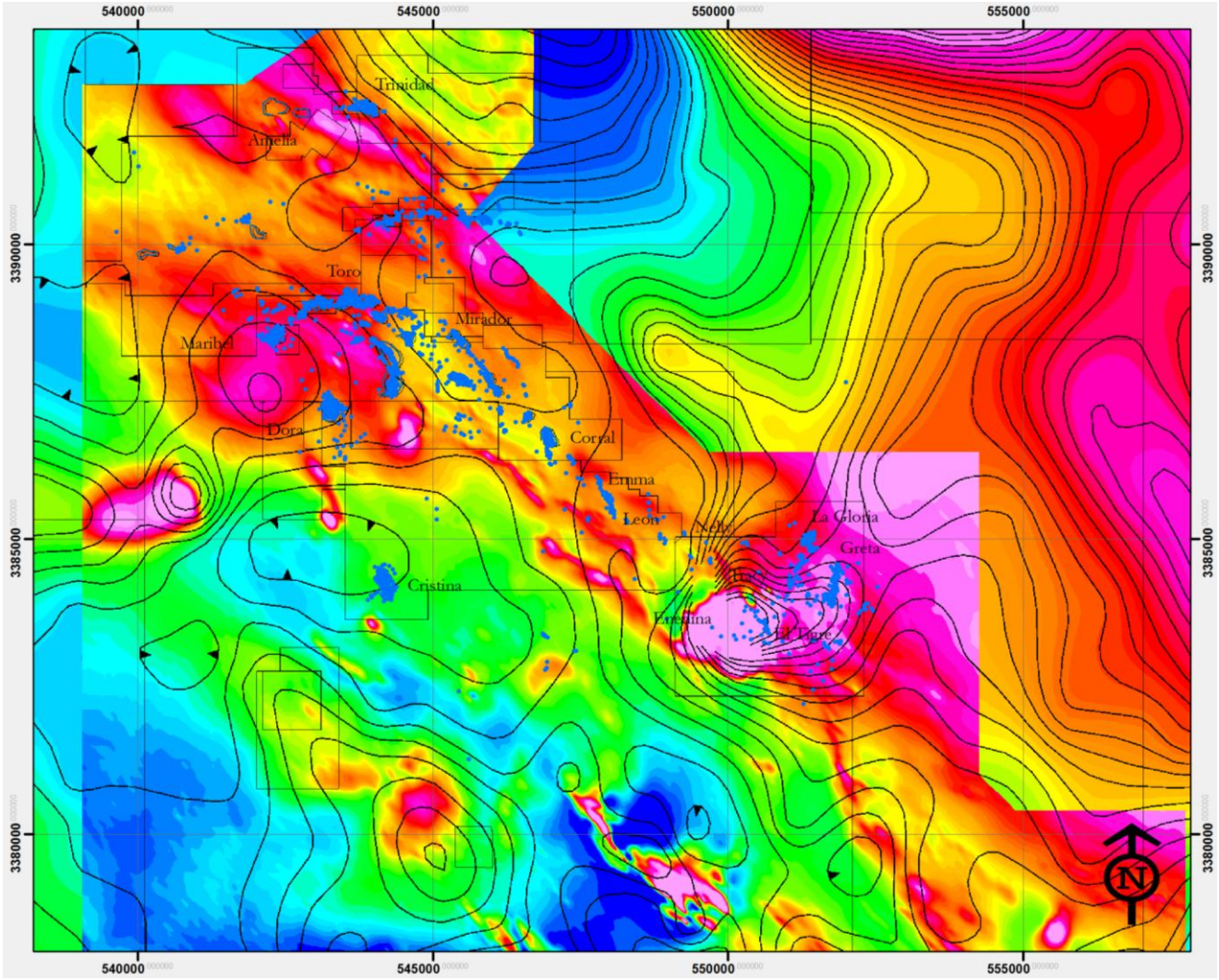

Figure C-2 RTP of the entire district, with select prospect names and drill collars. District map overlain on S.G.M. Magnetics Map. Courtesy of Durango Geophysics, 2008.

APPENDIX D
CROSS SECTIONS

Toro-to-Gregorio cross sections drawn and digitized by Bryan MacFarlane from Animas Resources mapping, drilling and core review.

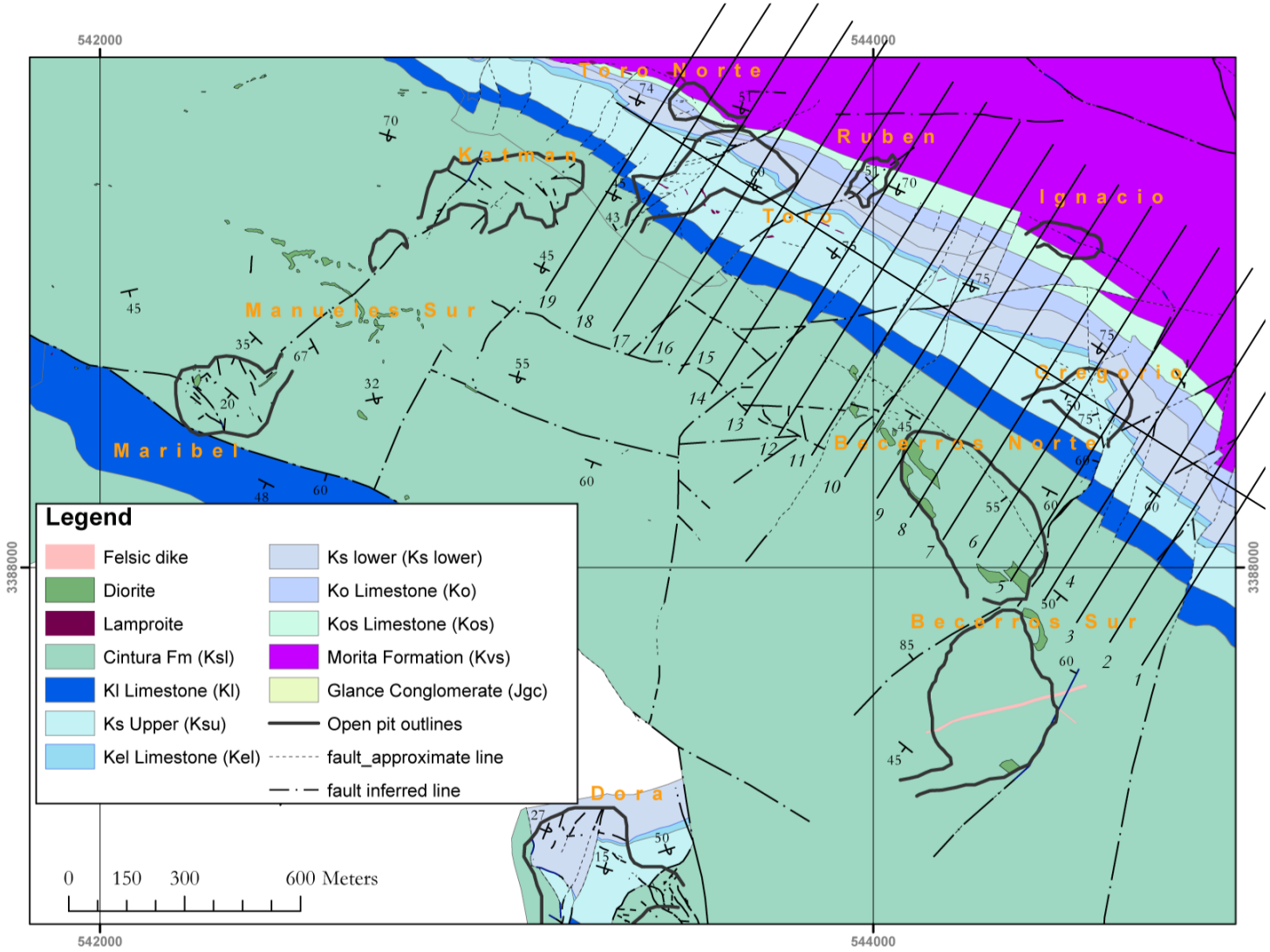

Figure D-1 Cross section line locations for the Toro-to-Gregorio study area

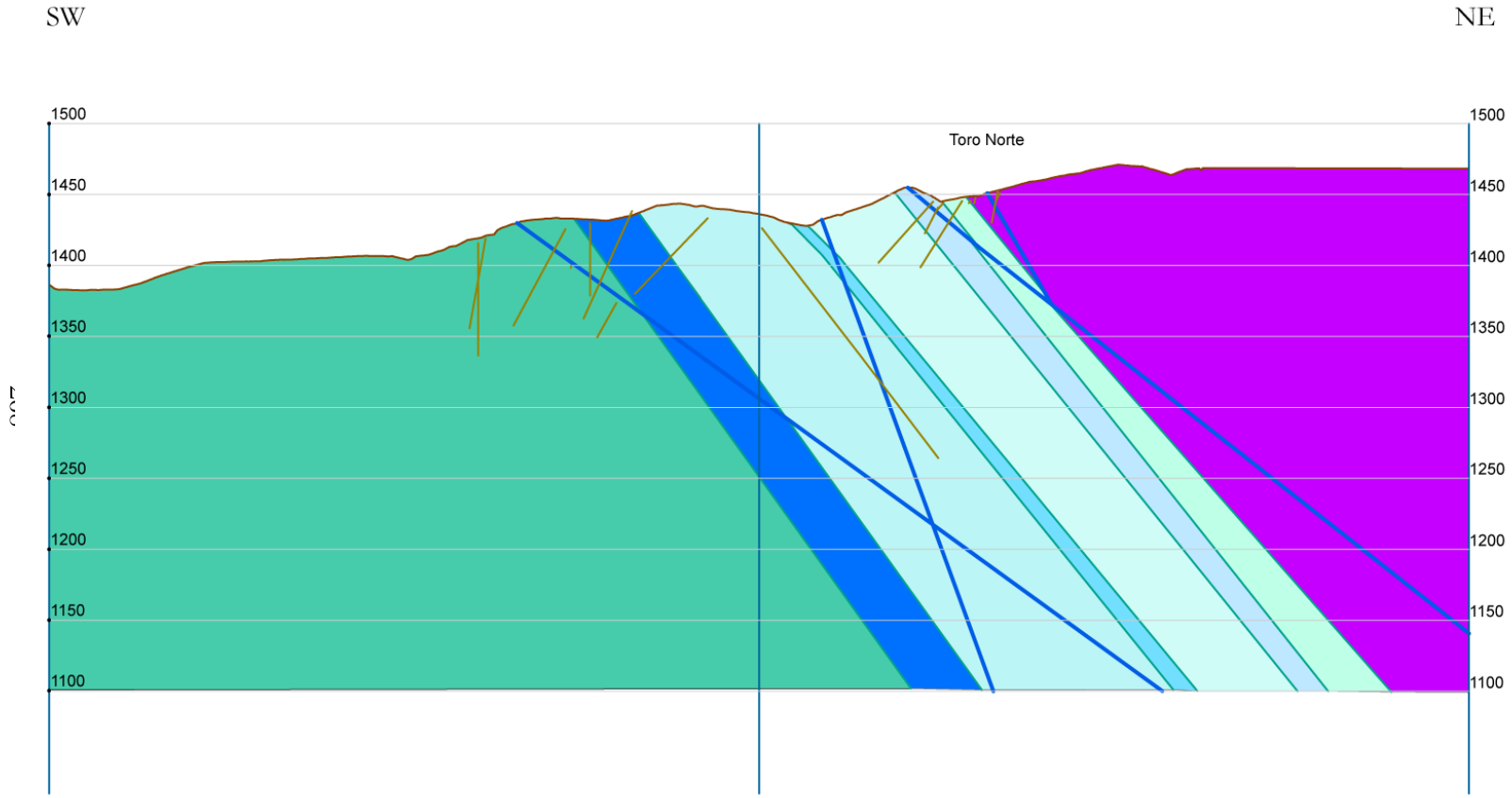

Figure D-2 Cross section *19*

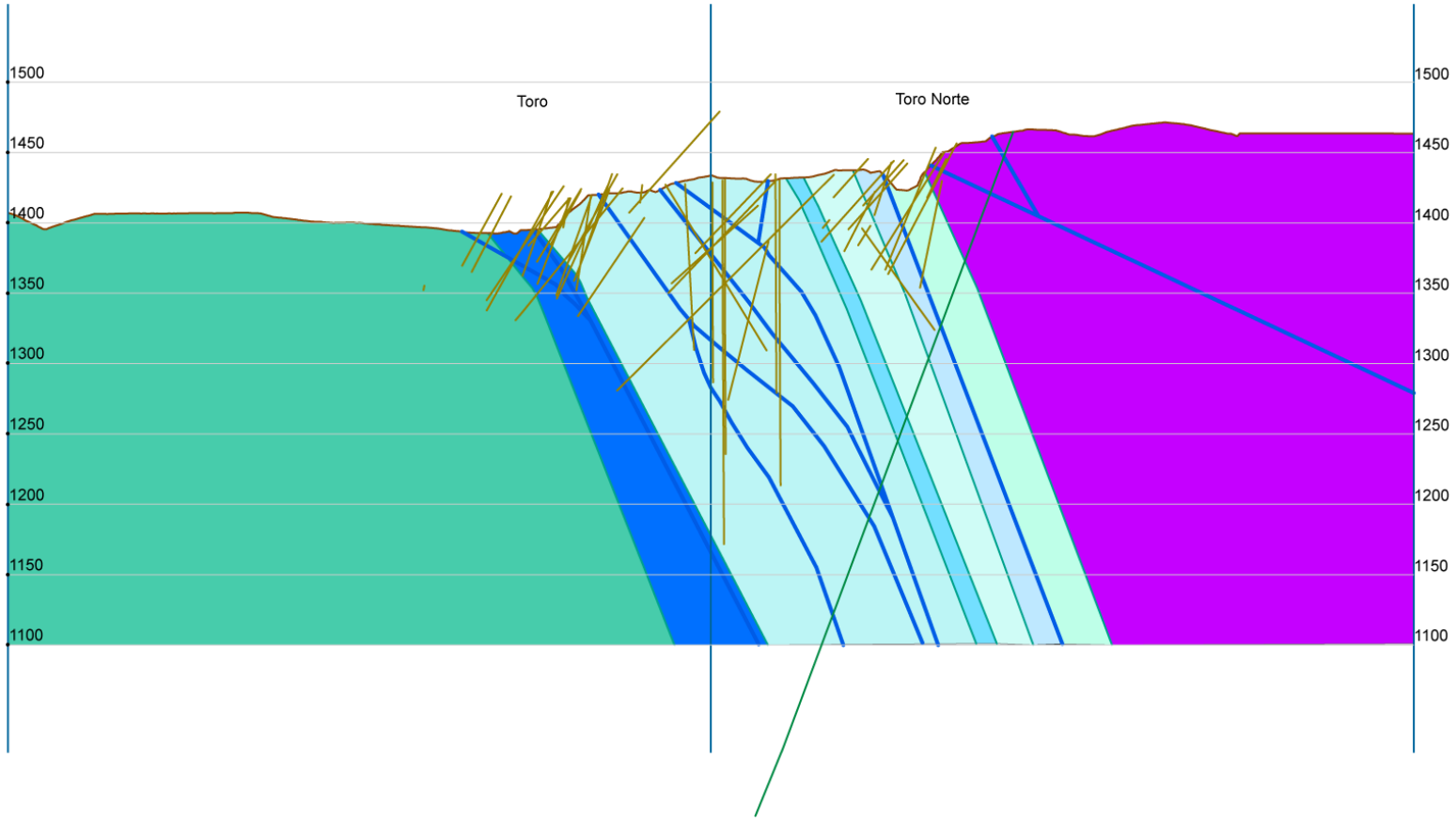

Figure D-3 Cross section *18*

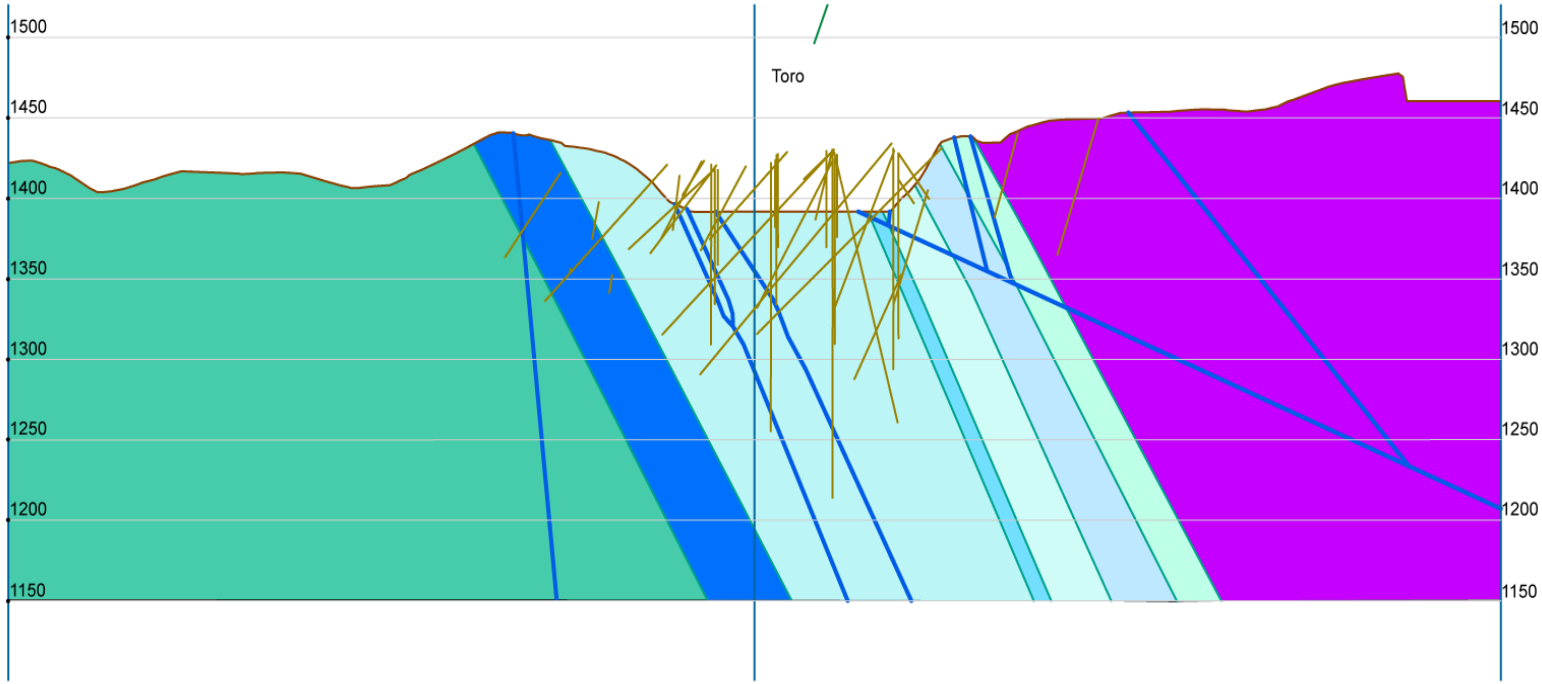

Figure D-3 Cross section *17*

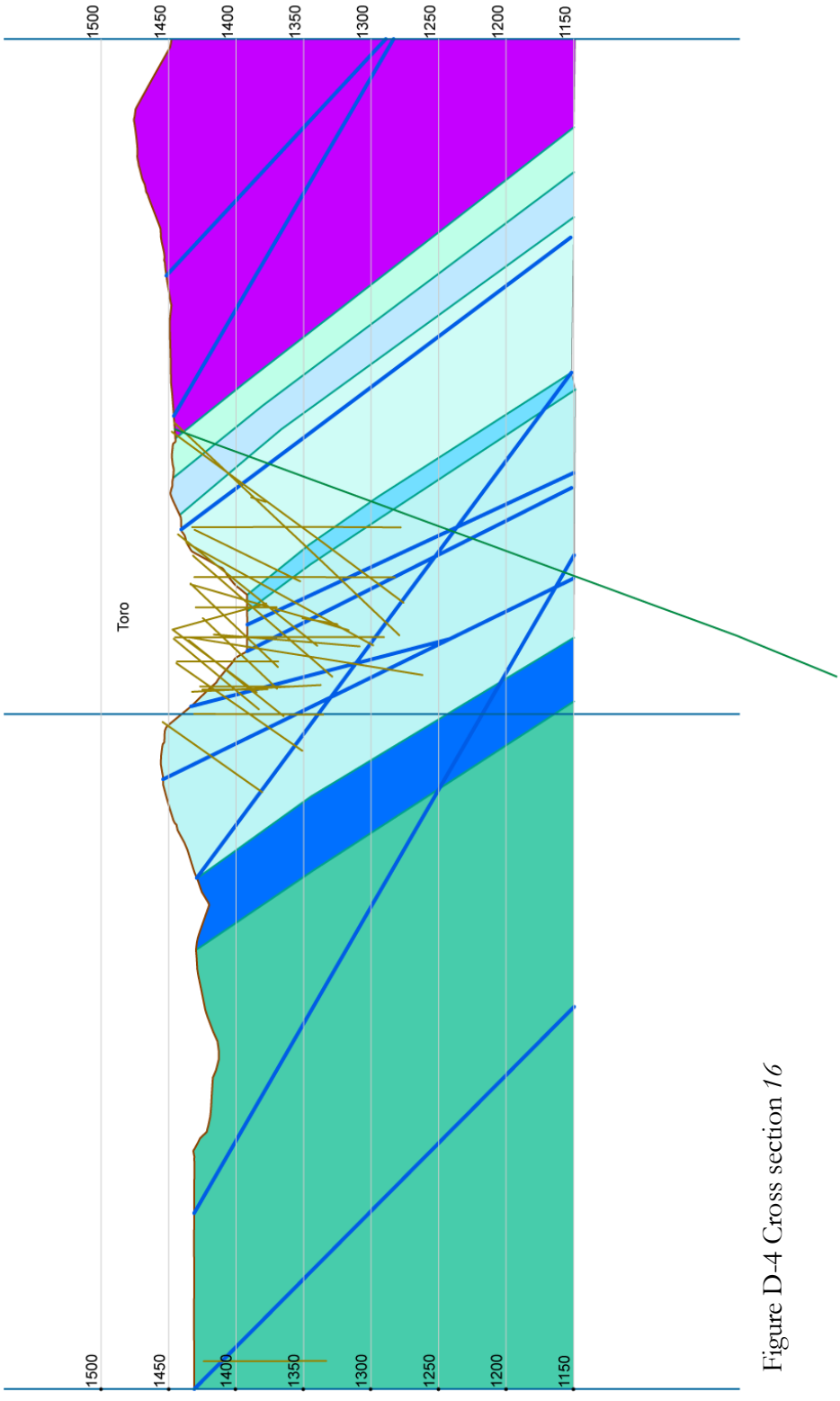

Figure D-4 Cross section *16*

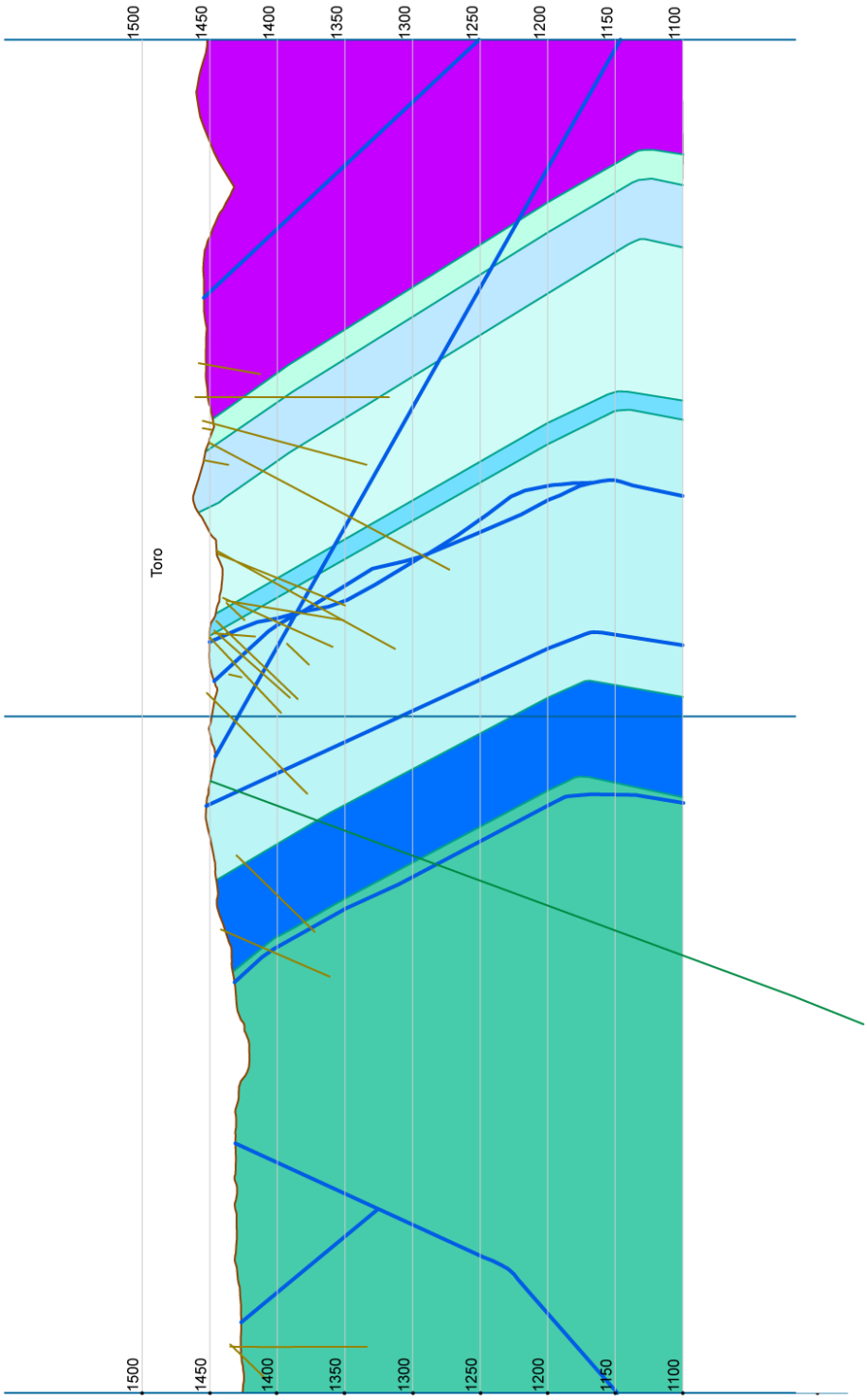

Figure D-5 Cross section *15*

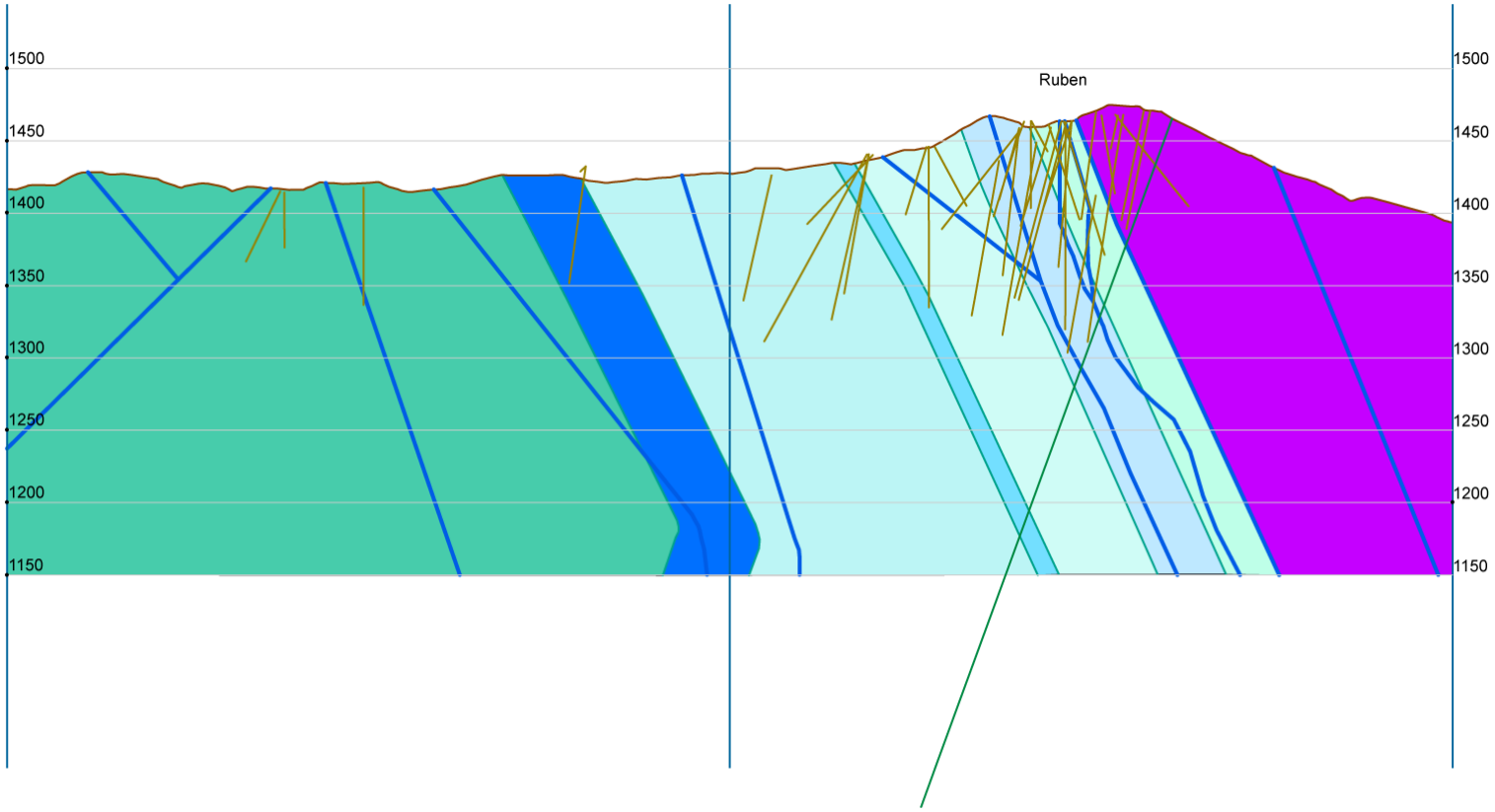

Figure D-6 Cross section *14*

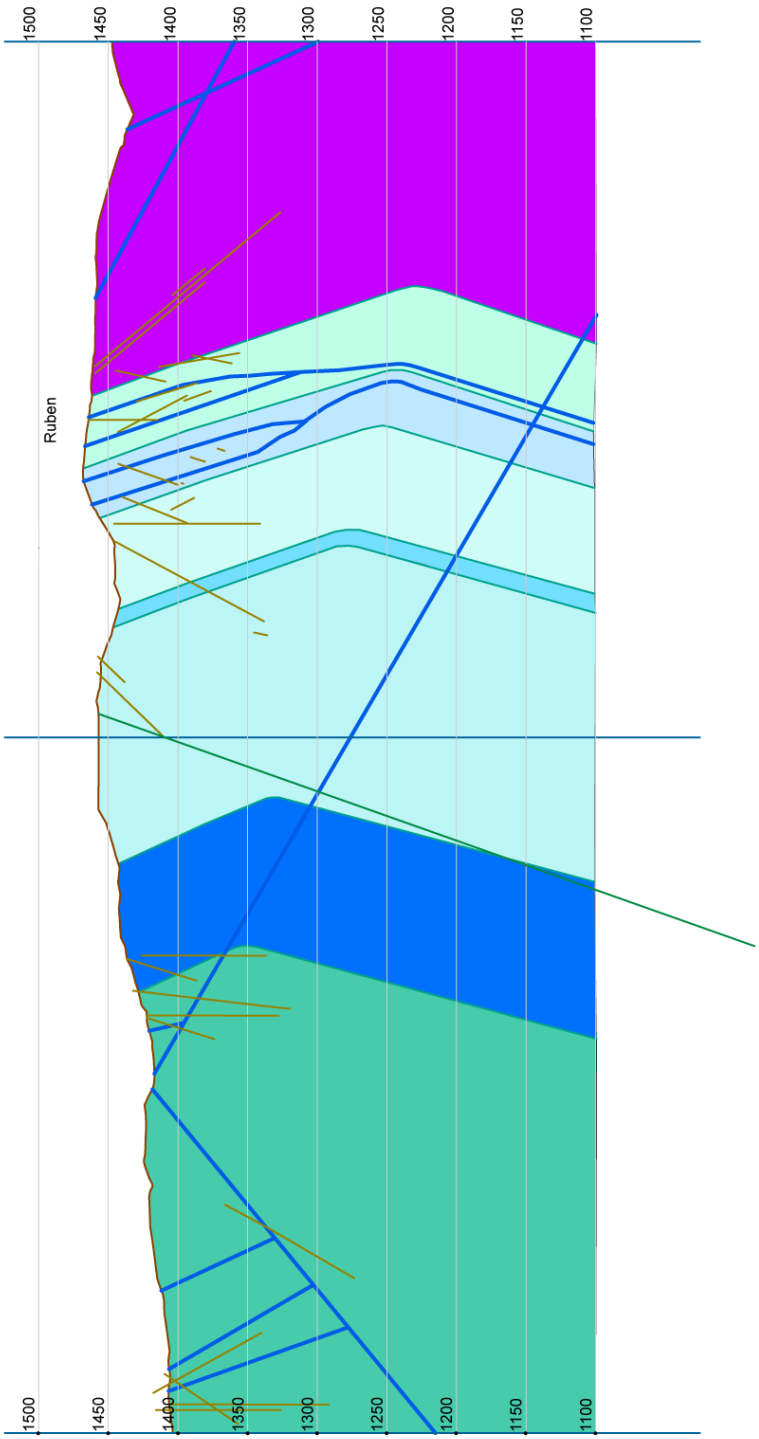

Figure D-7 Cross section *13*

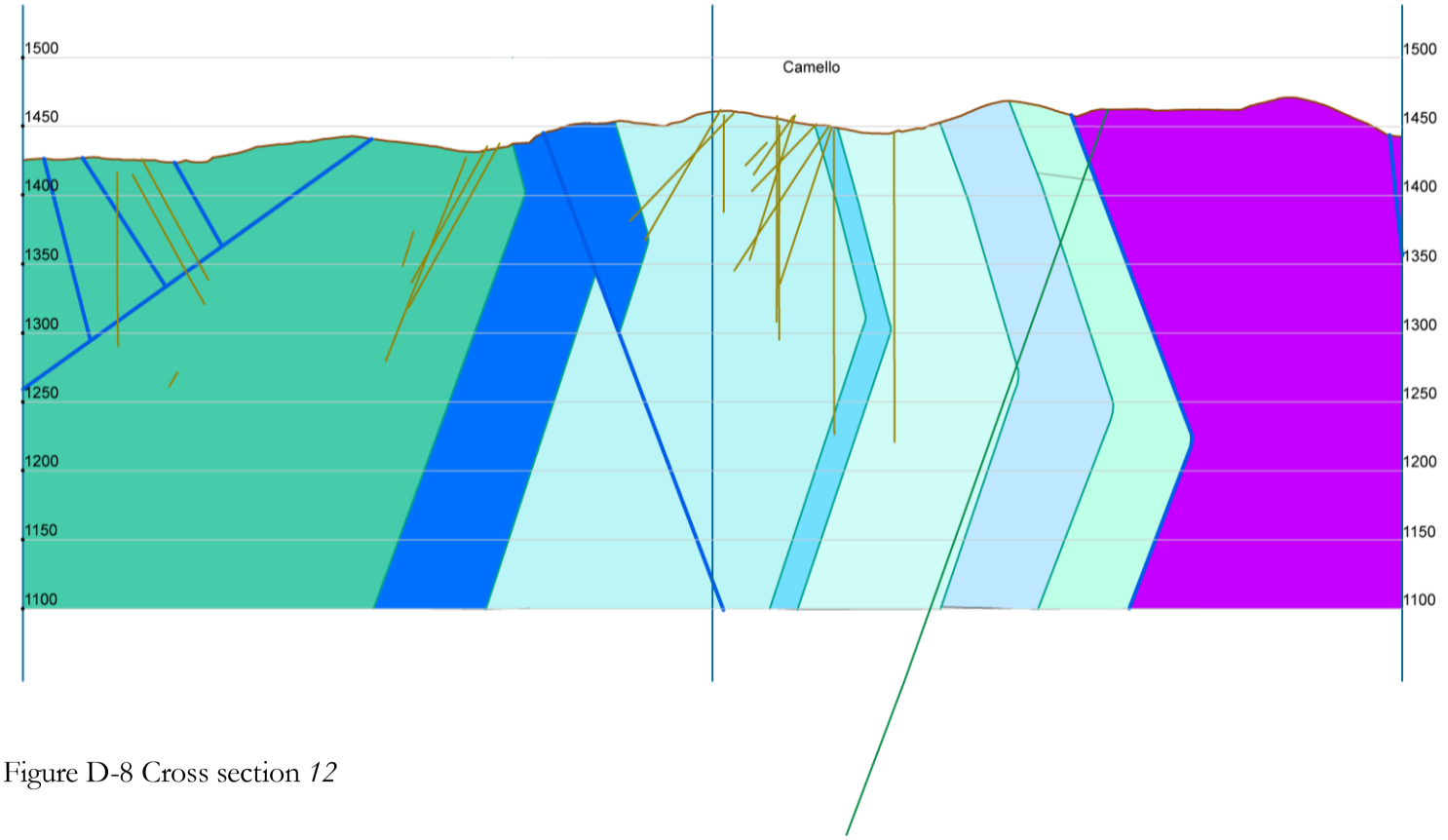

Figure D-8 Cross section *12*

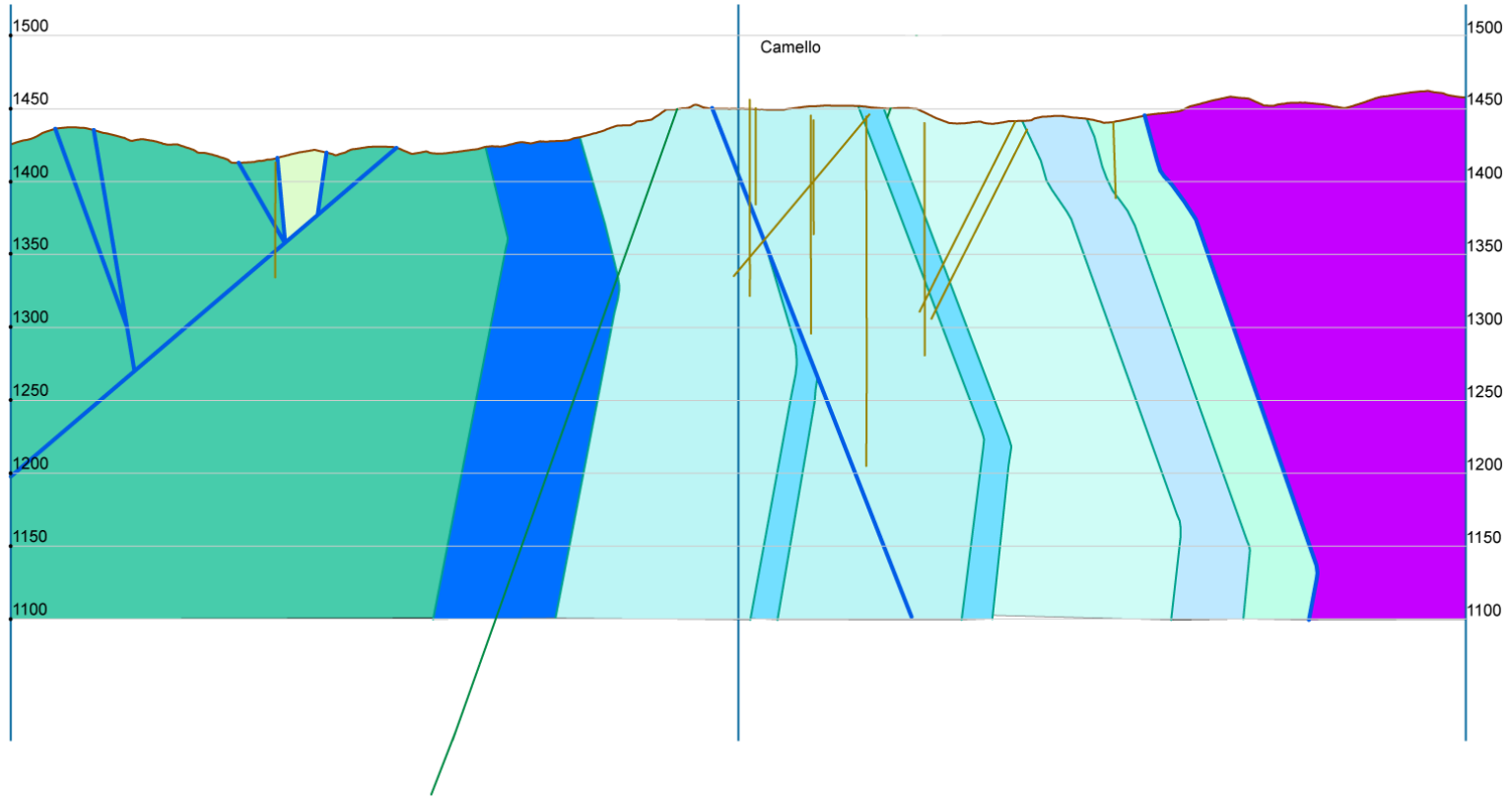

Figure D-9 Cross section *11*

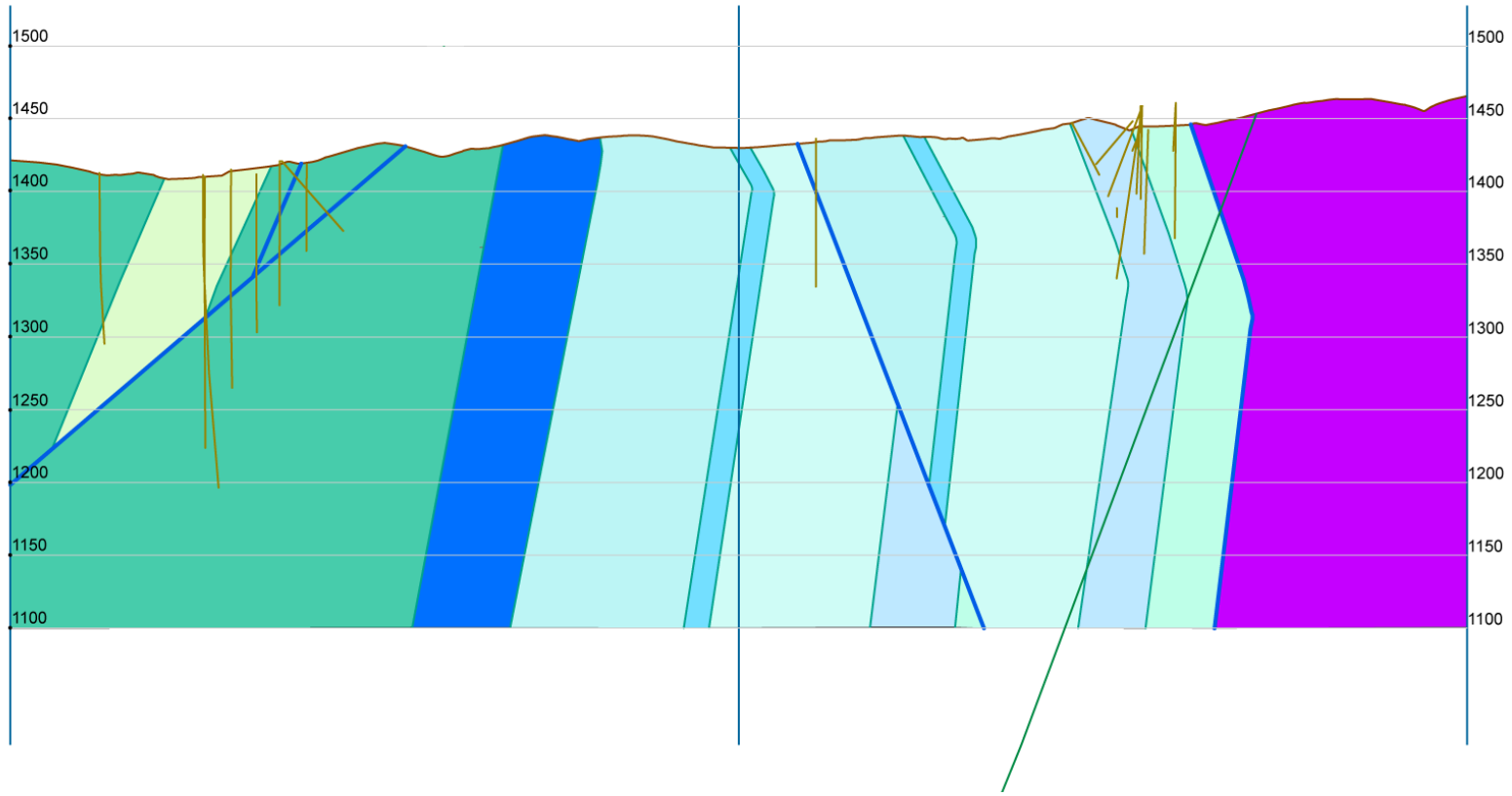

Figure D-10 Cross section *10*

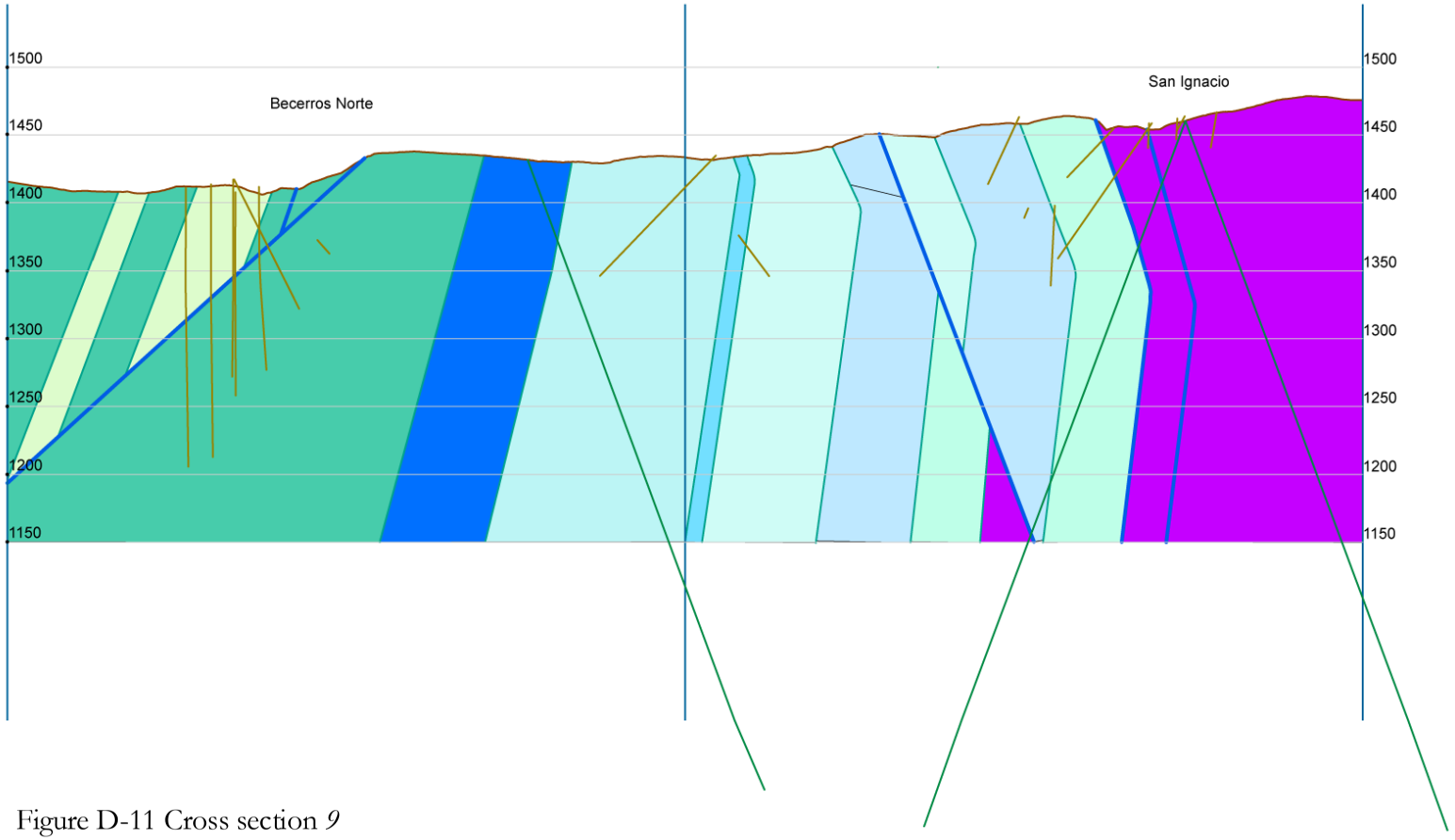

Figure D-11 Cross section *9*

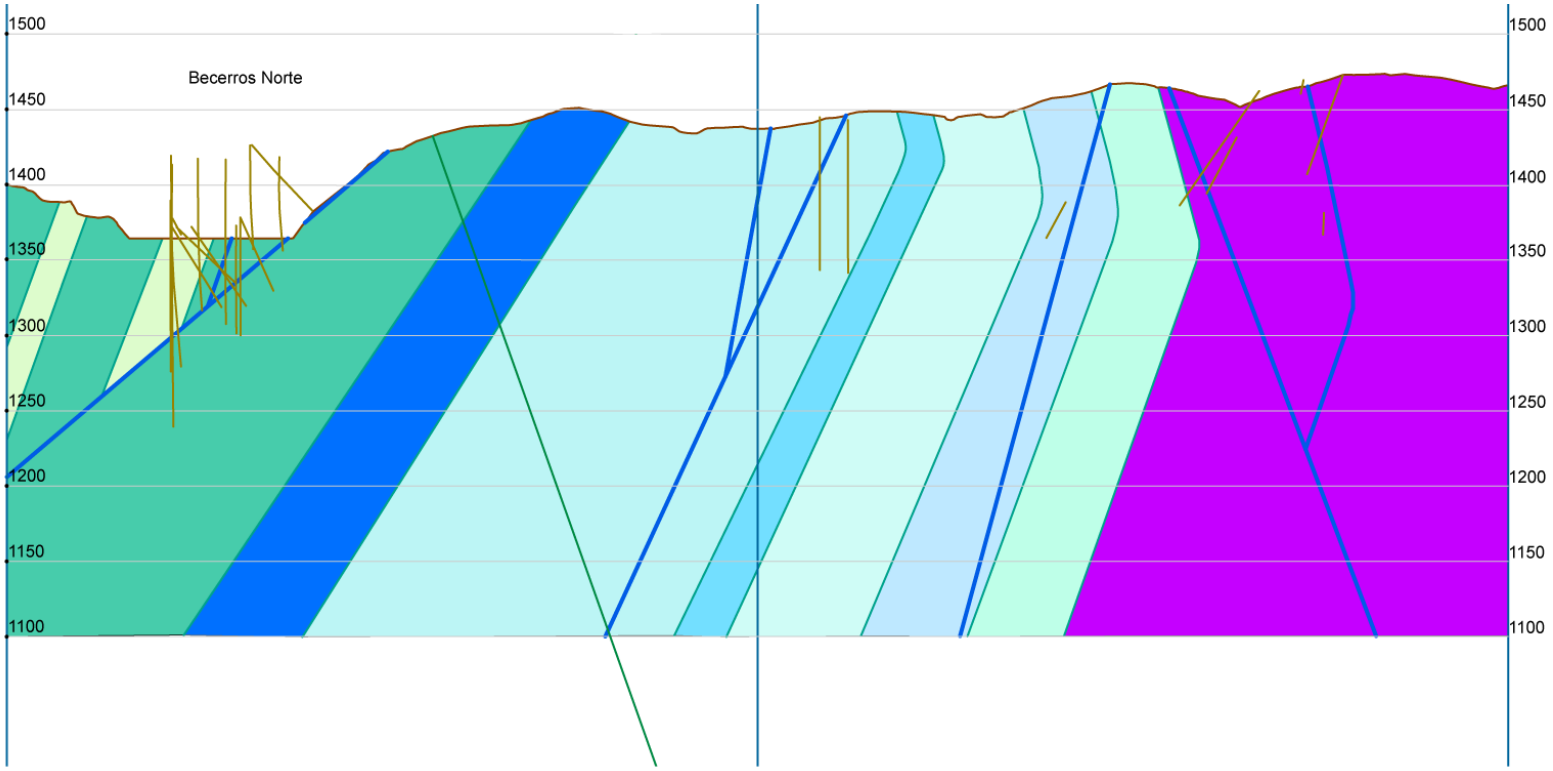

Figure D-12 Cross section *8*

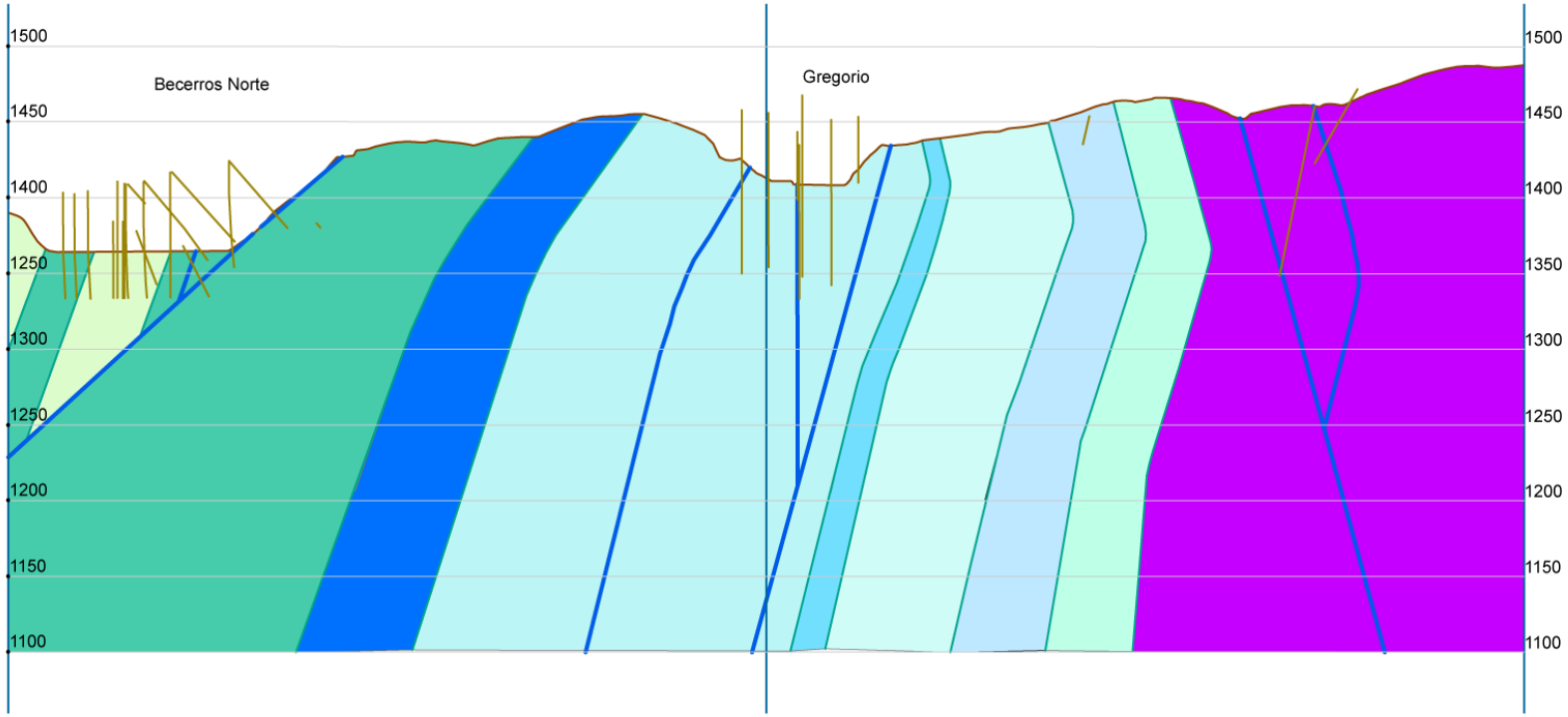

Figure D-13 Cross section *7*

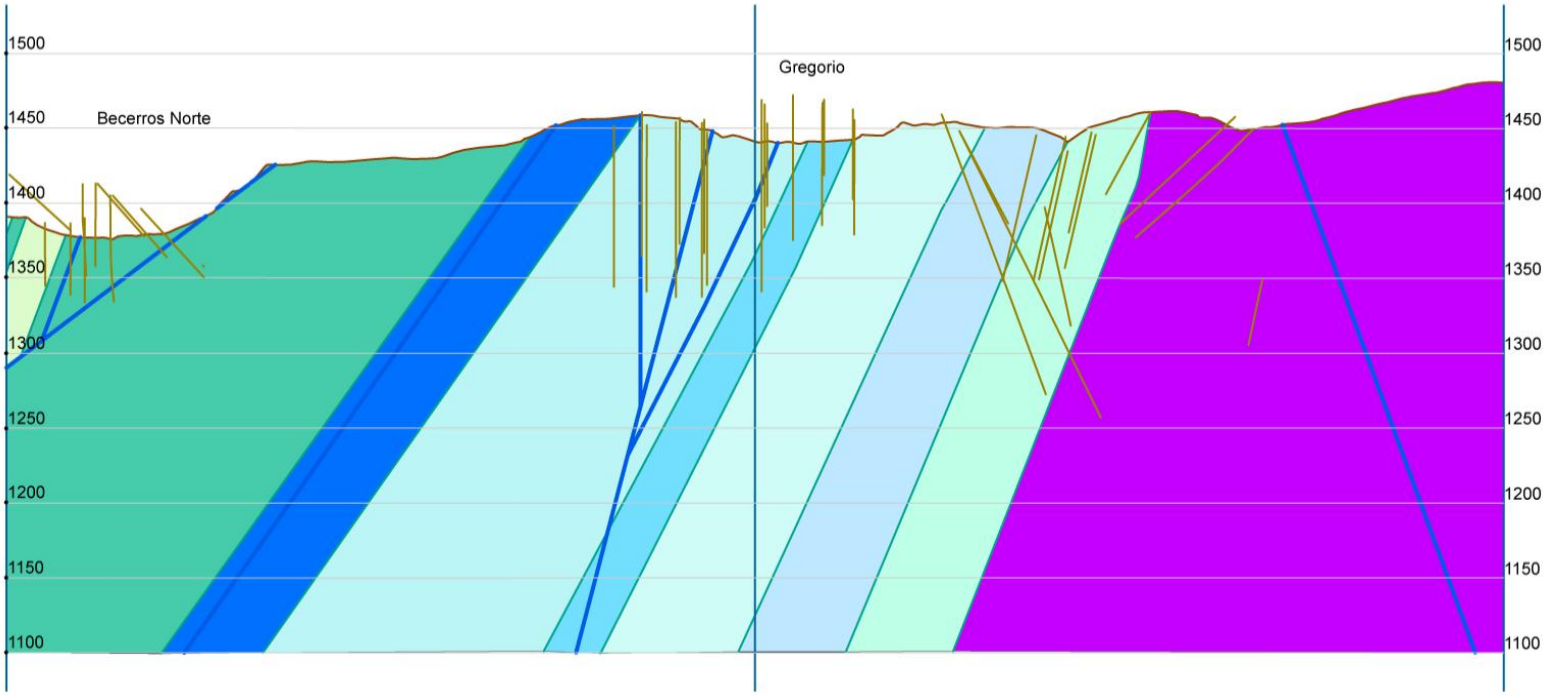

Figure D-14 Cross section *6*

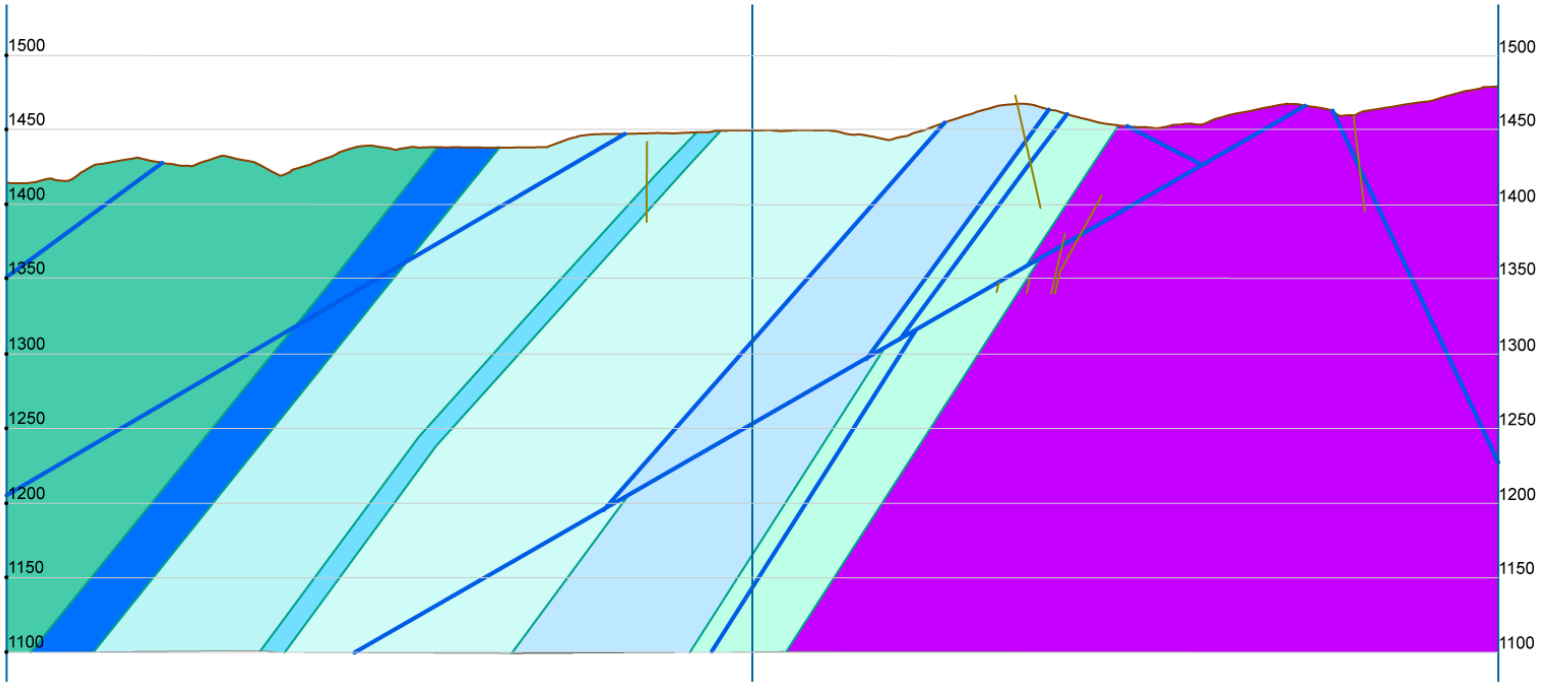

Figure D-15 Cross section *5*

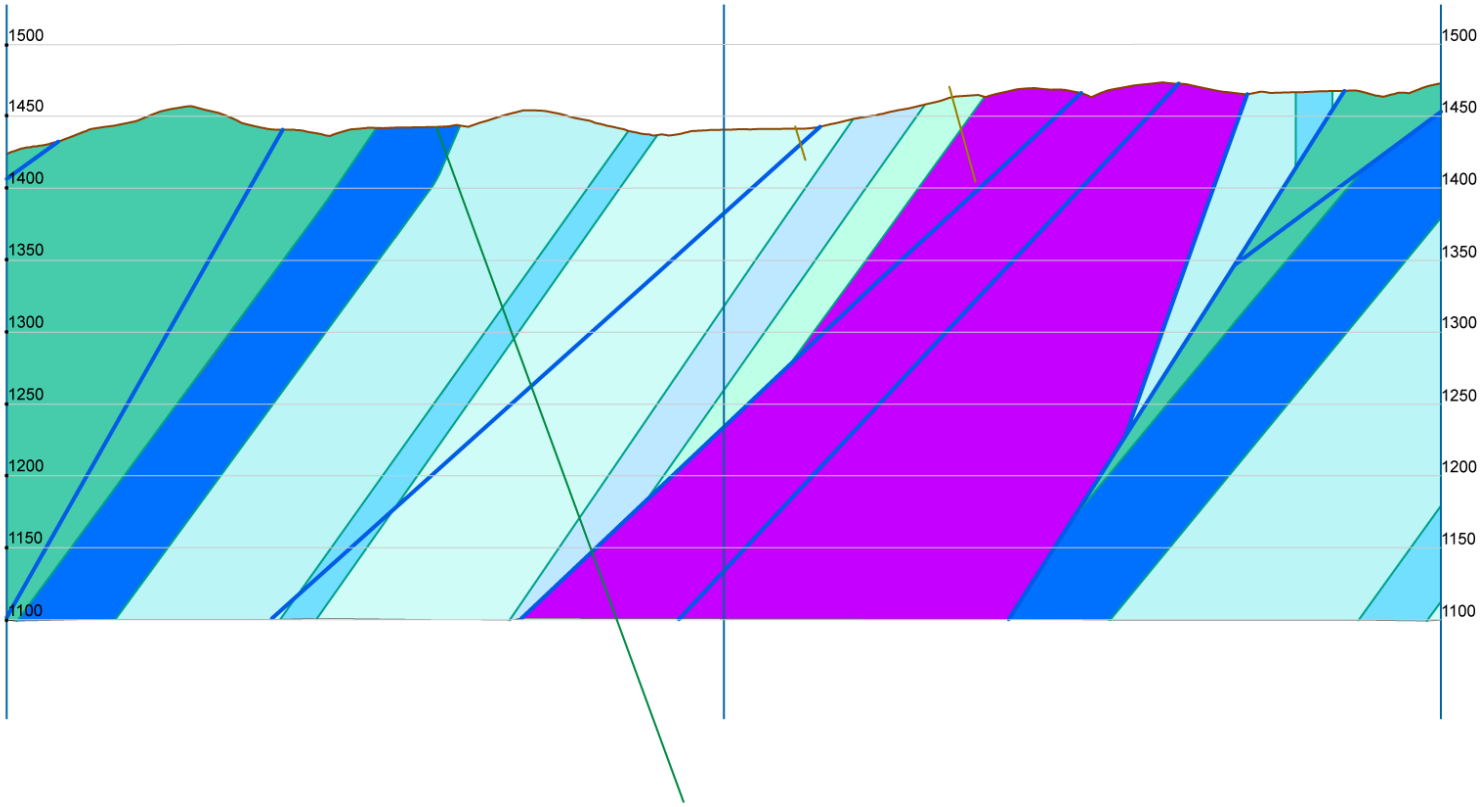

Figure D-16 Cross section *4*

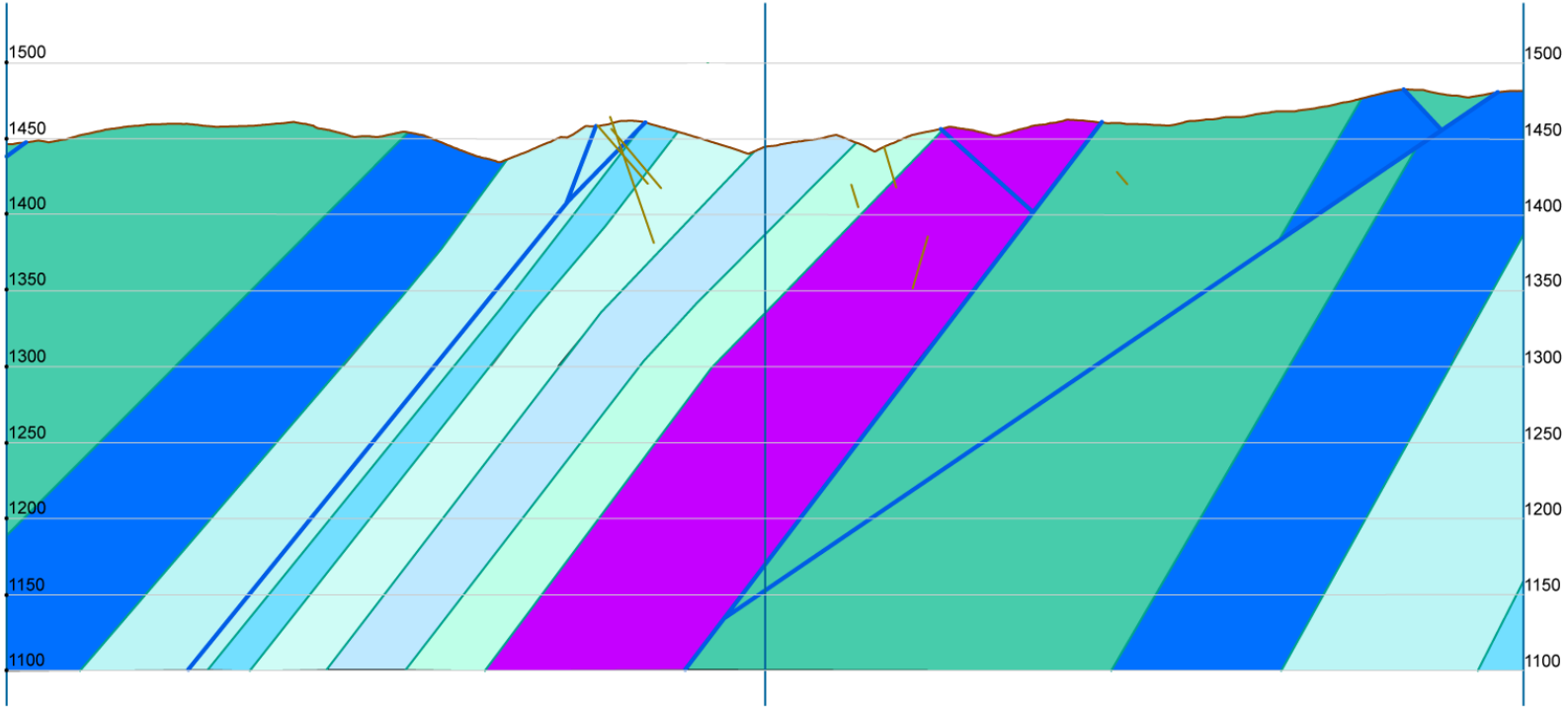

Figure D-17 Cross section *3*

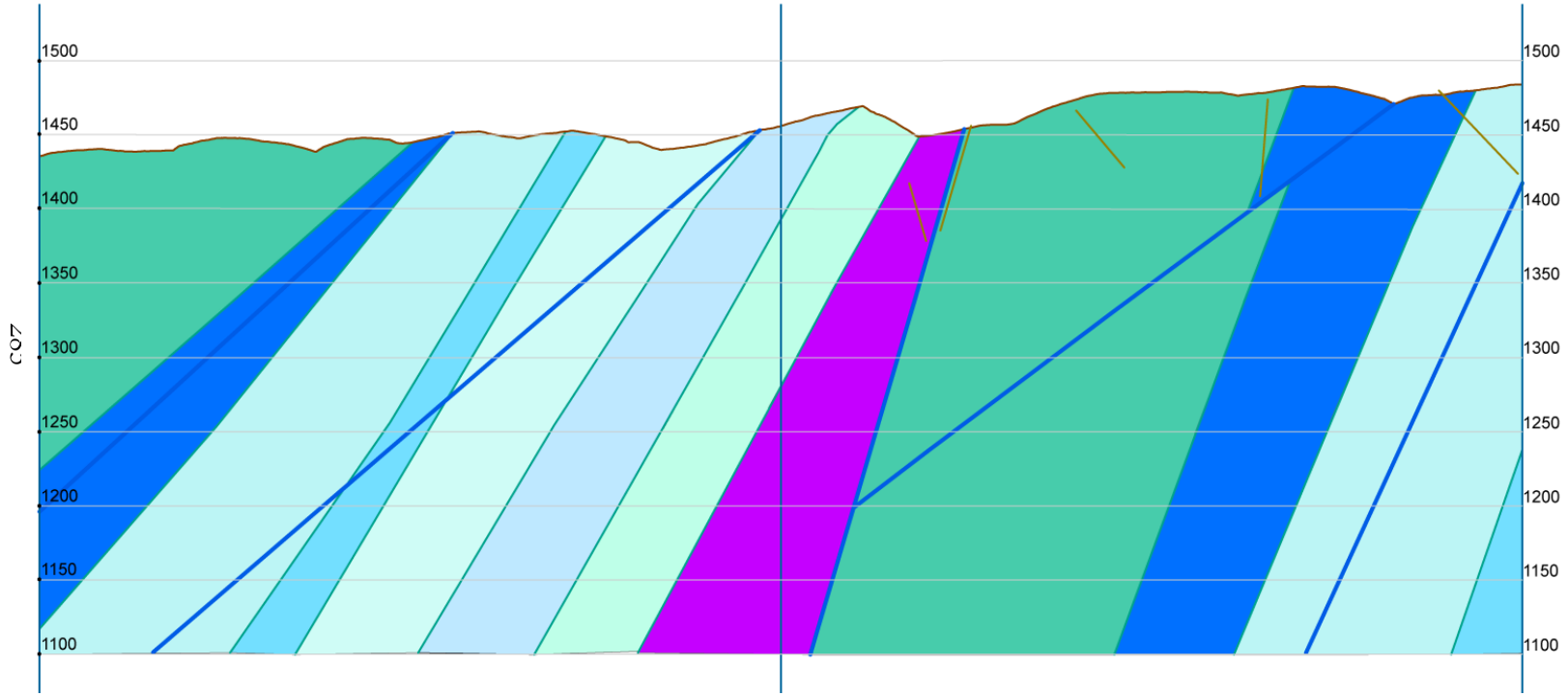

Figure D-18 Cross section *2*

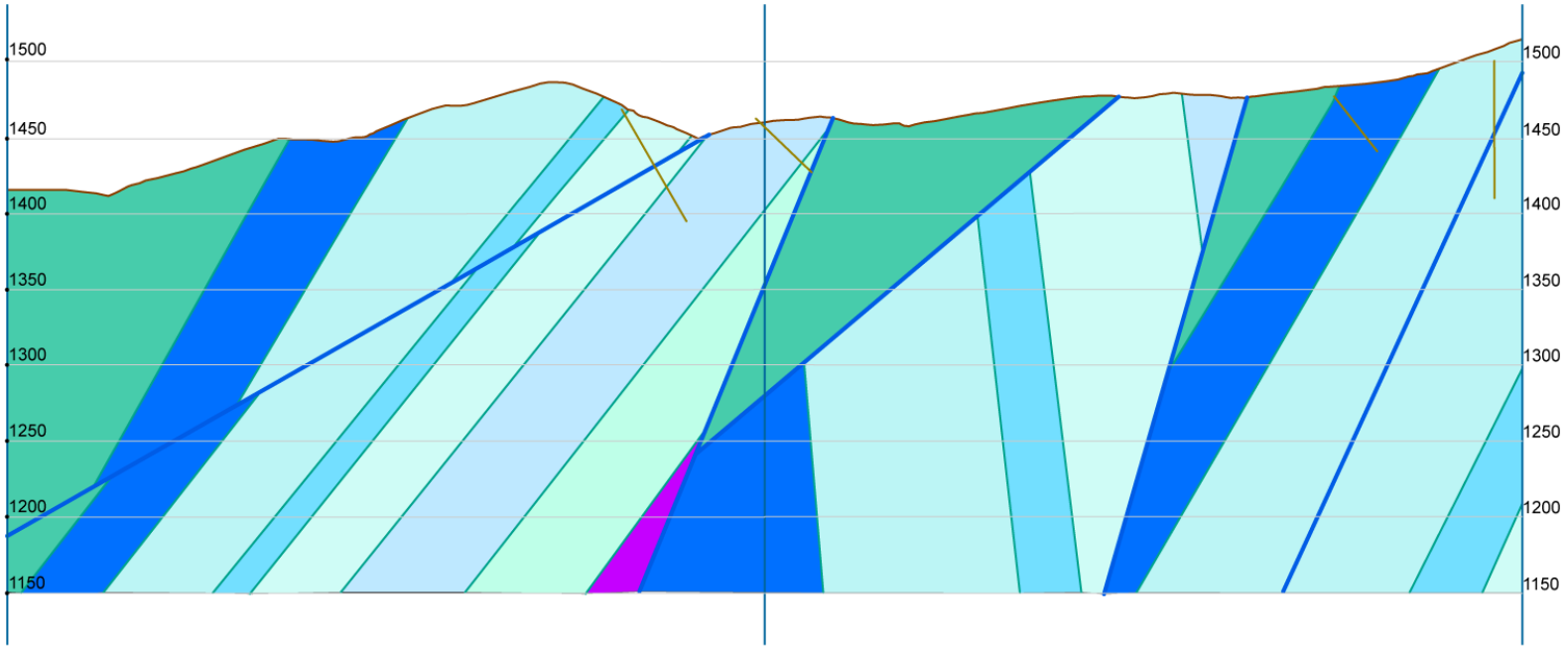

Figure D-19 Cross section *1*